

SLC4A11 in Blinding Endothelial Corneal Dystrophies:  
Characterization, Molecular Defect and Potential Therapeutic Strategy

by

Darpan Malhotra

A thesis submitted in partial fulfillment of the requirements for the degree of

Doctor of Philosophy

Department of Biochemistry  
University of Alberta

© Darpan Malhotra, 2019

## ABSTRACT

Endothelial Corneal Dystrophies (ECD), genetic blinding diseases with a heterogeneous pathophysiology, are the leading cause of endothelial keratopathy (corneal transplants). Patients manifest symptoms, including corneal edema with increased corneal thickness and loss of corneal endothelial cells (CEnC), which form the corneal endothelium and rest on their basement membrane, the Descemet's membrane (DM). Patients suffer blurred vision with progressive deterioration until partial or complete blindness arises. We lack a clear understanding of ECD and no effective therapeutic options are available for patients, leaving them to undergo corneal transplants. Global shortage of donor corneas is a growing concern that makes it essential to understand the defects underlying these dystrophies, to create new therapeutic strategies.

Two prominent blinding corneal dystrophies, rare pediatric-onset congenital hereditary endothelial dystrophy (CHED) and some cases of late-onset and prevalent (4-12% incidence) Fuchs endothelial corneal dystrophy (FECD), are caused by SLC4A11 mutations. SLC4A11, an integral membrane solute transport protein, is expressed in the endothelial layer of the cornea. More than 90 ECD mutations have been reported in SLC4A11, but the underlying mechanisms of the disease are incompletely understood. Three N-terminal variants of SLC4A11 (v1, v2, v3) are expressed in humans but recent controversies in the corneal expression of these variants demands studies to conclusively identify the relevant SLC4A11 isoform for corneal studies. Using a combination of bioinformatic analysis, RNA quantification and protein analysis with variant-specific custom antibodies, we identified SLC4A11 v2 as predominant in human corneal endothelium. We also found the transcription start site in v2 is Methionine at position 36 in human cornea, as opposed to the originally reported Methionine 1.

We further attempted to understand ECD in light of SLC4A11 and the mechanisms by which its mutations cause ECD. SLC4A11 functions as a solute transporter in removing excessive

fluid from the cornea which is essential to maintain corneal transparency and clear vision. Mutations compromising SLC4A11-mediated solute transport lead to fluid accumulation in the cornea, which explains corneal edema and increased corneal thickness. However, loss of solute transport does not explain the progressive decline in CEnC density in patients. We found that SLC4A11 is a cell adhesion molecule (CAM) adhering CEnC to their basement membrane, the DM, in human cornea. We designed a fluorescent *in vitro* cell adhesion assay using bovine DM and HEK293 cell expression system that enabled testing of multiple samples in 96-well format.

Results in this thesis revealed that SLC4A11 interacts with DM to promote cell adhesion. SLC4A11's CAM function is conserved across mammalian species. SLC4A11's third extracellular loop (SLC4A11-EL3) anchors human CEnC to DM as revealed by inhibition of adhesion by anti-SLC4A11-EL3 antibody. ECD-causing mutations in SLC4A11-EL3 ablate its cell adhesion function, without affecting cell surface trafficking, or transport activity. In an energy-minimized three-dimensional model of SLC4A11-EL3, these mutations cluster and are buried within EL3 structure, suggesting they do not directly form the binding site. SLC4A11 interacts with principal DM protein, COL8A2, as revealed by GST pull-down and mass-spectrometry. Experiments in primary CEnC isolated from donor human corneas confirmed the physiological role of SLC4A11 as a CAM in promoting adhesion to DM. Primary human CEnC lose SLC4A11 when cultured. Growing primary cultured human CEnC on bovine DM restored SLC4A11 expression along with its interaction partner, COL8A2. Engineered SLC4A11-EL3-containing chimeric protein, STIC (SLC4A11-EL3 Transmembrane-GPA Integrated Chimer), restores cell adhesion to DM, confirming the role of EL3 in cell adhesion and its potential applications in ECD therapeutics. SLC4A11 is the first solute transport protein to be discovered as a CAM. SLC4A11-mediated cell adhesion to DM is defective in ECDs, providing an explanation for pathological CEnC loss in patients and a potential therapeutic strategy for ECD treatment.

## PREFACE

The research conducted in this thesis is a part of an international research collaboration led by my supervisor, Dr. Joseph Casey. We collaborated with Dr. Richard Zimmermann at University of Saarland, Germany and Dr. Jodhbir Mehta at Singapore Eye Research Institute, Singapore. The thesis is my original work with experiments performed in Canada, Germany and Singapore. All the experiments were designed by Dr. Casey and me. Some data in Chapter 3 were collected by Chris Lukowski (Fig. 3.1), Dr. Sampath Loganathan and Anthony M. Chiu (Figs. 3.5-3.7) from University of Alberta. Chapter 4 includes some data collected by Dr. Martin Jung and Dr. Claudia Fecher-Trost (Fig. 4.8, Table 4.1) from University of Saarland, Dr. Matthew Lovatt and Dr. Gary S. Peh (Fig. 4.9B) from Singapore Eye Research Institute and Dr. Sergei Noskov (Fig. 4.6A) from University of Calgary. The research projects, of which thesis is a part, received ethics approval from University of Alberta Human Research Ethics Board (HREB) ("Towards therapies for genetic corneal dystrophies", Pro00036249, Dec.11, 2013) and human tissues were obtained from the Comprehensive Tissue Centre, University of Alberta Hospital. The study performed in Singapore was approved by SingHealth institutional review board (Ref: 2016/2839).

Chapter 3 of this thesis is accepted for publication as Darpan Malhotra, Sampath K. Loganathan, Anthony M. Chiu, Chris M. Lukowski and Joseph R. Casey. Human Corneal Expression of SLC4A11, a Gene Mutated in Endothelial Corneal Dystrophies. *Scientific Reports* (2019).

Chapter 4 of this thesis is submitted for publication as Darpan Malhotra, Martin Jung, Claudia Fecher-Trost, Matthew Lovatt, Gary S.L. Peh, Sergei Noskov, Jodhbir S. Mehta, Richard Zimmermann and Joseph R. Casey. Defective Cell Adhesion Function of Solute Transporter, SLC4A11, in Endothelial Corneal Dystrophies.

*“Defeat the defeat before defeat defeats you”*

-Naresh Malhotra (Dad)

*“Never allow someone’s thoughts to limit your imagination”*

-Prem Malhotra (Mom)

*To Mom, Dad and my sister (Khushboo Malhotra) who always believed in me, made me believe in me, made my dreams their own and supported me unconditionally.*

## ACKNOWLEDGEMENTS

*“Only after you build an “attitude of gratitude” can you begin to grow your happiness and achieve a measurable level of success”*

This degree has been an incredibly educational and life experience, and it would not have been possible without significant contributions from a lot of people who I want to thank here.

This degree would have been impossible if Dr. Joseph Casey, my PhD supervisor, wouldn't have believed in me and given me a chance to work with him. Joe gave me the best training that I could have hoped for and worked extremely hard with me. He is an excellent mentor who allowed me to explore my ideas and fueled my confidence every time I thought I was failing. Joe always prioritized things that are beneficial for my career and taught me great deal about life in science. Outside science, he also taught me how to ski, picked me up every time I fell and shared experiences over Indian food and beer. I am filled with immense gratitude and respect and will always be grateful for the experiences and lessons I learnt from Joe.

I am extremely thankful to my supervisory committee members, Dr. Howard Young and Dr. Todd Alexander for their guidance, support and valuable insights which helped me tailor me work for making an impactful contribution. They are extraordinary scientists who have ensured my progress in this program and I am glad to get their continued support. I am also thankful to Dr. Robert Molday and Dr. Ordan Lehmann for agreeing to be my external examiner and internal examiners. I am thankful to my collaborators Dr. Richard Zimmermann (University of Saarland, Germany) and Dr. Jodhbir Mehta (Singapore Eye Research Institute, Singapore) who welcomed me in their labs and ensured that I get the best experience and support in my work. I am grateful to Dr. Martin Jung, Dr. Claudia Fecher-Trost from Germany and Dr. Matthew Lovatt and Dr. Gary Peh from Singapore who helped me closely in my work and ensured a smooth workflow during my time in their labs. I am thankful to my collaborator, Dr. Sergei Noskov (University of Calgary), for his expertise and the time he put in my project and made a significant contribution to my work.

I am also thankful to members of the Membrane Protein Disease Research Group and International Research and Training Group in Membrane Biology for their valuable inputs and support. I want to especially thank Drs. Joanne Lemieux, Emmanuelle Cordat, Nicholas Touret, Elaine Leslie, Richard Fahlman and Jack Moore for their support at innumerable times during my PhD. Special thanks to Dr. Rachel Wevrick for her encouragement and delicious food. A big appreciation to the administrative and other staff of the Biochemistry department always ensure a smooth functioning environment and infrastructure for the students.

I acknowledge the privilege of conducting research at the University of Alberta and thank funding agencies CIHR and NSERC. I am extremely grateful for the stipend support I received from Vanier Canada Graduate Scholarships, Alberta Innovates Graduate Scholarships, IRTG in Membrane Biology Scholarship, Faculty of Medicine and Dentistry and Faculty of Graduate Studies and Research Awards, and the unknown Canadian taxpayers.

This journey would have been impossible without the continued support from Katie Badior who has been an incredible support in the lab, a great listener over coffee breaks and a compassionate friend. I am thankful to Dr. Sampath Loganathan, Mike Chiu, Nada Alshumaimeri, Dr. Arghya Basu, Chris Lukwoski and Kamala Lamsal for their continued help and support.

I want to thank my friends Silvia Sgaramella, Gaurav Suri and Samridhi Sharma for being there whenever I needed them. They are the source of my strength and a vital part of this journey.

I am indebted to The Rohrschach's: Doris (Mama), Wilhelm, Jutta and Gregory for providing me a home away from home. They became my family, fed me so much delicious food and supported me unconditionally. I feel blessed to have amazing people like them in my life.

No words will ever be enough to thank my parents and sister for all they have done to bring me where I am today. My aunts, Prem Rajpal, Veena Maggo, Vijay Arora, Chitra Arora and cousin Geetika Gakhar who keep sending me their love from oceans away. My uncles, cousins, nieces, nephews, and all family members for believing in me and loving me unconditionally.

# Table of Contents

1) CHAPTER 1: GENERAL INTRODUCTION.....	1
1.1 THESIS OVERVIEW.....	2
1.2 THE HUMAN EYE .....	3
1.3 THE CORNEA.....	4
1.3.1 Epithelium.....	4
1.3.2 Bowman’s Layer .....	7
1.3.3 Stroma .....	7
1.3.4 Descemet’s membrane .....	8
1.3.5 Endothelium.....	8
1.4 PHYSIOLOGICAL REGULATION OF CORNEA BY ENDOTHELIOUM .....	9
1.4.1 Supplying nutrition to the cornea.....	10
1.4.2 Maintenance of corneal transparency by the endothelial pump.....	10
1.5 CORNEAL DYSTROPHIES .....	11
1.6 ENDOTHELIAL CORNEAL DYSTROPHIES AND PATHOPHYSIOLOGY .....	14
1.6.1 Fuchs Endothelial Corneal Dystrophy (FECD) .....	14
1.6.2 Congenital Hereditary Endothelial Dystrophy (CHED).....	18
1.6.3 Harboyan Syndrome (HS).....	19
1.7 TREATMENT OPTIONS FOR ENDOTHELIAL CORNEAL DYSTROPHIES .....	19
1.8 GENE ALTERATIONS IN ENDOTHELIAL CORNEAL DYSTROPHIES .....	24
1.9 SOLUTE CARRIER 4 FAMILY OF TRANSPORTERS .....	26
1.10 SLC4A11 .....	27
1.10.2 Expression Profile .....	30
1.10.3 Transcripts.....	30

1.10.4 Structure .....	31
1.10.5 Oligomerization .....	32
1.10.6 Functions .....	32
1.10.7 Mutations .....	33
1.11 SLC4A11 MUTATIONS CAUSE ENDOTHELIAL CORNEAL DYSTROPHIES.....	36
1.11.1 Trafficking defect.....	36
1.11.2 Functional defect.....	37
1.12 SLC4A11 TRANSLATIONAL PRODUCT IN HUMAN CORNEA.....	37
1.13 ROLE OF SLC4A11 IN EXPLAINING THE PATHOPHYSIOLOGY OF ECD .....	41
1.13.1 Corneal edema and increase in corneal thickness .....	41
1.13.2 Progressive decline in CEnC density, increase DM thickness and guttae formation.....	41
1.14 CELL ADHESION TO BASEMENT MEMBRANES .....	42
1.15 HYPOTHESES .....	44
1.16 THESIS OBJECTIVES .....	45
<b>2) CHAPTER 2: MATERIALS AND METHODS .....</b>	<b>46</b>
2.1 MATERIALS.....	47
2.2 DNA CONSTRUCTS.....	49
2.2.1 Mammalian Expression constructs.....	49
2.2.2 Bacterial Expression constructs .....	51
2.3 RESEARCH-GRADE HUMAN CORNEOSCLERAL TISSUES .....	51
2.4 PREPARATION OF ANTI-SLC4A11 ANTIBODIES.....	58
2.5 BIOINFORMATIC ANALYSIS .....	58
2.6 BACTERIAL TRANSFORMATION .....	59

2.7 PLASMID PREPARATION.....	59
2.8 CELL CULTURE AND TRANSFECTION .....	60
2.8.1 HEK293 cells: .....	60
2.8.2 Primary HCEnC .....	60
2.9 PREPARATION OF HUMAN CORNEAL LYSATES.....	61
2.10 REVERSE TRANSCRIPTION PCR .....	62
2.11 REAL TIME QUANTITATIVE PCR .....	63
2.12 IMMUNOBLOTS AND DENSITOMETRY .....	63
2.13 CELL SURFACE PROCESSING ASSAYS.....	66
2.14 ASSAYS OF OSMOTICALLY DRIVEN WATER FLUX .....	67
2.15 QUANTIFICATION OF SLC4A11 VARIANT 2 AND 3 PROTEINS IN ENDOTHELIAL CELL LYSATES	68
2.16 HOMOLGY MODELING OF SLC4A11 V2-M36 AND V3 CYTOPLASMIC DOMAINS .....	69
2.17 PREPARATION OF BOVINE DM EXTRACTS .....	69
2.18 CELL ADHESION ASSAY.....	70
2.19 COMPETITION FOR ADHESION TO DM-COATED DISHES .....	71
2.20 ASSAY OF ANTI-SLC4A11-EL3 ANTIBODY EFFECT ON TRANSFECTED HEK293 CELL ADHESION.....	71
2.21 STRUCTURAL MODELLING OF SLC4A11 EXTRACELLULAR LOOP 3 .....	72
2.22 GST-SLC4A11-EL3 PULL DOWN ASSAYS .....	73
2.23 MASS SPECTROMETRY.....	74
2.24 GENE EXPRESSION ANALYSIS .....	75
2.25 CULTURE OF PRIMARY HCENC ON DM AND FIBRONECTIN-COATED DISHES .....	75
2.26 ASSAY OF PRIMARY HCENC ADHESION USING XCELLIGENCE REAL-TIME CELL ANALYZER...	77
2.27 ASSAY OF ANTI-SLC4A11-EL3 ANTIBODY ON PRIMARY HCENC ADHESION .....	77
2.28 STATISTICAL ANALYSIS.....	78

<b>3) CHAPTER 3: HUMAN CORNEAL EXPRESSION OF SLC4A11, A GENE MUTATED IN</b>	
<b>    ENDOTHELIAL CORNEAL DYSTROPHIES.....</b>	<b>79</b>
3.1 INTRODUCTION .....	80
3.2 RESULTS.....	82
3.2.1 Bioinformatic analyses of human SLC4A11 .....	82
3.2.2 Expression of SLC4A11 transcripts in human cornea.....	85
3.2.3 SLC4A11 v2 and v3 protein expression in human corneal endothelium .....	89
3.2.4 Identification of SLC4A11 v2 translation start site in total human corneal lysates.....	90
3.2.5 Plasma membrane localization of SLC4A11 v2-M1 and v2-M36. ....	92
3.2.6 Osmotically driven water flux activity of SLC4A11 v2-M1 and v2-M36.....	94
3.2.7 Functional and structural differences between v2-M36 and v3-SLC4A11.....	98
3.3 DISCUSSION .....	106
<b>4) CHAPTER 4: DEFECTIVE CELL ADHESION ROLE OF SOLUTE TRANSPORTER,</b>	
<b>    SLC4A11, IN ENDOTHELIAL CORNEAL DYSTROPHIES.....</b>	<b>108</b>
4.1 INTRODUCTION .....	109
4.2 RESULTS.....	112
4.2.1 Role of SLC4A11 in cell adhesion to DM.....	112
4.2.2 Characterization of SLC4A11 extracellular loop 3 as the DM adhesion site .....	113
4.2.3 FECD and CHED mutations in SLC4A11 compromise cell adhesion .....	117
4.2.4 Structural analysis of SLC4A11 extracellular loop 3 .....	121
4.2.5 STIC (SLC4A11-EL3 Transmembrane-GPA Integrated Chimera) restores cell adhesion... ..	124
4.2.6 SLC4A11-EL3 interacts with DM components.....	127
4.2.7 Role of DM in regulating SLC4A11 expression in primary HCEnC .....	127

4.2.8 Restoration of SLC4A11 expression increases HCEnC adhesion to DM.....	133
4.2.9 Anti-SLC4A11-EL3 antibody reduces primary HCEnC adhesion to DM.....	136
4.3 DISCUSSION.....	141
<b>5) CHAPTER 5: SUMMARY AND FUTURE DIRECTIONS .....</b>	<b>148</b>
5.1 SUMMARY .....	149
5.1.1 Human Corneal Expression of SLC4A11, a Gene Mutated in ECD.....	149
5.1.2 Defective Cell Adhesion Role of Solute Transporter, SLC4A11, in ECD.....	150
5.2 FUTURE DIRECTIONS .....	152
5.2.1 Key amino acid residues involved in SLC4A11 and COL8A2 interaction.....	152
5.2.2 SLC4A11 and COL8A2 co-chaperone each other to maintain DM organization?...	153
5.2.3 Potential association of SLC4A11 with corneal integrins and focal adhesions.....	155
5.2.4 Role of SLC4A11 in anoikis.....	156
5.2.5 Potential exploitation of SLC4A11-mediated cell adhesion by cancer cells .....	157
5.2.6 SLC4A11 and TCF4.....	158
5.2.7 Cell adhesion in the inner ear.....	159
5.2.8 Role of SLC4A11 during development .....	161
5.2.9 Strategies to use STIC as a therapeutic molecule in ECD.....	162
<b>BIBLIOGRAPHY.....</b>	<b>171</b>

## List of Figures

<i>Figure 1.1: Structure of the human eye and the cornea.</i> .....	5
<i>Figure 1.2: The Corneal Endothelial Pump maintains fluid-balance in the cornea and corneal transparency.</i> .....	12
<i>Figure 1.3: Clinical presentation of corneal edema in FECD and CHED patients.</i> .....	21
<i>Figure 1.4: Clinical presentation of CEnC loss in FECD and CHED patients.</i> .....	22
<i>Figure 1.5: Clinical presentation of guttae in FECD patients.</i> .....	23
<i>Figure 1.6: Phylogenetic Dendrogram of SLC4 family of transporters.</i> .....	28
<i>Figure 1.7: SLC4A11 topology model highlighting structural aspects of the protein and ECD-causing mutations.</i> .....	34
<i>Figure 3.1: Bioinformatic analysis of human SLC4A11.</i> .....	83
<i>Figure 3.2: Studying the expression of SLC4A11 transcripts in human cornea by RT-PCR.</i> .....	87
<i>Figure 3.3: Expression of SLC4A11 transcripts in human cornea assessed by quantitative PCR.</i> .....	88
<i>Figure 3.4: SLC4A11 v2 and v3 expression in human corneal endothelium.</i> .....	91
<i>Figure 3.5: Identification of SLC4A11 v2 translation start site in total human corneal lysates.</i> ....	93
<i>Figure 3.6: Plasma membrane localization of SLC4A11 v2-M1 and v2-M36.</i> .....	96
<i>Figure 3.7: Osmotically driven water flux activity of SLC4A11 v2-M1 and v2-M36.</i> .....	99
<i>Figure 3.8: Osmotically driven water flux activity of SLC4A11 v2-M36 and v3.</i> .....	101
<i>Figure 3.9: Homology model of SLC4A11 v2-M36 and SLC4A11 v3 cytoplasmic domains.</i> ....	103
<i>Figure 3.10: Alternative homology model of SLC4A11 v2-M36 and SLC4A11 v3 cytoplasmic domains.</i> .....	105
<i>Figure 4.1: Role of SLC4A11 in cell adhesion to DM</i> .....	114
<i>Figure 4.2: SLC4A11 cell adhesion role is conserved across mammals.</i> .....	116

<i>Figure 4.3: SLC4A11 extracellular loop 3 forms the DM adhesion site.....</i>	<i>118</i>
<i>Figure 4.4: Effect of N-linked glycosylation in SLC4A11-EL3 on cell adhesion.....</i>	<i>120</i>
<i>Figure 4.5: FECD and CHED mutations in SLC4A11 compromise cell adhesion. ....</i>	<i>122</i>
<i>Figure 4.6: Structural analysis of SLC4A11 Extracellular Loop 3. ....</i>	<i>125</i>
<i>Figure 4.7: STIC (SLC4A11-EL3 Transmembrane-GPA Integrated Chimera) restores cell adhesion. ....</i>	<i>128</i>
<i>Figure 4.8: Identification of DM proteins interacting with SLC4A11-EL3.....</i>	<i>132</i>
<i>Figure 4.9: Role of DM in regulating SLC4A11 expression in primary HCEnC.....</i>	<i>134</i>
<i>Figure 4.10: Restoration of SLC4A11 expression increases HCEnC adhesion to DM.....</i>	<i>137</i>
<i>Figure 4.11: Anti-SLC4A11-EL3 antibody reduces primary HCEnC adhesion to DM. ....</i>	<i>139</i>
<i>Figure 4.12: SLC4A11 cell adhesion role in corneal physiology and endothelial corneal dystrophies.....</i>	<i>142</i>
<i>Figure 4.13: SLC4A11 Cell Adhesion Role explains differences in FECD and CHED onset. ..</i>	<i>145</i>
<i>Figure 5.1: Potential amino acids in SLC4A11-EL3 involved in DM interaction are surface exposed. ....</i>	<i>154</i>
<i>Figure 5.2: Proposed cell biological pathway defective in FECD.....</i>	<i>160</i>

## List of Tables

<i>Table 1.1: Corneal Dystrophies classified on the basis of anatomical location in the cornea.....</i>	<i>16</i>
<i>Table 1.2: Transport mechanism and tissue distribution of SLC4 family of transporters.....</i>	<i>29</i>
<i>Table 1.3: List of SLC4A11 mutations causing different Endothelial Corneal Dystrophies. ....</i>	<i>38</i>
<i>Table 2.1: Primers used to clone human SLC4A11 v2-M36, SLC4A11 v3 and nHA-AE1 mammalian expression constructs. ....</i>	<i>52</i>
<i>Table 2.2: Primers used to create FECD, CHED and N-glycosylation mutants of human SLC4A11. ....</i>	<i>53</i>
<i>Table 2.3: Primers to create STIC construct for mammalian expression.....</i>	<i>54</i>
<i>Table 2.4: Primers to clone SLC4A11-EL3 into pJET1.2.....</i>	<i>55</i>
<i>Table 2.5: Donor information for samples collected from Comprehensive Tissue Centre (University of Alberta).....</i>	<i>56</i>
<i>Table 2.6: Donor information for samples collected from Lions Eye Institute for Transplant and Research. ....</i>	<i>57</i>
<i>Table 2.7: cDNA synthesis from isolated corneal RNA using SuperScript III First strand synthesis system.....</i>	<i>64</i>
<i>Table 2.8: Primers for reverse transcription PCR amplification of SLC4A11 transcripts.....</i>	<i>65</i>
<i>Table 2.9: TaqMan® gene expression assay probes used for real-time PCR. ....</i>	<i>76</i>
<i>Table 3.1: Review of Human SLC4A11 Variants used in studies from 2001-2019. ....</i>	<i>95</i>
<i>Table 4.1: Proteins associated with GST-SLC4A11-EL3 as identified by nano-liquid chromatography and mass spectrometry (nano-LC-ESI-MS<sup>2</sup>). ....</i>	<i>130</i>

## List of Abbreviations

Abbreviation	Full form
<b>A</b>	
A	Absorbance
ACD	Avellino corneal dystrophy
AD	Autosomal dominant
AE	Anion exchanger
AR	Autosomal recessive
AGBL1	ATP/GTP binding-protein like 1
ATPB1	Na <sup>+</sup> K <sup>+</sup> transporting ATPase, beta-1 polypeptide
AQP	Aquaporin
<b>B</b>	
bHLH	Basic helix-hoop-helix
B.I.	Band intensities
BK	Bullous keratopathy
BSA	Bovine serum albumin
BTR1	Borate transporter 1
Bp	Base pair
<b>C</b>	
C <sub>T</sub>	Threshold cycle
CACC	Calcium activated chloride channel
CAM	Cell adhesion molecule
CDPD	Corneal dystrophy and perceptive deafness
CEnC	Corneal endothelial cell
CFTR	Cystic fibrosis transmembrane conductance regulator
CFU	Colony forming unit
CHED	Congenital hereditary endothelial dystrophy
COL8A1	Collagen VIII alpha chain 1
COL8A2	Collagen VIII alpha chain 2
COSMIC	Catalogue of somatic mutations in cancer
CS	Calf serum
CSCD	Congenital stromal corneal dystrophy

<b>D</b>	
DM	Descemet's membrane
DEPC	Diethyl pyrocarbonate
DMEM	Dulbecco's modified eagle's medium
DMEK	Descemet's membrane endothelial keratoplasty
DSAEK	Descemet stripping automated endothelial keratoplasty
DTT	Dithiothreitol
<b>E</b>	
EBMD	Epithelial basement membrane dystrophy
ECD	Endothelial corneal dystrophies
ECM	Extracellular matrix
eGFP	Enhanced green fluorescent protein
EK	Endothelial keratoplasty
EL3	Extracellular loop 3
ER	Endoplasmic reticulum
ERAD	Endoplasmic reticulum-associated degradation
<b>F</b>	
F	Fluorescence
FBS	Fetal bovine serum
FCD	Fleck corneal dystrophy
FECD	Fuchs endothelial corneal dystrophy
FNC	Fibronectin
<b>G</b>	
GAPDH	Glyceraldehyde-3-phosphate dehydrogenase
GCD	Granular corneal dystrophy
GDL	Gelatinous drop-like corneal dystrophy
GST	Glutathione-S-transferase
GPA	Glycophorin-A
GWAS	Genome-wide association study
<b>H</b>	
HA	Hemagglutinin
HCD	High energy collision dissociation
HCEnC	Human corneal endothelial cell
HS	Harboyan syndrome

HRP	Horseradish peroxidase
HGMD	Human gene mutation database
HREB	Human research ethics board
<b>I</b>	
IC3D	International committee for classification of corneal dystrophies
IgCAM	Immunoglobulin cell adhesion molecule
IP	Immunoprecipitation
IPTG	Isopropyl- $\beta$ -D-thiogalactoside
I-TASSER	Iterative threading assembly refinement
ITGAV	Integrin $\alpha_v$
ITGB3	Integrin $\beta_3$
ITGB5	Integrin $\beta_5$
ITS	Insulin transferrin selenium
<b>K</b>	
KANK4	KN motif and ankyrin repeat domain containing protein 4
<b>L</b>	
LAMC1	Laminin gamma-1 protein
LB	Luria broth
LCD	Lattice corneal dystrophy
LECD	Lisch epithelial corneal dystrophy
LOXHD1	Lipoxygenase homology domain-containing 1
LMX1B	LIM homeobox transcription factor 1 beta
<b>M</b>	
M1	Methionine 1
M36	Methionine 36
MBSS	Mops buffered saline solution
MBNL1	Muscleblind like 1
MCD	Macular corneal dystrophy
MCT	Monocarboxylate transporter
MD	Molecular dynamics
MECD	Meesmann corneal dystrophy
MIM	Mendelian inheritance in man
<b>N</b>	
NCAD	N-cadherin

NCC	Neural crest cells
NHE	Na <sup>+</sup> /H <sup>+</sup> exchanger
NKCC1	Na <sup>+</sup> :K <sup>+</sup> :2Cl <sup>-</sup> cotransporter
NT	Non-transfected
<b>P</b>	
P0	Passage 0
P1	Passage 1
P2	Passage 2
PACD	Posterior amorphous corneal dystrophy
PAGE	Polyacrylamide gel electrophoresis
PBS	Phosphate buffered saline
Phyre <sup>2</sup>	Protein homology/analogy recognition engine V 2.0
PMSF	Phenylmethylsulfonyl fluoride
PK	Penetrating keratoplasty
PKC	Protein kinase C
PPCD	Posterior polymorphous corneal dystrophy
PRDX6	Peroxiredoxin 6
PSG	Penicillin-streptomycin-glutamine
PSM	Peptide spectrum matches
PVDF	Polyvinylidene difluoride
<b>R</b>	
RBCD	Reis-bucklers corneal dystrophy
RT	Reverse transcriptase
<b>S</b>	
SCN	Schnyder corneal dystrophy
SDS	Sodium dodecyl sulfate
SEM	Standard error of the mean
SFM	Serum free medium
SLC4A11	Solute carrier family 4 member 11
SMCD	Subepithelial mucinous corneal dystrophy
SNSB	Sulfo-NHS-SS-biotin
SOC	Super optimal catabolite
STIC	<u>SLC4A11-EL3</u> <u>Transmembrane-GPA</u> <u>Integrated</u> <u>Chimera</u>
<b>T</b>	

T	Total protein
TBCD	Thiel-behnke corneal dystrophy
TBST-M	Tris buffered saline tween20-milk
TCF4	Transcription factor 4
TCF8	Transcription factor 8
TCGA	The cancer genome atlas
THPA	The human protein atlas
TFIID	Transcription factor IID
TM	Transmembrane
<b>U</b>	
U	Unbound fraction
<b>V</b>	
v1	Variant 1
v2	Variant 2
v3	Variant 3
VAP-1	Vascular adhesion protein-1
<b>X</b>	
XECD	X-linked endothelial corneal dystrophy
XLD	eX-linked
<b>Z</b>	
ZEB1	Zinc-finger E-box binding homeobox 1
ZO-1	Zonula occludens-1

---

# **Chapter 1: General Introduction**

---

## 1.1 Thesis Overview

The objective of this thesis is to understand SLC4A11, a membrane protein, in the human cornea and its roles beyond membrane transport that underlie the pathophysiology of endothelial corneal dystrophies (ECD). Mutations of SLC4A11 cause these genetic blinding diseases which are genetically heterogeneous and have a diverse clinical presentation, including corneal edema, increase in corneal thickness and painful loss of corneal endothelial cells (CEnC). The defective transport role of SLC4A11 explains the manifestation of corneal edema in patients but it fails to explain the progressive decline in CEnC density. We considered that SLC4A11 has functions beyond membrane transport and tested its role as a cell adhesion molecule (CAM) in the corneal endothelium, which could explain loss of CEnC. We also characterized the human SLC4A11 variants expressed in the corneal endothelium using bioinformatic, RNA and protein-based approaches to identify the relevant variant that should be used for corneal studies.

SLC4A11 is expressed in various tissues of the body, but the focus of this thesis is to explore its role in the human cornea and its diseases. Chapter 1 provides a broad introduction to facilitate a better understanding of following chapters. This introductory chapter begins with a general structure of human eye and then focuses on its outermost layer; the cornea, its architecture and function. The introduction further discusses the physiological regulation of the cornea by the inner most layer, endothelium, which is crucial in understanding the mechanisms maintaining corneal transparency and how diseases affect visual acuity. The introductory chapter further discusses the ECD, their types, treatment options and genetic alterations in patients. This is followed by introducing SLC4A11 as the focus of the thesis, its expression, transcripts, structure, functions and mutations that cause these genetic blinding diseases. The introduction chapter briefly introduces cell adhesion, followed by our hypothesis and objectives to set the stage for the remainder of the thesis.

## 1.2 The Human Eye

The eye, one of the most complex organs in the human body, provides a colored, three-dimensional moving image in day light. The human eye is not a perfect sphere with an approximate volume of  $6.5 \text{ cm}^3$  and an anterior to posterior diameter of 24 mm in adults<sup>1</sup>.

There are three distinguishable layers in the eye: the external layer, the middle layer and the inner layer<sup>2</sup> (Fig. 1.1A). The external layer consists of the cornea and the sclera. The cornea is the protective layer of the eye that refracts and transmits the light to the lens and the retina. The sclera is the white part of the eye, formed of a connective tissue that maintains the shape of the eye and protects the inner layers. The visible part of the sclera is covered by a mucous membrane called the conjunctiva<sup>2</sup>. The middle layer consists of the iris, the ciliary body, the lens and the choroid. Iris, the pigmented muscle giving the eye its color, modulates the size of the central pupil to control the light entering the eye. The ciliary body controls the shape and the refractive power of the lens. The lens is a transparent body located behind the iris and connected to the ciliary body. It focuses the light on the retina by the contraction and relaxation of the ciliary body. The choroid is a vascular tissue which provides oxygen and nutrition to the outer retinal layers<sup>2,3</sup>. The inner layer is the sensory region of the eye called the retina, comprised of the light-sensing sensory neurons which receive the light, process and transmit the signal to the brain<sup>2</sup>.

There are three fluid filled cavities in the eye, the anterior chamber between cornea and iris, the posterior chamber between iris and lens and the vitreous chamber between lens and retina. The anterior and posterior chambers are filled with aqueous humor and the vitreous chamber is filled with vitreous humor which is more viscous than aqueous humor<sup>3</sup>.

## 1.3 The Cornea

Cornea is the anterior most part of the eye which is biconcave, transparent, avascular, and acts as a primary structural, protective barrier. It is the most densely innervated tissue of the body and most of its nerves are sensory. Human cornea has a prolate shape, with a steeper center and flattened periphery. The average horizontal diameter of the human cornea is about 11.5 mm, about 1 mm longer than its vertical diameter. The average central corneal thickness is 0.5 mm and the diameter of the optic zone, the central region which refracts most of the light<sup>2,4</sup>, is 4 mm.

Human cornea consists of five recognized layers: three cellular layers: epithelium, stroma and endothelium, and two acellular membranes: Bowman's layer and Descemet's membrane (DM) (Fig. 1.1B).

### 1.3.1 Epithelium

Epithelium, the anterior most layer of the cornea which has a thickness of 50  $\mu\text{m}$  and is made of 5-7 layers of non-keratinized stratified squamous epithelial cells. Epithelium secretes a tear film that separates the epithelial cells from the atmosphere and is symbiotic with the epithelium. The tear film prevents the cornea from chemicals, toxins and microbial invasion and provides the epithelium with immunological and growth factors that are critical for epithelial health and repair. Tear film also smooths the irregularities of the epithelial surface. Three types of epithelial cells in this layer are: superficial, wing and basal cells. Two to three superficial cell layers are followed by a single layer of wing cells and an innermost monolayer of basal cells. A basement membrane called the basal lamina, which consists of collagen IV and laminin, is secreted by the basal cells and prevents epithelial detachment from the cornea. Basal lamina can be regenerated by the basal cells, if damaged<sup>5</sup>. The posterior surface of basal lamina is in contact with the underlying Bowman's layer.

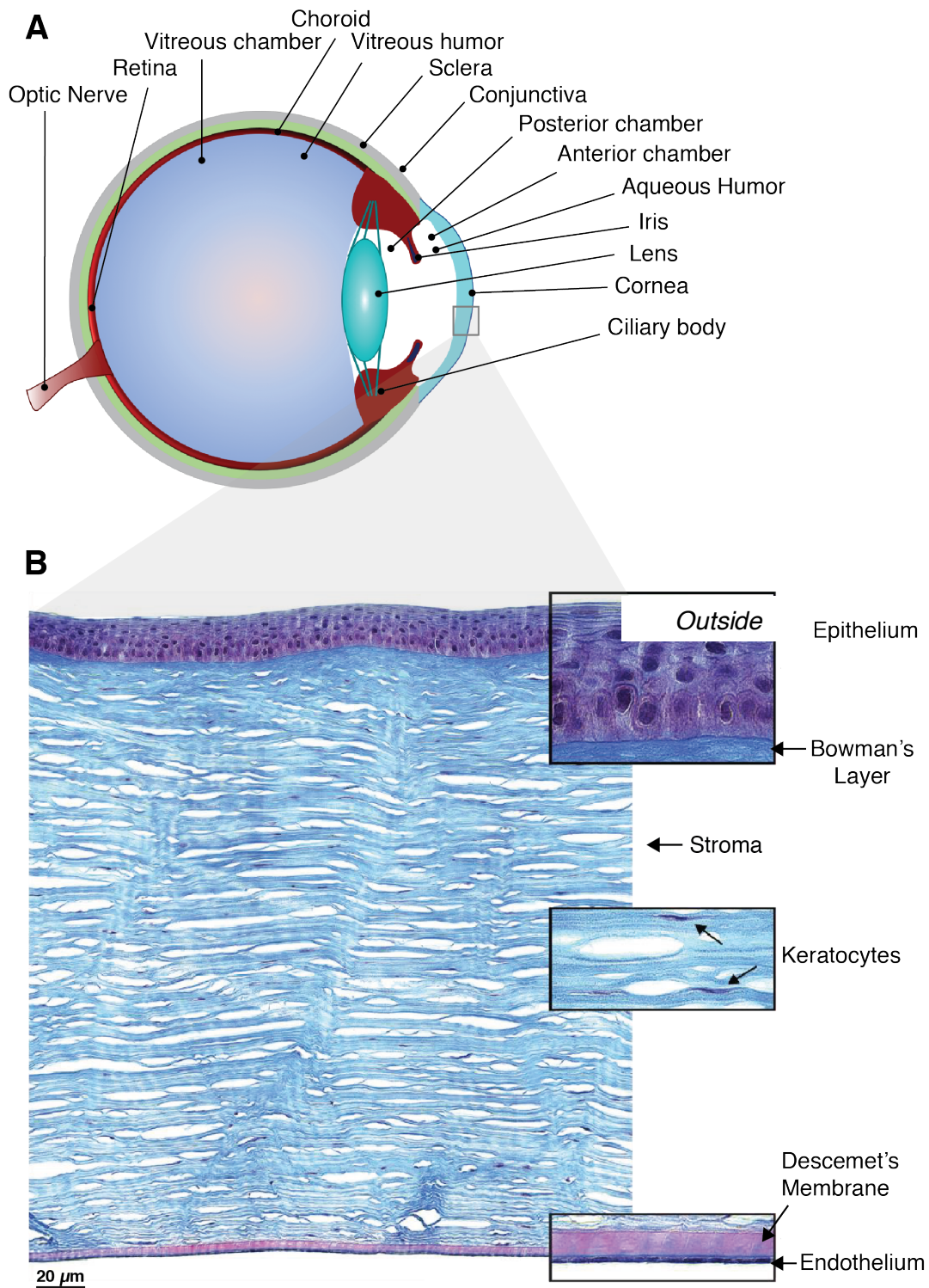


**Figure 1.1: Structure of the human eye and the cornea.**

**A.** Schematic representation of the human eye showing three layers. The outside of the eye is on the right. The outermost layer consists of cornea (where the light enters the eye) and the sclera

which is covered by a transparent mucous layer of conjunctiva. Middle layer consists of the lens (that receives the eye and focuses it to the retina in the inner layer), ciliary body, iris and the choroid. The inner layer consists of the retina, the sensory region that receives the light and transmits the signal to the brain through the optic nerve. **B.** Stained cross-section of the cornea showing five corneal layers, courtesy of Dr. Mathieu Thériault, University of Laval. Outside of the eye is on top and marked. The epithelium is the outermost layer of the cornea. Going towards the interior is the Bowman's layer, the stroma, DM and the endothelium. Aqueous humor is adjacent to the endothelium.

### **1.3.2 Bowman's Layer**

Bowman's layer, between the basal lamina of the epithelium and the stroma, is an acellular condensate of the most anterior region of the stroma that is absent in non-primate mammals. Composed of Collagens I, III, V and VII, Bowman's layer has a thickness of  $15\ \mu\text{m}^6$  and is believed to be secreted by the keratocytes in the anterior portion of the stroma. Some studies also suggest that epithelium contributes to the formation of Bowman's layer during development<sup>7</sup>. Bowman's layer helps to maintain the biconcave shape of the cornea. Once damaged, Bowman's layer does not regenerate and forms a scar.

### **1.3.3 Stroma**

Stroma is the central corneal layer with an average thickness of  $450\ \mu\text{m}$  in humans. Stroma comprises the bulk structural framework of the cornea and about 90% of the total corneal volume<sup>8</sup>. The major components of stroma are collagen fibrils, Collagen I and V, which are present as heterodimers with a unique narrow diameter. These stromal fibrils are surrounded by proteoglycans (chondroitin sulfate and keratan sulfate), which maintain corneal hydration. Collagen fibers in stroma have a very precise arrangement to sustain stromal transparency. The collagen fibrils are arranged in parallel bundles called fibrils which are further packed in parallel layers called lamellae. Stroma contains about 200-250 lamellae where each layer is arranged at right angle to the fibers in the adjacent lamellae, resulting in reduced forward light scattering and transparency of the cornea<sup>9,10</sup>. Keratocytes, the resident cells of the stroma, secrete the collagens and the glycosamines, and are located in the anterior stroma towards the Bowman's layer. These cells, like the lens, contain water soluble proteins, crystallins, that reduce light backscatter from keratocytes and maintain corneal transparency. Stromal avascularity critically contributes to corneal transparency. Corneal architecture and its hydration state are essential to maintain its refractive index and clarity. Epithelium and endothelium have critical roles as fluid barriers and to

remove excess fluid to maintain the desired stromal hydration state. Compromised epithelial and endothelial barrier functions cause fluid accumulation in the stroma that distorts the collagen lamellae arrangement to induce light scattering and edema, thereby compromising visual acuity<sup>9</sup>.

#### **1.3.4 Descemet's membrane**

DM is a basement membrane, composed of extracellular matrix (ECM) proteins secreted by the corneal endothelium, on which endothelial cells adhere. DM's collagenous and non-collagenous proteins have a more complex structure than other basement membranes in the body. DM was first described by Descemet in 1758 when it was considered to be structureless<sup>11</sup>. DM is secreted throughout life by endothelium, which leaves a record of aspect of endothelial cell function. With the advancement in technology, we know that DM has an anterior banded layer and a posterior non-banded layer. In the anterior banded layer, collagen fibrils show a lattice-like organization with continuous banding pattern at 110 nm intervals. Unlike other basement membranes in which collagen IV is common, collagen VIII is the specific major structural component of DM. Other DM proteins include collagen I, collagen IV, collagen XII, collagen XVIII, fibronectin (FNC), laminins, osteonectin and versican<sup>12</sup>. While FNC and vitronectin are concentrated on the stromal side of DM, remaining proteins are prominent on the endothelial side. Two different collagen VIII proteins are present in DM: collagen VIII alpha chain 1 (COL8A1) and collagen VIII alpha chain 2 (COL8A2). Two chains of COL8A1 and one chain of COL8A2 form trimers that further arrange into hexagonal lattices in the DM<sup>13</sup>. The functions of DM include providing a structural support for the endothelium and maintaining the corneal dehydration<sup>14</sup>.

#### **1.3.5 Endothelium**

Corneal endothelium is comprised of a single flat monolayer of highly specialized cells called CEnC that rest on their basement membrane, the DM. CEnC have a depth of 5  $\mu\text{m}$  and a diameter

of 20  $\mu\text{m}$  and are arranged in hexagonal lattices that appear as a honeycomb-like mosaic when viewed from the posterior side. Humans are born with a significant reserve of CEnC, about 5000-7000 cells/ $\text{mm}^2$ . The CEnC density and morphology change continuously throughout life; cell density declines rapidly by 45% in the first year and then it continues to decrease until the mid-twenties. CEnC density declines more gradually between 20-80 years of age at a constant rate of 0.52% per year<sup>15,16</sup>. The endothelium plays an important role in maintaining corneal hydration state, which is critical for clear vision. CEnC have ion-transport systems that form an “endothelial pump” which works continuously to produce a net fluid flux from stroma to aqueous humor to maintain a constant hydration state of the stroma at 78% (% water in stroma by weight). This process is called corneal deturgescence. It is critical in maintaining the precise organization of the collagen fibrils in stroma which is essential for clear vision<sup>2</sup>.

Unlike epithelial cells, CEnC do not proliferate in the cornea<sup>17</sup>. Cell damage caused by different pathologies or trauma lead to irreplaceable CEnC loss. CEnC do, however, enlarge (polymegathism), change shape (pleomorphism) and migrate to cover the space left by cell death in order to maintain an intact endothelial monolayer. With constant loss in number, increased polymegathism and pleomorphism arise in CEnC, reflecting a reduced ability of CEnC to deturgesce the cornea. Decline in CEnC count to an average of 500 cells/ $\text{mm}^2$  (symptomatic threshold) disturbs the organization of endothelial monolayer, the endothelial pump and gives rise to corneal edema<sup>4</sup>.

A sixth layer between the stroma and DM was recently discovered, called the Dua's layer<sup>18</sup>. It is a well-defined, acellular pre-DM layer, whose significance is unknown.

## **1.4 Physiological Regulation of Cornea by Endothelium**

Cornea is an exquisite example of natural engineering that solves the challenge of an optically clear protective layer by precise organization of collagen stromal fibrils. This ensures transmission

of light to the lens and further to the retina. While stroma is the unique structural component of the cornea, the endothelium plays a crucial role in maintaining healthy corneal physiology.

#### **1.4.1 Supplying nutrition to the cornea**

Corneal avascularity is another factor required for corneal transparency. Lack of blood supply, however, makes it difficult to provide nutrients and other molecules to stromal keratocytes and corneal epithelial cells. Endothelium, therefore, has a key role in providing nutrients and other molecules to these cells from the aqueous humor. Corneal epithelium receives oxygen, calcium, magnesium, potassium and sodium chloride through the tears<sup>19</sup>. In contrast, other nutrients, including glucose, are virtually absent in tear fluid. The adjacent limbal vasculature provides about 20% of the glucose demand to the cornea, yet ablation of this source does not disrupt the corneal physiology<sup>20</sup>. Aqueous humor is the main source of glucose and others essential nutrients. This supply is achieved by the “leaky” nature of the endothelium. The endothelium acts as a partially leaky barrier to allow for the diffusion of these solutes from the aqueous humor into the stroma, which in turn supplies them to the epithelium (Fig. 1.2). Blocking this natural supply route causes stromal and epithelial degeneration<sup>19</sup>. However, with the diffusion of solutes and due to the osmotic gradients across the endothelium, aqueous humor fluid also leaks into the stroma, which increases the corneal deturgescence. This is rectified by the endothelial pump function.

#### **1.4.2 Maintenance of corneal transparency by the endothelial pump**

Stromal hydration is maintained by several factors including endothelial tight junctions, endothelial pump function and the ability of CEnC to accommodate for the continuously lost cells by changing their shape and size. CEnC are polarized cells with the basolateral surface facing the DM and the apical surface at the aqueous humor. Cadherin along with alpha-catenin, beta-catenin and plakoglobin form a pericellular band at the apical cell junctions of CEnC<sup>21</sup>. Tight junctions

associated with Zonula occludens 1 (ZO-1) are also present near the apical surface of the cells<sup>22</sup>. These contribute to the structural integrity of the endothelial monolayer. Actins maintain the cell shape and migration and are located at the apical surface of the cells as dense bands<sup>23</sup>.

An active endothelial pump moves the excessive fluid back from stroma to aqueous humor against its osmotic gradient (Fig. 1.2). This process requires large amounts of energy provided by abundant mitochondria in the cytoplasm of metabolically active CEnC<sup>24</sup>. Fluid pumping is carried out by CEnC proteins including, SLC4A11, Na<sup>+</sup>/K<sup>+</sup>-ATPase, Na<sup>+</sup>/H<sup>+</sup> exchanger (NHE1), Cl<sup>-</sup>/HCO<sub>3</sub><sup>-</sup> Anion exchanger 2 (SLC4A2 or AE2), a 1Na<sup>+</sup>: 2HCO<sub>3</sub><sup>-</sup> cotransporter SLC4A4 (NBCe1), Na<sup>+</sup>:K<sup>+</sup>:2Cl<sup>-</sup> cotransporter (NKCC1), cystic fibrosis transmembrane conductance regulator (CFTR), Calcium activated chloride channels (CACCC1), Monocarboxylate transporters 1 and 4 (MCT1 and 4) and Aquaporins (AQPs). Several models have been proposed to explain the endothelial pump mechanism. Movement of ions across the basolateral and apical surface of CEnC is predicted to generate localized osmotic gradients, sometimes driven by negative membrane potential, which leads to the movement of fluid from the stroma to the aqueous humor<sup>24-27</sup>. Studies on a membrane transport protein, SLC4A11, which localizes at the basolateral surface of CEnC (facing stroma) show that it facilitates the direct movement of water into the cells, which could be further moved into the aqueous humor by AQP1 at the apical surface (facing aqueous humor) of CEnC<sup>28</sup>. The combined leaky barrier function and the fluid pump, referred to as the pump-leak mechanism, is essential in maintaining healthy corneal physiology and transparency.

## **1.5 Corneal Dystrophies**

Corneal dystrophies are heterogeneous, genetically-determined, bilateral, spontaneous, non-inflammatory disorders of the cornea. These diseases have no reported systemic manifestations

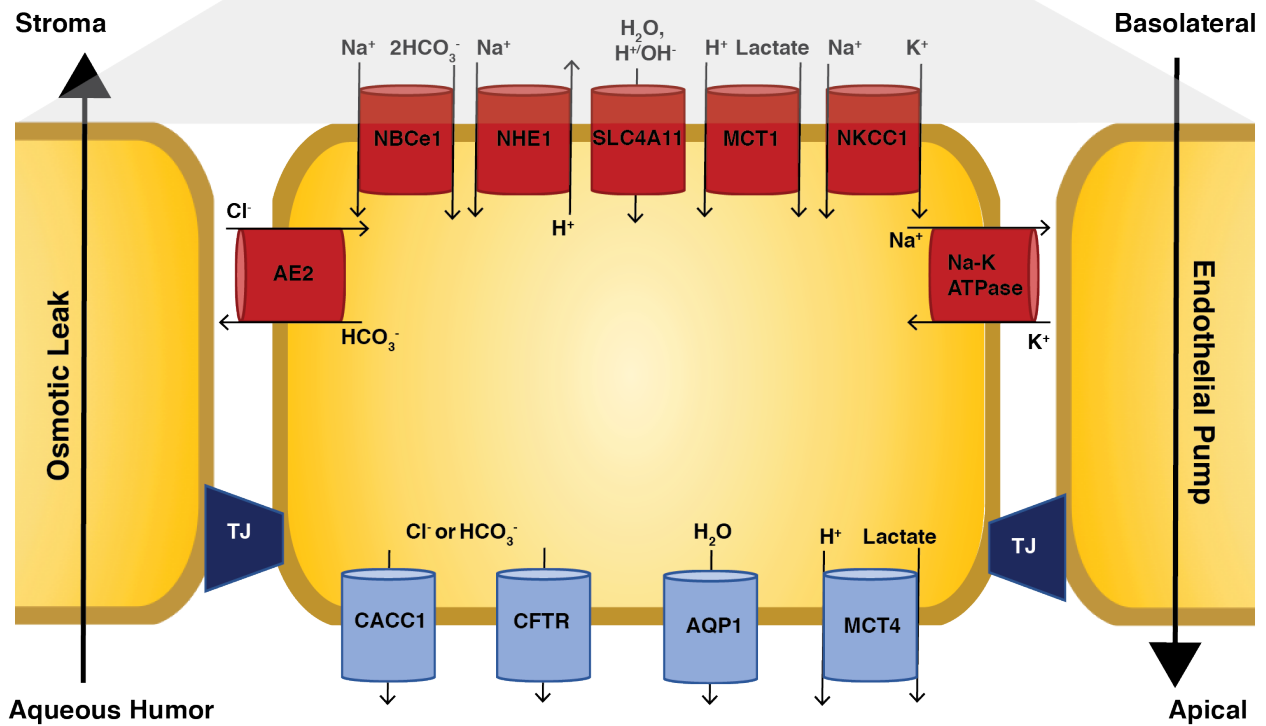
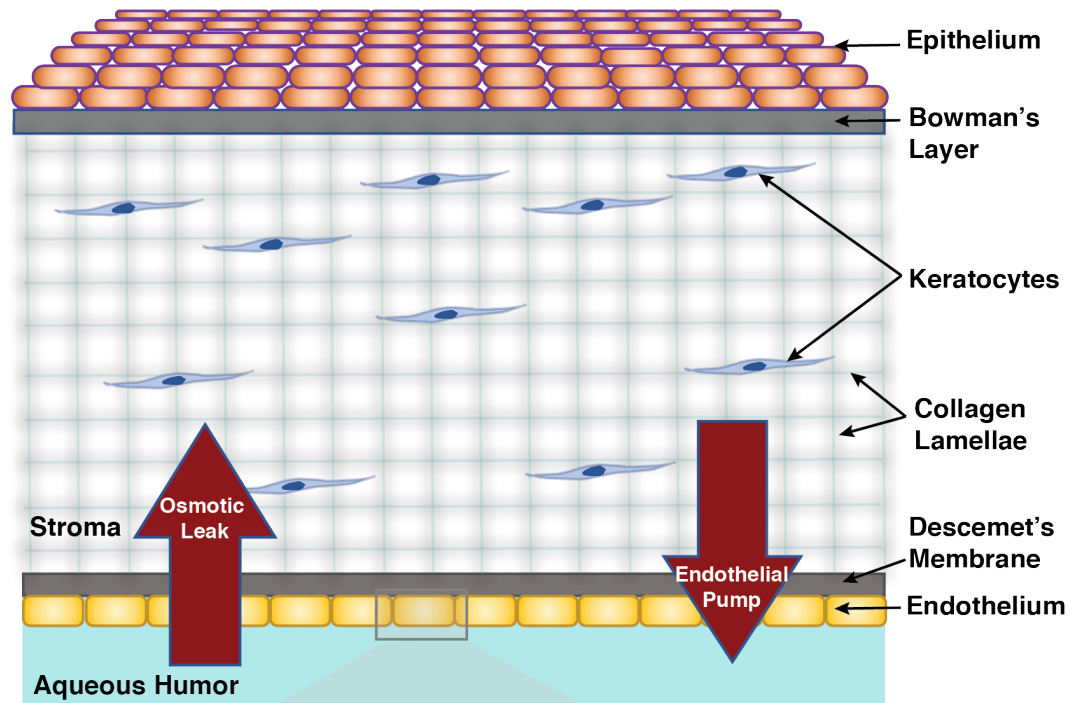


**Figure 1.2: The Corneal Endothelial Pump maintains fluid-balance in the cornea and corneal transparency.**

The upper panel represents the structure of the cornea showing the five distinct layers. Stroma features collagen lamellae organized in a distinct fashion to prevent light scattering, and keratocytes with vital roles in stromal biology. The osmotic leak represents the leaky barrier of the endothelium to allow the diffusion of nutrients to the stroma. Fluid osmotically leaks into the stroma and is pumped back to the aqueous humor by the endothelial pump as shown. The lower panel represents a zoomed view of the CEnC showing its basolateral side facing the stroma and the apical side facing the aqueous humor. It shows the proteins that contribute to the endothelial pump. The basolateral components are NBCe1, NHE1, SLC4A11, MCT1, NKCC1, AE2 and Na<sup>+</sup>-K<sup>+</sup> ATPase. Apical proteins that work in coordination with the basolateral transporters are CACC1, CFTR, AQP1 and MCT4. TJ represents Tight junctions. HCO<sub>3</sub><sup>-</sup> transport by basolateral NBCe1 and AE2 and lactate transport by MCT1 into the cell drives fluid secretion. Apical CACC1 and CFTR move HCO<sub>3</sub><sup>-</sup> and MCT4 moves lactate across the apical surface which drives fluid movement into the aqueous humor. Basolateral SLC4A11 and apical AQP1 form a water permeation pathway from stroma to aqueous humor (Adapted from <sup>24,28</sup>).

and present with variable corneal opacity resulting in corneal edema and compromised visual acuity<sup>29</sup>. Clinically, they are classified by their anatomical location in the layer where the defect lies. There are three classes of corneal dystrophies: 1. Superficial or anterior corneal dystrophies caused by defects in the epithelium, basal lamina or the Bowman's layer, 2. Stromal Corneal dystrophies caused by the defects in the corneal stroma and, 3. Posterior or Endothelial Corneal Dystrophies caused by defects in the DM or the endothelium. Most of these diseases follow a Mendelian pattern of inheritance ((autosomal dominant (AD), autosomal recessive (AR) or X-linked (XLD)) and have variable clinical presentation with different ages of onset<sup>30</sup>. Table 1.1 summarizes corneal dystrophies by their type, modes of inheritance and causative genes. This thesis focuses on the defects that arise due to defects in the DM or the endothelium and hence the ECD.

## **1.6 Endothelial Corneal Dystrophies and Pathophysiology**

ECD are a group of diverse diseases characterized by defects in the corneal endothelium or the DM secreted by the endothelium. These defects disrupt the endothelial monolayer and compromise the endothelial pump. This results in accumulation of excessive fluid from the aqueous humor in the stroma, causing corneal edema and a decline in visual acuity (Fig. 1.3). The three prominent diseases discussed in this thesis are Fuchs Endothelial Corneal Dystrophy (FECD), Congenital Hereditary Endothelial Dystrophy (CHED) and Harboyan Syndrome (HS).

### **1.6.1 Fuchs Endothelial Corneal Dystrophy (FECD)**

FECD, which arises due to defects in the corneal endothelium, has a regional prevalence from 4-12% in individuals over 40 years of age and is the primary reason for endothelial transplants in the United States<sup>31</sup>. The disease has an AD mode of inheritance and is characterized by a progressive decline in CEnC density, CEnC polymegathism and pleomorphism in patients<sup>31,32</sup>

(Fig. 1.4). In FECD patients, CEnC density declines until the endothelial pump fails (symptomatic threshold), which compromises corneal deturgescence. Fluid accumulation in stroma increases corneal thickness and cloudiness, causing corneal edema which compromises visual clarity (Fig. 1.3). Patients also show bead-like deposits of ECM on DM, called guttae. Non-confluent guttae on the peripheral DM are normal with progressing age (Hassall-Henle warts). FECD show guttae in the central cornea which enlarge and grow confluent as the disease progresses<sup>33</sup> (Fig. 1.5).

FECD symptoms arise in fourth to fifth decade of life and the disease usually progresses in four stages: Stage I is non-symptomatic, however, slit lamp and specular microscopy reveal non-confluent guttae in the central cornea. In stage II, guttae become confluent with loss of CEnC along with polymegathism and pleomorphism. In stage III, the endothelial pump is compromised, and corneal edema is observed. By stage IV, the corneal edema severity increases which causes corneal scarring, diminishing visual acuity<sup>31</sup>. With the compromised endothelial pump, stromal fluid accumulation in stroma produces a blue-gray haze anterior to the DM. Eventually this fluid accumulation increases corneal thickness and gives the cornea a round glass like appearance (Fig. 1.3D). The excessive fluid reaches and accumulates between epithelial cells and sub-epithelium. These bubbles burst through the epithelium and cause painful corneal erosions, called Bullous Keratopathy (BK). Symptoms of epithelial edema subsequently reduce but visual acuity continues to decline as the epithelium secretes connective tissue to repair itself<sup>29</sup>. FECD starts in the central cornea and radially progresses to peripheral cornea with extensive DM wrinkling. In advanced FECD, abnormalities are found in all corneal layers, but consistent changes are observed in DM and endothelium. Cornea continuously loses CEnC over the guttae and abnormal CEnC are significantly larger in size, have widened intercellular spaces, swollen mitochondria and dilated rough endoplasmic reticulum (ER). Some CEnC also show fibroblast-like morphology.

**Table 1.1: Corneal Dystrophies classified on the basis of anatomical location in the cornea.**

*AD: Autosomal Dominant, AR: Autosomal recessive, XLD: X-Linked, UK: Unknown, means the causative gene(s) have not been identified. MIM# can be used to find more information about the disease on the Online Mendelian Inheritance in Man (OMIM) database (<https://www.omim.org>)*

Disease	MIM#	Mode of Inheritance	Altered Gene
<b>Anterior or Superficial Corneal Dystrophies</b>			
Epithelial Basement Membrane Dystrophy (EBMD)	121820	AD	TGFβ1
Reis-Bucklers Corneal Dystrophy (RBCD)	608470	AD	TGFβ1
Gelatinous Drop-like Corneal Dystrophy (GDLD)	204870	AR	TACSTD2
Thiel-Behnke Corneal Dystrophy (TBCD)	602082	AD	TGFβ1
Lisch Epithelial Corneal Dystrophy (LECD)	300778	XLD	UK
Meesmann Corneal Dystrophy (MECD)	122100	AD	KRT3
Meesmann Corneal Dystrophy (MECD)	122100	AD	KRT12
Subepithelial Mucinous Corneal Dystrophy (SMCD)	612867	AD	UK
<b>Stromal Corneal Dystrophies</b>			
Congenital Stromal Corneal Dystrophy (CSCD)	610048	AD	DCN
Fleck Corneal Dystrophy	121850	AD	PIKFYVE
Macular Corneal Dystrophy (MCD)	217800	AR	CHST6
Avellino Corneal Dystrophy (ACD)	607541	AD	TGFβ1
Schnyder Corneal Dystrophy (SCN)	121800	AD	UBIAD1
Lattice Corneal Dystrophy 1 (LCD1)	122200	AD	TGFβ1

Lattice Corneal Dystrophy 2 (LCD2)	105120	AD	GSN
Lattice Corneal Dystrophy 3A (LCD3A)	608471	AD	TGFβ1
Granular Corneal Dystrophy I (GCD1)	121900	AD	TGFβ1
<b>Endothelial Corneal Dystrophies</b>			
Congenital Hereditary Endothelial Dystrophy (CHED)	217700	AR	SLC4A11
Corneal Dystrophy and Perceptive Deafness (CDPD) or Harboyan Syndrome	217400	AR	SLC4A11
Fuchs Endothelial Corneal Dystrophy 1 (FECD1)	136800	AD	COL8A2
Fuchs Endothelial Corneal Dystrophy 2 (FECD2)	610158	AD	UK
Fuchs Endothelial Corneal Dystrophy 3 (FECD3)	613267	AD	TCF4, LOXHD1
Fuchs Endothelial Corneal Dystrophy 4 (FECD4)	613268	AD	SLC4A11
Fuchs Endothelial Corneal Dystrophy 5 (FECD5)	613269	UK	UK
Fuchs Endothelial Corneal Dystrophy 6 (FECD6)	613270	AD	ZEB1
Fuchs Endothelial Corneal Dystrophy 7 (FECD7)	613271	UK	UK
Fuchs Endothelial Corneal Dystrophy 8 (FECD8)	615523	AD	AGBL1
Posterior Polymorphous Corneal Dystrophy 1 (PPCD1)	122000	AD	OVOL2
Posterior Polymorphous Corneal Dystrophy 2 (PPCD2)	609140	AD	COL8A2
Posterior Polymorphous Corneal Dystrophy 3 (PPCD3)	609141	AD	ZEB1
Posterior Polymorphous Corneal Dystrophy 4 (PPCD4)	609141	AD	GRHL2
Posterior Amorphous Corneal Dystrophy (PACD)	618031	AD	UK
EDICT Syndrome	614303	AD	MIR184
X-Linked Endothelial Corneal Dystrophy (XECD)	300779	XLD	UK

DM thickness increases to about four-times than a healthy DM due to excessive ECM deposition, especially in the regions of guttae. The size and confluence of guttae also increases in the central DM and they start to protrude in the anterior chamber<sup>34</sup>.

FECD arises due to a complex combination of genetic factors with two different ages of onsets in patients. Early-onset happens around the second to third decade of life and is well characterized, but very rare. The late-onset occurs around the fourth to fifth decade and accounts for the majority of patients, with heterogeneous genetics and physiological etiology<sup>35</sup>.

### **1.6.2 Congenital Hereditary Endothelial Dystrophy (CHED)**

CHED also arises due to defects in corneal endothelium but is a rare dystrophy in which symptoms present in infancy or arise within the first few years of life. CHED has an AR mode of inheritance and is thus prevalent in countries with high incidences of consanguineous marriages<sup>36</sup>. CHED is characterized by corneal opacification in infants with corneas about two-three times thicker than in healthy infants (Fig. 1.3C-D). Patient corneas have a ground glass-like appearance and are swollen due to extensive stromal edema. Patients are born with a significantly decreased CEnC density, and their CEnC have a fibrotic morphology. Patients also manifest varying degrees of amblyopia (lazy eye due to developmental defects) and nystagmus (rapid uncontrolled movement of the eye affecting vision, depth perception, balance and coordination)<sup>31</sup>. Patients also have thickened DM, however, guttae are not evident. DM has a normal anterior banded layer and a posterior non-banded layer, but with an additional 20-40 nm thick fibrous layer at the posterior surface consisting of a mixture of ECM-like fibrous material. CHED is not a progressive disease with symptoms that remain stable throughout the patient's life<sup>29</sup>.

### **1.6.3 Harboyan Syndrome (HS)**

HS or Corneal Dystrophy and Perceptive Deafness (CDPD) is sensorineural hearing disorder associated with some cases of CHED, although HS is also seen as a manifestation of CHED. Infants with HS are born with a compromised visual acuity, but they develop progressive hearing deficits usually around 10 to 15 years of age<sup>37</sup>.

One study looked at the genetic alterations in a single pedigree and showed that CHED patients eventually progress to develop HS, although their hearing is not routinely examined, which may be due to lack of information and infrastructure in developing countries. It also shows that both parents of CHED patients are affected by stage I FECD and are carriers of disease alleles. This places all three diseases in the same pedigree and suggests changes in clinical practices to monitor for HS in all CHED patients and for FECD in their parents<sup>38</sup>.

Lack of reports on non-corneal symptoms could be due to prevalence of CHED patients in developing countries. Parents of these patients may fail to report non-corneal symptoms due to lack of information/infrastructure. Symptoms in FECD patients arise around 40-50 years of age and other disorders may be confused with growing age. More thorough investigations in patients are needed to understand disease manifestation in non-corneal tissues.

## **1.7 Treatment options for Endothelial Corneal Dystrophies**

There are no treatment options for ECD that directly correct the underlying defects. Full thickness penetrating keratoplasty (PK) which replaces the complete cornea were the standard method for transplantation in the 1950s because PK provides visual correction and symptomatic relief. However, PK came with undesirable consequences, including high rates of graft rejection, prolonged visual rehabilitation, increased vulnerability to trauma and high postoperative astigmatism. Endothelial keratoplasty (EK) which replaces specific layers of cornea, is most

popularly used now for late-stage FECD patients. Descemet Stripping Automated Endothelial Keratoplasty (DSAEK) and Descemet's Membrane Endothelial Keratoplasty (DMEK) are two popular types of EK<sup>39</sup>. DSAEK replaces diseased DM, endothelium and stroma with lenticules containing healthy stroma, DM and endothelium. DMEK, which is more surgically challenging, replaces the diseased DM and endothelium with their healthy donor counterparts. Shortage of donor corneas pose a major concern in alleviating pain in these patients through transplants.

Patients in early stages of disease or with poor visual potential are usually prescribed alternative methods to alleviate pain and discomfort and also potentially improve visual acuity. Use of topical osmotic solutions like 5% hyperosmotic sodium chloride eye drops and glycerin eye drops can help dehydrate the stroma and improve visual clarity temporarily but must be used multiple times daily. Bandage contact lenses, which are silicon hydrogel or 85% Sauflon bandages containing hypertonic solutions, are also used to alleviate corneal pain. Anterior stromal punctures with a large bore needle (20G, 25G and 26G) are used to remove the excessive corneal fluid in patients showing BK and decrease ocular discomfort. Unfortunately, the depth of all the punctures cannot be reproduced and it changes expression of epithelial proteins. Other methods, including Gunderson conjunctival flaps, phototherapeutic keratectomy, amniotic membrane transplantation and collagen cross-linking also alleviate some ocular discomfort<sup>29,31,33,34</sup>. All these methods are, however, temporary, uncomfortable, and do not prevent disease progression. This underscores the need to improve the understanding of ECD, to design potential new strategies to correct the underlying defects and permanently increase visual acuity in patients.

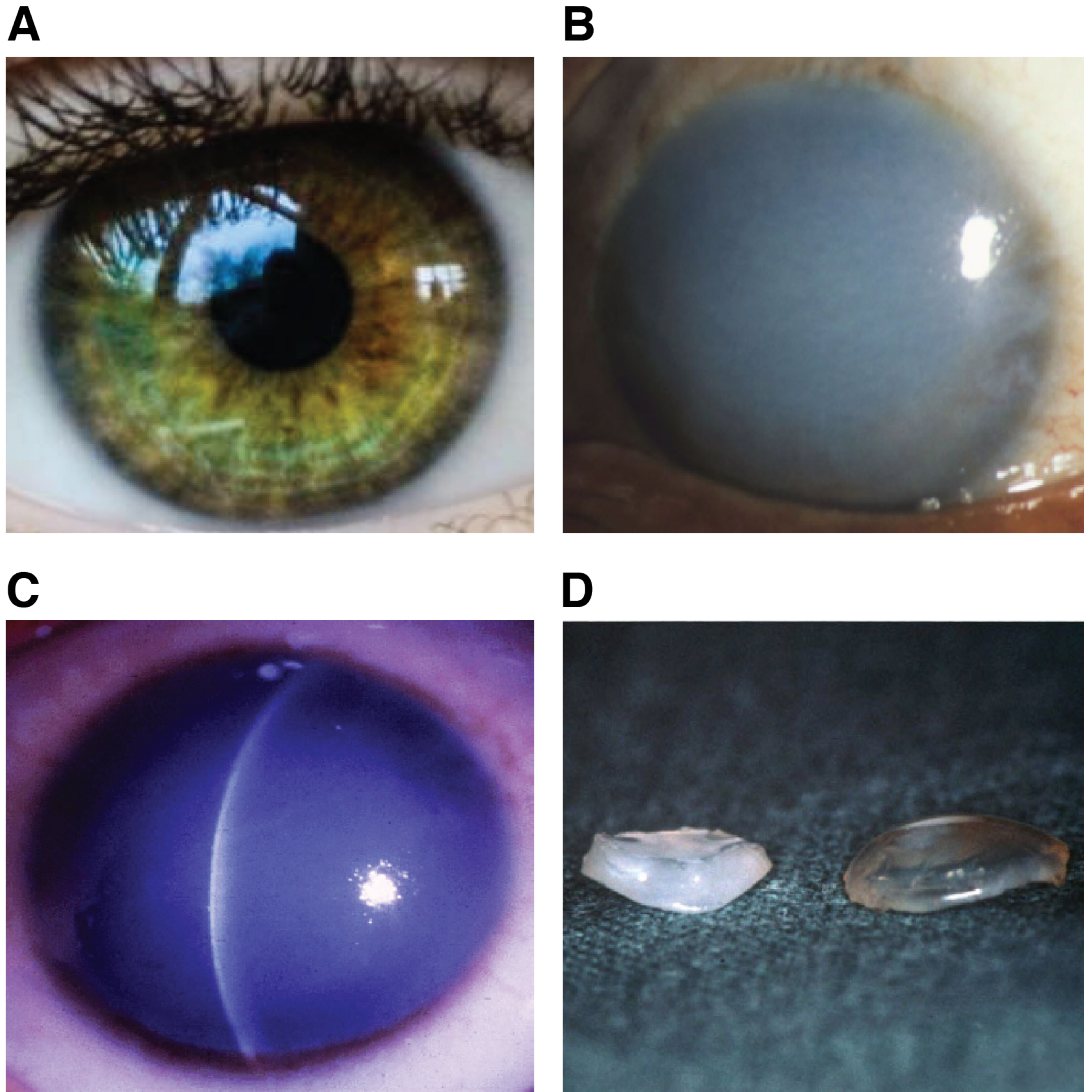


**Figure 1.3: Clinical presentation of corneal edema in FECD and CHED patients.**

**A.** Representative image of a healthy cornea. **B,C.** Slit lamp examination of FECD and CHED patient corneas, respectively, show corneal opacity and edema due to loss of CEnC that disrupt the endothelial pump and compromise stromal deturgescence state. The difference in corneal clarity can be compared between A, B and C which compromises visual acuity in patients. **D.** Macroscopic comparison of excised corneas from a CHED patient (left), which is thicker due to swelling and has a diffuse ground glass appearance, when compared to the control cornea (right). (Modified and reproduced from<sup>29</sup> under Creative Commons Attributions License).

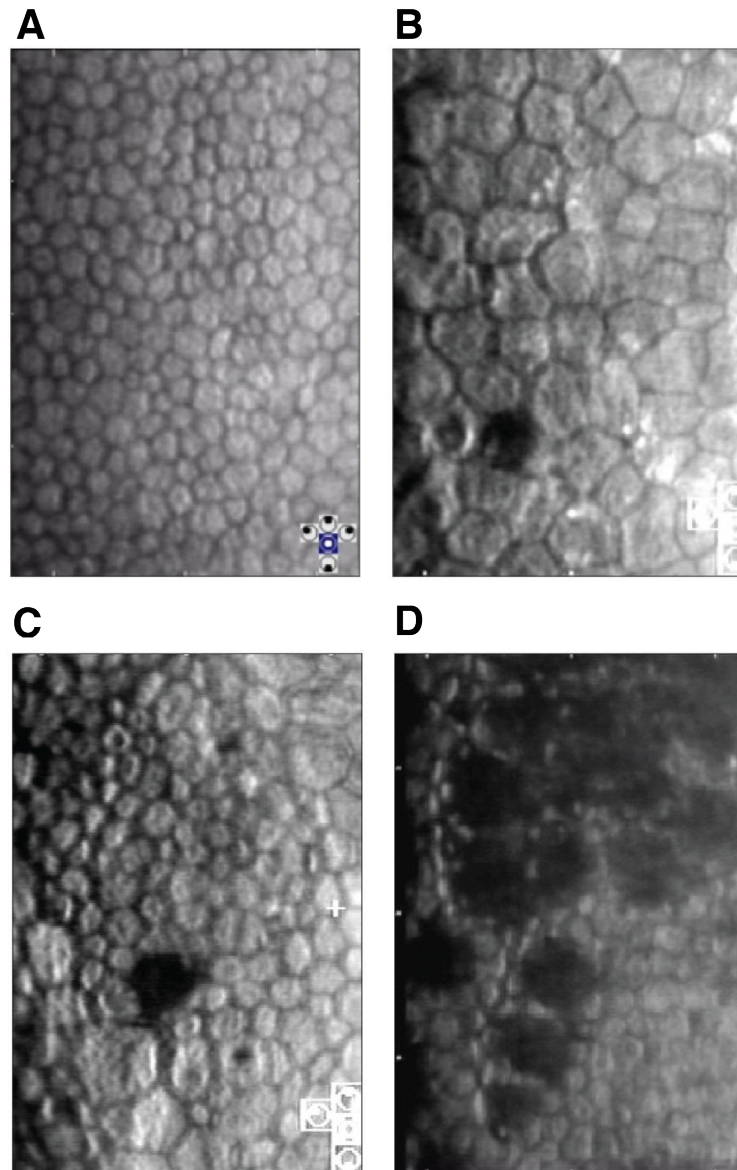


**Figure 1.4: Clinical presentation of CEnC loss in FECD and CHED patients.**

Representative images of specular microscopy examination of ECD patient eyes reveal the change in CEnC shape, density and appearance of DM. **A.** Healthy corneal endothelium with hexagonal shaped CEnC arranged tightly in monolayer. **B-C.** Loss of CEnC is visible along with polymegathism, pleomorphism and exposed underlying DM (black). **D.** Significant CEnC loss in advanced stages of FECD exposes the underlying DM (black), which disrupts corneal endothelium integrity and the endothelial pump. (Procured and modified with consent from Konan Medical, CA, USA).

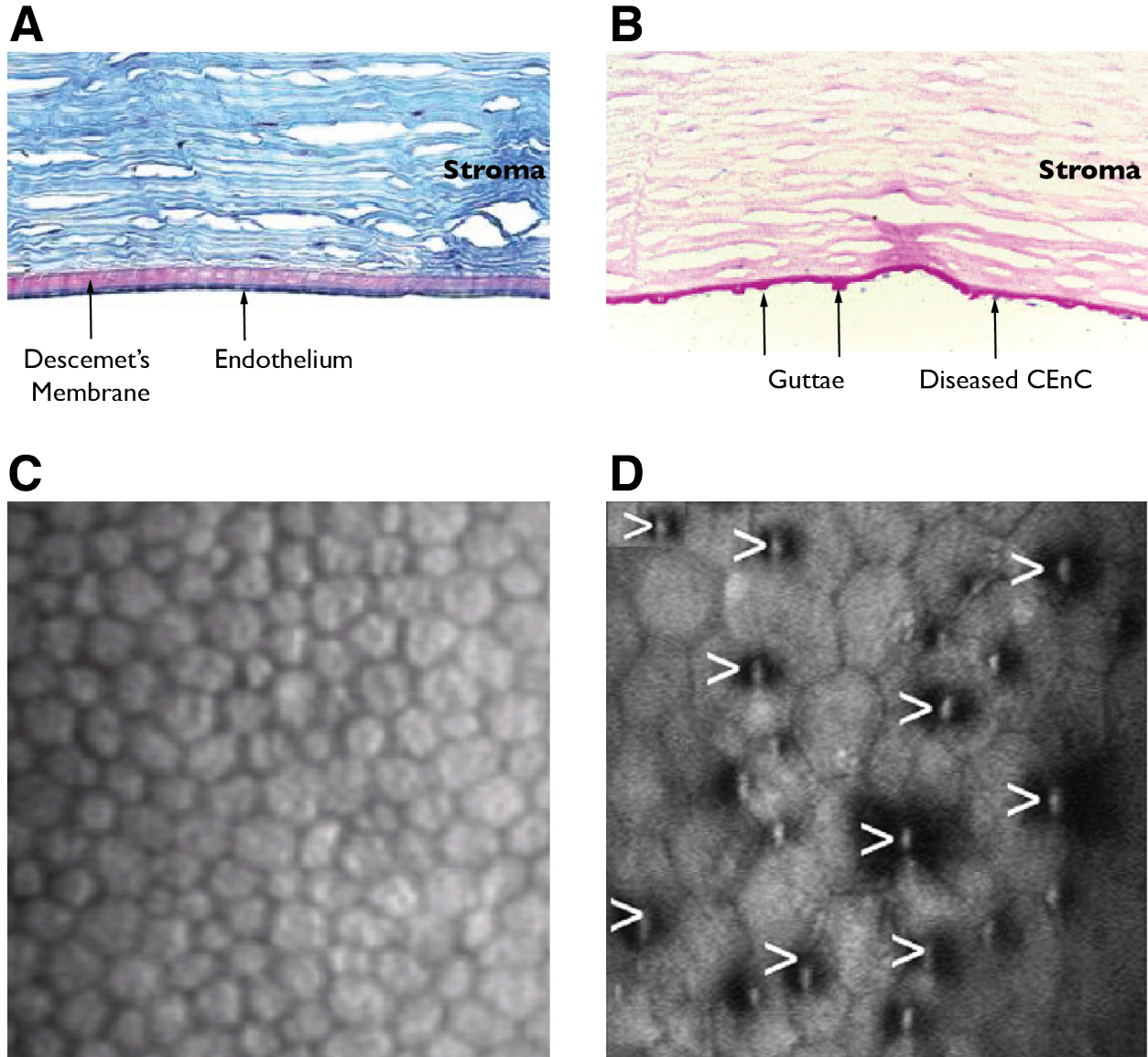


**Figure 1.5: Clinical presentation of guttae in FECD patients.**

**A.** Stained cross-section of a healthy cornea reveals DM stained (purple) and a healthy endothelial monolayer at the bottom (dark blue). **B.** Stained cross-section of a FECD cornea shows disorganized DM with button-like excrescences called guttae (purple) and scarce unhealthy CEnC (in blue). **C.** Specular microscopy image of a healthy endothelial monolayer. **D.** Specular microscopy of advanced stage FECD cornea showing button-like guttae (marked) disrupting CEnC organization. (A,B and D obtained and from<sup>29</sup> under Creative Commons Attributions License, and C from Konan Medical, CA, USA with consent).

## 1.8 Gene Alterations in Endothelial Corneal Dystrophies

Multiple genes cause corneal dystrophies with differing patterns of inheritance (Table 1.1). Amongst ECD, FECD has an AD mode of transmission, although sporadic cases are more prevalent. Multiple genetic and environmental factors underlie the FECD pathology. The genetic basis of FECD is heterogeneous with incomplete penetrance and variable expressivity. Alterations in multiple genes have been implicated in FECD<sup>40,41</sup>. Alterations in genes *COL8A2*<sup>35</sup>, *SLC4A11*<sup>42</sup>, *TCF4*<sup>43</sup>, *TCF8*<sup>44</sup>, *AGBL1*<sup>45</sup> and *LOXHD1*<sup>46</sup> have been mapped to specific chromosomal loci but new mutations and genes are still being identified. Genome-wide association studies (GWAS) have implicated *KANK4*<sup>47</sup>, *LAMC1*<sup>47</sup> and *ATPB1*<sup>47</sup> in the pathogenesis of FECD.

- ***COL8A2* gene:** *COL8A2* codes for COL8A2 protein which is the principal component of DM and secreted by CEnC. It associates with COL8A1 to form heterotrimers organized into highly ordered three-dimensional arrays in DM<sup>48</sup>. Two mutations, L450W<sup>49</sup> and Q455K<sup>35</sup>, cause abnormal intracellular accumulation and distort the trimeric protein arrangement. Knock-in mouse models of both mutations mimic the early onset FECD phenotype in mice<sup>50,51</sup>. *COL8A2* mutations also cause PPCD2<sup>35</sup>.
- ***SLC4A11* gene:** *SLC4A11* encodes a membrane transport protein, SLC4A11 that belongs to the SLC4 family of bicarbonate transporters. Several heterozygous point mutations have been identified in *SLC4A11* which are distributed throughout the protein with no clear pattern<sup>52</sup>. The effect of these mutations on the protein are still not completely understood.
- ***TCF4* gene:** *TCF4* or transcription factor 4 gene encodes the transcription factor 4 that belongs to the E-protein family of class I basic helix-loop-helix (bHLH) transcription factors<sup>43</sup>. A CTG (cytosine-thymine-guanine) trinucleotide repeat expansion in the third intron of *TCF4* has been associated with FECD. The CTG repeat expansion alters the TCF4 expression by affecting its

transcription and translation. The mRNA carrying the repeats undergo toxic accumulation leading to cell stress and is predicted to cause CEnC death<sup>53</sup>. CTG repeat length of >50 has been predicted to be pathogenic and a strong determinant of disease risk<sup>54</sup>. *TCF4* alterations represent about 70-80% genetic load in FECD<sup>40</sup>.

- ***TCF8* gene:** *TCF8* or transcription factor 8 gene encodes Zing-finger E-box binding Homeobox 1 protein (ZEB1) which is a transcription factor, also known as TCF8. Five late-onset FECD-causing mutations have been identified in *TCF8*, however, its role in FECD is unclear<sup>44</sup>. ZEB1 and TCF4 modulate each other's expression<sup>55</sup> and are hypothesized to be a part of the same pathway that causes FECD.
- ***AGBL1* gene:** *AGBL1* gene encodes the ATP/GTP binding-protein like 1 or AGBL1 which is a metallo-carboxypeptidase that mediates glutamylation of target proteins. One nonsense mutation, R1028\* and one mis-sense mutation C990S were identified in *AGBL1*, however their roles underlying the FECD pathology are unclear. AGBL1 interacts with TCF4 and both identified mutations affect AGBL1-TCF4 interaction which may contribute to the disease through the same pathway as TCF4<sup>56</sup>.
- ***LOXHD1* gene:** *LOXHD1* gene encodes Lipoxygenase Homology Domain-containing 1 protein or LOXHD1, a plasma membrane protein that has been implicated in progressive hearing loss. Fifteen mis-sense mutations have been identified in *LOXHD1* which localize on the surface of the protein and are predicted to affect its interaction with other proteins. Accumulation of the mutant proteins in the cytoplasm may also lead to cytotoxicity and cause CEnC death<sup>46</sup>.
- ***KANK4* gene:** *KANK4* gene encodes KN motif and ankyrin repeat domain containing protein 4 or KANK4 which is a cytoplasmic protein speculated to be involved in actin polymerization and control of cytoskeletal formation. GWAS identified *KANK4* as a locus in FECD, however, its correlation to the disease pathophysiology remains unclear<sup>47</sup>.

- **LAMC1 gene:** *LAMC1* gene encodes Laminin gamma-1 protein or LAMC1 which is an ECM protein present in DM. GWAS identified *LAMC1* as a locus in FECD, however, its correlation to the disease pathophysiology remains unclear<sup>47</sup>.
- **ATPB1 gene:** *ATPB1* gene encodes Na<sup>+</sup> K<sup>+</sup> transporting ATPase, beta-1 polypeptide or ATPB1. GWAS identified *ATPB1* as a locus in FECD, however, its correlation to the disease pathophysiology remains unclear<sup>47</sup>.

Amongst the other factors, smoking has been linked to increased guttae in patients. Smoking in female FECD patients increases the risk of progressing to advanced stages, perhaps due to increased oxidative stress. Diabetes in FECD patients also increases central corneal thickness which is independent of FECD. An association between myocardial infarction, angina pectoris, cardiac insufficiency and ECD has been explained, possibly due to a common endothelial factor that effects all these conditions<sup>40</sup>.

CHED pathophysiology, on the contrary, is only linked to mutations in the *SLC4A11* gene<sup>57</sup>, most of which have been characterized and discussed later in this chapter.

## 1.9 Solute Carrier 4 Family of Transporters

Human Genome Organization categorizes proteins that transport substances across the plasma membrane as Solute Carrier (SLC) proteins<sup>58</sup>. SLC is a group of more than 300 integral membrane proteins that transport a wide range of substrates across biological membranes and play essential roles in maintaining a healthy cellular physiology<sup>59</sup>.

The fourth SLC family (SLC4) are broadly known as bicarbonate transporters. Within the SLC4 family, there are three subfamilies of transporters: Electroneutral Na<sup>+</sup>-independent Cl<sup>-</sup>/HCO<sub>3</sub><sup>-</sup> exchangers (SLC4A1 or Anion Exchanger 1 or AE1, SLC4A2 or Anion Exchanger 2 or AE2, SLC4A3 or Anion Exchanger 3 or AE3), Electrogenic Na<sup>+</sup>-coupled HCO<sub>3</sub><sup>-</sup> co-transporters

(SLC4A4 or NBCe1, SLC4A5 or NBCe2) and Electroneutral Na<sup>+</sup>-coupled HCO<sub>3</sub><sup>-</sup> co-transporters (SLC4A7 or NBCn1, SLC4A8 or NBCBE, SLC4A9 or AE4, SLC4A10 or NBCn2)<sup>60</sup>.

SLC4A11 is the last member for this family, but it does not transport bicarbonate<sup>61</sup>. An early report suggested it to be a borate transporter<sup>62</sup> (the function of plant SLC4A11 orthologues), but human SLC4A11 does not transport borate<sup>63</sup>. Instead, it facilitates transmembrane H<sub>2</sub>O movement, and OH<sup>-</sup>/H<sup>+</sup><sup>63-66</sup> and NH<sub>3</sub>/H<sup>+</sup><sup>63,67</sup> transport. Phylogenetic analysis (Fig. 1.6) also reveals that SLC4A11 is the most distant member of the SLC4 family while other transporters cluster together in three defined categories. SLC4 family proteins are widely distributed in the body and have specific transport mechanisms as reported in Table 1.2.

Most SLC4 family members transport bicarbonate to maintain physiological pH, cell volume and acid-base secretion. CO<sub>2</sub>/HCO<sub>3</sub><sup>-</sup> is an important buffering system in the body, whose defects are implicated in several diseases, including cardiac hypertrophy<sup>68</sup>, proximal and distal renal tubular acidosis, autism, to mention a few<sup>60</sup>. AE1 or SLC4A1, which makes up 50% of erythrocyte membrane proteins, is one of the most studied members of this family<sup>69</sup>. SLC4A11 mutations cause ECD, as discussed previously. SLC4A11 has about 26% sequence identity to AE1. With increasing reports of SLC4A11 mutations in ECD, its structural and functional studies are becoming increasingly important.

## 1.10 SLC4A11

SLC4A11 is a large (891 amino acids, Accession no. NP\_114423.1) multi-domain integral membrane protein encoded by SLC4A11 gene (RefSeq ID: NG\_017072.1) located on chromosome 20 at locus 20p12. It was first discovered in 2001 as BTR1 or Borate Transporter 1, belonging to the bicarbonate transport superfamily<sup>70</sup>.

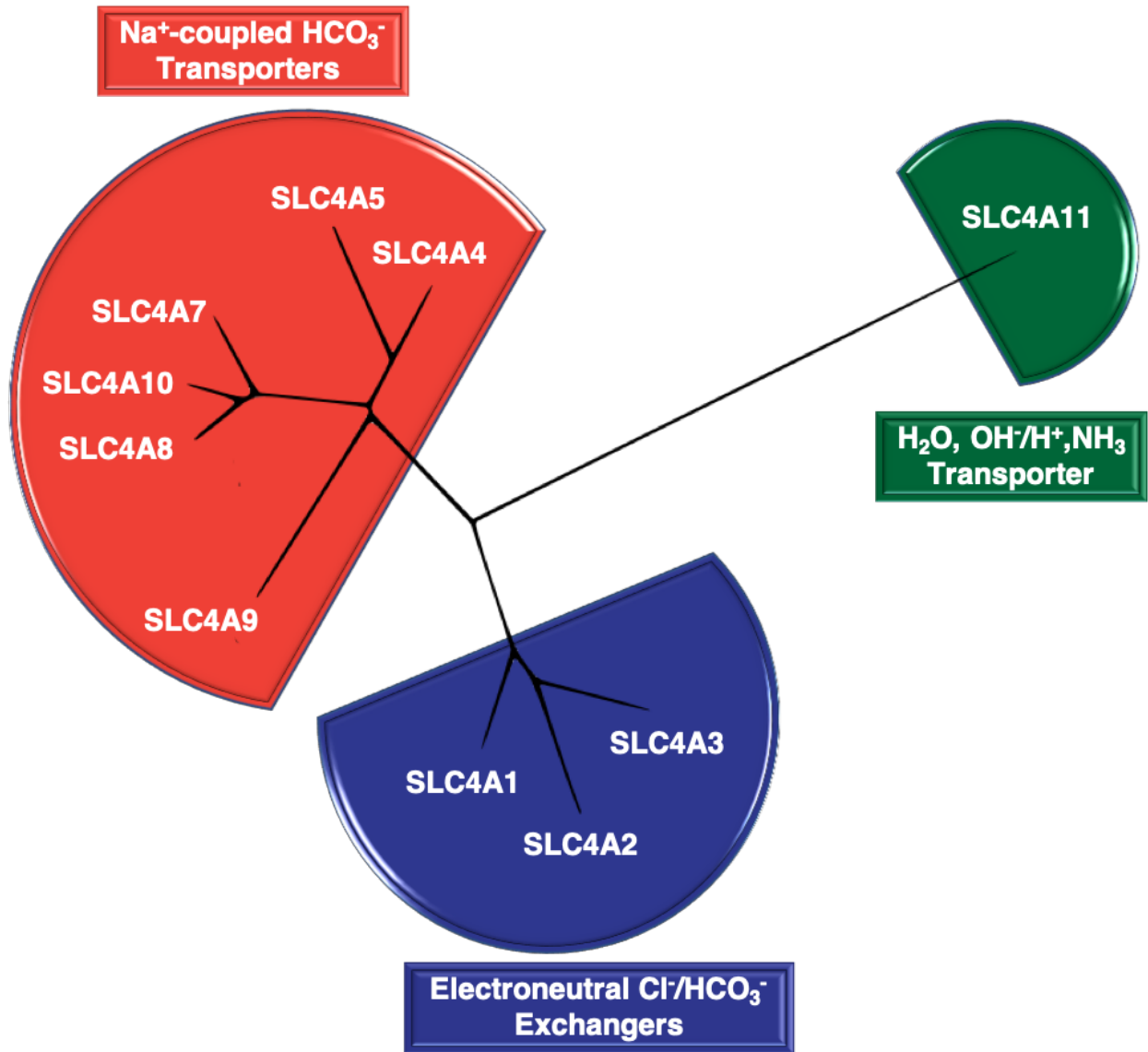


**Figure 1.6: Phylogenetic Dendrogram of SLC4 family of transporters.**

Amino acid sequences for each SLC4 member were obtained from the NCBI database and aligned using the Clustal Omega software to create a phylogenetic dendrogram. The length of each line represents the relative evolutionary distance between proteins. SLC4 members cluster in three categories, with SLC4A11 being the most distant member of the family.

**Table 1.2: Transport mechanism and tissue distribution of SLC4 family of transporters**

Adapted and modified from<sup>60,69</sup>

<b>Name</b>	<b>Other names</b>	<b>Transport mechanism</b>	<b>Tissue distribution</b>
SLC4A1	AE1, Band 3	Electroneutral Cl <sup>-</sup> /HCO <sub>3</sub> <sup>-</sup> exchanger	Erythrocytes, kidney, heart
SLC4A2	AE2	Electroneutral Cl <sup>-</sup> /HCO <sub>3</sub> <sup>-</sup> exchanger	Widespread (mostly basolateral)
SLC4A3	AE3	Electroneutral Cl <sup>-</sup> /HCO <sub>3</sub> <sup>-</sup> exchanger	Brain, retina, retina, kidney, smooth muscle, GI tract, adrenal and pituitary gland
SLC4A4	NBCe1, NBC1	Electrogenic Na <sup>+</sup> -coupled HCO <sub>3</sub> <sup>-</sup> cotransporter	Heart, kidney, prostate, pancreas, colon, brain, stomach, thyroid
SLC4A5	NBCe2, NBC4	Electrogenic Na <sup>+</sup> -coupled HCO <sub>3</sub> <sup>-</sup> cotransporter	Brain, liver, choroid plexus, epididymis, spleen, testis, cardiac and smooth muscles, kidney, spleen
SLC4A7	NBCn1, NBC2	Electroneutral Na <sup>+</sup> -coupled HCO <sub>3</sub> <sup>-</sup> cotransporter	Heart, liver, kidney, pancreas, lungs, spleen, stomach, skeletal muscle, smooth muscle, submandibular gland
SLC4A8	NDCBE, NBC3	Electroneutral Na <sup>+</sup> -coupled Cl <sup>-</sup> /HCO <sub>3</sub> <sup>-</sup> exchanger	Cardiomyocytes, testis, kidney, prefrontal cortex, oocytes
SLC4A9	AE4	Electroneutral Na <sup>+</sup> /HCO <sub>3</sub> <sup>-</sup> cotransporter	Kidney, pancreas, testis
SLC4A10	NBCn2, NCBE	Electroneutral Na <sup>+</sup> -dependent Cl <sup>-</sup> /HCO <sub>3</sub> <sup>-</sup> exchanger or HCO <sub>3</sub> <sup>-</sup> dependent Cl <sup>-</sup> /Cl <sup>-</sup> exchanger	Neurons, choroid plexus, kidney, adrenal cortex, uterus, cardiomyocytes
SLC4A11	BTR1, NaBC1	H <sub>2</sub> O, OH <sup>-</sup> /H <sup>+</sup> , NH <sub>3</sub> /H <sup>+</sup>	Cornea, kidney, cerebral cortex, gall bladder, testis, small intestine, epididymis, cerebellum, adrenal glands, breast, ovary, pancreas, lungs, urinary bladder, cardiac muscle

### **1.10.2 Expression Profile**

SLC4A11 is expressed in most body tissues with high expression in cornea, cerebral cortex, epididymis, gall bladder, small intestine, testis, kidney, breast, cerebellum, lungs, ovaries, pancreas and stomach<sup>71</sup>. In cornea, it is expressed in the epithelium and endothelium. SLC4A11 localizes at the basolateral surface of CEnC where its extracellular region faces the DM<sup>28,61</sup>. It is one of the most abundantly expressed proteins of the corneal endothelium<sup>72,73</sup>. In kidneys, it is expressed in the thin descending and thick ascending limb of the loop of Henle<sup>74</sup>, glomerular podocytes, basolateral membrane of proximal tubule epithelia, apical membrane of cortical collecting duct epithelia and in collecting duct<sup>75</sup>. SLC4A11 immunoreactivity is also seen in apical membrane of the choroid plexus epithelia<sup>75</sup>. In the inner ear, SLC4A11 is present in fibrocytes of spiral ligament under the stria vascularis in cochlea and the sensory epithelia of the vestibular system<sup>75</sup>.

Data from The Human Protein Atlas and The Cancer Genome Atlas show that SLC4A11 expression differences arise in tumors, including ovaries, thyroid, lung, pancreas, glioma and melanomas<sup>71,76</sup>.

### **1.10.3 Transcripts**

Three N-terminal variants of human SLC4A11 have been reported in the genome database which arise due to differential splicing of the mRNA: SLC4A11 Variant 1 (v1) which encodes for a 918 amino acid protein (NCBI Reference Sequence: NP\_001167561.1), SLC4A11 Variant 2 (v2) which encodes for an 891 amino acid splice form 2 (NP\_114423) and SLC4A11 Variant 3 (v3) which encodes for an 875 amino acid splice form 3 (NP\_001167560). These variants have also been respectively called SLC4A11-A, -B and -C<sup>66</sup>. These variants differ in their N-termini by 20-60 amino acids. SLC4A11 v2 was the first variant to be cloned in 2001 when the protein was discovered and is the most widely used variant in *in vitro* studies.

#### **1.10.4 Structure**

SLC4A11 is an integral membrane protein with the molecular weight of ~95 kDa. It has a 26% sequence identity with SLC4A1 or AE1. A topology model of SLC4A11-v2 has been created using hydropathy analysis and the topology model of AE1, that highlights the structural features of the protein<sup>77</sup>. The topology model (Fig. 1.7) predicts the protein to have a large N-terminal cytoplasmic domain spanning amino acid residues 1-374, a membrane domain spanning amino acid residue 375-873, and a short cytoplasmic tail from residues 874-891. The membrane domain is arranged in 14 transmembrane (TM) helices which have multiple extracellular and intracellular loops. The largest of these is extracellular loop 3 (EL3) which is 64 amino acids long (Fig. 1.7) from amino acids 514-577 between TM helices 5 and 6. The loop has is predicted to have two sites for N-linked glycosylation at N545 and N553. When expressed in HEK293 cells, SLC4A11 migrates as two bands on a denaturing sodium dodecyl sulfate-polyacrylamide gel electrophoresis (SDS-PAGE) gel. The lower band corresponds to non-glycosylated/core-glycosylated immature form of the protein running at ~95 kDa and the upper band corresponding to the complex glycosylated mature form running around 120 kDa<sup>78</sup>.

The homology model of SLC4A11-v2 cytoplasmic domain<sup>79</sup> and membrane domain<sup>80</sup> based on the crystal structures of AE1 cytoplasmic domains and membrane domain respectively, have been created. These validate the structural details highlighted in the SLC4A11 topology model. In addition, the membrane domain is predicted to have a core (TM1-4, 8-11) and gate domain (TM5-7,12-14), similar to AE1. A substrate translocation pathway is predicted in the middle of the membrane domain running through the open region at the interface of the core and the gate domain that is potentially used by the protein to move solutes across the plasma membrane. No structure could be predicted for SLC4A11-EL3 because of the low resolution of

the extracellular loops of AE1 and lack of sequence conservation in this region. With all these advances, we still wait to have crystallographic information of the structure of SLC4A11.

### **1.10.5 Oligomerization**

SLC4A11 is dimeric when expressed in HEK293 cells. Non-denaturing perfluoro-octanoic acid PAGE, extracellular cross-linking and co-immunoprecipitation (co-IP) show that SLC4A11 exists as a dimer in HEK293 cells<sup>78</sup>. Under denaturing conditions, the protein migrates as a monomer on an SDS-PAGE gels. SLC4A11 membrane domain when expressed without the cytoplasmic domain is unstable and does not accumulate in the cell. However, the cytoplasmic domains accumulate when expressed individually in HEK293 cells. The cytoplasmic domains of SLC4A11 associate to form dimers irrespective of the membrane domains. The homology models of SLC4A11 cytoplasmic domain predicts the amino acid residues Q301-P331 are involved in forming the dimeric interface, based on the crystal structure of AE1 cytoplasmic domain which is also dimeric<sup>79</sup>. The SLC4A11 membrane domain homology model also predicts that TM5 and 6 in each monomer are involved in the dimeric interface with contributions from TM7. EL3 lies at the dimeric interface of SLC4A11, however, we do not know if the two EL3s from the two monomers interact<sup>80</sup>.

### **1.10.6 Functions**

SLC4A11 transport function has been controversial in the past decade. SLC4A11 was identified as a sodium-coupled borate transporter because its plant orthologue, BOR1, transports borate<sup>62,70,81</sup>. Borate is critical to the structural integrity of cell walls of bacteria, plants and fungi because it cross-links vicinal diols<sup>82</sup>. Mammals do not have cell wall and insignificant to no borate in their system. Hence, the borate transport function of SLC4A11 does not hold physiological relevance. Studies later showed that indeed, SLC4A11 is not a borate transporter. SLC4A11 is

member of the SLC4 family, whose other members are all bicarbonate transporters, yet SLC4A11 does not transport bicarbonate<sup>61,63</sup>. Human SLC4A11-v2 was reported to function as an EIPA-sensitive  $\text{Na}^+$ -OH<sup>-</sup> ( $\text{H}^+$ ) transporter<sup>83</sup>, however, recent reports show that it functions in a  $\text{Na}^+$ -independent electrogenic  $\text{H}^+$  ( $\text{OH}^-$ ) permeation pathway<sup>66</sup>.

SLC4A11, localized at the basolateral surface of CEnC, promotes a water flux from stroma to aqueous humor in collaboration with the apical AQP1<sup>28</sup>. *Xenopus* oocytes and HEK293 cells displayed increased rates of hypo-osmotic medium-induced cell swelling when they transiently express SLC4A11<sup>28</sup>. This suggests that SLC4A11 increases water movement either directly by moving solutes like  $\text{Na}^+$  to drive osmotic flow, or indirectly by functioning as a pore for direct movement of water, like AQP1. Further studies showed no  $\text{Na}^+$ -dependency on water movement, suggesting that SLC4A11 moves the water directly, potentially through its translocation pore<sup>28</sup>. The water flux function of SLC4A11 contributes to the endothelial pump to maintain a healthy corneal physiology, transparency and clear vision.

Recent reports have shown that SLC4A11 functions as a  $\text{NH}_3/\text{H}^+$  co-transporter in corneal endothelium<sup>67</sup>. CEnC are metabolically active cells which use glutamate catabolism (glutaminolysis) as a source of ATP through TCA cycle. Glutaminolysis generates  $\text{NH}_3$  as a by-product which can be toxic to the cells in high concentrations. SLC4A11 helps efflux  $\text{NH}_3$  with  $\text{H}^+$  to avoid CEnC ammonia toxicity<sup>84</sup>. A recent report, however, argues that SLC4A11 promotes an electroneutral transport of  $\text{NH}_3$ <sup>63</sup>. Another report suggests that mouse SLC4A11 does not move  $\text{NH}_3$ , but only  $\text{H}^+/\text{OH}^-$  ions<sup>65</sup>.

### **1.10.7 Mutations**

The Human Gene Mutation database (HGMD) shows 57 mis-sense mutations, 12 pre-mature termination mutations, 4 splicing mutations, 13 small deletions, 1 small insertion, 7 small insertion-

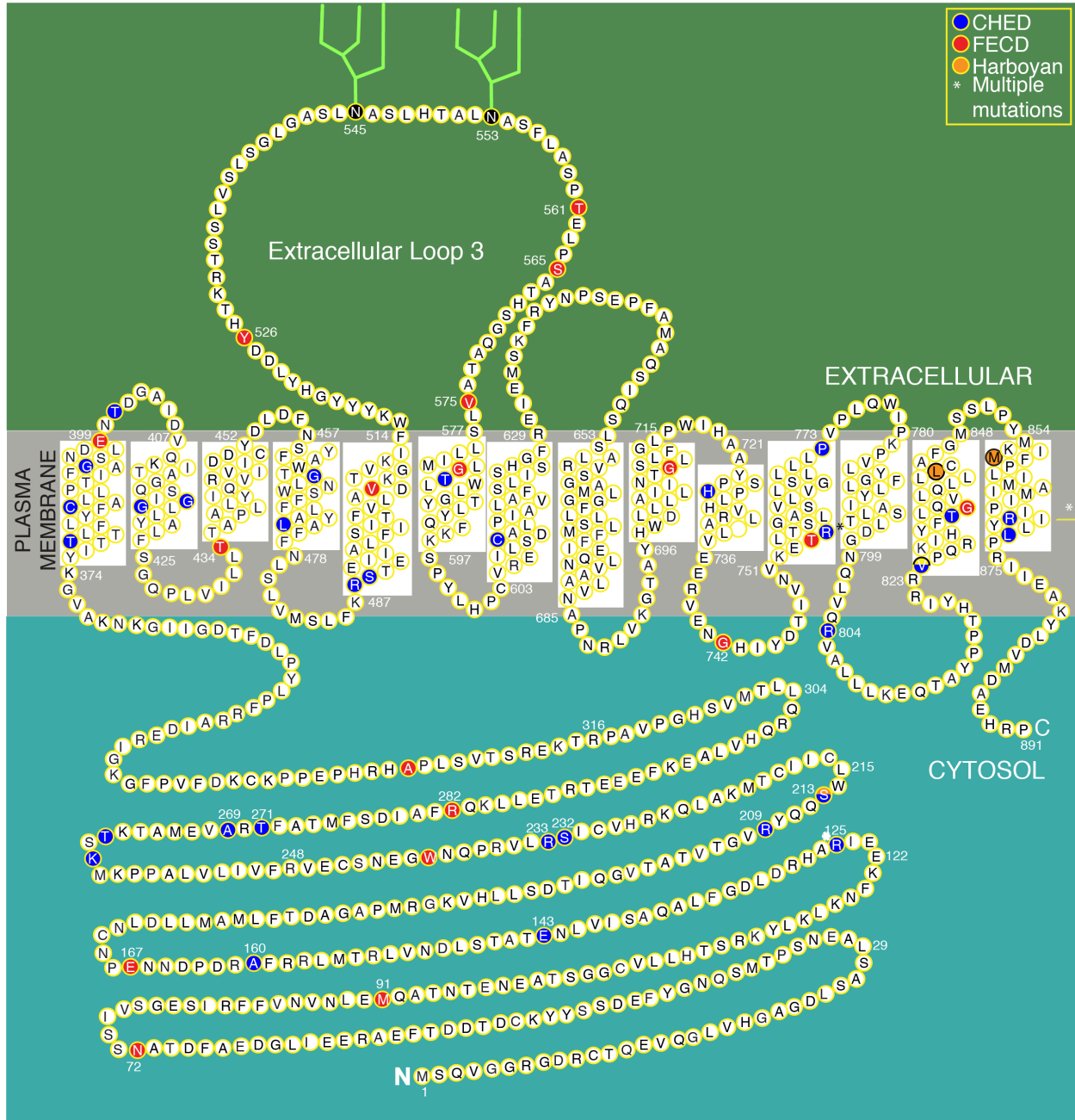


**Figure 1.7: SLC4A11 topology model highlighting structural aspects of the protein and ECD-causing mutations.**

SLC4A11 topology model is based on hydropathy analysis and the topology model and crystal structure of SLC4A1 (AE1), which has the lowest evolutionary sequence divergence from SLC4A11. SLC4A11 protein showing its membrane domain inserted in the plasma membrane

(grey), a large N-terminal domain and the short C-terminal tail in the cytosol (blue) and the loops in the extracellular region (green). EL3 has 64 amino acids with two predicted sites for N-linked glycosylation at N545 and N553. Fifty-seven ECD causing point mutations are shown throughout the protein. Highlighted residues for CHED (blue), FECD (red) and HS (orange) represent the sites for mis-sense mutations. \* represents the residues that are mutated in two or more diseases.

-deletions and 4 gross deletions. These genetic alterations all cause ECD, Peters anomaly (eye disease) and Keratoconus (eye disease)<sup>85</sup>. The COSMIC (Catalogue of Somatic Mutations in Cancer) database reports 318 mutations (mis-sense, non-sense, frameshift, insertion, substitution and deletion) in patients with different cancers. The majority of mutations were found in patients affected by cancers of breast, central nervous system, kidneys, large intestine, liver, lungs and haemopoietic and lymphoid cancers<sup>86</sup>. Similarly, The Cancer Genome Atlas (TCGA) shows 151 mutations (133 mis-sense, 10 frameshift and 8 termination) identified in patients with different cancers<sup>76</sup>. Mutations in SLC4A11 have known implications in ECD (Table 1.3) and some new studies have shown its relation to poor survival rates in cancer<sup>87</sup>. However, the effect of all these mutations are still not clearly understood and need further investigation.

## **1.11 SLC4A11 Mutations cause Endothelial Corneal Dystrophies**

About 57 ECD-causing mis-sense mutations have been reported in SLC4A11 which are distributed throughout the sequence of the protein (Fig. 1.7), with no obvious pattern (Table 1.3). Out of the 55 mutations, 18 mutations cause FECD, 35 mutations cause CHED and five mutations cause HS. Two out of these five HS causing mutations also cause CHED. There are geographical variations in the occurrence of these mutations, where some are more prominent in one ethnic group over the other. There are two known mechanism by which SLC4A11 mutations cause disease: 1. Trafficking defects 2. Functional defect.

### **1.11.1 Trafficking defect**

Some mutations cause the SLC4A11 protein to mis-fold which causes the protein to be retained in the ER and targeted for degradation by the ER-Associated degradation (ERAD) pathway<sup>88</sup>. This results in little or no protein at the cell surface, thereby causing disease due to a lack of

protein at the cell surface. Out of 55 mutation, 31 cause partial or complete ER-retention of the protein. 65% of CHED -causing mutations cause ER-retention of the protein<sup>52,89</sup>.

### **1.11.2 Functional defect**

Some SLC4A11 mutations do not affect protein folding. The mutated protein traffics to the cell surface but still causes disease by potentially compromising one or more of its known functions. 24 out of 55 known mutations cause disease by potentially affecting SLC4A11 function. 67% of the FECD causing mutants are not ER-retained and thus may cause disease by defective function at the cell surface. Out of these 24 mutations, only four mutations affect SLC4A11 function: R125H affects the SLC4A11 water flux function<sup>28</sup> and R125H, W240S, C386R, V507I affect the ammonia transport function<sup>90</sup>. Two mutations, V507I and V575M are present at the dimeric interface of SLC4A11 as predicted by the homology model and are predicted to distort the SLC4A11 dimerization which might affect the protein's function<sup>80</sup>.

## **1.12 SLC4A11 translational product in human cornea**

As discussed earlier, three different N-terminal variants of human SLC4A11, v1 v2 and v3, are reported. SLC4A11-v2 was the first variant to be discovered in 2001. Since then, all *in vitro* experiments aimed at understanding the role of SLC4A11 in cornea and its diseases have used v2 (Table 3.1). However, a recent study shows v3 as the SLC4A11 isoform expressed in the human cornea with no v2 expression<sup>91</sup>. This study had a few drawbacks because it only examined the SLC4A11 variant expression at the mRNA level and the source of the mRNA was unclear. Although the two variants differ by 19 amino acids at their N-terminus, it still raises two questions:

1. What is the relevant SLC4A11 variant that should be used for studies on human cornea and its diseases?
2. If v3 is the relevant corneal isoform, are the studies from the past decades on v2 still valid?

**Table 1.3: List of SLC4A11 mutations causing different Endothelial Corneal Dystrophies.**

The position of mutations is based on SLC4A11 v2 amino acid sequence. The references indicate the original studies which identified these mutations. \*The processing and function defects caused by the mutations were identified in<sup>28,52,89,90,92</sup>.

Sl. No.	Mis-sense mutation	Type of ECD	Reference	Defect*
1	p.Asn72Thr	FECD	Vithana <i>et al</i> (2008) <sup>42</sup>	Functional
2	p.Met91Val	FECD	Vithana <i>et al</i> (2008) <sup>42</sup>	Functional
3	p.Arg125His	CHED	Hemadevi <i>et al</i> (2008) <sup>93</sup>	Functional
4	p.Arg125Cys	CHED	Hemadevi <i>et al</i> (2010) <sup>94</sup>	Functional
5	p.Phe133Leu	CHED	Siddiqui <i>et al</i> (2014) <sup>38</sup>	Unknown
6	p.Glu143Lys	CHED	Ramprasad <i>et al</i> (2007) <sup>95</sup>	Trafficking
7	p.Ala160Thr	CHED	Hemadevi <i>et al</i> (2008) <sup>93</sup>	Functional
8	p.Glu167Asp	FECD	Riazuddin <i>et al</i> (2010) <sup>96</sup>	Functional
9	p.Arg209Trp	CHED	Sultana <i>et al</i> (2007) <sup>57</sup>	Trafficking
10	p.Ser213Pro	CHED/HS	Desir <i>et al</i> (2007) <sup>97</sup>	Trafficking
11	p.Ser213Leu	CHED	Sultana <i>et al</i> (2007) <sup>57</sup>	Trafficking
12	p.Ser232Asn	CHED	Aldave <i>et al</i> (2007) <sup>98</sup>	Trafficking
13	p.Arg233Cys	CHED	Sultana <i>et al</i> (2007) <sup>57</sup>	Trafficking
14	p.Trp240Ser	FECD	Soumitra <i>et al</i> (2014) <sup>99</sup>	Trafficking
15	p.Lys260Glu	CHED	Puangrucharern <i>et al</i> (2014) <sup>100</sup>	Functional
16	p.Thr262Ile	CHED	Kodaganur <i>et al</i> (2013) <sup>101</sup>	Functional
17	p.Ala269Val	CHED	Hemadevi <i>et al</i> (2008) <sup>93</sup>	Functional

18	p.Thr271Met	CHED	Shah <i>et al</i> (2008) <sup>102</sup>	Functional
19	p.Arg282Pro	FECD	Riazuddin <i>et al</i> (2010) <sup>96</sup>	Trafficking
20	p.Ala327Val	FECD	Vithana <i>et al</i> (2008) <sup>42</sup>	Functional
21	p.Cys386Arg	CHED	Ramprasad <i>et al</i> (2007) <sup>95</sup>	Functional
22	p.Gly394Arg	CHED	Aldahmesh <i>et al</i> (2009) <sup>103</sup>	Trafficking
23	p.Glu399Lys	FECD	Vithana <i>et al</i> (2008) <sup>42</sup>	Trafficking
24	p.Thr401Lys	CHED	Sultana <i>et al</i> (2007) <sup>57</sup>	Trafficking
25	p.Ser415Asn	CHED	Kumawat <i>et al</i> (2016) <sup>104</sup>	Unknown
26	p.Gly417Arg	CHED	Kodaganur <i>et al</i> (2013) <sup>101</sup>	Trafficking
27	p.Gly418Asp	CHED	Sultana <i>et al</i> (2007) <sup>57</sup>	Trafficking
28	p.Thr434Ile	FECD	Soumitra <i>et al</i> (2014) <sup>99</sup>	Trafficking
29	p.Gly464Asp	CHED	Vithana <i>et al</i> (2006) <sup>36</sup>	Trafficking
30	p.Leu473Arg	CHED	Sultana <i>et al</i> (2007) <sup>57</sup>	Trafficking
31	p.Arg488Lys	HS	Desir <i>et al</i> (2007) <sup>97</sup>	Trafficking
32	p.Ser489Leu	CHED	Vithana <i>et al</i> (2006) <sup>36</sup>	Trafficking
33	p.Val507Ile	FECD	Soumitra <i>et al</i> (2014) <sup>99</sup>	Functional
34	p.Tyr526Cys	FECD	Riazuddin <i>et al</i> (2010) <sup>96</sup>	Functional
35	p.Thr561Met	FECD	Vithana <i>et al</i> (2008) <sup>42</sup>	Functional
36	p.Ser565Leu	FECD	Riazuddin <i>et al</i> (2010) <sup>96</sup>	Functional
37	p.Val575Met	FECD	Riazuddin <i>et al</i> (2010) <sup>96</sup>	Functional
38	p.Gly583Asp	FECD	Riazuddin <i>et al</i> (2010) <sup>96</sup>	Trafficking
39	p.Thr584Lys	CHED	Sultana <i>et al</i> (2007) <sup>57</sup>	Trafficking

40	p.Cys611Arg	CHED	Kodaganur <i>et al</i> (2013) <sup>101</sup>	Trafficking
41	p.Glu657Ala	CHED	Kaul <i>et al</i> (2016) <sup>105</sup>	Unknown
42	p.Gly709Glu	FECD	Vithana <i>et al</i> (2008) <sup>42</sup>	Trafficking
43	p.His724Asp	CHED	Kodaganur <i>et al</i> (2013) <sup>101</sup>	Trafficking
44	p.Gly742Arg	FECD	Riazuddin <i>et al</i> (2010) <sup>96</sup>	Functional
45	p.Thr754Met	FECD	Vithana <i>et al</i> (2008) <sup>42</sup>	Functional
46	p.Arg755Gln	CHED	Vithana <i>et al</i> (2006) <sup>36</sup>	Trafficking
47	p.Arg755Trp	CHED	Ramprasad <i>et al</i> (2007) <sup>95</sup>	Trafficking
48	p.Pro773Leu	CHED	Sultana <i>et al</i> (2007) <sup>57</sup>	Trafficking
49	p.Arg804His	CHED	Jiao <i>et al</i> (2007) <sup>106</sup>	Functional
50	p.Val824Met	CHED/HS	Desir <i>et al</i> (2007) <sup>97</sup>	Functional
51	p.Thr833Met	CHED	Jiao <i>et al</i> (2007) <sup>106</sup>	Trafficking
52	p.Gly834Ser	FECD	Riazuddin <i>et al</i> (2010) <sup>96</sup>	Functional
53	p.Leu843Pro	HS	Desir <i>et al</i> (2007) <sup>97</sup>	Trafficking
54	p.Met856Val	HS	Desir <i>et al</i> (2007) <sup>97</sup>	Functional
55	p.Arg869His	CHED	Hemadevi <i>et al</i> (2008) <sup>93</sup>	Trafficking
56	p.Arg869Cys	CHED	Vithana <i>et al</i> (2006) <sup>36</sup>	Functional
57	p.Leu873Pro	CHED	Hemadevi <i>et al</i> (2008) <sup>93</sup>	Trafficking

## **1.13 Role of SLC4A11 in explaining the pathophysiology of ECD**

As SLC4A11 mutations cause CHED and some cases of FECD, studies have tried to relate the role of SLC4A11 to clinical presentations of ECD: cornea edema, increase in corneal thickness, progressive loss of CEnC, increased DM thickness and guttae.

### **1.13.1 Corneal edema and increase in corneal thickness**

SLC4A11 functions in maintenance of stromal deturgescence by moving excessive fluid from stroma to aqueous humor. SLC4A11 mutations that affect the water-flux function can compromise the endothelial pump. R125H is the only characterized mutation that compromises the water flux function<sup>28</sup>. Other SLC4A11 mutations that affect protein trafficking will compromise the cell surface abundance of SLC4A11, which in turn will compromise the water flux function in the plasma membrane<sup>52</sup>. 30 out of 55 mis-sense mutations compromise cell surface trafficking of the protein (Table 1.3). These mutations with R125H can lead to a compromised endothelial pump which will result in fluid accumulation in the stroma causing edema and increase in corneal thickness. The accumulated fluid distorts the arrangement of collagen lamellae resulting in increased scattering of light and compromised visual acuity.

Indeed, *slc4a11*<sup>-/-</sup> mice develop symptoms of corneal edema and increased central corneal thickness, resembling the clinical presentations of ECD in patients<sup>28,107</sup>. This confirms that loss of SLC4A11 contributes to ECD pathophysiology of corneal edema.

### **1.13.2 Progressive decline in CEnC density, increase DM thickness and guttae formation**

Loss of water flux function provides one possible explanation for the manifestation of corneal edema and increase in corneal thickness. However, compromised solute transport function does not adequately explain CEnC loss in patients. The *slc4a11*<sup>-/-</sup> mice also show a

progressive decline in CEnC density with age, along with distorted cell shape and size, mimicking the ECD patients<sup>28,107</sup>. Does SLC4A11 play additional roles that can explain CEnC loss?

SLC4A11 promotes efflux of ammonia which is a by-product of glutaminolysis in CEnC<sup>84</sup>. Loss of ammonia transport functions due to SLC4A11 could lead to ammonia toxicity in CEnC which could result in cell death. However, ammonia can diffuse out of the cell through the plasma membrane following its concentration gradient. Alterations in TCF4 due to CTG repeats in its third intron can lead to mRNA toxicity, which can contribute to CEnC loss<sup>108</sup>. However, not all FECD patients show CTG expansion which can cause mRNA toxicity and a direct co-relation between mRNA toxicity and the underlying mechanisms of CEnC loss has not been established<sup>109</sup>. Adhesion of CEnC to their underlying DM seems crucial in the cornea and can be one potential cause of CEnC loss. Although CEnC adhesion to DM has not been explored in the context of ECD yet.

## **1.14 Cell adhesion to basement membranes**

Cell attachment to their basement membrane is the hallmark of epithelial structures. Cells attach to their ECM in a highly organized and distinctive patterns. Cell adhesions are sites of cell attachment, which also connect the inside of the cell to the extracellular environment and transduce the signals to maintain a healthy physiology<sup>110</sup>. Cell adhesion is accompanied by multi-protein complexes made of three broad classes of proteins: the CAM or receptors, the ECM proteins and the cytoplasmic/ancillary/peripheral membrane proteins. CAMs are integral membrane proteins categorized in five super families: integrins, immunoglobulin cell adhesion molecules (IgCAMs), selectin, cadherins and proteoglycans<sup>111</sup>. They act as a connection link between the cytosolic proteins and ECM. ECM proteins are secretory proteins that constitute the basement membrane to which the cells adhere. Cells usually secrete ECM to make their own basement membranes. ECM proteins include collagens, laminins, FNCs and proteoglycans that

assemble into macromolecular arrays to create a defined basement membrane arrangement<sup>112</sup>. ECM proteins interact with their plasma membrane receptors to hold the cells tightly in their place. Cytosolic/peripheral membrane proteins are the regulatory proteins which connect with the cytosolic regions of the CAMs to the cytoskeletal proteins to transduce the signals to the inner regions of the cell. These multimeric complexes usually cluster in focal adhesions to promote cell attachment and to regulate other cellular functions<sup>113</sup>.

Loss of epithelial cell anchorage from their ECM triggers programmed cell death called anoikis, a physiological defense mechanism in multi-cellular organisms that prevents re-attachment and growth of detached cells on foreign matrices that can disturb the organ's microenvironment<sup>114</sup>. Alterations in the proteins of this complex cause diverse pathologies, including vascular diseases, cancer, inflammation<sup>115</sup>.

Attachment of CEnC to DM and to each other is critical to maintain the endothelial barrier and thus corneal transparency. Integrins have been identified in the corneal endothelium that contribute to CEnC-DM attachment. Integrins function as heterodimers consisting of  $\alpha$  and  $\beta$  chains. Integrin  $\alpha_V$  (ITGAV), Integrin  $\beta_3$  (ITGB3) and integrin  $\beta_5$  (ITGB5) are the corneal endothelial integrins and exist in heterodimers of  $\alpha_V\beta_3$  and  $\alpha_V\beta_5$ . They interact with collagens, FNC and laminins in DM by binding to their RGD motifs<sup>116</sup>.  $\alpha_4\beta_1$  and  $\alpha_6\beta_1$ , discovered recently in CEnC, interact with their binding partners in the DM through their large extracellular domains that extend from the cell surface towards the DM<sup>76</sup>.

ECD patients show progressive CEnC loss suggesting that defective cell adhesion could be one of the potential underlying causes of the disease. However, none of the CAMs have been implicated in ECD. Amongst the genes mutated in ECD, SLC4A11 is the transmembrane protein which has a large extracellular loop (EL3) extending towards the DM. Single point mutations in the loop cause FECD. Does the solute carrier protein, SLC4A11, also function as a CAM?

## 1.15 Hypotheses

This thesis addresses the hypothesis that SLC4A11 acts as a CAM to promote CEnC adhesion to DM. SLC4A11-EL3 is the anchoring site for CEnC to DM. Mutations that affect SLC4A11 cell adhesion function compromise integrity of endothelium and contribute to CEnC loss in patients.

SLC4A11 is a plasma membrane protein with a large EL3, that is not reported to be involved in any transport functions of the protein. Disrupting the loop by insertion of a double-hemagglutinin tag (HA-Tag) does not affect the water flux function of the protein<sup>92</sup>. FECD causing point mutations in the loop can give rise to disease symptoms suggesting that EL3 has a certain function that is compromised by these mutations. SLC4A11-EL3 is large and can potentially come in close proximity to the DM. SLC4A11 is also one of the most abundant proteins of CEnC that has a basolateral localization, making it an excellent candidate to promote cell attachment to DM. The homology model shows that the two SLC4A11-EL3s are present at the dimeric interface where they can function together to promote a stronger cell attachment by avidity. *slc4a11*<sup>-/-</sup> mice have the clinical manifestation of progressive CEnC loss, pleomorphism and polymegathism, as seen in patients. Additionally, out of the 24 mutations that affect the protein SLC4A11 function (Table 1.3), only four have been linked to the transport function of the protein<sup>28,90</sup>. This suggests there may be additional functions of SLC4A11 that are still undiscovered and the remaining 20 mutations cause disease by affecting these functions. COL8A2, whose mutations also cause FECD, is one of the most abundant proteins of DM making it a feasible binding partner of SLC4A11. Altogether, these facts support the hypothesis that SLC4A11 functions as a CAM to promote CEnC adhesion to DM.

This thesis also addresses the hypothesis that one of the three N-terminal SLC4A11 variants is predominant in corneal endothelium. The relevant SLC4A11 variant needs to be identified in corneal endothelium before studying the role of SLC4A11 in CEnC adhesion to DM.

## 1.16 Thesis Objectives

There are two broad objectives of this thesis:

1. To characterize the SLC4A11 variant(s) expressed in the human cornea and its endothelium. This will identify the relevant SLC4A11 variant(s) that should be used in studies related to cornea and its diseases.
2. To test if SLC4A11 functions as a CAM in the corneal endothelium to promote CEnC adhesion to DM via its large EL3. Additionally, to test if SLC4A11 interacts with COL8A2, a principal component of DM whose mutations cause FECD.

Chapter 2 of this thesis summarizes all the materials and detailed methodologies used in addressing the two objectives outlined above. Chapter 3 focuses on identifying the SLC4A11 variant(s) expressed in the human cornea and its endothelium. We combine bioinformatic, RNA and protein-based studies to conclusively quantify the abundance of different SLC4A11 variants in the corneal endothelium. Chapter 4 focuses on testing the hypothesis on the role of SLC4A11 as a CAM in the corneal endothelium. I designed an *in vitro* cell adhesion assay that can test multiple samples in a 96-well format using HEK293 cells as the expression system. This chapter also characterizes the four FECD-causing mutations in SLC4A11-EL3 and their effect on the potential cell adhesion function of the protein. Along with identification of the interaction partner of SLC4A11 in DM, we also test the hypothesis in primary human corneal endothelial cells (HCEnC) to validate the potential adhesion role of SLC4A11. This chapter will help create a better understanding of SLC4A11 and its role in ECD. Chapter 5 summarizes the key findings of this thesis and discusses the potential avenues where these findings can be applied to create a better understanding of human biology and disease.

---

## **Chapter 2: Materials and Methods**

---

## 2.1 Materials

Materials used	Source
<b>DNA constructs and cloning</b>	
Oligonucleotides	Integrated DNA Technologies (Coralville, IA)
Q5 Site-directed mutagenesis kit	New England Biolabs (Ipswich, USA)
CloneJET PCR Cloning Kit, Taq DNA polymerase PCR kit	Thermo Fisher Scientific (Ottawa, ON, Canada)
<b>Mammalian Cell culture and Transfection</b>	
Dulbecco's modified Eagle's medium (DMEM), fetal bovine serum (FBS), calf serum (CS), penicillin-streptomycin-glutamine (PSG), Ham's F12 Medium 199, Human Endothelial-serum free medium (SFM), Insulin/Transferrin/Selenium (ITS), Collagenase Type I, TrypLE™ Select, gentamycin	Life Technologies (Carlsbad, CA, USA)
Recombinant basic fibroblast growth factor	R&D Systems (Minneapolis, MN, USA)
T75 flask, 6-well, 12-well, 48-well and 100-mm cell culture dishes	Sarstedt (Montreal, QC, Canada)
96-well black flat clear bottom dishes with lids, Falcon® 60 mm TC-treated Center Well Organ Culture Dish	Corning (NY, USA).
FNC coating mix	United States Biologicals (Swampscott, MA, USA)
<b>Biochemical Assays</b>	
Bovine Eyeballs	Kastelen Sausage and Meats (Ardrossan, AB, Canada), Capital Fine Meats (Edmonton, AB, Canada)

Trizol, SuperScript III First Strand synthesis kit, chicken anti-mouse IgG conjugated with Alexa Fluor 594 and chicken anti-rabbit Alexa Fluor 488	Life Technologies (Carlsbad, CA, USA)
E-Plate 96	ACEA Biosciences (San Diego, CA, USA).
Complete Protease Inhibitor cocktail tablets, Pepstatin	Roche Applied Science (Indianapolis, IN, USA)
BCA Protein Assay Kit	Pierce (Rockford, IL, USA)
High Capacity Immobilized Streptavidin Agarose Resin, electroporation cuvettes, SuperSignal West Femto Maximum Sensitivity Substrate, phenyl methane sulfonyl fluoride (PMSF), glass coverslips, DNaseI and anti-GFP antibody	Thermo Fisher Scientific (Ottawa, ON, Canada)
Poly-L-lysine and Isopropyl thiogalactoside (IPTG), Pepsin from porcine gastric mucosa	Sigma-Aldrich (Oakville, ON, Canada)
Immobilon-P Polyvinylidene difluoride (PVDF) membranes, Luminata TM Crescendo Western horseradish peroxidase (HRP) Substrate chemiluminescence reagent	Millipore (Billerica, MA, USA)
HA monoclonal antibody (Clone 16B12)	BioLegend, Inc. (San Diego, CA, USA)
Anti-Glyceraldehyde-3-phosphate dehydrogenase (GAPDH), anti-Transcription factor IID (TFIID) and HRP-conjugated secondary donkey anti-rabbit antibodies	Santa Cruz Biotechnology (Santa Cruz, CA, USA)
Custom antibodies: Rabbit polyclonal SLC4A11-EL3, SLC4A11-v2-M1, SLC4A11-common, SLC4A11-v3	Primm Biotech (Cambridge, MA, USA)
HRP-conjugated sheep anti-mouse antibody	GE Healthcare Bio-Sciences Corp. (Piscataway, NJ, USA).

Glutathione Sepharose resin, PreScission Protease	GE Healthcare (Little Chalfont, Buckinghamshire, UK)
iQ-SYBR green super mix	Bio-Rad Laboratories (Hercules, CA, USA)
LiChroCART RP-18 (5 $\mu$ m particle size) columns	Merck KgaA (Darmstadt, Germany)
Common chemicals and reagents (Highest grade)	Sigma-Aldrich (Oakville, ON, Canada), Thermo Fisher Scientific (Ottawa, ON, Canada), EMD Millipore (Burlington, MA, USA)

## 2.2 DNA Constructs

Integrity of all constructs was confirmed by DNA sequencing (Institute of Biomolecular Design, Department of Biochemistry, University of Alberta, Edmonton, AB, Canada).

### 2.2.1 Mammalian Expression constructs

Eukaryotic-expression construct for splicing variant 2 of human SLC4A11 encoding an 891 amino acid protein (NCBI Reference Sequence: NG\_017072.1), N-terminally tagged with the HA epitope (pSKL1) and its point mutant, R125H ((C.374G>A (p.Arg125His)) were reported earlier<sup>52</sup>. This construct encodes “long” SLC4A11, starting at presumed start codon Met 1 (SLC4A11 v2-M1). A shortened version of pSKL1, removing the first 35 amino acids of the protein, resulting in an expression construct (pAMC1) encoding an 856 amino acid protein (SLC4A11 v2-M36)<sup>92</sup>, was created using the Q5<sup>®</sup> site directed mutagenesis kit using primers in Table 2.1. gBlock gene fragment encoding the first 135 amino acids of SLC4A11 variant 1 (NCBI Reference Sequence:

NM\_001174090.1) with a *Bam* HI site at the 5' end was from Integrated DNA technologies and cloned blunt in pJET1.2 vector (pDM16) using the CloneJET PCR cloning kit. SLC4A11 variant 3 (NCBI Reference Sequence: NM\_001174089.1) was made using pAMC1 as the template and the primers in Table 2.1. The forward primer contains bases that encode for variant 3 specific N-terminal residues. The PCR product was cloned into pcDNA 3.1 using *Nhe* I and *Xho* I. Nucleotide sequences corresponding to the amino acids (YPYDVPDYA) of an HA epitope tag (5'-TACCCCTACGACGTGCCCGACTACGCC-3') were added at the C-terminus (pCML13). Eukaryotic expression construct of amino-terminally HA-tagged-AE1 encoding a 911 amino acid protein (NCBI Reference: NG\_007498.1) was cloned into pcDNA3.1 (pDM1) using primers in Table 2.1. Eukaryotic expression construct of amino-terminally HA-tagged version of bovine SLC4A11 encoding an 851-amino acid protein (NCBI Reference: NM\_001191314.2) was made using gBlocks gene fragments from Integrated DNA Technologies (Coralville, IA, USA), and cloned into pcDNA3.1. Mouse SLC4A11 cDNA encoding an 862-amino acid protein (NCBI Reference: NM\_001081162.1) with an N-terminal HA tag cloned in pCDNA3.1 (pDM2) was from GenScript. All mutations were introduced into human SLC4A11 (c.1577A>G (Y562C), c.1682C>T (T561M), c.1694C>T (S565L), c.1723G>A (V575M) and c.[427G>A] +[427G>A] (E143K), c.[1633A>G] +[1635C>G] (N545Q), c. [1657A>G] +[1659C>G] (N553Q)) using Q5 Site-Directed Mutagenesis Kit, pSKL1 as the template and the primers listed in Table 2.2. Eukaryotic expression construct of enhanced green fluorescent protein or eGFP (peGFP-C1) was from Cedarlane Corporation. STIC (SLC4A11-EL3 Transmembrane-GPA Integrated Chimera) expression construct was made in two steps using primers listed in Table 2.3: 1. Sub-cloning cDNA encoding human Glycophorin-A (GPA) precursor (NCBI Reference: NM\_002099.8) into pcDNA3.1 (pDMCT1), 2. *In vivo* homologous recombination cloning in DH5 $\alpha$ <sup>117</sup> to replace the extracellular region of GPA precursor with SLC4A11-EL3, simultaneously mutating signal peptidase cleavage site (pDMCT2).

### **2.2.2 Bacterial Expression constructs**

Bacterial expression construct of GST-SLC4A11-EL3 fusion protein was made in two steps: 1. Cloning PCR product of SLC4A11-EL3 (primers in Table 2.4) into pJET1.2 (pDM3) using CloneJET PCR cloning kit. 2. Direct sub-cloning of the SLC4A11-EL3 from pDM3 to bacterial expression vector pGEX-6P-1 with N-terminal GST (pDM4) using restriction enzymes, *Bam* HI and *Xho* I.

## **2.3 Research-grade human corneoscleral tissues**

The human cadaver corneas used in this study were obtained post-mortem from the Lions Eye Institute for Transplant and Research (Tampa, FL, USA) and the Comprehensive Tissue Centre (University of Alberta Hospital, Edmonton Canada) with informed consent of the next of kin of deceased donors and we adhered to the principles outlined in the Declaration of Helsinki. Human corneas used in this study were deemed unsuitable for transplant and made available for research. Experiments using human corneas were approved by the University of Alberta Human Research Ethics Board (HREB) (Ref: Pro00036249) and SingHealth institutional review board (Ref: 2016/2839), and experiments followed guidelines from HREB and SingHealth. Corneal tissues were preserved in Optisol-GS (Bausch & Lomb, Rochester, NY, USA) at 4 °C until use.

Seven corneal pairs used in studies in chapter 3 were procured from Comprehensive Tissue Centre (University of Alberta Hospital, Edmonton Canada). Donor corneas had minimum endothelial cell count of 2000 cells/mm<sup>2</sup> (patient details in Table 2.5). Eleven corneal pairs used in studies in chapter 4 were procured from Lions Eye Institute for Transplant and Research (Tampa, FL, USA). Donor corneas had minimum endothelial cell count of 2200 cells/mm<sup>2</sup> (patient details in Table 2.6).

**Table 2.1: Primers used to clone human SLC4A11 v2-M36, SLC4A11 v3 and nHA-AE1 mammalian expression constructs.**

FP: forward primer; RP: reverse primer;

Construct	Primers used	Description
<b>pAMC1</b>	FP: ATCTCGCAGAATGGATACTTCG RP: GCTAGCCAGCTTGGGTCT	Shortened version of pSKL1 removing first 35 amino acids (SLC4A11 v2-M36)
<b>pCML13</b>	FP: 5'AGTC <u>GCTAGC</u> <i>GCCACCATGGCC</i> <b>GCGGCCACCAGGCGCGTGTTCATCT</b> <b>GCAGCCGTGCGAAA</b> ACTCTCCCACC ATGTCGCAGAATGGATACTTCGAGGATTC-3' RP: CAGT <u>CTCGAGT</u> CAAGGCCTGTGCTCAG	SLC4A11 v3 created by adding specific residues at the N-terminus of pAMC1 and a c-terminal HA- tag. <i>Nhe</i> I and <i>Xho</i> I restriction sites are underlined in FP and RP, the italicized sequence in FP represents the Kozak consensus <sup>118</sup> and the bold sequences represent v3 specific cDNA.
<b>pDM1</b>	FP: <u>GCTAGC</u> <i>GCCACCATGT</i> <b>TACCCATACGATGTT</b> <b>CCAGATTACGCTGAGGAGCTGCAGGATGAT</b> RP: <u>CTCGAGT</u> CACACAGGCATGGCCACTTCG	HA-tagged-AE1 encoding a 911 amino acid protein. <i>Nhe</i> I and <i>Xho</i> I restriction sites are underlined in FP and RP, the italicized sequence in FP represents the Kozak consensus and the bold sequences represent HA-tag,

**Table 2.2: Primers used to create FECD, CHED and N-glycosylation mutants of human SLC4A11.**

FP: forward primer; RP: reverse primer; N-Gly-Mut: N-linked Glycosylation site mutation.

\*Mutations in the forward primers are underlined.

<b>Mutation (cDNA)</b>	<b>Mutation (Protein)</b>	<b>Primers used*</b>	<b>Relevance</b>
c.1577A>G	p.Tyr526Cys p.Y526C	FP: CCTGGACGACT <u>G</u> CCACACAAAAAG RP: TAATGCCCATAGTAGTACTTC	FECD
c.1682C>T	p.Thr561Met p.T561M	FP: CGCCAGCCCC <u>A</u> TGGAGCTGCCCT RP: AGGAAGCTGGCGTTGAGGGCAGTG	FECD
c.1694C>T	p.Ser565Leu p.S565L	FP: GGAGCTGCCCT <u>T</u> GGCCACACACT RP: GTGGGGCTGGCGAGGAAG	FECD
c.1723G>A	p.Val575Met p.V575M	FP: GGCGACCGCC <u>A</u> TGCTCAGCCTCC RP: TGGCCTGAGTGTGTGGCCG	FECD
c.[427G>A	p.Glu143Lys p.E143K	FP: CGTCCTGAACA <u>A</u> GACGGCCACCTC RP: ATGCTGGCCTGCGCCAGG	CHED
c.[1633A>G] +[1635C>G]	p.Asn545Gln p.N545Q	FP: CGCCAGCCTC <u>C</u> AGGCCAGCCTCC RP: CCGAGGCCTGACAGGCTG	N-Gly-Mut
c [1657A>G] +[1659C>G]	p.Asn553Gln p.N553Q	FP: CACTGCCCTC <u>C</u> AGGCCAGCTTCC RP: TGGAGGCTGGCGTTGAGG	N-Gly-Mut

**Table 2.3: Primers to create STIC construct for mammalian expression.**

FP: forward primer; RP: reverse primer.

Construct	Primers used	Details
pDMCT1	FP: <u>GCTAGCATGTATGGAAAAATAATC</u> RP: <u>CTCGAGTCAGGCGTAGTCGGGC</u>	<i>Nhe</i> I and <i>Xho</i> I restriction sites underlined in FP and RP
pDMCT2	SLC4A11-EL3 FP: <u>CAGCAATTGTGAGCATATCATGGAAGTACTACTAT</u> GGG  SLC4A11-EL3 RP: <u>CCAAAAATAATGAGTGTTATCTGGCCTGAGTGTGT</u> GGC	Underlined are sequences homologous to GPA sequence around the insertion site. TGG (Tryptophan) in FP replaces Alanine (GCA) to mutate signal peptidase cleavage site
	GPA FP: <u>CGGCCACACACTCAGGCCAGATAACACTCATTAT</u> TTTTGG  GPA RP: <u>TGCCCATAGTAGTACTTCCATGATATGCTCACAAT</u> TGCTG	Underlined are sequences homologous to SLC4A11-EL3 insert

**Table 2.4: Primers to clone SLC4A11-EL3 into pJET1.2.**

FP: forward primer; RP: reverse primer.

<b>Construct</b>	<b>Primers used</b>	<b>Details</b>
<b>pDM3</b>	FP: <u>GGATCCGGCACGGTTAAAATCTTCTGG</u> RP: <u>CTCGAGGCTGAGCACGGCGGTCGC</u>	<i>Bam</i> HI and <i>Xho</i> I restriction sites underlined in FP and RP

**Table 2.5: Donor information for samples collected from Comprehensive Tissue Centre (University of Alberta).**

Listed are the donor information along with their use in studies described here. UK - unknown.

Serial No.	Age/Sex	HCEnC count (OS/OD)	Cause of death	Figure			
				3.2	3.3	3.4	3.5
JC-MC-015	50/M	2087/2262	Pulmonary embolism				*
JC-DM-017	47/M	2923/3267	Pontine Hemorrhage stroke	*	*		
JC-DM-018	58/M	3194/3436	Myocardial infarction	*	*		
JC-DM-018	53/M	3021/n/a	UK	*	*		
JC-DM-023	67/M	2457/2288	Heart failure			*	
JC-DM-024	62/F	2674/2558	Metastatic invasion/Ductal carcinoma of breast			*	
JC-DM-025	40/F	3021/2849	Cardiac arrest due to Nitric Oxide intoxication			*	

**Table 2.6: Donor information for samples collected from Lions Eye Institute for Transplant and Research.**

Listed are the donor information along with their use in my studies.

Serial No.	Age/ Sex	HCEnC count (OS/OD)	Cause of death	Figure				
				4.9A	4.9B	4.9C-D	4.10	4.11
(GPO36)P 1 & P2	21/M	3289/2639	Exsanguination	*				*
(GPK533) P1	23/M	2899/2817	Overdose					*
(GPK489) P1	29/F	2481/2469	Pancreatitis					*
(GPK495) P1	28/M	2564/2618	Acute Cardiac Crisis					*
(GPK531) P1 & P2	22/F	2538/2551	Anoxic Brain Injury				*	*
(GPK547) P2	4/M	3610/3774	Respiratory Failure	*			*	
(GPK537) P2	30/F	2551/2667	Brain Aneurysm				*	
(GPK497) P2	33/F	2725/2604	Overdose		*	*		
(GPK557) P2	21/M	3401/3367	Blunt Head Trauma		*	*		
(GPK524) P2	27/F	3003/3030	MVA		*	*		
(GPK533) P2	22/F	2101/2309	Anoxic Brain Injury			*		

## **2.4 Preparation of anti-SLC4A11 antibodies.**

Four polyclonal antibodies were raised in rabbits against synthetic peptides, corresponding to regions of human SLC4A11, by PrimmBiotech (Cambridge, MA USA). Antibody “SLC4A11-v2-M1” corresponded to amino acids 11-26 of variant 2, starting at the presumed start Met1, NH<sub>2</sub>-MCTQEVQGLVHGAGDLS-COOH. Antibody “SLC4A11-common” corresponded to amino acids 37-50 of variant 2, starting at M36, NH<sub>2</sub>-MSQNGYFEDSSYYKC-COOH. Antibody “SLC4A11-v3” was generated against the N-terminal residues of the unique exon in SLC4A11 variant 3, NH<sub>2</sub>-MAAATRRVFLHQLQPC-COOH. Antibody SLC4A11-Extracellular Loop 3 (SLC4A11-EL3) was generated against the peptide NH<sub>2</sub>-HTKRTSSLVSLSGL-COOH corresponding to amino acids 527-540 of human v2 SLC4A11-EL3.

## **2.5 Bioinformatic analysis**

SLC4A11 v2-M1 nucleotide sequences immediately upstream of the first and second possible translation initiation start codons (ATG) were compared to the human Kozak consensus sequence (GCCACC). To identify SLC4A11 genes in other organisms, human SLC4A11 sequence was used as a BLAST query of other species genome databases available through Ensembl. Genomic DNA surrounding and inclusive of SLC4A11 coding sequence was exported and used to search for DNA sequences corresponding to the unique 297 bp, 184 bp and 147 bp regions of human SLC4A11 v1, 2, and 3, respectively. Genomic DNA was manually searched since many databases only contain predicted transcripts, not fully sequenced cDNAs. High sequence conservation allowed identification of the M36 codon readily. Sequences upstream of the M36 codon were carefully examined for the presence of an upstream M1 start codon corresponding to human v2-M1. Translated upstream sequences were aligned to human SLC4A11-v2-M1 amino acid sequences.

## 2.6 Bacterial transformation

Electrocompetent *E. coli* (DH5 $\alpha$ ) cells were prepared<sup>119</sup> and cells with a minimum transformation efficiency of  $1 \times 10^9$  Colony Forming Units (CFU)/ $\mu$ g of cDNA were used for transformations. Frozen aliquots of electrocompetent cells (50  $\mu$ l) were thawed on ice for 5 min. Electroporation cuvettes were chilled on ice for 5 min and the cells were transferred to the cuvette. High quality (super-coiled and low salt) cDNA (10 pg) was added to the cells and mixed gently. The cuvette was dried and placed in the holder of the Eppendorf Electroporator 2510. Cells were transformed at 1800 V with time constant close to 5 ms, and immediately incubated in 450  $\mu$ l of Super Optimal Catabolite (SOC) medium (0.2% bactotryptone, 0.5% yeast extract, 10 mM NaCl, 2.5 mM KCl, 10 mM MgSO<sub>4</sub>, 10 mM MgCl<sub>2</sub>, 20 mM glucose) at 37 °C in shaker incubator for 30 min for the cells to recover. Desired volume of cells was plated on antibiotic selective standard Luria Broth (LB) agar plates and incubated overnight at 37 °C. Total number of colonies were counted and used for plasmid preparation.

## 2.7 Plasmid preparation

Colonies from antibiotic selective agar plates were inoculated in 3 ml of LB medium with selective antibiotics for 8 h at 37 °C in shaker incubator at 220 rpm. Bacterial concentration was estimated by measuring the absorbance (A) of the sample at 600 nm in a spectrophotometer. The sample with the maximum A was used as a starter culture and added to 250 ml standard LB media with selected antibiotics in a baffled flask and incubated at 37 °C in shaker incubator at 220 rpm for 16 h. Bacterial cells were harvested by centrifugation at 6,000 x g for 20 min at 4 °C. Cells were lysed and plasmids were isolated using the Qiagen Plasmid Plus midi kit (Qiagen, Hilden, Germany). The quality of the isolated plasmid was tested by 1% agarose gel electrophoresis and

the integrity of the preps were confirmed by DNA sequencing (Institute of Biomolecular Design, Department of Biochemistry, University of Alberta, Edmonton, AB, Canada).

## **2.8 Cell culture and transfection**

All cells were maintained at 37 °C in 5% CO<sub>2</sub>-air environment All experiments were carried out 40-48 h post-transfection.

### **2.8.1 HEK293 cells:**

HEK293 cells were maintained in complete DMEM (DMEM with 5% (v/v) FBS, 5% (v/v) CS and 1% (v/v) PSG. cDNAs were transiently transfected in HEK293 cells using the calcium phosphate method<sup>120</sup> on 100 mm dishes. For cell adhesion assays, peGFP-C1 (1.6 µg) was co-transfected with indicated cDNAs (3.8 µg, unless stated otherwise). For other assays, 3.8 µg of indicated cDNAs were transfected.

### **2.8.2 Primary HCEnC**

Primary HCEnC were isolated and expanded using the dual media system<sup>121</sup>. Briefly, The DM attached to corneal endothelium was enzymatically digested for 4 h with 2 mg/ml collagenase in the corneal M5 endothelial stabilization medium ((M5-Endo; Human Endothelial serum free medium (SFM) with 5% serum)) to dislodge the HCEnC from DM. This resulted in tightly packed HCEnC clusters. These clusters were further dissociated into single cells by treatment with TrypLE reagent for 5 min. The cells were washed twice with phosphate buffered saline (PBS, 140 mM NaCl, 3 mM KCl, 6.5 mM Na<sub>2</sub>HPO<sub>3</sub>, 1.5 mM KH<sub>2</sub>PO<sub>3</sub>, pH 7.4), and then seeded onto ECM (FNC coating mix)-coated 60 mm center well organ culture dishes in the corneal endothelial stabilization medium, overnight. Cells were washed and switched into M4 proliferative medium ((M4-F99; Ham's F12/M199, 5% serum, 20 µg/ml ascorbic acid, 1X ITS (Insulin Transferrin

Selenium) and 10 ng/ml Basic Fibroblast Growth factor)) to expand the isolated CEnCs. After cells reached 80-90% confluence, they were maintained in M5-Endo stabilization medium. This is described as passage 0 (P0). Cells were further expanded to passage 1 (P1) and passage 2 (P2) by de-plating using TrypLE reagent and expanding again as described.

For transfection, CEnCs at P2 were washed with PBS and de-plated using 0.25% Trypsin-EDTA for 5 min followed by addition of serum containing medium and counting cells. Cells were transfected using the Neon transfection system (Thermo Fisher Scientific) as per the manufacturer's protocol. Briefly,  $4 \times 10^6$  cells were aliquoted, washed with PBS, centrifuged and re-suspended in 120  $\mu$ l of proprietary Buffer R and 2.5  $\mu$ g of nHA-SLC4A11 cDNA was added. Cells were transfected in the specialized neon pipette tips using the following protocol (Pulse voltage: 1300 V, pulse width: 30 ms, pulse number 1) and added to 2 ml M4-F99 proliferative medium in ECM-coated 12-well dishes for 24 h. Cells were switched to 2 ml of M5-Endo stabilization medium after 24 h.

## **2.9 Preparation of human corneal lysates**

Protein lysates from intact corneas and endothelial layer were prepared separately. Briefly, two intact human cadaver corneas of a donor with 50 years of age and average endothelial cell density of 2174 cells/mm<sup>2</sup> (Table 2.5) were frozen in liquid nitrogen and crushed using a mortar and pestle. The resulting tissue powder was solubilized in 500  $\mu$ l Immuno-precipitation (IP) buffer (1% (v/v) IGEPAL CA-630, 5 mM EDTA, 150 mM NaCl, 0.5% (w/v) sodium deoxycholate, 10 mM Tris, pH 7.5), containing Complete Protease Inhibitor cocktail (mini-complete, Roche) and freshly prepared 1 mM PMSF (used 100 mM PMSF stock made in ethanol). For endothelial cell lysates, six human cadaver corneas with average age of donors was 54 years and average endothelial cell density was 2641 cells/mm<sup>2</sup> (Table 2.5) were micro-dissected and the endothelial layers were peeled off along with the DM and pooled. Tissues were also lysed in 200  $\mu$ l IP buffer, containing Complete

Protease Inhibitor cocktail and freshly prepared 1 mM PMSF. Both samples were incubated on ice for 20 min and were centrifuged at 13200 x g for 20 min at 4 °C and supernatant was collected. Protein concentration was determined by BCA Assay<sup>122</sup>.

## 2.10 Reverse Transcription PCR

Human corneas, deemed unfit for transplantation, were from the Comprehensive Tissue Centre, University of Alberta Hospital. Corneas were either used intact or subjected to dissection to isolate corneal endothelium with DM. Total corneal RNA and isolated endothelial cell RNA each came from three corneas, respectively with average donor age of 52 years and average endothelial cell density 3168 cells/mm<sup>2</sup>. RNA was isolated from tissues using Trizol reagent (Life Technologies) according to the manufacturer's instructions. The resulting RNA was used as template with SuperScript™ III First Strand synthesis system (Invitrogen) ((with or without reverse transcriptase (RT) enzyme)) to generate cDNA according to manufacturer's instructions (Table 2.7). Resulting cDNA (100 ng) was used as template in PCR with Taq Polymerase along with the corresponding primers (Table 2.8). PCR was performed using an MJ Research Inc. PTC-100 thermal cycler and the following reaction: 2 ng cDNA, 1 μM forward and reverse primer, 1.5 mM MgCl<sub>2</sub>, 1X Taq buffer and 1.25 U Taq Polymerase. PCR conditions were: 2 min 95 °C, 40 cycles of (30 s at 95 °C, 30 s at 54 °C (variant 1, 2, 3 primers), 15 s at 72 °C) and 10 min at 72°C. Resulting PCR products were visualized by agarose gel electrophoresis. To check the specificity of each primer pair, PCR was performed using the primer pairs for each variant with three synthetic templates (pDM16, pSKL1 and pCML13), using similar conditions as mentioned above. Resulting PCR products were visualized by 2% agarose gel electrophoresis.

## 2.11 Real Time quantitative PCR

cDNA from total cornea and isolated endothelium were used with primer pairs for variant 1, 2, 3 and GAPDH (Table 2.8) and iQ SYBR green super mix on Rotor Gene RG-3000 real time analysis system (Corbett life Science, San Francisco, CA, USA). SYBR green super mix is an optimized pre-blend containing SYBR green I dye, iTaq DNA polymerase, dNTPs and reaction buffers. Reactions were performed in 20  $\mu$ l reaction mixture with cDNA (from 1 ng RNA), 1X SYBR green super mix and 300 nM of forward and reverse primer. Reactions without RT enzyme samples were used to quantify the background and reactions without template were used as a negative control for each group. Primers for GAPDH were used as an internal control. PCR conditions were: 10 min for 95 °C, 40 cycles of (10 s at 95 °C, 15 s at 54 °C, 20 s at 72 °C). To quantify transcript abundance, a standard curve was constructed for each variant using a range of copies for each synthetic template (2.5 to  $2.5 \times 10^4$  copies) in the similar reaction conditions as above. Fluorescence was recorded at the end of each elongation step. After 40 cycles, a melting curve was generated by slowly increasing the temperature (0.1 °C/s) from 54 °C to 95 °C, while the fluorescence was measured. The threshold cycle ( $C_T$ ) was calculated manually and kept consistent throughout. A standard curve was constructed for each variant by plotting the  $\text{Log}_{10}$  of the copies against the  $C_T$  values. The  $C_T$  for the samples were normalized for GAPDH and plotted in the standard curve to estimate the number of copies of each transcript per reaction. The values for No RT control were subtracted for each variant in each group.

## 2.12 Immunoblots and densitometry

Forty to 48 h post transfection, culture medium was removed, and cells were rinsed with PBS. Cells were lysed in IP buffer, containing Complete Protease Inhibitor Cocktail and freshly prepared 1 mM PMSF for 20 min on ice and centrifuged at 13,400 x g for 10 min. Supernatant

**Table 2.7: cDNA synthesis from isolated corneal RNA using SuperScript III First strand synthesis system.**

SL. No. stands for serial number, U stands for units, 1X stands for 1 times dilution of the original stock. Oligo(dT)<sub>20</sub> means it is a 20-mer string of deoxythymine residues.

SL. No.	Reaction components	Final concentration
1.	Oligo(dT) <sub>20</sub>	50 $\mu$ M
2.	Total RNA	20 ng
3.	dNTP mix	10 mM total
4.	Diethyl Pyrocarbonate (DEPC)-treated water	To final volume
Mix and heat to 65 °C followed by incubation on ice for 2 min. Centrifuge briefly to collect the contents and add:		
5.	5X First Strand Buffer	1X
6.	Dithiothreitol (DTT)	100 mM
7.	RNAseOUT	40 U
8.	SuperScript III RT enzyme	200 U

**Table 2.8: Primers for reverse transcription PCR amplification of SLC4A11 transcripts.**

FP: forward primer; RP: reverse primer.

<b>Transcript</b>	<b>Primer Pairs</b>	<b>Product Size (bp)</b>
<b>SLC4A11 Variant 1</b>	FP: 5'-GGGCAGGGTTTTCTCAGGAA-3' RP: 5'-CATTCTCAGTGTTGGTGGCCT-3'	244
<b>SLC4A11 Variant 2</b>	FP: 5'-GGCTGGTGACCTTTCTGCTT-3' RP: 5'-CATTCTCAGTGTTGGTGGCCT-3'	233
<b>SLC4A11 Variant 3</b>	FP: 5'-CAGGCGCGTGTTCCATCTG-3' RP: 5'-CATTCTCAGTGTTGGTGGCCT-3'	233
<b>GAPDH</b>	FP: 5'-CAGCCTCAAGATCATCAGCA-3' RP: 5'-TGTGGTCATGAGTCCTTCCA-3'	106

was collected, and protein concentration was quantified by Pierce BCA protein assay. Total lysate (50  $\mu$ g per sample) was mixed with SDS-PAGE sample buffer ((10% (v/v) glycerol, 2% (w/v) SDS, 0.5% (w/v) bromophenol blue, 75 mM Tris, pH 6.8)). Lysates were made to 1% (v/v) 2-mercaptoethanol, heated at 65 °C for 5 min and insoluble material was removed by centrifugation at 9,000 x g for 1 min. Samples were resolved on SDS-PAGE on 10% (w/v) polyacrylamide gels. Mouse anti-HA or mouse anti-TFIID or rabbit anti-SLC4A11-v2-M1 or rabbit anti-SLC4A11-common or rabbit anti-SLC4A11-v3 or mouse anti-GAPDH were used to probe for the HA-tagged proteins or TFIID or SLC4A11-v2-M1 or SLC4A11-v2-M36 or SLC4A11-v3 or GAPDH on immunoblots at 1:2000 or 1:1000 or 1:500 or 1:500 or 1:500 or 1:3000 dilution respectively, in Tris buffered saline-tween20-milk (TBST-M) ((0.1% (v/v) Tween-20, 0.15 M NaCl, 50 mM Tris, pH 7.5 and 5% (w/v) skim milk powder)) 12-16 h at 4 °C. HRP-conjugated sheep anti-mouse or donkey-anti-rabbit were used as secondary antibody at 1:5000 dilution each in TBST-M for 1 h at 20 °C. Immunoblots were developed, using Luminata Crescendo Western HRP Substrate for 1 min or Super Signal™ West Femto maximal sensitivity substrate for 5 min and imaged on ImageQuant LAS4000 Image Analyzer (GE Healthcare). Quantitative densitometric analysis was performed using ImageQuant TL 1D gel analysis software (GE Healthcare). Band intensities (B.I.) for each protein were normalized to their respective TFIID or GAPDH B.I. to correct for loading differences.

## **2.13 Cell surface processing assays**

Cell surface processing assays were performed as described earlier<sup>123</sup>. Transfected cells were rinsed with 4 °C PBS washed with 4 °C Borate buffer (154 mM NaCl, 7.2 mM KCl, 1.8 mM CaCl<sub>2</sub>, 10 mM boric acid, pH 9.0) and labelled with Sulpho-NHS-SS-Biotin (0.5 mg/ml). After washing three times with 4 °C Quenching buffer (192 mM glycine, 25 mM Tris, pH 8.3), cells were solubilised in 500  $\mu$ l of IP buffer, containing Complete Protease Inhibitor Cocktail and freshly

prepared 1 mM PMSF. For each sample, half of the recovered supernatant was retained for later SDS-PAGE analysis (Total Protein, T). The remaining half of the recovered supernatants was combined with 100  $\mu$ l of 50% suspension of High Capacity Streptavidin Agarose resin to precipitate the biotinylated proteins and the supernatant was collected (Unbound Protein, U). The T and U fractions of each sample were processed for SDS-PAGE analysis and immunoblotting as described above. Densitometry using GE image analysis Software and the formula  $(T-U)/T \times 100\%$  was used to calculate the percentage of biotinylated protein.

## **2.14 Assays of osmotically driven water flux**

HEK293 cells were grown on 25 mm diameter poly-L-lysine coated round glass coverslips and co-transfected with peGFP-C1 and cDNA encoding WT-SLC4A11 or pcDNA 3.1 (empty vector) or indicated SLC4A11 mutant constructs in a 1:8 molar ratio<sup>28</sup>. Post-transfection (48 h), coverslips were mounted on a 35 mm-diameter cell chamber (Attofluor, Molecular Probes). The chamber was further mounted on a motorized xy stage with piezo focus drive (MS-4000 xyz automated stage, ASI Imaging), on a spinning-disk confocal microscope (Wave FX, Quorum Technologies, Guelph, ON, Canada) with a scanning head (CSU10, Yokogawa). The chamber was perfused with iso-osmotic Mops Buffered Saline Solution (MBSS) buffer (90 mM NaCl, 5.4 mM KCl, 0.4 mM MgCl<sub>2</sub>, 0.4 mM MgSO<sub>4</sub>, 3.3 mM NaHCO<sub>3</sub>, 2 mM CaCl<sub>2</sub>, 5.5 mM glucose, 100 mM D-mannitol, 10 mM HEPES, pH 7.4, 300 mosmol/kg) for 1 min and then with hypo-osmotic MBSS buffer (iso-osmotic MBSS minus D-mannitol, 200 mosmol/kg) for 3 min. Osmolality of each solution was measured, using a 3D3 Advanced Osmometer (Advanced Instruments Inc., Norwood, MA, USA). Data acquisition was performed with a Hamamatsu C9100–13 Digital Camera (EM-CCD; Chamlide) and a 20X objective with a laser (Spectral Applied Research, Richmond Hill, ON, Canada) excitation at 491 nm. GFP fluorescence, acquired at 1 point.s<sup>-1</sup>, was collected using a dichroic cube (Quorum Technologies) at wavelength range from 520 nm to 540 nm. Selected

regions of each HEK293 cell were subjected to quantitative image analysis, using Volocity 6.0 software (PerkinElmer, Waltham, MA, USA). The baseline was set using the fluorescence signal collected during perfusion with iso-osmotic MBSS buffer. The rate of cell swelling was calculated for the first 15 s after switching to hypo-osmotic buffer, using linear change in GFP fluorescence as a surrogate for cell swelling. Data were corrected for background and normalized to the value for WT-SLC4A11.

## **2.15 Quantification of SLC4A11 variant 2 and 3 proteins in endothelial cell lysates**

HEK293 cells transfected with cDNA encoding SLC4A11 v2, v3 and empty vector were lysed as explained above. v2 lysate (10  $\mu$ g protein), v3 lysates (5  $\mu$ g, 10  $\mu$ g and 20  $\mu$ g protein), vector control lysate (20  $\mu$ g protein) and pooled HCEnc lysate (20  $\mu$ g protein) were processed on immunoblots in duplicates. Blots were probed with SLC4A11-common antibody and SLC4A11-v3 antibody, respectively followed by Donkey anti-rabbit secondary antibody and developed. GAPDH, used as a loading control, was detected with monoclonal antibody against GAPDH from Santa Cruz Biotechnology and secondary antibody was sheep anti-mouse (GE Healthcare Bio-Sciences Corp. (Piscataway, NJ, USA). B.I. were determined by densitometry. The ratio of v3 detection by anti-SLC4A11-common and anti-SLC4A11-v3 antibodies was determined (Fig. 3.4C). This detection ratio (anti-SLC4A11-common/anti-SLC4A11-v3) was used to calculate the abundance of v2 and v3 in endothelial lysates as follows: Total SLC4A11 expression (detected with anti-SLC4A11-common antibody) = v2 + v3. To convert the abundance of v3 detected by anti-SLC4A11-v3 to the amount detected with anti-SLC4A11-common,  $v3 = B.I._{\alpha\text{-SLC4A11-v3}} \times$  Detection ratio. So,  $v2 = \text{Total SLC4A11 expression (detected with anti-SLC4A11-common}$

antibody) - v3 and thus v2 = Total SLC4A11 expression (detected with anti-SLC4A11-common antibody) - (B.I.<sub>α</sub>-SLC4A11-v3 X Detection ratio).

## **2.16 Homology modeling of SLC4A11 v2-M36 and v3 cytoplasmic domains**

Cytoplasmic domain sequence of SLC4A11 v2-M36 (M36-Y340) and SLC4A11 v3 (M1-Y359) were used to prepare their respective homology models using Protein Homology/Analogy Recognition Engine V 2.0 (Phyre<sup>2</sup>)<sup>124</sup> and Iterative Threading Assembly Refinement (I-TASSER)<sup>125</sup>. Crystal structure of human erythrocyte Band 3 (SLC4A1) cytoplasmic domain (PDB: 1HYN) was used as the template. Generated models were aligned with PyMOL molecular graphics system v 2.0.7 using segments that were modelled with 100% confidence (R90-P306 for SLC4A11-v2 and R109-P325 for SLC4A11-v3).

## **2.17 Preparation of bovine DM extracts**

The protocol was adapted<sup>13,126</sup> and modified to yield biochemical extracts suitable for cell adhesion assays. Briefly, fresh bovine eyes were obtained from a local slaughter house and corneas were dissected and rinsed in PBS (140 mM NaCl, 3 mM KCl, 6.5 mM Na<sub>2</sub>HPO<sub>4</sub>, 1.5 mM KH<sub>2</sub>PO<sub>4</sub>, pH 7.4). DM were micro-dissected and incubated in 1 ml of 0.05% sodium azide and stirred at 20 °C for 1 h. Following centrifugation at 5,000 x g for 5 min, the supernatant was discarded. Pellet was resuspended in 3% (v/v) Triton-X100 and 0.05% sodium azide and incubated at 20 °C for 3 h with end-over-end rotation, followed by centrifugation at 5,000 x g for 5 min. The supernatant was discarded and nuclei were removed by digestion with DNase I (20 U/μl in a 200 μl reaction) for 1 h at 37 °C and centrifuged again at 5,000 x g for 5 min. Pellets were further treated in 1 ml 4% sodium deoxycholate, 0.05% sodium azide and incubated at 20

°C for 3 h with end-over-end rotation, followed by centrifugation at 5,000 x g for 5 min. Purified DM was aliquoted (25 mg each). Pepsin stock (250  $\mu$ l of 0.05 mg/ml in 0.5 M acetic acid) was added to 25 mg of DM (1:2,000 w/w) and digested at 37 °C for 24 h with end-over-end rotation. Pepsin activity was inhibited by adding pepstatin in 1:1 molar ratio (pepsin: pepstatin). Undigested material was sedimented at 10,000 x g for 10 min and the supernatant was collected. Extracts were aliquoted, frozen at -80 °C and lyophilized overnight. Extracts were reconstituted in PBS and quantified by BCA assay, following the manufacturer's instructions, and used further in the cell adhesion assays.

## 2.18 Cell Adhesion Assay

The protocol was adapted from different sources and modified<sup>127-129</sup>. The base of 96-well dishes (Costar, Black Plate, Clear bottom with lid) were coated with 0.5  $\mu$ g reconstituted DM extract/well (50  $\mu$ l) at 4 °C for 12-16 h. Solution was aspirated and wells were blocked with 100  $\mu$ l of 10 mg/ml bovine serum albumin (BSA) in PBS for 1 h at 37 °C. Transiently transfected cells were de-plated using 0.25% Trypsin-EDTA and centrifuged at 500 x g for 2 min to remove trypsin. The cell pellet was reconstituted in fresh DMEM and cells were counted using an automated cell counter (Countess II Automated Cell Counter, Thermo Scientific, AMQAX1000). Cells were diluted to 6 x 10<sup>5</sup> cells/ml in DMEM. BSA from plates was aspirated and 3 x 10<sup>4</sup> cells (50  $\mu$ l of cell suspension) were added to each well and allowed to adhere for 3 h at 37 °C in 5% CO<sub>2</sub>-air environment. Each sample was studied in quadruplicate. Post incubation, total GFP fluorescence from each well was measured using a SynergyMX Plate Reader (BioTek, Winooski, VT, USA) with excitation and emission wavelengths at 485 nm and 512 nm, respectively (eGFP fluorescence<sub>pre-disruption</sub>). Loosely/non-adhering cells were removed by inverted centrifugation at 6.8 x g for 45-75 s, using an Eppendorf 5810R centrifuge with an A-4-62 MTP rotor with bucket microplate-F carrier, and eGFP fluorescence was measured again (eGFP fluorescence<sub>post-disruption</sub>). The percentage of

adhering cells was measured by calculating the fractional cell adhesion ( $\text{eGFP fluorescence}_{\text{post-disruption}} / \text{eGFP fluorescence}_{\text{pre-disruption}} \times 100\%$ ). Converting the data to % eGFP fluorescence ensures correction for variable GFP expression across different samples.

## **2.19 Competition for adhesion to DM-coated dishes**

HEK293 cells transfected with SLC4A11 cDNA or vector (pCDNA3.1) were counted and volume adjusted to  $6 \times 10^5$  cells/ml DMEM. DM extract (0, 2.5, 5 and 10  $\mu\text{g}$  per 50  $\mu\text{l}$  cell suspension) was added to 250  $\mu\text{l}$  cell suspension each and incubated at 37 °C for 30 min with end-over end-rotation. Cells were centrifuged at 500 x g for 2 min and medium was removed by aspiration. Cell pellets were re-suspended in 250  $\mu\text{l}$  of DMEM and pipetted up and down gently to disperse cell clusters into single cells. Cells were added to the DM-coated 96 well plates and the cell adhesion assay was repeated as described above.

## **2.20 Assay of anti-SLC4A11-EL3 antibody effect on transfected**

### **HEK293 cell adhesion**

Immune serum containing custom anti-SLC4A11-EL3 antibody was incubated with SLC4A11 cDNA and vector-transfected cells at a 1: 500 dilution for 30 min at 37 °C with end-over end-rotation. Cells were centrifuged at 500 x g for 2 min, and the supernatant was removed. Cells were re-suspended in fresh DMEM and pipetted up and down gently to obtain a single cell suspension. These cells were added to the DM-coated 96-well plates and the cell adhesion assays were carried out as described above. Pre-immune serum was used as negative control.

## 2.21 Structural modelling of SLC4A11 extracellular loop 3

A structural model of human SLC4A11 was prepared by homology to human Band 3 (SLC4A1)<sup>130</sup>. The available crystal structure contains many of the highly conserved topological elements, but structure corresponding to highly-mobile EL3 was missing. To model secondary elements that may be present in SLC4A11-EL3, we used ROSETTA-Membrane<sup>131,132</sup> de novo protein folding software (ROSETTA-MP) to generate initial seed-structures for the distributed replica exchange simulations described below. The conserved folding elements were restrained and only residues from G509 to S597 were used for loop modelling and optimization with ROSETTA-MP. We further performed a global search of the conformational space for protein tertiary structures to select conformations especially low in free energy for the amino acid sequence of EL3 and immediately adjacent elements<sup>133</sup>. Approximately, 25000 low-resolution models were generated, side-chains were rebuilt and then clustered as described previously<sup>132</sup>. This resulted in eight distinct structural clusters used as inputs for the distributed replica-exchange molecular dynamics (MD) simulations. The distributed replica exchange MD simulations were run for 260 ns per replica with 24 replica windows exponentially distributed from  $T = 300.0$  to  $501.1$  K. The exchanges between replica simulations run in parallel at different temperatures enable enhanced rapid sampling of the conformational space explored by EL3 in the dimer of SLC4A11. The aggregated length of the simulation was over  $10 \mu\text{s}$ . All simulations were performed with CHARMM 40b1 program using REPD module<sup>134</sup>, CHARMM-19 force-field with EEF1 implicit membrane model<sup>135</sup>. The temperature-weighted histogram analysis was used to determine the low-free energy structural states of SLC4A11-EL3 dominant at  $298$  K<sup>136</sup> corresponding to replicas with  $T$  between  $300.0$  to  $316.4$  K.

## 2.22 GST-SLC4A11-EL3 pull down assays

BL-21 *E. coli* cells were transformed with pDM4 and pGEX-6P-1 alone and grown at 37 °C to  $A_{600}$  of 0.6 before protein expression was induced by medium supplementation to 300  $\mu$ M IPTG for 4 h at 37 °C. Protein expression was confirmed by SDS-PAGE on 10% (w/v) polyacrylamide gels and staining with Coomassie blue. Cells were sedimented at 6,000 x g for 10 min and the pellets were resuspended in 1X PBSKM (150 mM NaCl, 3 mM KCl, 1 mM  $MgCl_2$ , 25 mM  $NaPO_4$ , pH 7.3). Cells were sonicated (1 min on, 1 min off, three cycles) in the presence of 0.3 mM DTT and Complete Protease Inhibitor Cocktail, followed by centrifugation at 20,000 x g for 30 min at 4 °C. Supernatants were incubated with glutathione-Sepharose resin in the presence of 0.2% Tween-20, 12-16 h at 4 °C and centrifuged at 1,000 x g for 1 min. Glutathione resin bound to GST-SLC4A11-EL3 fusion protein and GST-alone were incubated with 500  $\mu$ g of DM extract each, for 12-16 h at 4 °C. Samples were centrifuged at 1,000 x g for 5 min and supernatant was collected to remove the unbound DM. The fusion protein consists of a PreScission protease cleavage site upstream of the SLC4A11-EL3. The resin was washed with ten bed volumes of PreScission protease cleavage buffer (150 mM NaCl, 1 mM EDTA, 1 mM DTT, 50 mM Tris, pH 7.0) and incubated with 500 U PreScission protease, for 12-16 h at 4 °C to cleave off the SLC4A11-EL3. Resin was sedimented at 1,000 x g for 1 min and the supernatant containing the cleaved SLC4A11-EL3 bound to its potential interaction peptide was collected. Supernatants were further purified on a Hitachi EliteLaChrom System HPLC connected to an RP-18 (250-25) column (Merck KGaA) with a linear gradient (10-90%) of  $H_2O$  (0.1%) /  $CH_3CN$  (0.1% TFA) (75 min). Eluted peaks were collected on a fraction collector and lyophilized.

## 2.23 Mass Spectrometry

Pepsin-digested peptides were resuspended in 20  $\mu\text{l}$  of 0.1% formic acid and analyzed by nanoflow LC-HR-MS/MS (Ultimate 3000 RSLC nano system equipped with an Ultimate3000 RS autosampler coupled to an LTQ Orbitrap Velos Pro, ThermoFisher Scientific, TF, Dreieich, Germany). Peptides were trapped on a C18 trap column (75  $\mu\text{m}$  x 2 cm, Acclaim PepMap100C18, 3  $\mu\text{m}$  particle size, ThermoFisher) and separated on a reversed phase column (nano viper Acclaim PepMap capillary column, C18; 75  $\mu\text{m}$  x 50 cm, 2  $\mu\text{m}$  particle size; ThermoFisher) at a flow rate of 200 nl/min with buffer A (water and 0.1% formic acid) and B (90% acetonitrile and 0.1% formic acid), using a gradient from 4 to 55% buffer B in 85 min and 55 to 90% B in 15 min. Chromatography eluate was directly sprayed into the mass spectrometer through a coated silica electrospray emitter (PicoTipEmitter, 30  $\mu\text{m}$ , New Objective, Woburn, MA, USA) and ionized at 2.2 kV. MS spectra were acquired in a data-dependent mode. For the high energy collision dissociation (HCD) top3 method, full scan MS spectra ( $m/z$  300–1700) were recorded in the orbitrap analyzer with resolution of  $r = 60,000$ . The three most intense peptide ions with charge states  $>2$  were sequentially isolated and fragmented in the HCD collision cell with normalized collision energy of 30%. The resulting fragments were detected in the Orbitrap system with resolution  $r = 7,500$ . The fragmented peptides were identified by using MASCOT algorithm and TF Proteome Discoverer 1.4 software. Peptides were matched to tandem mass spectra by Mascot version 2.4.0 by searching a SwissProt database (version2015\_01 with 547.599 protein sequences from all taxonomies, 66091 mammalia) and imported in Scaffold. MS<sup>2</sup> spectra were matched with a mass tolerance of 7 ppm for precursor masses and 0.5 Da for fragment-ions. We used Pepsin A digest and allowed for up to two missed cleavage sites. Deamidation of asparagine and glutamine, acetylation of lysine and oxidation of methionine were set as variable modifications. Scaffold (version Scaffold\_4.0.7, Proteome Software Inc., Portland, OR) was used

to validate MS/MS based peptide and protein identifications. Peptide identifications were accepted if they could be established at greater than 90.0% probability by the Scaffold Local FDR algorithm. Protein identifications were accepted if they could be established at greater than 95.0% probability and contained at least two identified peptides.

## **2.24 Gene expression analysis**

Primary HCEnC from three age-matched donors were cultured to P2 and further de-plated and counted. Cells ( $2 \times 10^5$ ) from each donor were added to each well of DM-coated 48-well dishes and maintained in M5-Endo stabilization medium for 14 days with media change every 2 days. At Day 0 and 14, total RNA was extracted using PureLink micro kit (Thermo Fisher Scientific). Total RNA (400 ng) was reverse transcribed with high-capacity cDNA reverse transcription kit (Applied Biosystems, Thermo Fisher Scientific). Real time PCR was performed using TaqMan® gene expression assays (Table 2.9) and TaqMan® fast master mix.  $2^{-\Delta\Delta CT}$  were calculated for each gene and normalized to their GAPDH expression.

## **2.25 Culture of primary HCEnC on DM and fibronectin-coated dishes**

Primary HCEnC from four donors belonging to the same age-range were expanded to P2 (in culture for 7 days after P1) and further de-plated and counted. Cells ( $2 \times 10^5$ ) from each donor were added to each well of DM or FNC-coated 48-well dishes and maintained in M5-Endo stabilization medium for 7 and 14 days with media change every two days. Cells were harvested at Day 7 and Day 14. Cells were lysed and stored at  $-80^\circ\text{C}$ . Cells ( $1 \times 10^5$ ) from each donor were lysed at Day 0 (the day cells were plated on DM-coated dishes) and stored at  $-80^\circ\text{C}$ . FNC-coated dishes were used as control.

**Table 2.9: TaqMan® gene expression assay probes used for real-time PCR.**

Probe Assay IDs can be used to find the respective primer information on the TaqMan gene expression assays database<sup>137</sup>.

<b>Gene name</b>	<b>Probe Assay ID</b>	<b>Exon Boundary</b>	<b>Amplicon Length</b>
GAPDH	Hs02758991_g1	6-7	93
SLC4A11	Hs00984689_g1	11-12	59
COL8A1	Hs00156669_m1	4-5	71
COL8A2	Hs00697025_m1	3-4	85
LMX1B	Hs00158750_m1	2-3	99

## **2.26 Assay of primary HCEnC adhesion using xCELLigence real-time cell analyzer**

Adhesion of primary HCEnC to DM-coated dishes was analyzed using an xCELLigence real-time cell analyzer and E-Plate 96 dishes (ACEA Bioscience, San Diego, CA, USA). Primary HCEnC were de-plated, using 0.25% Trypsin-EDTA for 5 min and dissociated into single cell suspension and counted. E-Plate 96 dishes were coated overnight with 0.5  $\mu$ g reconstituted DM extract/well (50  $\mu$ l) at 4 °C for 12-16 h. Solution was aspirated, and equal number of cells were seeded on DM-coated wells at a density of  $1.25 \times 10^4$  cells.cm<sup>-2</sup> in M5-Endo stabilization medium at 37 °C in 5% CO<sub>2</sub>-air environment. The electrical impedance readings (Cell Index) of cell adherence were recorded for up to 30 h.

## **2.27 Assay of anti-SLC4A11-EL3 antibody on primary HCEnC adhesion**

Primary HCEnC from five donors belonging to the same age-range were expanded to P1 (in culture for 7 days after P0) and kept in M5-Endo stabilization medium until use. Cells were de-plated using 0.25% Trypsin-EDTA for 5 min and dissociated into single cell suspension and counted. Cells ( $5 \times 10^4$ ) were aliquoted in 500  $\mu$ l M5-Endo stabilization medium. Immune serum containing custom anti-SLC4A11-EL3 antibody (as described above) or the pre-immune serum were added to the aliquoted cells at 1:50 dilution and incubated at 37 °C for 30 min with end-over end-rotation. HCEnC ( $1.25 \times 10^4$  cells.cm<sup>-2</sup>) incubated with the serum were added to the DM-coated E-Plate 96 and the cell adherence (Impedance or Cell Index) was analyzed using the xCELLigence real-time cell analyzer.

## **2.28 Statistical analysis**

Numerical values represent mean±standard error of the mean (SEM). The statistical analysis was performed using GraphPad Prism 7.0. (GraphPad software). The significance of difference between two or more groups was determined using one-way ANOVA or two-way ANOVA with Sidak or Bonferroni-post tests, or Student's t-test.  $P < 0.05$  was considered significant.

---

## **Chapter 3: Human Corneal Expression of SLC4A11, a Gene Mutated in Endothelial Corneal Dystrophies**

---

A version of this paper is accepted for publication as Darpan Malhotra, Sampath K. Loganathan, Anthony M. Chiu, Chris M. Lukowski and Joseph R. Casey. Human Corneal Expression of SLC4A11, a Gene Mutated in Endothelial Corneal Dystrophies. *Scientific Reports* (2019).

All experiments were performed by Darpan Malhotra except bioinformatics analysis (Fig. 3.1) was performed by Chris M. Lukowski, and characterization of SLC4A11 v2-M1 and v2-M36 (Figs. 3.5-3.7) were performed by Sampath K. Loganathan and Anthony M. Chiu.

### 3.1 Introduction

Cornea, the outer surface of the eye, serves as a physical barrier to protect the inner layers of the eye and contributes to refractive power in focusing the visual image<sup>29</sup>. Within the cornea are three major layers: outermost is the epithelium; the middle layer is the stroma, a dissolved proteoglycan and collagen layer, sparsely populated by keratocytes; innermost is the endothelium, a monolayer of specialized endothelial cells. Because of the stroma's high solute concentration, there is a strong drive for osmotic fluid accumulation from the aqueous humor, across the endothelium. The endothelial layer's principle role is to remove this fluid through a "pumping" mechanism, which reabsorbs fluid into the aqueous humor<sup>25</sup>.

Defects in the endothelial "pump" give rise to stromal fluid accumulation, significantly thickening the layer. The edematous stroma blurs vision, significantly compromising visual acuity. Defects in endothelial function cause posterior ECD, which are responsible for 24% of corneal transplantation procedures<sup>32</sup>. Among ECD, FECD is most common, with a lifetime incidence of about 4% and disease onset typically over age 40<sup>29</sup>. Although genetically heterogeneous, mutations of the gene SLC4A11, cause many cases of dominantly inherited FECD<sup>42,96</sup>. Recessively-inherited, childhood onset CHED arises from SLC4A11 mutations<sup>29,36,57,93,95,106,138</sup>. Finally, SLC4A11 mutations also cause HS, characterized by childhood endothelial dystrophy and progressive sensorineuronal deafness<sup>139</sup>, although recently HS has been interpreted as a manifestation of CHED<sup>38</sup>.

SLC4A11 is an integral membrane protein, with a 41 kDa cytoplasmic domain and a 57 kDa membrane domain. Consistent with an important role in the endothelial cell fluid "pump", SLC4A11 facilitates transmembrane water movement<sup>28,52</sup>, Na<sup>+</sup>/OH<sup>-</sup> co-transport<sup>61,83</sup>, Na<sup>+</sup>-independent H<sup>+</sup> (OH<sup>-</sup>) transport<sup>65,66</sup>, and NH<sub>3</sub> transport<sup>67,140</sup>. Although plant SLC4A11 orthologs can transport borate<sup>141</sup>, the report that human SLC4A11 can<sup>142</sup> has been disputed<sup>61,83</sup>. Most

disease alleles of SLC4A11 result in protein misfolding and protein retention in the ER<sup>36,42,143</sup>, but some affect the protein's transport function<sup>28,66,144</sup>.

The genome database reveals three N-terminal variants of human SLC4A11: 918 amino acid splice form 1 (NCBI Reference Sequence: NP\_001167561.1), 891 amino acid splice form 2 (NP\_114423) and 875 amino acid splice form 3 (NP\_001167560). These variants have also been respectively called SLC4A11-A, -B and -C<sup>66</sup>. Differences in the three sequence variants arise at the N-terminus within the first 20-60 amino acids. One RT-PCR analysis of RNA from corneal endothelium suggested that only splice form 3 was present<sup>66</sup>. Studies of recombinant SLC4A11 are ongoing, working to understand SLC4A11 function and ultimately to ameliorate corneal dystrophy symptoms associated with defective SLC4A11. Yet, all earlier studies have explored the function of recombinant splice form 2<sup>28,36,42,52,61,67,79,83,99,123,145</sup>.

Definitively establishing the form of SLC4A11 protein in human cornea is critical to guide relevant future studies of the protein. Approximately 55 point mutations are spread throughout the two domains of SLC4A11<sup>36,42,57,93,95,98-101,103,106,139,146,147</sup>. Recently, important roles of the N-terminal SLC4A11 cytoplasmic domain were revealed<sup>79</sup>. Sequence variants at the SLC4A11 N-terminus thus may affect the protein's function. To determine the form of SLC4A11 in human cornea, we performed RT-PCR and real-time quantitative PCR of RNA from whole human cornea and isolated corneal endothelium. We developed antibodies able to detect all SLC4A11 variants, variant 2 initiating translation at two possible start Met residues, and variant 3. We further characterized the cell surface trafficking, transport functions and structural differences of SLC4A11 variants.

## 3.2 Results

### 3.2.1 Bioinformatic analyses of human SLC4A11

To begin to examine what forms of SLC4A11 are expressed in human cornea, we performed bioinformatic analysis (Fig. 3.1). Three variant transcripts of human SLC4A11 have been identified by cDNA sequencing efforts: variant 1 (v1), variant 2 (v2) and variant 3 (v3). These share 18 common exons and differ only in the sequence of their first exon (Fig. 3.1A). According to their cDNA sequences deposited into genome databases, transcript v1 and v3 splice into the middle of the first exon of v2. The genetic basis for this observation is unclear as normally splicing occurs at intron-exon boundaries, not in the middle of an exon. Nonetheless, sequences of transcripts are consistent with the splicing diagram presented (Fig. 3.1B).

We next examined coding sequences for the equivalent of v2 amongst mammalian species (Fig. 3.1C). In the case of human v2, we aligned the sequences around the first (M1) and second (M36) potential start methionine residues. Nucleotide sequence conservation was clearly much stronger starting at the start codon for Met36 than the upstream M1, which was even more evident at the amino acid level (Fig. 3.1D). This led us to consider whether M36 might act as the translational start site for the protein. The nucleotide sequence surrounding the start codon, the Kozak consensus sequence, is important in establishing translational start efficiency<sup>118</sup>. We thus mapped the translational start efficiency of nucleotides surrounding human SLC4A11 variant 2 at M1 (v2-M1) and M36 (v2-M36), as well as the other mammalian sequences (Fig. 3.1C). For translational start at v2-M1, only one of six nucleotides match optimal Kozak consensus (Fig. 3.1C). Yet, v2-M36, shows 5/6 upstream nucleotides as agreeing with consensus for efficient translational start. Moreover, all analyzed mammalian sequences revealed adequate-strong prediction around the ATG corresponding to human v2-M36 as translational start site, on the basis of Kozak consensus, GCCACCATG.

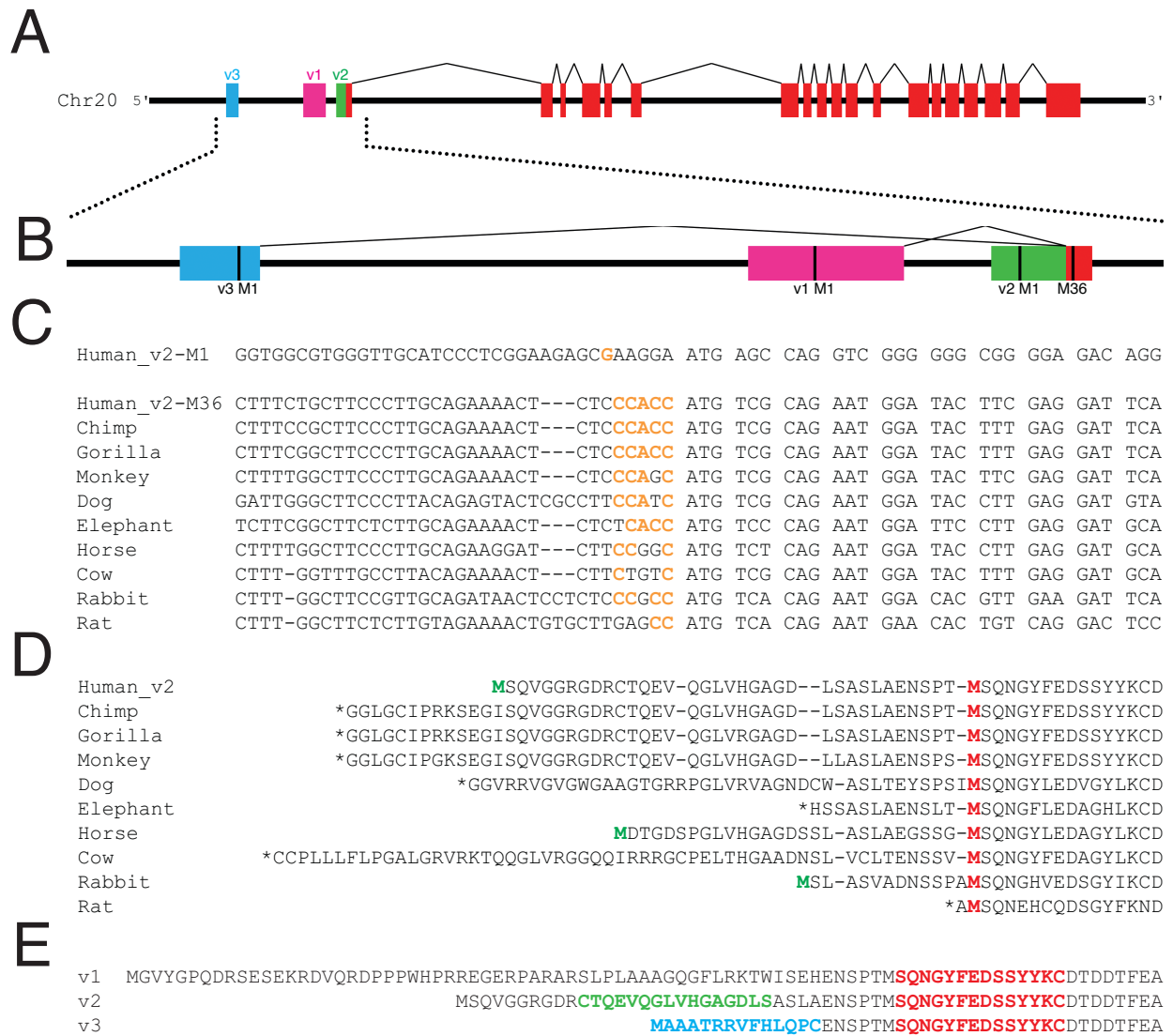


**Figure 3.1: Bioinformatic analysis of human SLC4A11.**

(A) cDNA sequences of known human SLC4A11 transcripts were mapped onto a 15 kb segment of Human chromosome 20 genomic DNA to show transcript structure (colored boxes), connected by introns (black lines). Each transcript variant (v1, v2 and v3) has a unique starting exon which results in unique N-terminal regions of the predicted protein and a common core region (red). (B) Magnified view of the 5' end of the SLC4A11 gene. Each variant has a predicted start codon (M1; vertical black line). M36 (numbering based on predicted sequence of v2) marks the start of the

common coding sequence for all transcripts. **(C)** Alignment of DNA sequences surrounding the predicted start codons in SLC4A11 v2 for multiple species. Kozak translational start sequence efficiency<sup>118</sup> is indicated with bases matching the consensus shown in orange. For human SLC4A11, Kozak analysis is indicated for v2 start at Met 1 and 36 (v2-M1 and v2-M36). **(D)** Alignment of amino acid sequences for v2 SLC4A11 for the indicated mammals. Red Methionine (M) residue indicates the position corresponding to human v2-M36. Green Met indicates in frame Met upstream of v2-M36. Stop codons are indicated (\*). **(E)** Amino acid sequences of SLC4A11 v1-v3 are aligned with sequences of peptides used to generate splice form-selective antibodies highlighted in red: SLC4A11-common, green: SLC4A11-v2-M1 and blue: SLC4A11-v3.

We next aligned amino acid sequences predicted for SLC4A11 v2 transcripts in ten mammals, including human (Fig. 3.1D). The alignment shows a high degree of amino acid identity starting at M36 of human SLC4A11. Moreover, only a small proportion of mammals (2/9 shown) had a potential start Met codon upstream of the position corresponding to human Met36. Together these observations suggest that in humans SLC4A11 v2 translational start occurs at the second Met in the sequence, Met36.

To determine the form of SLC4A11 expressed in cornea, antibodies able to detect specific sequences of SLC4A11 were prepared. Synthetic peptides were synthesized and used to immunize rabbits. Antibody SLC4A11-common was raised against a sequence immediately after the v2-M36, thus detecting a region common to all SLC4A11 variants (Fig. 3.1E, red). Antibody SLC4A11-v2-M1 was raised against a sequence uniquely present in the region between M1 and M36 of v2 (Fig. 3.1E, green). Finally, antibody SLC4A11-v3 was raised against a peptide corresponding to the unique region of v3 (Fig. 3.1E, blue).

### **3.2.2 Expression of SLC4A11 transcripts in human cornea**

Bioinformatics analysis indicates three SLC4A11 variants at the 5' end of the mRNA (Fig. 3.1). Mutations of SLC4A11 are associated with defects in the corneal endothelial layer, making the cornea the most important tissue to establish the expression profile for SLC4A11. We thus obtained human corneas deemed by a tissue bank as unsuitable for transplant. Whole cornea contains three predominant cell types. There is an outer epithelial cell layer, a stromal layer largely acellular, but containing some keratocytes, and an inner endothelial cell layer. RNA prepared from whole cornea thus represents the contribution of at least three cell types. Since defects in the endothelial layer underlie corneal dystrophies, we also prepared RNA from micro-dissected human corneal endothelium.

RT-PCR was performed using primer pairs (Table 2.8) producing products spanning intron-exon boundaries to avoid background arising from genomic DNA contamination of RNA samples. Primers were designed to amplify each of the three reported SLC4A11 mRNA variants, which differ in their first exon (Fig. 3.1A). Products were observed using agarose gel electrophoresis. To verify the ability of PCR primers to detect all SLC4A11 variants, PCR was performed on SLC4A11 v1, v2 and v3 cDNA cloned into a plasmid vector. v2 and v3 were expression constructs cloned into pcDNA3.1. In the case of v1, synthetic DNA including the entire v1 PCR amplicon was cloned into pJET1.2 plasmid to use as PCR template. PCR was carried out using the same molar amount of plasmid template for each variant, and with the specific PCR primer sets for the three variants on each template. Using cloned templates, v1 PCR product was obtained with a similar intensity to the bands found for the v2 and v3 amplicons (Fig. 3.2A). Thus, v1 reverse transcription product would be detected if its expression in human cornea were similar to v2 or v3. Specificity of RT-PCR was confirmed by the presence of PCR product only when PCR was performed with the primer pair designed for each variant, but not when tested on the other templates (Fig. 3.2A).

Reverse transcription reactions were performed with and without RT enzyme. RT-PCR of samples produced without RT did not produce any product, indicating that bands observed arose from reverse transcription of RNA (Fig. 3.2B-C). Using RNA from whole cornea, bands of the expected amplicon size were observed using v2 and v3-specific primers, but no band was observed for v1 (Fig. 3.2B). RT-PCR of human corneal endothelium RNA also revealed presence of v2 and v3 but no band was observed for v1 (Fig. 3.2C).

To measure the expression level of each variant in human cornea, we performed quantitative RT-PCR with cDNA from total cornea and isolated corneal endothelium from three different donors. Amounts of SLC4A11 RNA were normalized to GAPDH RNA level in each sample. Cloned cDNA for each variant ( $2.5 - 2.5 \times 10^4$  copies) was used to construct standard

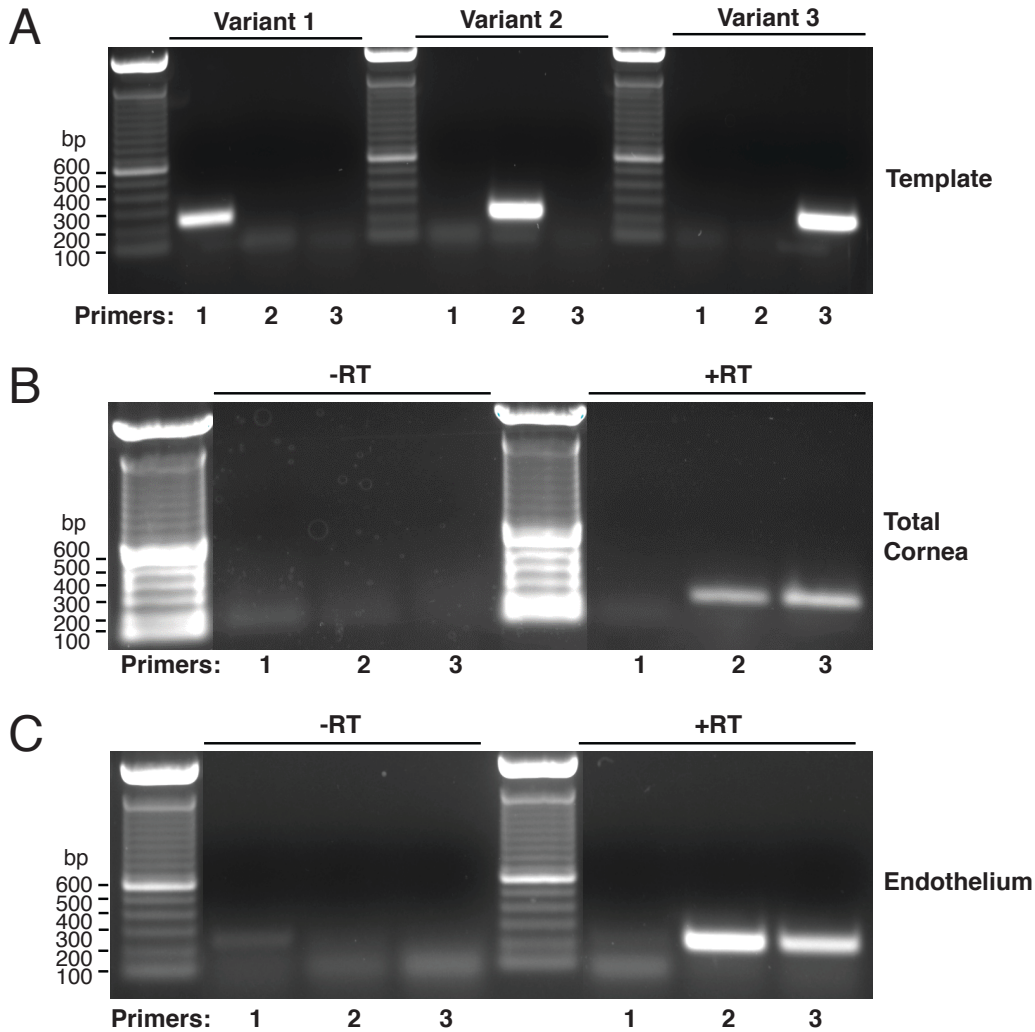


**Figure 3.2: Studying the expression of SLC4A11 transcripts in human cornea by RT-PCR.**

(A) Plasmid-cloned SLC4A11 v1, v2 and v3 were each used as a template with specific forward primers for v1, v2 and v3, respectively and a common reverse primer. PCR reaction was set up for 40 cycles, and total reaction mixture was loaded on a 1% agarose gel. (B-C) RNA isolated from total cornea and micro-dissected endothelial layer were subjected to reverse transcription reaction with (+RT) or without (-RT) enzyme. PCR was performed using cDNA template generated from (B) total cornea and (C) isolated endothelium, with forward primers corresponding to v1, v2 and v3 along with common reverse primer. Expected amplicon sizes were 244, 233 and 233 bp for v1, v2 and v3, respectively.

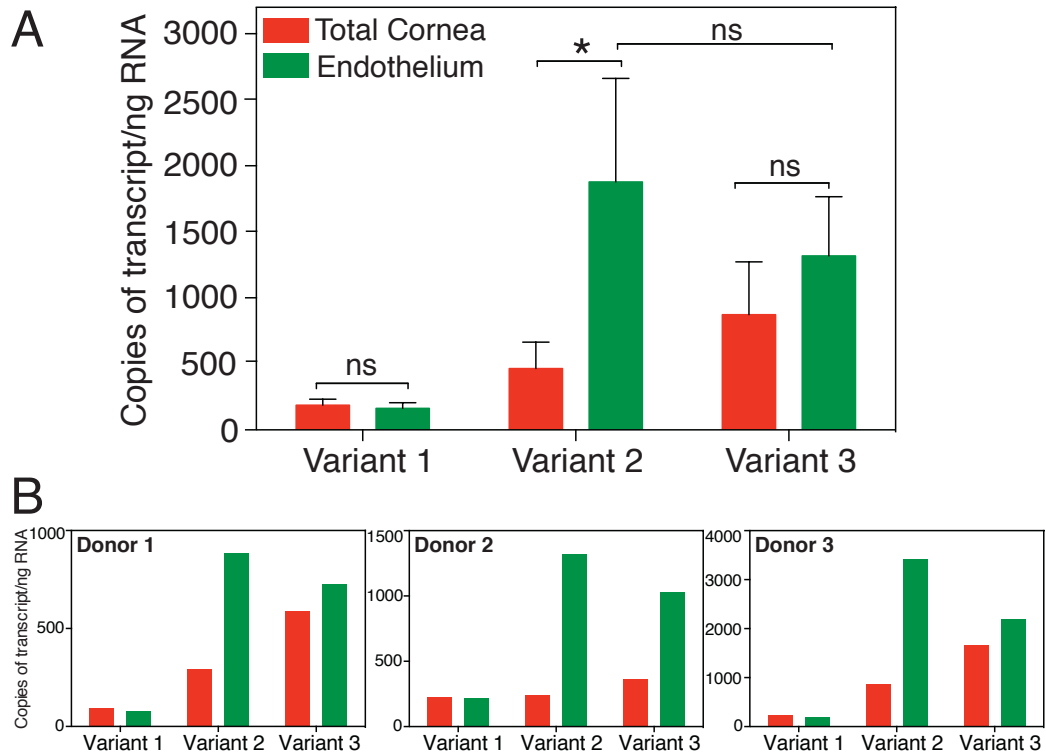


**Figure 3.3: Expression of SLC4A11 transcripts in human cornea assessed by quantitative PCR.**

qPCR was performed on cDNA from corneal endothelium and total cornea using iQ SYBR green mix along with forward and reverse primers for v1, v2 and v3 and GAPDH. Reactions were carried out for 40 cycles and fluorescence was recorded at each elongation step. Standard curve was constructed for each variant by using respective synthetic templates in the range of  $2.5 - 2.5 \times 10^4$  copies and plotting  $\text{Log}_{10}$  (template copies) against their  $C_T$  values. The sample  $C_T$  values were corrected to GAPDH for every experiment and number of copies of each variant was calculated, using their respective standard curves. Background (-RT control) values were subtracted from the samples. The average number of copies per ng RNA were plotted for each variant in corneal endothelium and total cornea for (A) pooled samples and (B) Individual donors. Data are presented as mean  $\pm$  SEM from three biological replicates (Two-way ANOVA and Sidak's multiple comparison test). \* $p=0.02$ , ns=not significant.

curves to enable comparisons of numbers of transcript copies present in each sample, for each SLC4A11 variant (Fig. 3.3A). This approach confirmed that there is little or no v1 expressed in human cornea. Expression of v2 was enriched in corneal endothelium, in comparison to total cornea. In contrast, there was no significant difference in v3 abundance between total cornea and endothelium. In endothelium samples, no significant difference was observed between v2 and v3 abundance. v2 expression in endothelium, however, was higher in each of the three human corneas analyzed when compared to v3 (Fig. 3.3B). Expression level differences between patients, however, led to standard error values, that failed to reach significance when values from the three corneas were pooled.

### **3.2.3 SLC4A11 v2 and v3 protein expression in human corneal endothelium**

RNA analysis revealed SLC4A11 v2 and v3 expression in human corneal endothelium. To examine expression of the translation products of these transcripts, we generated two antibodies against synthetic peptides corresponding to SLC4A11 amino acid sequences (Fig. 3.1E). Anti-SLC4A11-common antibody detects an epitope common to all three variants of SLC4A11 and anti-SLC4A11-v3 antibody detects the unique region in v3. On immunoblots, SLC4A11-common antibody detected HEK293 cell-expressed SLC4A11 v2 as well as variant 3 (Fig. 3.4A). Specificity of the SLC4A11-common antibody was indicated by the absence of signal in vector-transfected cells. Similarly, anti-SLC4A11-v3 antibody did not detect v2, although a faint non-specific band was visible at a molecular weight lower than v2 in transfected HEK293 cells (Fig. 3.4B, vector lane). Band sizes are consistent with their expected sizes (Fig. 3.1).

To quantify the abundance of v2 and v3 SLC4A11 in human corneal endothelium, corneal endothelial lysates pooled from six human corneas were processed on immunoblots. These samples were probed with the antibodies: anti-SLC4A11-common and anti-SLC4A11-v3. Both anti-SLC4A11-common and anti-SLC4A11-v3 revealed immunoreactive material consistent with

SLC4A11 (Fig. 3.4A-B). To quantify the absolute levels of v2 and v3 protein abundance in corneal endothelium, the following approach was used. Anti-SLC4A11-common detected both v2 and v3 proteins since they share the epitope for the antibody. Conversely, anti-SLC4A11-v3 detected only v3 protein since the epitope is unique to v3. We reasoned that the signal intensity observed for anti-SLC4A11-common antibody represents the sum of v2 and v3. We performed an experiment in which varied amounts of recombinant v3 SLC4A11 protein were detected with anti-SLC4A11-common and anti-SLC4A11-v3 antibodies (Fig. 3.4A-B). This enabled calibration of the efficiency of v3 protein detection by the two antibodies (Fig. 3.4C). Using this detection ratio, we converted the v3 signal from human endothelial cell lysate probed with anti-SLC4A11-v3 antibody, to the amount of signal that would arise using the anti-SLC4A11-common antibody. In this way, amount of v2 in lysate = total v2 detected by anti-SLC4A11-common antibody – (v3 protein detected by anti-SLC4A11-v3 antibody x detection ratio). From this analysis, v2 is about four times more abundant than v3 in human corneal endothelium (Fig. 3.4D).

### **3.2.4 Identification of SLC4A11 v2 translation start site in total human corneal lysates**

Bioinformatic analyses suggested the second methionine (M36) downstream of M1 as a potential start site on SLC4A11 v2 (Fig. 3.1C-D). To determine whether the translational product of SLC4A11 v2 starts at M1 or M36 in the human cornea, we generated an antibody called anti-SLC4A11-v2-M1 that detects “long” form of SLC4A11 v2 starting at M1. Anti-SLC4A11-v2-M1 was raised against a peptide corresponding to a specific region up stream of M36 (Fig. 3.1E, green). Lysates were prepared from human cornea and from HEK293 cells transfected with cDNA encoding v2-M1 or v2-M36 SLC4A11. These samples were probed on immunoblots with the antibodies: anti-SLC4A11-v2M1 and anti-SLC4A11-common. While anti-SLC4A11-v2M1 antibody only detected the HEK293 cell-expressed SLC4A11 v2 with the translation start site at

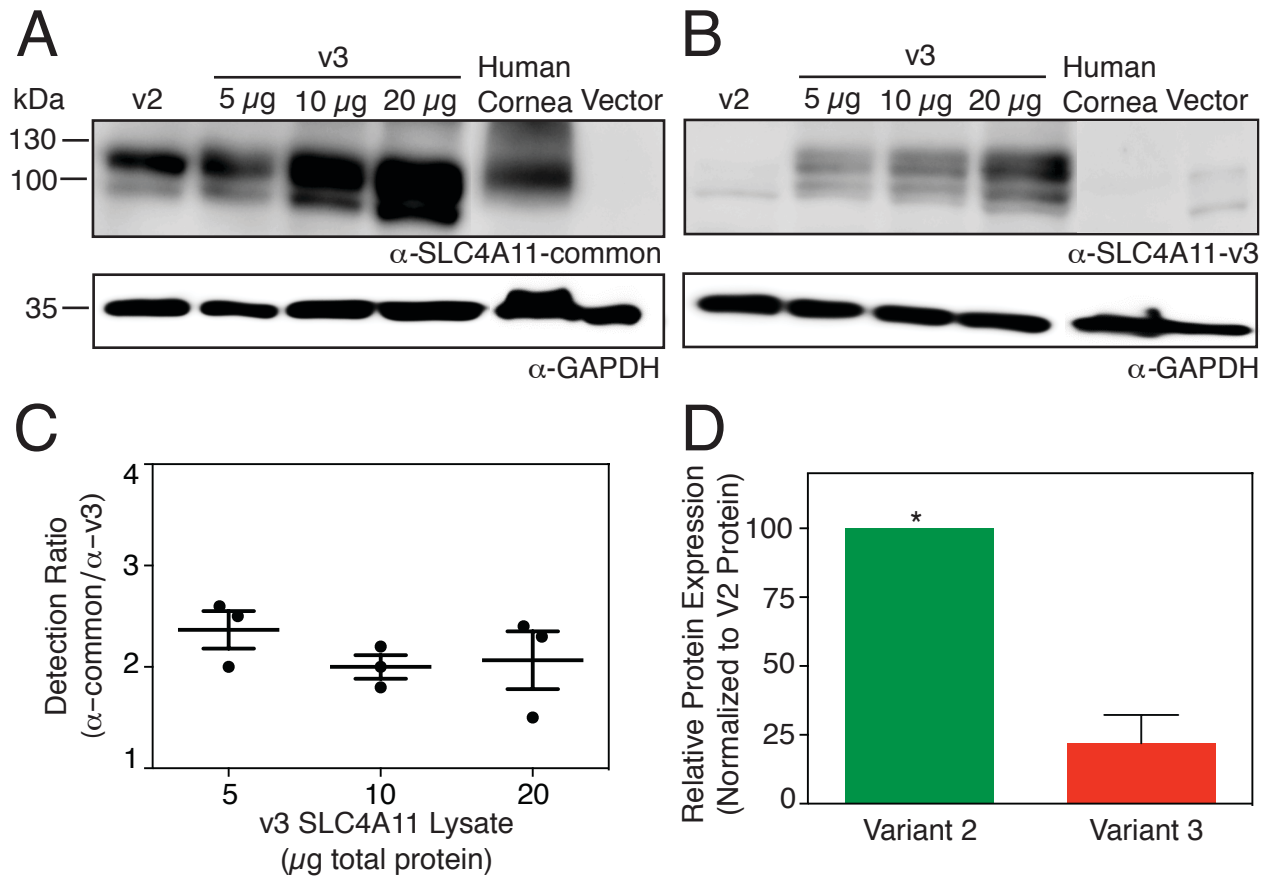


**Figure 3.4: SLC4A11 v2 and v3 expression in human corneal endothelium.**

Corneal endothelium was micro-dissected from six human corneas. Protein lysates from pooled human corneal endothelium (20  $\mu$ g protein) along with HEK293 cells transfected with cDNA encoding SLC4A11 v2 (10  $\mu$ g protein lysate), v3 (5, 10, 20  $\mu$ g protein lysates, indicated) and empty vector (20  $\mu$ g protein lysate) were processed for immunoblots. Blots were probed with **(A)** SLC4A11-common antibody and **(B)** SLC4A11-v3 antibody, along with GAPDH antibody as a loading control. **(C)** Densitometry quantified the B.I. Ratio of SLC4A11 band intensity from  $\alpha$ -SLC4A11-common and  $\alpha$ -SLC4A11-v3 antibodies was calculated for each amount of total lysate and plotted to establish Detection Ratio. **(D)** Data from each trial were normalized to SLC4A11 v2 abundance. Data represent mean  $\pm$  SEM from three replicates (Two-tailed t-test). \*p=0.005 when compared to v3.

M1 (Fig. 3.5A), SLC4A11-common antibody detected SLC4A11 v2 with translational start at M1 and M36 (Fig. 3.5B). Band sizes are consistent with the differences in their expected sizes (Fig. 3.1). Specificity of the antibody was confirmed in analysis of lysates from non-transfected (NT) cells. Importantly, the SLC4A11-common antibody detected a band in human corneal lysates, migrating at a position consistent with v2-M36 (Fig. 3.5B), while anti-SLC4A11-v2-M1 antibody did not detect immunoreactivity in corneal cell lysates (Fig. 3.5A). This indicates that the SLC4A11 v2 translation start site in the human cornea is at M36 and is consistent with bioinformatic analyses.

### **3.2.5 Plasma membrane localization of SLC4A11 v2-M1 and v2-M36.**

Until now, SLC4A11 v2 with M1 start site has been the focus of studies (Table 3.2)<sup>28,36,42,52,61,67,79,83,99,123,145</sup>. Data presented here indicate that for v2, M36, not M1, is the translational start site. The question thus arises: are these earlier reports valid? Do the properties of SLC4A11 differ depending on translational start site? We, therefore, compared the ability of these SLC4A11 variants to traffic to the cell surface and to facilitate transport function at the cell surface.

cDNA encoding SLC4A11 v2-M1 or v2-M36 were expressed in HEK293 cells. Cells were treated with membrane impermeant biotinylating reagent to measure the fraction of SLC4A11 at the cells surface. Total cell lysates were incubated with streptavidin resin to remove biotinylated protein, allowing the fraction of SLC4A11 biotinylated to be assessed from the difference between total and unbound (Fig. 3.6A). Examining the migration position of SLC4A11 v2-M1 and v2-M36 in total lysates reveals a clear difference in migration position (Fig. 3.6A), which indicates that M1 is preferentially used as translational start site over M36. Thus, earlier reports of SLC4A11 studied the protein starting at the M1 of variant 2, which does not exist in the cornea.

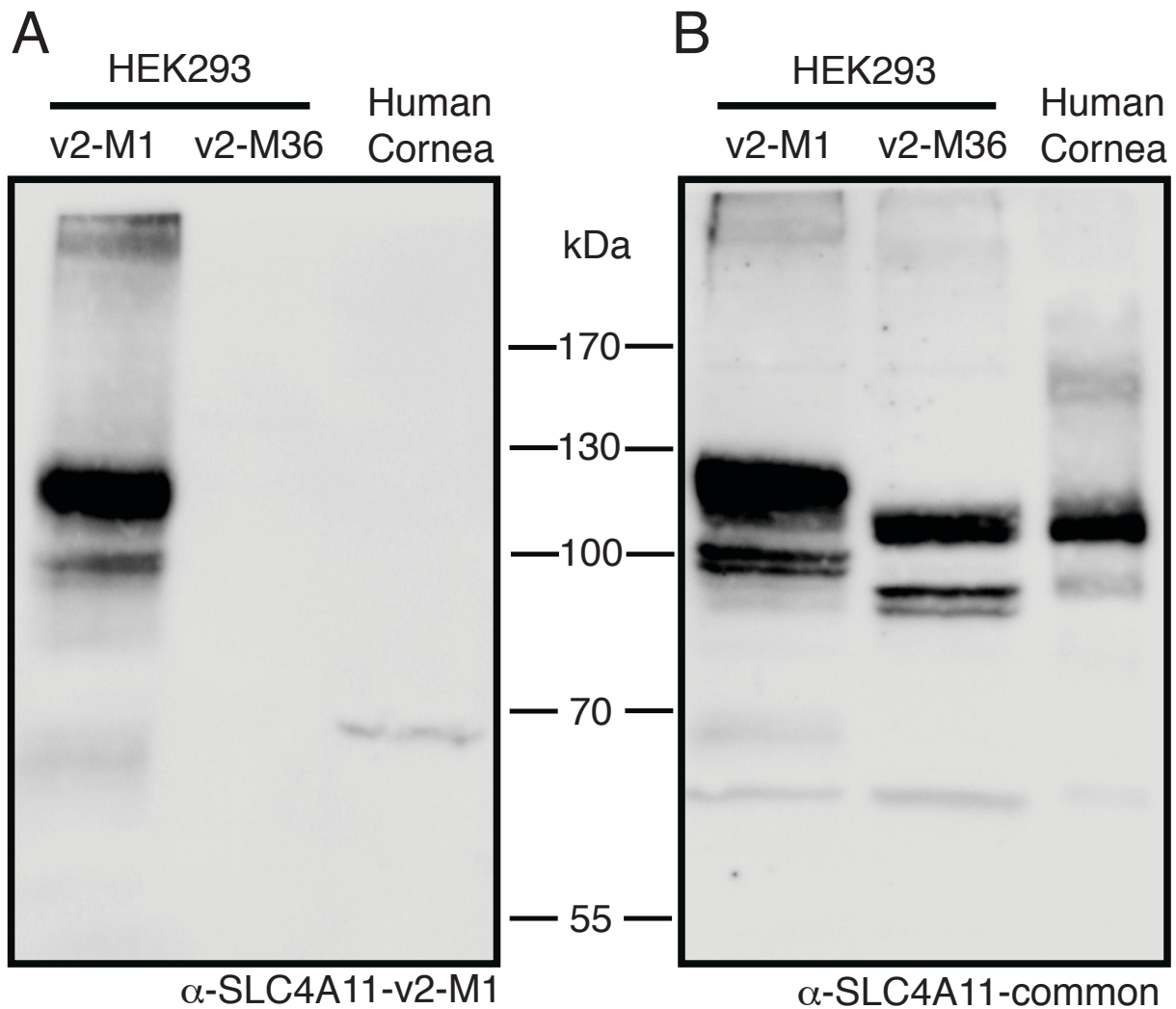


**Figure 3.5: Identification of SLC4A11 v2 translation start site in total human corneal lysates.**

HEK293 cells were transfected with cDNA encoding: SLC4A11 v2 starting at Met1 (SLC4A11 v2-M1) or SLC4A11 v2 starting at Met36 (SLC4A11 v2-M36). Whole human cornea samples were flash frozen with liquid nitrogen, crushed, solubilized and then combined with 2X SDS-Page sample buffer. Samples were electrophoresed on 7.5% acrylamide gels. Corresponding immunoblots were probed with antibodies (A) Anti-SLC4A11-v2-M1 and (B) Anti-SLC4A11-common.

The presence of two immune-reactive bands for SLC4A11 expressed in HEK293 cells has previously been attributed to an upper, mature-glycosylated form predominately present at the cell surface and a lower molecular weight form, receiving core glycosylation and associated with ER retention<sup>123</sup>. Cell surface biotinylation assays revealed no significant difference in cell surface trafficking of SLC4A11 v2 with M1 or M36 start site (Fig. 3.6B).

Plasma membrane localization of v2-M1 and v2-M36 SLC4A11 was further assessed by confocal immunofluorescence (Fig. 3.6C). Endogenous Na<sup>+</sup>-K<sup>+</sup>-ATPase was used as a plasma membrane marker. Indeed, pericellular staining was observed for Na<sup>+</sup>-K<sup>+</sup>-ATPase, consistent with its expected plasma membrane localization. Specificity of the SLC4A11-common antibody (Fig. 3.1E) was indicated by the absence of staining in vector-transfected cells (Fig. 3.6C). In cells expressing v2-M1 and v2-M36, SLC4A11 was detected with the SLC4A11-common antibody with pericellular and intracellular staining, consistent with plasma membrane and ER localizations, respectively. This staining pattern supports the conclusion from biotinylation assays that SLC4A11 protein, whether initiated at M1 or M36 does not affect the protein trafficking to the plasma membrane.

### **3.2.6 Osmotically driven water flux activity of SLC4A11 v2-M1 and v2-M36.**

A role of SLC4A11 N-terminal cytoplasmic domain in the transport function of the protein has been suggested<sup>79</sup>. Thus, variations at the SLC4A11 N-terminus might affect the protein's membrane transport function. SLC4A11 mediates accumulation of water into cells when exposed to hypo-osmotic challenge, whereas the cell surface trafficked mutant SLC4A11 R125H does not<sup>28</sup>. To assess water flux function, SLC4A11 N-terminal start site variants, v2-M1 and v2-M36 were expressed in HEK293 cells. Cells were co-transfected with eGFP. Immunoblots of cells used for water flux assays revealed similar levels of SLC4A11 expression for the two variants and as expected v2-M36 SLC4A11 migrated at a lower molecular weight than v2-M1 (Fig. 3.7A).

**Table 3.1: Review of Human SLC4A11 Variants used in studies from 2001-2019.**

Studies using different SLC4A11 variants since 2001 are listed below. Variant 1, variant 2 starting at first methionine (M1), variant 2 starting at second methionine (M36) and variant 3 are shown as v1, v2-M1, v2-M36 and v3, respectively.

<b>SLC4A11 Variant used</b>	<b>Literature Citations</b>
v1	Zhang <i>et al.</i> (2015) <sup>67</sup>
v2-M1	Parker <i>et al.</i> (2001) <sup>70</sup> , Park <i>et al.</i> (2004) <sup>142</sup> , Vithana <i>et al.</i> (2006) <sup>36</sup> , Riazuddin <i>et al.</i> (2010) <sup>96</sup> , Vilas <i>et al.</i> (2011) <sup>145</sup> , Vilas <i>et al.</i> (2012) <sup>123</sup> , Jalimarada <i>et al.</i> (2013) <sup>61</sup> , Vilas <i>et al.</i> (2013) <sup>28</sup> , Ogando <i>et al.</i> (2013) <sup>83</sup> , Loganathan <i>et al.</i> (2014) <sup>52</sup> , Soumittra <i>et al.</i> (2014) <sup>99</sup> , Roy <i>et al.</i> (2015) <sup>148</sup> , Loganathan <i>et al.</i> (2016) <sup>79</sup> , Kao <i>et al.</i> (2016) <sup>91</sup> , Guha <i>et al.</i> (2017) <sup>149</sup> , Li <i>et al.</i> (2019) <sup>144</sup>
v2-M36	Chiu <i>et al.</i> (2016) <sup>92</sup> , Loganathan <i>et al.</i> (2016) <sup>140</sup> , Badior <i>et al.</i> (2017) <sup>80</sup> , Alka <i>et al.</i> (2018a) <sup>143</sup> , Alka <i>et al.</i> (2018b) <sup>150</sup>
v3	Kao <i>et al.</i> (2015) <sup>66</sup> , Kao <i>et al.</i> (2016) <sup>91</sup>

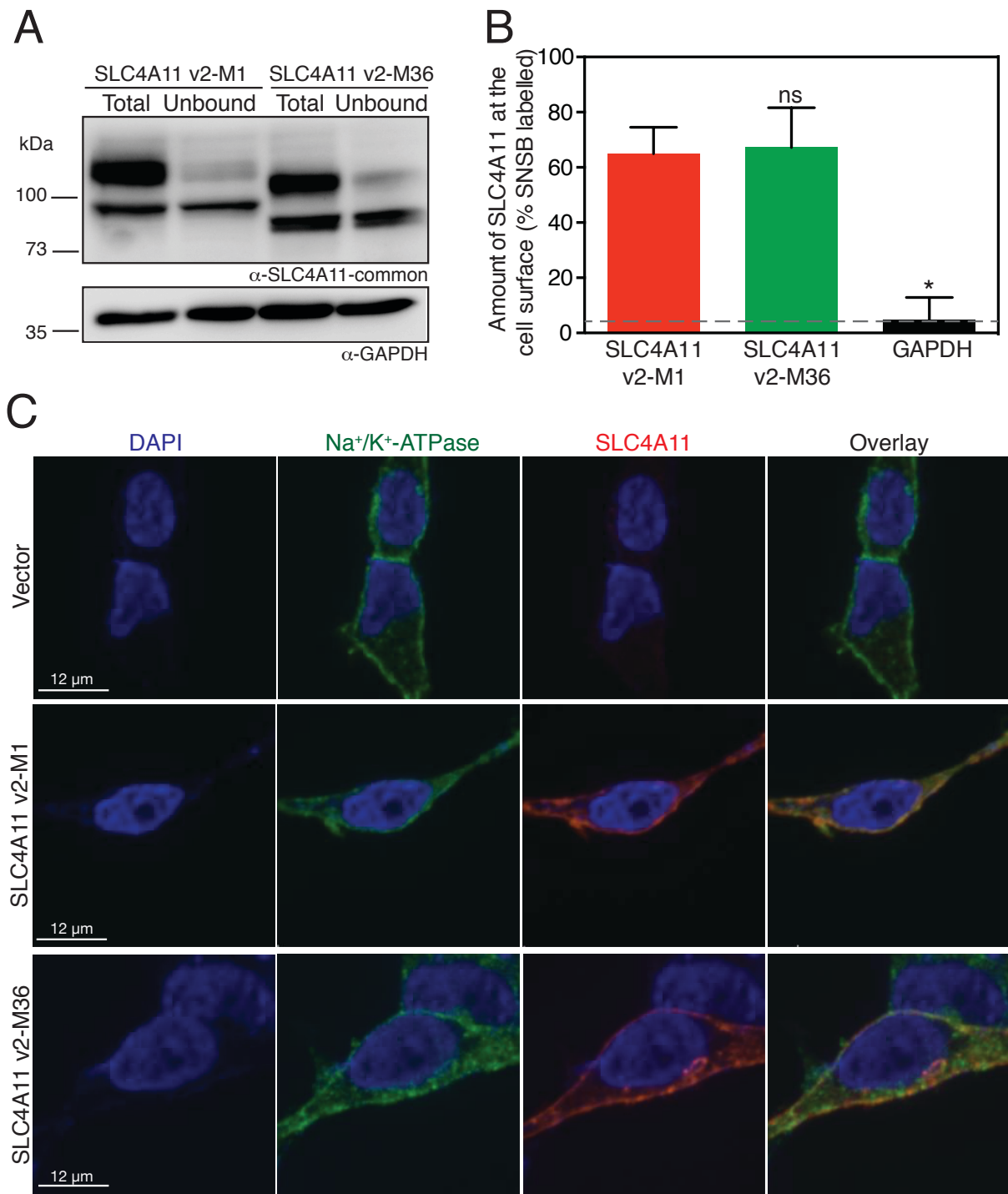


**Figure 3.6: Plasma membrane localization of SLC4A11 v2-M1 and v2-M36.**

HEK293 cells were transfected with cDNA encoding SLC4A11 v2-M1 or SLC4A11 v2-M36 as shown. **(A)** Cells were labeled with membrane-impermeant Sulfo-NHS-SS-biotin (SNSB) and the

cell lysates were divided into two equal fractions. One was incubated with streptavidin resin to remove biotinylated proteins. The unbound fraction (U) and the total cell lysate (T) were probed with SLC4A11-common antibody on immunoblots. GAPDH was used as an internal control. **(B)** The fraction of SLC4A11 and GAPDH labeled by SNSB was calculated. Dashed line indicates the background for this assay, as indicated by labeling of GAPDH. Data represent mean  $\pm$  SEM from five replicates (One-way ANOVA with Sidak's multiple comparisons test). \* $p < 0.0001$  when compared to SLC4A11 v2-M1, ns=not significant. **(C)** Cells were processed for immunofluorescence and images were collected by confocal microscopy (scale bars indicated in each row). Nuclei were detected with DAPI staining (blue). SLC4A11 was detected with SLC4A11-common antibody and chicken anti-rabbit IgG conjugated with Alexa Fluor 594 (red). Plasma membrane marker, Na<sup>+</sup>/K<sup>+</sup>-ATPase was detected with anti-Na<sup>+</sup>/K<sup>+</sup>-ATPase and Chicken anti-mouse Alexa Fluor 488 (green). Overlay represents merged images from all three channels.

The relative amount of cell lysate was revealed as similar by the intensity of GAPDH present. Cell lysates also expressed similar levels of transfected eGFP (Fig. 3.7A).

To assess the capacity of SLC4A11 variants to mediate a water flux, transfected cells were placed on a perfusion chamber on the stage of a confocal microscope. Cells were initially perfused with iso-osmotic medium, followed by hypo-osmotic medium. The level of green fluorescence in a region of interest of the cytosol was monitored, as a surrogate for cell volume (Fig. 3.7B). Exposure to hypo-osmotic medium induced cell volume increase, as indicated by a dilution of eGFP fluorescence intensity. The initial rate of cell volume increase (decrease of eGFP fluorescence) was quantified following shift to hypo-osmotic medium (Fig. 3.7C). Vector-transfected cells swelled at a rate significantly slower than SLC4A11-transfected cells. The rate of cell swelling was, however, not significantly different between cells expressing the v2-M1 and v2-M36 forms of SLC4A11. This indicates that SLC4A11 functional activity is unaltered between whether translation begins at M1 or M36.

### **3.2.7 Functional and structural differences between v2-M36 and v3-SLC4A11**

We next looked at the functional and structural differences between the two SLC4A11 variants of human corneal endothelium: v2-M36 and v3. We performed assays of osmotically driven water flux as described. No significant differences in water flux were found between HEK293 cells expressing v2-M36 and v3 (Fig. 3.8), suggesting the unique amino acids in v3 do not affect transport function.

To assess the structural differences between v2-M36 and v3, we created structural homology models for the cytoplasmic domains of v2-M36-SLC4A11 (M36-Y340) and v3-SLC4A11 (M1-Y359,) using the crystal structure of human erythrocyte Band 3 (SLC4A1) cytoplasmic domain (PDB: 1HYN) as the template<sup>130</sup>.

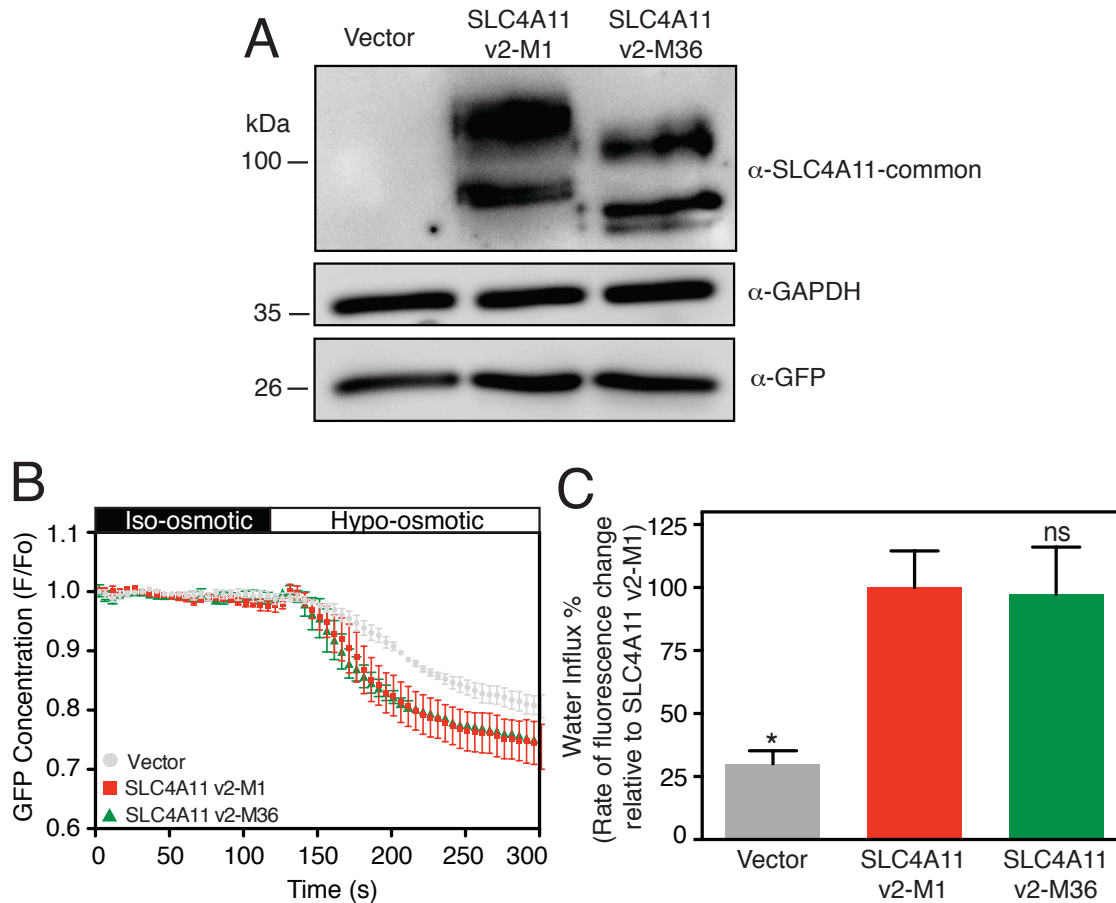


**Figure 3.7: Osmotically driven water flux activity of SLC4A11 v2-M1 and v2-M36.**

HEK293 cells were transiently transfected with peGFP-C1 along with empty vector or SLC4A11 v2-M1 or SLC4A11 v2-M36 cDNA. **(A)** After performing water flux assays, cells from the same dishes were lysed and probed on immunoblots, using SLC4A11-common antibody to detect the expression of SLC4A11 variants. GAPDH and eGFP were also detected using respective antibodies. **(B)** HEK293 cells transfected with v2-M1 or v2-M36 cDNA were perfused alternately with iso-osmotic (black bar) and hypo-osmotic (white bar) media. eGFP fluorescence (F) was normalized to F averaged for time 0-120 seconds ( $F_0$ ) and  $F/F_0$  plotted. **(C)** Rate of fluorescence change (a surrogate for cell volume change) was calculated. Data represent mean  $\pm$  SEM from 6-8 independent coverslips with 8-10 cells measured per coverslip (One-way ANOVA with Sidak's multiple comparisons test) \* $p < 0.0001$  when compared to SLC4A11 v2-M1, ns=not significant.

Earlier analysis indicated that SLC4A11 cytoplasmic domain had the same fold as Band 3<sup>79</sup>. Two different models were generated for each variant using Iterative Threading Assembly Refinement (I-TASSER)<sup>125</sup> and Protein Homology/Analogy Recognition Engine V 2.0 (Phyre<sup>2</sup>)<sup>124</sup>. Homology models predicted through I-TASSER (Fig. 8) had estimated TM-score of  $0.44 \pm 0.14$  (v2-M36) and  $0.41 \pm 0.14$  (v3) and estimated RMSD of  $12.0 \pm 4.4$  Å (v2-M36) and  $12.9 \pm 4.2$  Å (v3). While the two structures had a common fold at their C-termini, the N-termini had significant differences (Fig. 3.9C). The N-terminal loops of each variant are almost 180° apart. The unique sequence at the v3 N-terminus (M1-T19, highlighted in pink), however, is surface exposed, enabling a role in protein-protein interaction. Homology models generated by Phyre<sup>2</sup> revealed large differences in the N-terminal region of the two variants with a common conserved C-terminal fold (Fig. 3.10). Although these models highlight potential functional differences of the two variants, their N-termini were modeled with low confidence.

Computational predictions of eukaryotic phosphorylation sites in the unique N-terminal region of v3 (M1-T19) were performed using NetPhos 3.1<sup>151</sup> with a cut-off score of 0.8. Threonine at position 5 (N-MAAA**T**RRRVFHLQPC-C) was predicted as a potential phosphorylation site for Protein Kinase C (PKC) with high score (0.887). PKC is crucial in CEnC proliferation and cell cycle<sup>152</sup>. v3-SLC4A11 could be specifically phosphorylated at Thr5 as part of CEnC proliferative regulation.

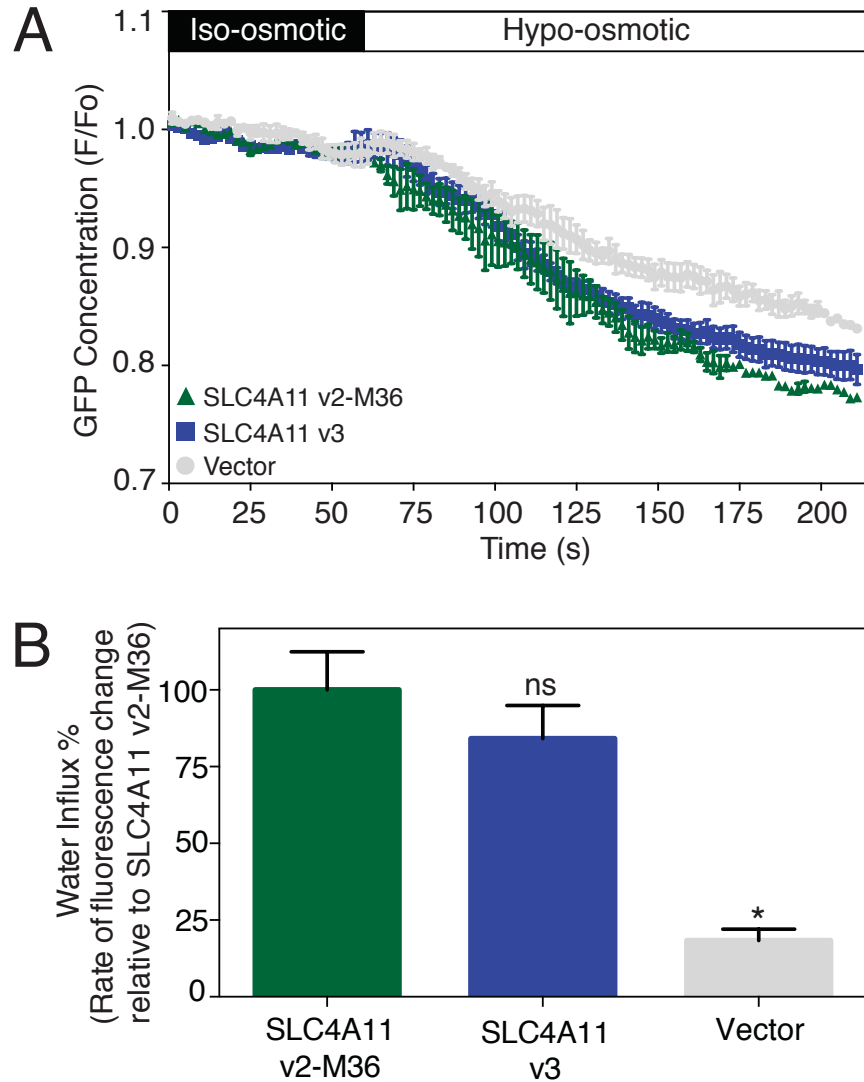


**Figure 3.8: Osmotically driven water flux activity of SLC4A11 v2-M36 and v3.**

HEK293 cells were transiently transfected with peGFP-C1 along with empty vector or SLC4A11 v2-M36 or SLC4A11 v3 cDNA. **(A)** Cells were perfused alternately with iso-osmotic (black bar) and hypo-osmotic (white bar) media. eGFP fluorescence (F) was normalized to F averaged for time 0-60 seconds ( $F_0$ ) and  $F/F_0$  plotted. **(B)** Rate of fluorescence change was calculated. Data represent mean  $\pm$  SEM from 4-6 independent coverslips with 12-18 cells measured per coverslip (One-way ANOVA with Sidak's multiple comparisons test) \* $p < 0.0001$  when compared to SLC4A11 v2-M36, ns=not significant.

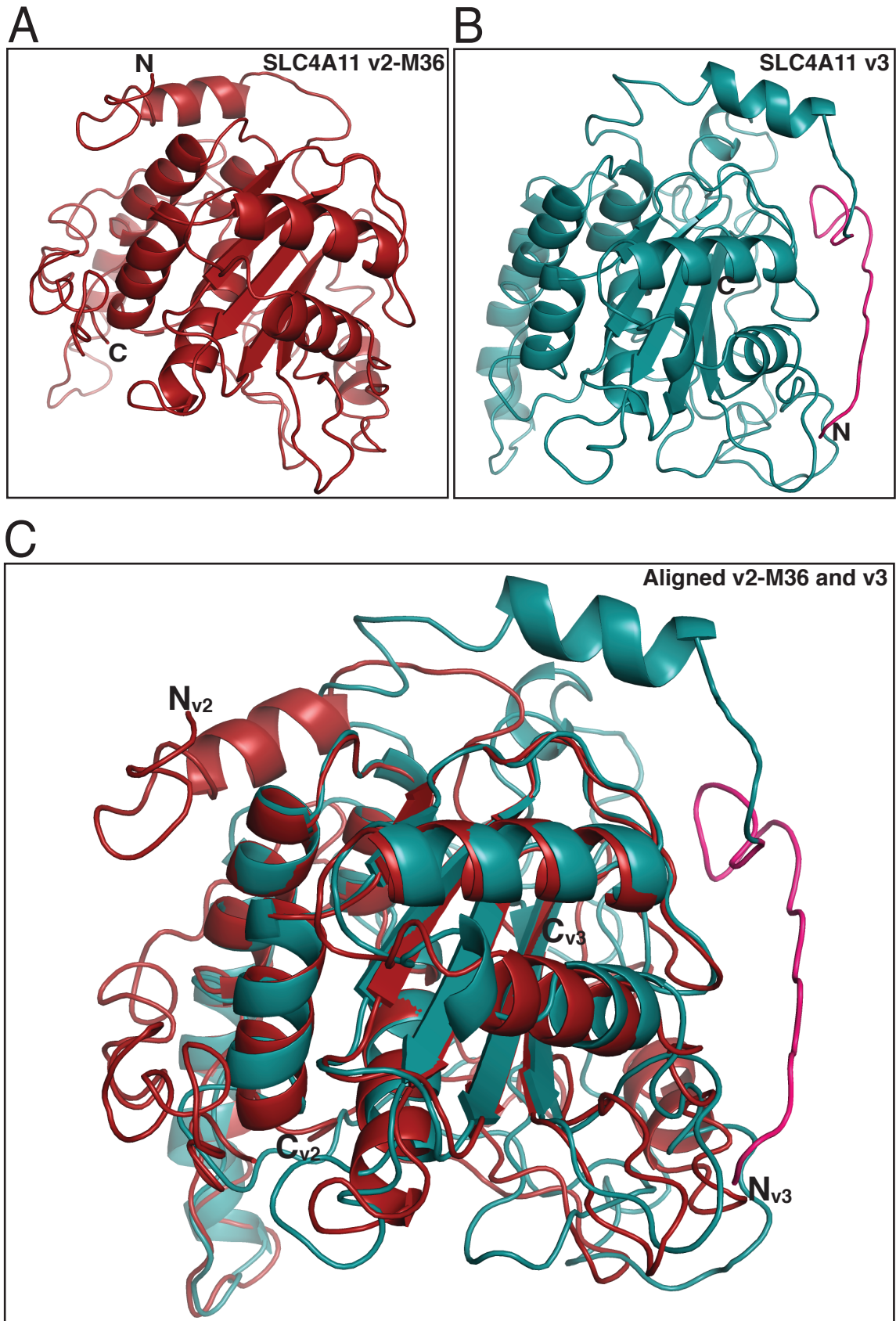


**Figure 3.9: Homology model of SLC4A11 v2-M36 and SLC4A11 v3 cytoplasmic domains.**

Homology models of cytoplasmic domains of (A) SLC4A11 v2-M36 (M36-Y340) and (B) SLC4A11 v3 (M1-Y359) generated by I-TASSER using crystal structure of human erythrocyte Band 3 cytoplasmic domain (PDB: 1HYN) as the template. Unique N-terminal sequence of v3 is highlighted in pink. (C) v2-M36 and v3 models aligned in PyMOL (molecular graphics system version 2.0.7), using segments that were modelled with 100% confidence (R90-P306 for v2-M36, R109-P325 for v3). N<sub>v2</sub>, N<sub>v3</sub> and C<sub>v2</sub>, C<sub>v3</sub> are the N and C termini for v2-M36 and v3, respectively.

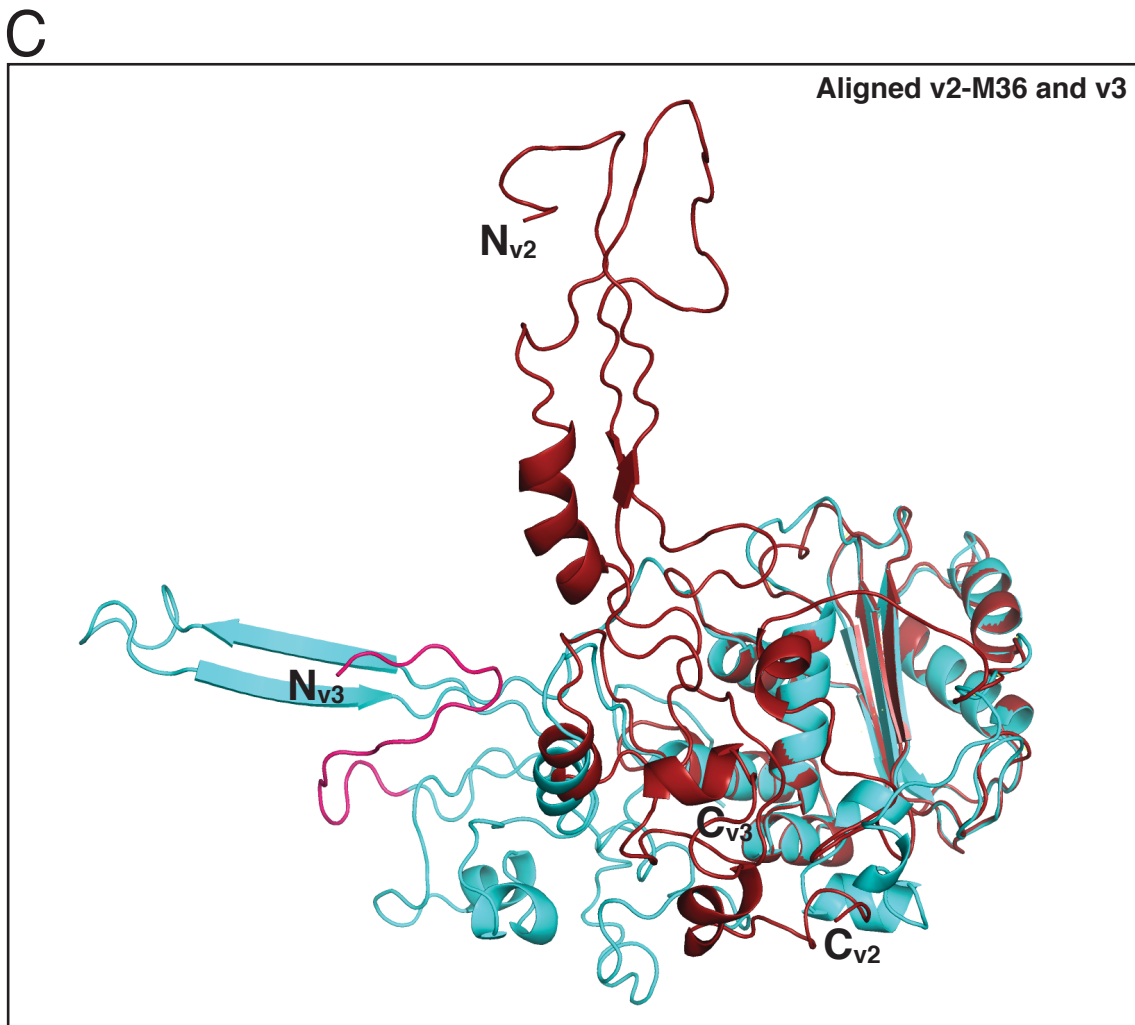
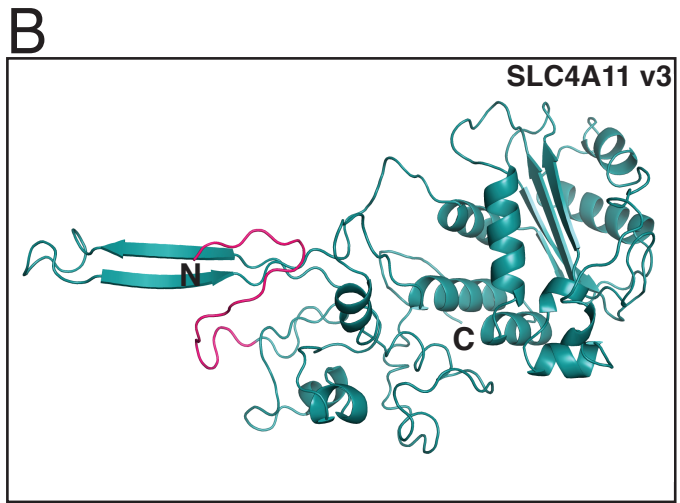
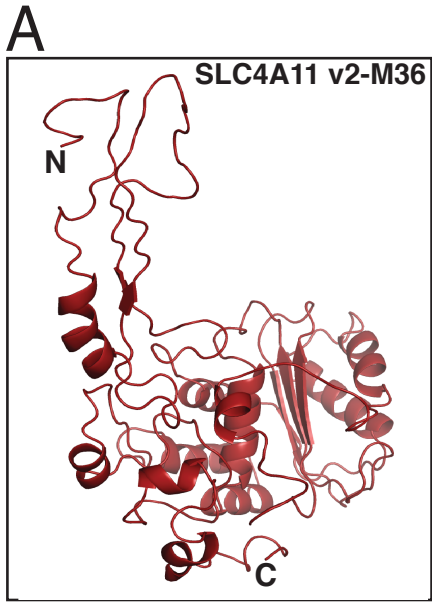


***Figure 3.10: Alternative homology model of SLC4A11 v2-M36 and SLC4A11 v3 cytoplasmic domains.***

Homology models of cytoplasmic domains of **(A)** SLC4A11 v2-M36 and **(B)** SLC4A11 v3 generated by Phyre2 fold recognition software, using crystal structure of human erythrocyte Band 3 cytoplasmic domain (PDB: 1HYN) as the template. Unique N-terminal sequence of v3 is highlighted in pink. **(C)** v2-M36 and v3 models aligned in PyMOL (molecular graphics system version 2.0.7), using segments that were modelled with 100% confidence (R90-P306 for v2-M36, R109-P325 for v3).  $N_{v2}$ ,  $N_{v3}$  and  $C_{v2}$ ,  $C_{v3}$  are the N and C termini for v2-M36 and v3, respectively.

### 3.3 Discussion

This study used bioinformatic, transcriptomic and protein level analyses to identify the SLC4A11 translational product in human cornea. Bioinformatic analysis predicted SLC4A11 v2 starting at Met36 to share highest nucleotide and amino acid sequence conservation with SLC4A11 from other mammals. RT-PCR and qRT-PCR further revealed the presence of only v2 and v3 transcripts in human cornea and the endothelium, where variant 2 is the predominant transcript in the endothelium. Protein analysis showed the predominance of v2 protein in the endothelium when compared to v3. Further, antibodies targeting v2-M1 and v2-M36 SLC4A11 confirmed the presence of SLC4A11 v2-M36 in the human cornea. Homology models of the cytoplasmic domains of v2-M36 and v3 displayed large differences in the N-termini of both variants with a common c-terminal fold. No differences were, however, observed in the water flux function of these variants. Data here support that v2-SLC4A11, with translation start at the transcript's second Met is the predominant SLC4A11 protein of human corneal endothelium, although the v3 variant is present at a significant level. No difference in cell surface trafficking or transport function could be detected arising from differences in the N-terminal region of SLC4A11.

Using custom-designed antibodies, we found v2 to be four-times more abundant than v3 in the human corneal endothelium. We also found higher v2 abundance than v3 at the transcript level with negligible v1 in the cornea. Mass spectrometry, unfortunately, was unable to differentiate between v2 and v3 in the human cornea due to the absence of specific tryptic sites in the short unique N-terminal region of v3-SLC4A11. An earlier study found SLC4A11 v3 to be the predominant corneal endothelial SLC4A11 transcript<sup>66</sup>, however, the source of the endothelial mRNA used was unclear and extraction method was not described. Additionally, the earlier study did not analyze the variants at the protein level.

Variant 2 in human cornea has an alternative start site at methionine 36 (v2-M36) but most studies of SLC4A11 variant 2 have used the protein starting at methionine 1 (v2-M1) (Table 3.2). We did not find significant difference in the cell surface abundance of the v2-M36 vs v2-M1. The N-terminal cytoplasmic domain of SLC4A11, however, is required for its transport function<sup>79</sup>. Since we did not observe a difference of SLC4A11 water flux function between SLC4A11 v2 starting at M1 or M36, earlier functional studies of SLC4A11 v2-M1 are likely reliable. Our recent studies have used SLC4A11 v2-M36 after being identified as the relevant isoform to be studied in the cornea (Table 3.2). Only one study mentions the use of SLC4A11 v1<sup>67</sup> for functional analyses (Table 3.2).

The presence of SLC4A11 v2-M36 and v3 in the cornea suggests unique functional roles of the two variants. Homology models of their respective cytoplasmic domains revealed large differences in the N-terminal region of the variants. The location of the unique region of v3-SLC4A11 (Fig. 3.9B-C) on the surface of the cytoplasmic domain is consistent with a role in protein-protein interaction. Potential phosphorylation sites in the unique region of v3 further suggests a role in protein-protein interaction and modulation by regulatory pathways. No functional differences were, however, found in osmotically driven water flux functions between the two variants. Other SLC4A11 substrates, H<sup>+</sup>/OH<sup>-</sup>/NH<sub>3</sub>, remain to be tested to explain the presence of two N-terminal splice variants of SLC4A11 in human cornea.

Studying the physiologically relevant form of SLC4A11 is crucial for future investigations of SLC4A11, in particular of molecular therapeutics. Our data indicate that SLC4A11 Variant 2 starting at Met36 is the principal variant of human corneal endothelium, but variant 3 also contributes to SLC4A11's role in corneal biology to a lesser extent.

---

## **Chapter 4: Defective Cell Adhesion Role of Solute Transporter, SLC4A11, in Endothelial Corneal Dystrophies**

---

A version of this paper has been submitted for publication as Darpan Malhotra, Martin Jung, Claudia Fecher-Trost, Matthew Lovatt, Gary S.L. Peh, Sergei Noskov, Jodhbir S. Mehta, Richard Zimmermann and Joseph R. Casey. Defective Cell Adhesion Function of Solute Transporter, SLC4A11, in Endothelial Corneal Dystrophies.

All experiments were performed by Darpan Malhotra except mass spectrometry (Table 4.1, Fig. 4.8) performed by Martin Jung and Claudia Fecher-Trost, Three-dimensional molecular dynamics experiments (Fig. 4.6) performed by Sergei Noskov, isolation and culture of primary HCEnc by Gary S.L. Peh and real-time PCR (Fig. 4.9B) was performed by Matthew Lovatt.

## 4.1 Introduction

Adhesion to underlying ECM layer is critical to the organization and polarity of epithelial and endothelial cell layers<sup>153</sup>. The cornea's innermost region is an endothelial cell monolayer that adheres to its ECM, the DM<sup>29</sup>. DM is a two dimensional highly structured array of ECM proteins secreted by CEnC, where COL8A1 and COL8A2 are its two principal proteins<sup>34</sup>. In genetic ECD, corneal endothelial function is disrupted, in some cases by increased rates of CEnC loss from the DM<sup>29</sup>. Mutations of the solute carrier protein, SLC4A11, cause rare, recessive CHED<sup>36,138</sup> (CHED; OMIM# 217700) and some cases of common, dominant FECD<sup>42</sup> (FECD; OMIM# 613268). However, the effect of these mutations on CEnC loss is unclear. Here we report SLC4A11 as a CAM in human CEnC, the first solute carrier (SLC) protein found with this function, which interacts with principal DM proteins COL8A1 and COL8A2. We identified SLC4A11 point mutations that can cause FECD by impairing SLC4A11 adhesion activity, while leaving transport activity intact. SLC4A11 CAM activity underscores the importance of cell adhesion in ECD and points towards a therapeutic direction.

SLC4A11 is a unique member of the SLC4 family of bicarbonate transport proteins, as it is not a bicarbonate transporter<sup>63,64</sup>. SLC4A11, localized at the basolateral surface of CEnC, contributes to osmotically-driven water flux from the stroma to aqueous humor to maintain corneal fluid-balance<sup>28</sup>. SLC4A11 also transports OH<sup>-</sup>/H<sup>+</sup><sup>63-66</sup> and NH<sub>3</sub><sup>63,67</sup>. SLC4A11 has a two-domain structure with a 41 kDa cytoplasmic domain and a 57 kDa integral membrane domain comprised of 14 transmembrane segments<sup>80</sup>. Prominent in the membrane domain is the large third extracellular loop, containing two sites of N-linked glycosylation.

SLC4A11 mutations cause some ECD<sup>36,42</sup>, one of the most common causes of visual impairment and corneal blindness worldwide<sup>154</sup>. ECD have a variable clinical presentation, often including progressive and painful corneal edema, increased rates of CEnC loss and focal

thickening of DM, with the formation of button-like DM excrescences called guttae<sup>29</sup>. Sixty ECD-causing point mutations have been found throughout SLC4A11, without obvious pattern<sup>89</sup>.

FECD and CHED arise from SLC4A11 mutations<sup>36,42</sup>. FECD is a progressive dominant disorder, which becomes symptomatic in the fourth to fifth decade of life, while CHED has a recessive mode of inheritance with symptoms evident at birth or within the first few years<sup>29</sup>. While CHED is rare, FECD regionally affects 4-12% of the North-American population above the age of 40 years and is the leading cause of corneal transplantation across the world. In addition to SLC4A11 mutations, FECD is also caused by alterations in the genes: COL8A2<sup>35</sup>, TCF4<sup>43</sup>, ZEB1<sup>44</sup>, AGL1<sup>45</sup> and LOXHD1<sup>46</sup>. KANK4, LAMC1 and ATP1B1 have also been implicated in the pathogenesis FECD in a GWAS<sup>47</sup>. In contrast, CHED is caused only by SLC4A11 mutations<sup>57</sup>.

SLC4A11 mutations cause two molecular defects: folding defects leading to ER retention of the protein, and impaired membrane transport function. About half of the ECD burden from SLC4A11 mutations arises from SLC4A11 retention in the ER. Defective transport activity has been identified in four SLC4A11 mutants<sup>28,155</sup>.

We considered whether SLC4A11 has a critical role beyond membrane transport. Ablation of the mouse *slc4a11* gene leads to corneal edema and disruption of CEnC packing, reminiscent of that seen in ECD patients<sup>107</sup>. This suggests that loss of SLC4A11 function, rather than toxic gain of function, underlies the pathology associated with SLC4A11 mutations. The third, large extracellular loop (EL3) of SLC4A11 contains four FECD mutations<sup>42,96</sup>, but has not been associated with any functional role. Indeed, introducing epitope tag sequences into EL3 did not affect SLC4A11-mediated water flux<sup>92</sup>, suggesting the region is not required for membrane transport. SLC4A11 is one of the most highly-expressed genes of CEnC<sup>72,73</sup>. Finally, Band 3 (SLC4A1), another member of the SLC4 family, is the most abundant protein of the erythrocyte membrane (50% of total)<sup>156</sup>. Through its cytoplasmic domain, Band 3 interacts with ankyrin, which in turn binds the underlying spectrin-actin cytoskeleton to maintain the biconcave erythrocyte

shape<sup>157</sup>. We thus considered whether SLC4A11, a highly abundant SLC4 protein of CEnC basolateral membrane, may serve as a CAM to anchor CEnC to their basement membrane, DM. Loss of endothelial (epithelial) cell attachment leads to anoikis, a specific form of programmed cell death<sup>158,159</sup>. Defective SLC4A11-DM attachment could thus explain increased cell death in FECD patients. Further, loss of endogenous SLC4A11 expression in HCEnc when removed from their native environment (DM)<sup>73,160,161</sup> also suggests an association between SLC4A11 and DM.

To explore a role of SLC4A11 in cell adhesion, we developed a high throughput *in vitro* cell adhesion assay on 96 well dishes coated with DM extract. An antibody against the SLC4A11 third extracellular loop probed the importance of this region in DM-binding. Affinity chromatography combined with mass spectrometry revealed SLC4A11 binding partners in DM. De novo modelling with ROSETTA-Membrane followed by Temperature Replica-Exchange Molecular Dynamics simulations provided a three-dimensional structural model for the SLC4A11 region we found to bind DM. Primary explanted human CEnC were used to quantify cell adhesion. A small chimeric protein was created using SLC4A11-EL3 as a potential therapeutic to restore cell adhesion. Together, data here reveal that SLC4A11 mediates adhesion to DM and its disease-causing mutations compromise this activity to cause ECD.

## 4.2 Results

### 4.2.1 Role of SLC4A11 in cell adhesion to DM

We tested the ability of HEK293 cells to bind to DM extracts coated onto 96 well dishes. HEK293 cells co-expressing eGFP and SLC4A11 or AE1 (SLC4A1) or pcDNA3.1 (empty vector) were grown on DM-coated or uncoated dishes. Cells associated with dishes were quantified by measuring GFP fluorescence before and after loosely/non-adhering cells were removed by inverted centrifugation. Fractional cell adhesion was quantified by measuring the ratio of GFP fluorescence before and after disruption. Adhesion of SLC4A11-expressing cells to DM-coated wells was much higher than to uncoated wells (Fig. 4.1A). AE1 (SLC4A1), a member of SLC4 family of bicarbonate transporters, has 40% similarity to SLC4A11 in the membrane domain<sup>80</sup>. Cells transfected with empty vector or cDNA encoding AE1 adhered to an extent not significantly different whether grown on DM-coated, or uncoated dishes (Fig. 4.1A). This suggests that SLC4A11 has a role in cell adhesion to DM that is not conserved across other SLC4 family members.

To further probe the interaction of SLC4A11 with DM components, we performed a competition binding experiment. We reasoned that if SLC4A11 interacts with DM, pre-incubation with free DM components would prevent adhesion to DM-coated dishes. SLC4A11 and vector-transfected cells were pre-incubated with increasing amounts of DM extract and excess DM was removed by centrifugation. Cell adhesion assays on DM-coated dishes without competing DM extract revealed that SLC4A11-transfected cells adhered to a much higher extent than the vector-transfected cells (Fig. 4.1B). Pre-incubation with DM extract, however, decreased adhesion of SLC4A11-expressing cells in proportion to the amount of DM in competition. Adhesion of vector-transfected cells was unaffected by pre-incubation with DM extract. These data support an interaction between SLC4A11 and DM to promote cell adhesion.

To test if cell adhesion depends on SLC4A11 expression, HEK293 cells were co-transfected with peGFP-C1 and varied amounts of SLC4A11 cDNA. Cell adhesion increased with SLC4A11 expression and was saturable (Fig. 4.1C-D). Cell adhesion thus depended on the amount of SLC4A11 expressed and reached a maximum, consistent with specific binding.

To test if the SLC4A11-mediated adhesion is conserved across mammals, we expressed human, bovine or murine SLC4A11 in HEK293 cells. On immunoblots, human, bovine and murine proteins migrate at their respective molecular weights and accumulate to comparable levels (Fig. 4.2A). The proteins migrated as two bands, previously ascribed to immaturely-glycosylated protein (lower band), resident in the ER, and mature-glycosylated protein (upper band) found at the plasma membrane<sup>77</sup>. In cell adhesion assays, the bovine and murine SLC4A11 proteins promoted cell adhesion to DM to similar levels as the human protein (Fig. 4.2B). Vector transfected cells had significantly lower adhesion than cells expressing SLC4A11 from all the species. A role in cell adhesion is a shared attribute across mammalian SLC4A11 proteins.

#### **4.2.2 Characterization of SLC4A11 extracellular loop 3 as the DM adhesion site**

What part of SLC4A11 binds DM? If the interaction is direct, the region must be able to extend from the cell surface to DM. EL3 is the largest extracellular loop of SLC4A11, on the basis of a structural model prepared by homology to the SLC4A1 (Band 3) crystal structure<sup>80,130</sup>. The presence of four FECD-causing point mutations in EL3 (Fig. 4.3A) further suggested involvement in DM adhesion. We raised an antibody against a 14-amino acid sequence in EL3 that was predicted to be antigenic (Fig. 4.3A). SLC4A11 and vector-transfected cells were pre-incubated with pre-immune and immune serum and subjected to cell adhesion assays on DM-coated plates. SLC4A11-transfected cells had significantly higher adhesion than vector-transfected cells when treated with pre-immune serum (Fig. 4.3B). Immune serum, however, suppressed adhesion of

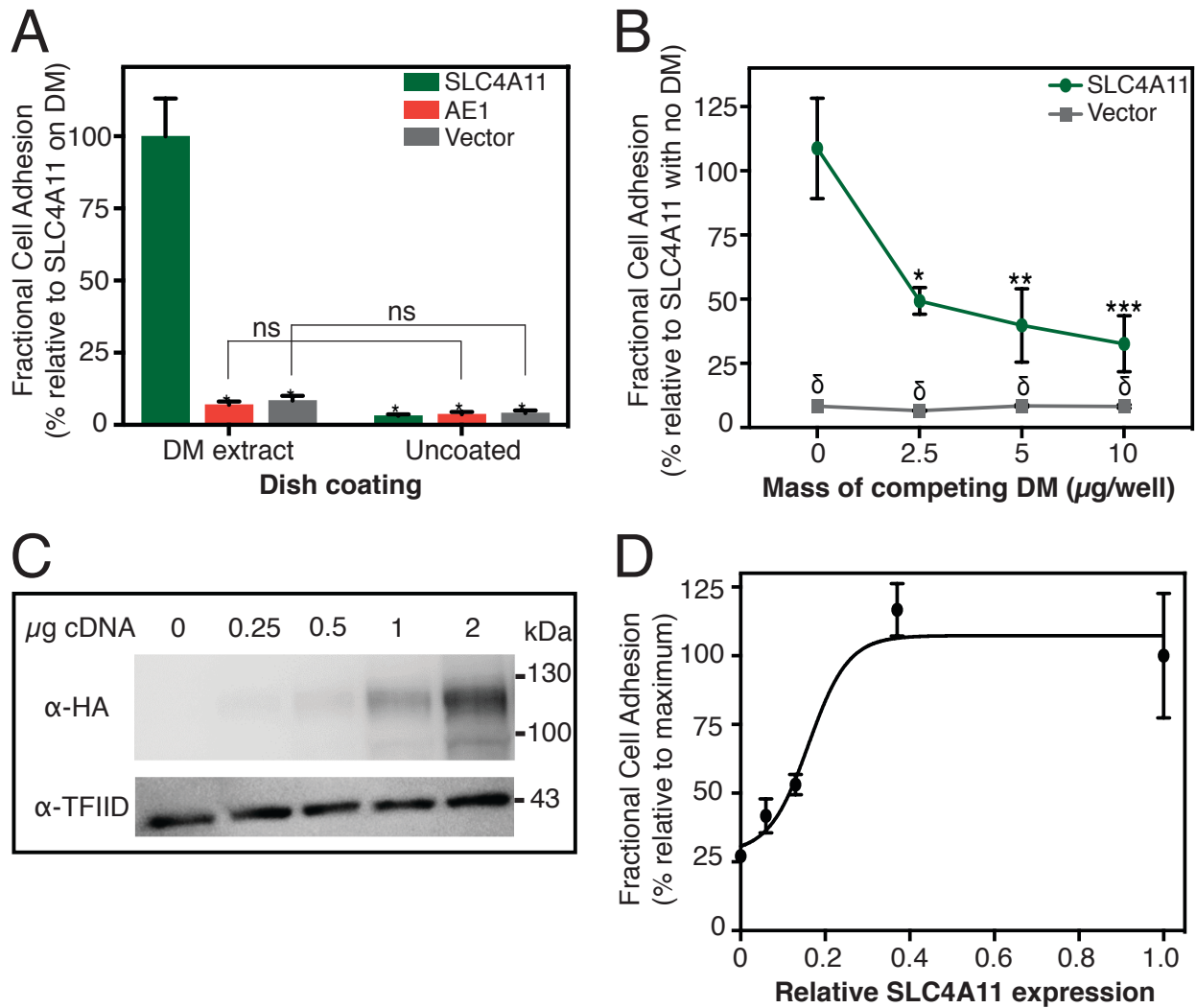


**Figure 4.1: Role of SLC4A11 in cell adhesion to DM**

(A) HEK293 cells, co-transfected with peGFP-C1 and cDNA encoding SLC4A11 or AE1 (SLC4A1) or empty vector, were grown on DM-coated and uncoated dishes. Cell adhesion was determined from the number of cells remaining on the dish following mild disruption by inverted centrifugation. Fractional cell adhesion was calculated as:  $(\text{eGFP fluorescence}_{\text{post-disruption}} / \text{eGFP fluorescence}_{\text{pre-disruption}}) \times 100\%$ . Cell adhesion assays were performed, and fractional cell adhesion was plotted relative to SLC4A11-transfected cells on DM-coated dish. (n=12 from three independent replicates). Data are presented as mean  $\pm$  standard error of mean (SEM). \*p<0.0001

versus SLC4A11 on DM-coated dishes (Two-way ANOVA and Bonferroni's post-tests). **(B)** SLC4A11 and vector-transfected cells were pre-incubated with DM extract and plated on DM-coated dishes. Cell adhesion assays were performed, and fractional cell adhesion was determined. (n=4). Data are presented mean  $\pm$  SEM. \*p=0.0007, \*\*p=0.0002, \*\*\*p<0.0001,  $\delta$ p<0.0001 vs. SLC4A11 with no DM incubation (Two-way ANOVA and Bonferroni's post-tests). **(C)** Lysates from cells transfected with indicated masses of SLC4A11 cDNA were analyzed on immunoblots, using anti-HA and anti-TFIID antibodies. **(D)** Densitometry of SLC4A11 expression was corrected for TFIID abundance and normalized to maximal expression of SLC4A11. Cell adhesion assays were performed on samples seen in c. Fractional cell adhesion was normalized to the maximal value. (n=4).

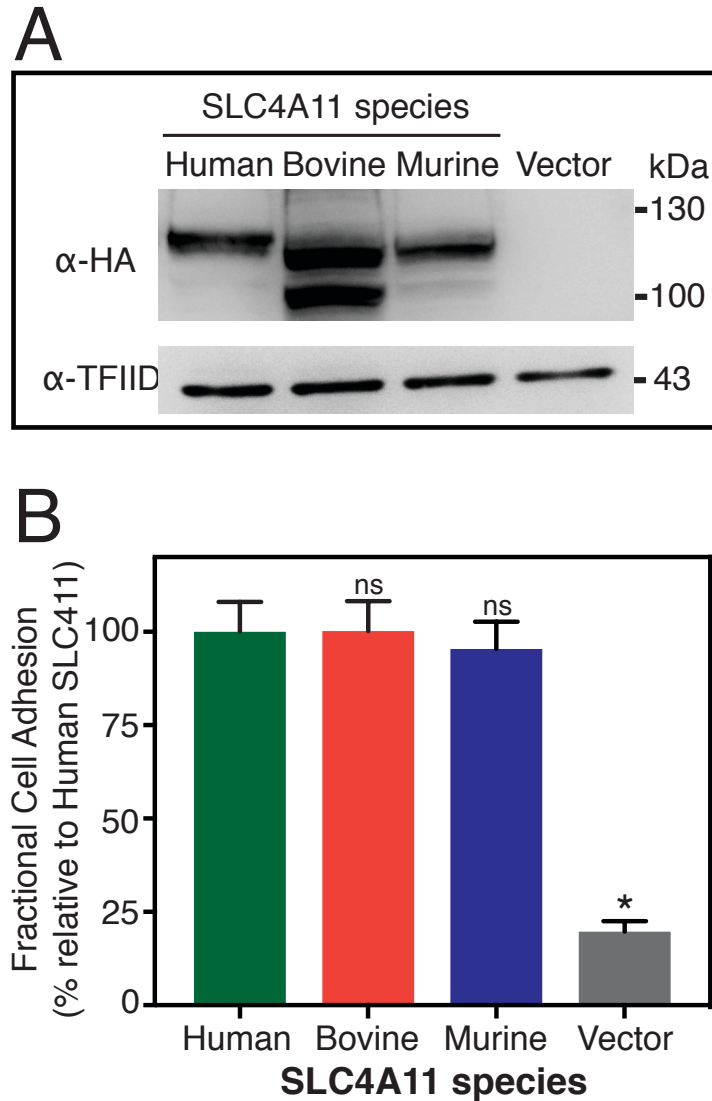


**Figure 4.2: SLC4A11 cell adhesion role is conserved across mammals.**

(A) Lysates from cells transfected with cDNA encoding HA-epitope tagged-SLC4A11 (human, bovine or murine) were probed on immunoblots using anti-HA and anti-TFIID antibodies. (B) HEK293 cells transfected with indicated constructs were tested in cell adhesion assays and fractional cell adhesion was normalized to value from human SLC4A11. (n=8 wells from two independent replicates). Data are presented as mean  $\pm$  SEM. \* $p < 0.0001$  versus human SLC4A11 (One-way ANOVA and Bonferroni's post-tests).

SLC4A11-expressing cells, without an effect on vector-transfected cells. This suggests that SLC4A11-EL3 has a central role in mediating cell adhesion to DM.

We next examined the two consensus N-linked glycosylation sites in EL3, N545 and N553 (Fig. 4.3A), to determine the role of glycosylation in cell adhesion. Both N545Q and N553Q-SLC4A11 traffic to the cell surface at levels similar to WT but their molecular weights are lower than WT-SLC4A11, consistent with loss of glycosylation at one of the sites (Fig. 4.4A). Loss of a single glycosylation site did not decrease the molecular weight of the mutant proteins to ~100 kDa (non-glycosylated SLC4A11), suggesting that both the sites on EL3 are glycosylated. SLC4A11 N545Q-N553Q double mutant however, did not accumulate in the cell, when assessed on immunoblots. This suggests that glycosylation at one site is needed for correct SLC4A11 folding.

We tested the effect of these mutations on SLC4A11-EL3 mediated cell adhesion (Fig. 4.4B). There was no significant difference between adhesion levels of cells expressing N545Q and N553Q-SLC4A11 when compared to WT-SLC4A11, suggesting that either one glycosylation suffices SLC4A11-mediated cell adhesion or glycosylation does not affect cell adhesion.

#### **4.2.3 FECD and CHED mutations in SLC4A11 compromise cell adhesion**

Cell adhesion assays were performed to determine if four FECD-causing mutations located in EL3 (Y526C<sup>96</sup>, T561M<sup>42</sup>, S565L<sup>42</sup> and V575M<sup>96</sup>) affect SLC4A11-cell adhesion function. E143K, a CHED-causing mutation that causes complete SLC4A11 ER-retention<sup>77</sup>, was included as negative control. Each of the FECD-causing mutations in SLC4A11-EL3 led to a significant decrease in cell adhesion when compared to cells expressing WT-SLC4A11 (Fig. 4.5A). Expression of E143K-SLC4A11 led to cell adhesion similar to the vector control. R125H-SLC4A11, a FECD-causing mutation that allows the protein to traffic to the cell surface but impairs solute transport (water flux) function<sup>28</sup>, showed no difference in cell adhesion when compared to

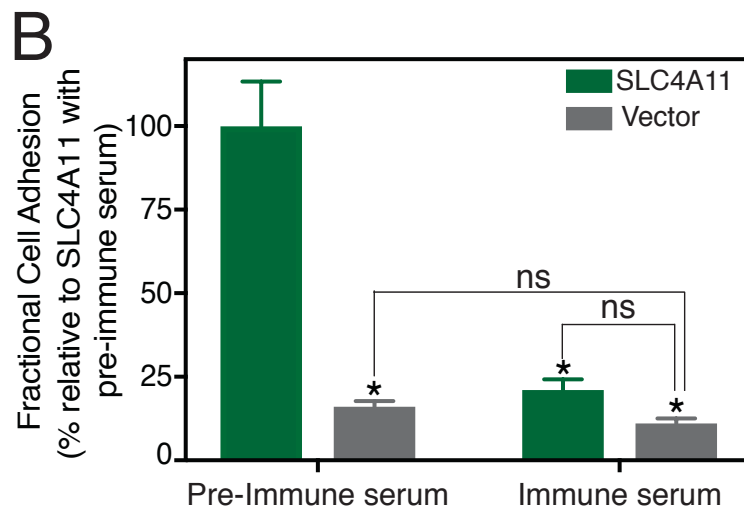
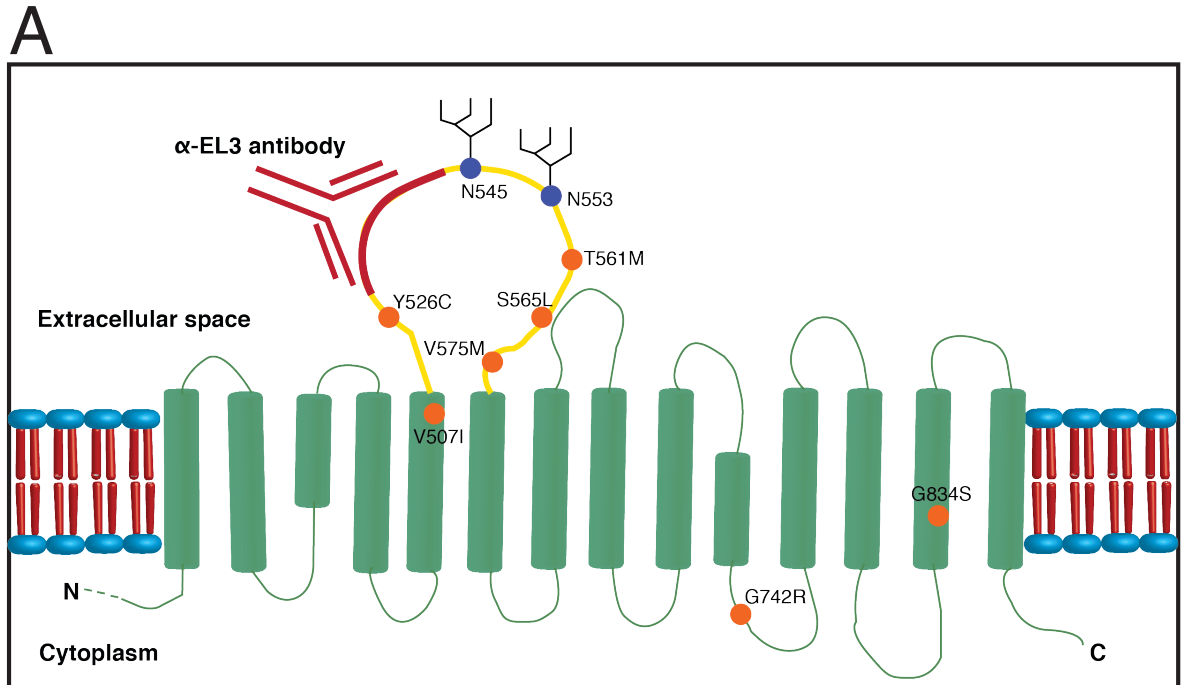


**Figure 4.3: SLC4A11 extracellular loop 3 forms the DM adhesion site.**

(A) Topology model for human SLC4A11 on the basis of homology to human SLC4A1 (Band 3) structure<sup>80,130</sup>. EL3 is yellow and the region corresponding to the peptide used to produce the anti-EL3 antibody (NH<sub>2</sub>-HTKRTSSLVLSLGL-COOH) is red, along with a cartoon of an IgG molecule attached to the epitope. The loop has two N-linked glycosylation sites (N545 and N553) in blue and four FECD-causing point mutations in orange (Y526C, T561M, S565L and V575M). SLC4A11

cytoplasmic domain is truncated in the model, with the first transmembrane residue at Y375. Lipid bilayer is represented by red and blue. **(B)** HEK293 cells transfected with SLC4A11 or empty vector were incubated with anti-SLC4A11-EL3 immune serum or pre-immune serum for 30 min at 37 °C. Cells were subjected to cell adhesion assays on DM-coated dishes. Fractional cell adhesion was normalized to the value for SLC4A11 with pre-immune serum (n=12 from three independent replicates). Data are presented as mean  $\pm$  SEM. \*p<0.0001 versus SLC4A11 incubated with pre-immune serum (Two-way ANOVA and Bonferroni's post-tests).

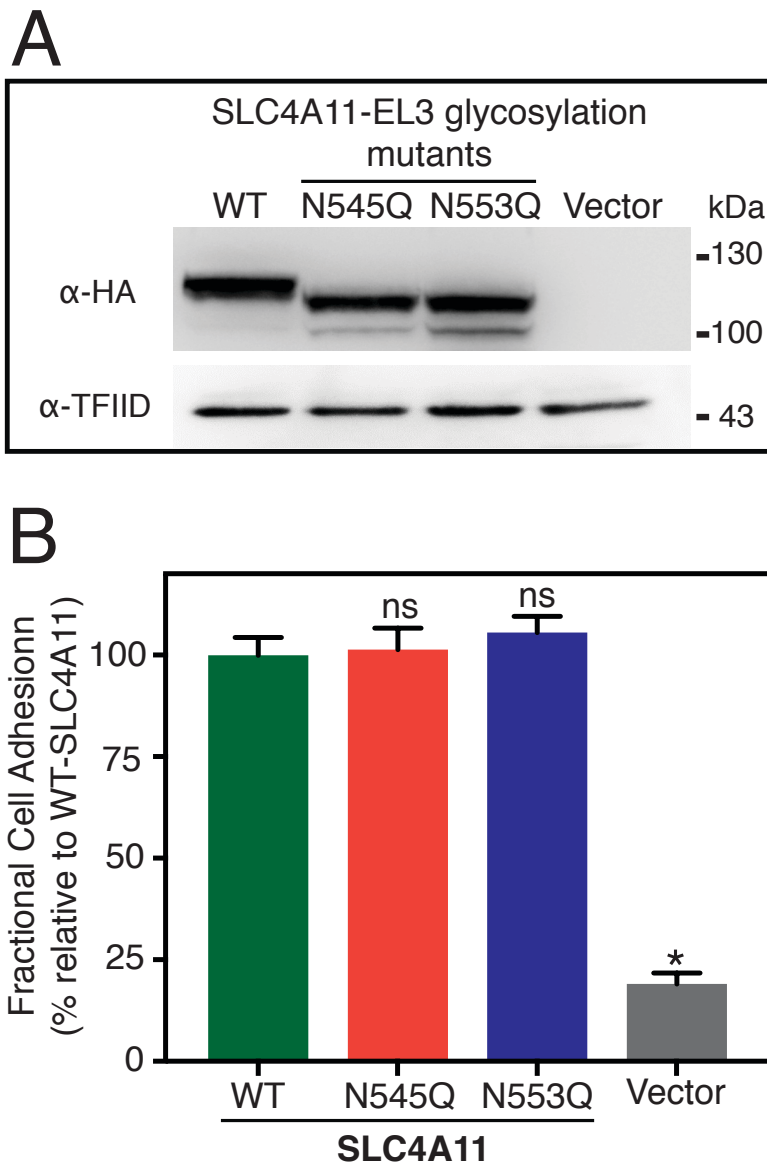


**Figure 4.4: Effect of N-linked glycosylation in SLC4A11-EL3 on cell adhesion.**

(A) Lysates of cells transfected with cDNA encoding WT, N545Q, N553Q SLC4A11 or empty vector, were probed with anti-HA and anti-TFIID antibodies. (B) HEK293 cells transfected with indicated constructs were subjected to cell adhesion assays and fractional cell adhesion was normalized to WT-SLC4A11. Data are presented as mean  $\pm$  SEM. \* $p < 0.0001$  versus WT-SLC4A11 (One-way ANOVA and Bonferroni's post-tests).

WT-SLC4A11. This indicates that FECD may arise from either a transport defect, or an adhesion defect.

Since some SLC4A11 mutations cause protein retention in ER<sup>89</sup>, we performed whole cell biotinylation assays on the EL3 mutants. The four FECD-causing EL3 mutants accumulate at the plasma membrane to similar levels as WT-SLC4A11 (Fig. 4.5B). The dashed line indicates the biotinylation level of GAPDH, a cytosolic protein, which represents the background level of the assay. These data confirm that the four EL3 FECD-causing mutations do not cause disease by intracellular protein retention. E143K-SLC4A11 has been established to be an ER-retained mutant while R125H-SLC4A11 processes normally to the cell surface<sup>52,92,162</sup>.

ECDs associated with SLC4A11 mutations have also been explained by a defect in SLC4A11 transport function, including R125H<sup>28,130</sup>. We next assessed the effect of four SLC4A11-EL3 mutations on osmotically-driven water-flux assays. The four SLC4A11-EL3 mutations did not significantly alter the water flux function of SLC4A11 (Fig. 4.5C). Previously, it was established that E143K-SLC4A11 does not support a water flux<sup>92</sup>, as the protein is ER-retained. Since the four FECD-causing mutations in SLC4A11 EL3 do not affect cell surface trafficking of the protein or its ability to mediate water flux, it suggests that disease arises because of some other defect in SLC4A11. The defective cell adhesion function of the EL3 mutants (Fig. 4.5A), suggests that loss of capacity for DM adhesion underlies the pathology of ECD patients with these mutations.

#### **4.2.4 Structural analysis of SLC4A11 extracellular loop 3**

We made use of a recently-published crystal structure for SLC4 family member SLC4A1 (Band 3)<sup>130</sup>, which has 40% similarity to SLC4A11 in the membrane domain<sup>80</sup>. De novo structural modelling performed with ROSETTA-Membrane on the developed three-dimensional homology modelling revealed EL3 to localize to the SLC4A11 dimeric interface (Fig. 4.6A). The loops are flexible, and topology depends on the inter-subunit interactions.

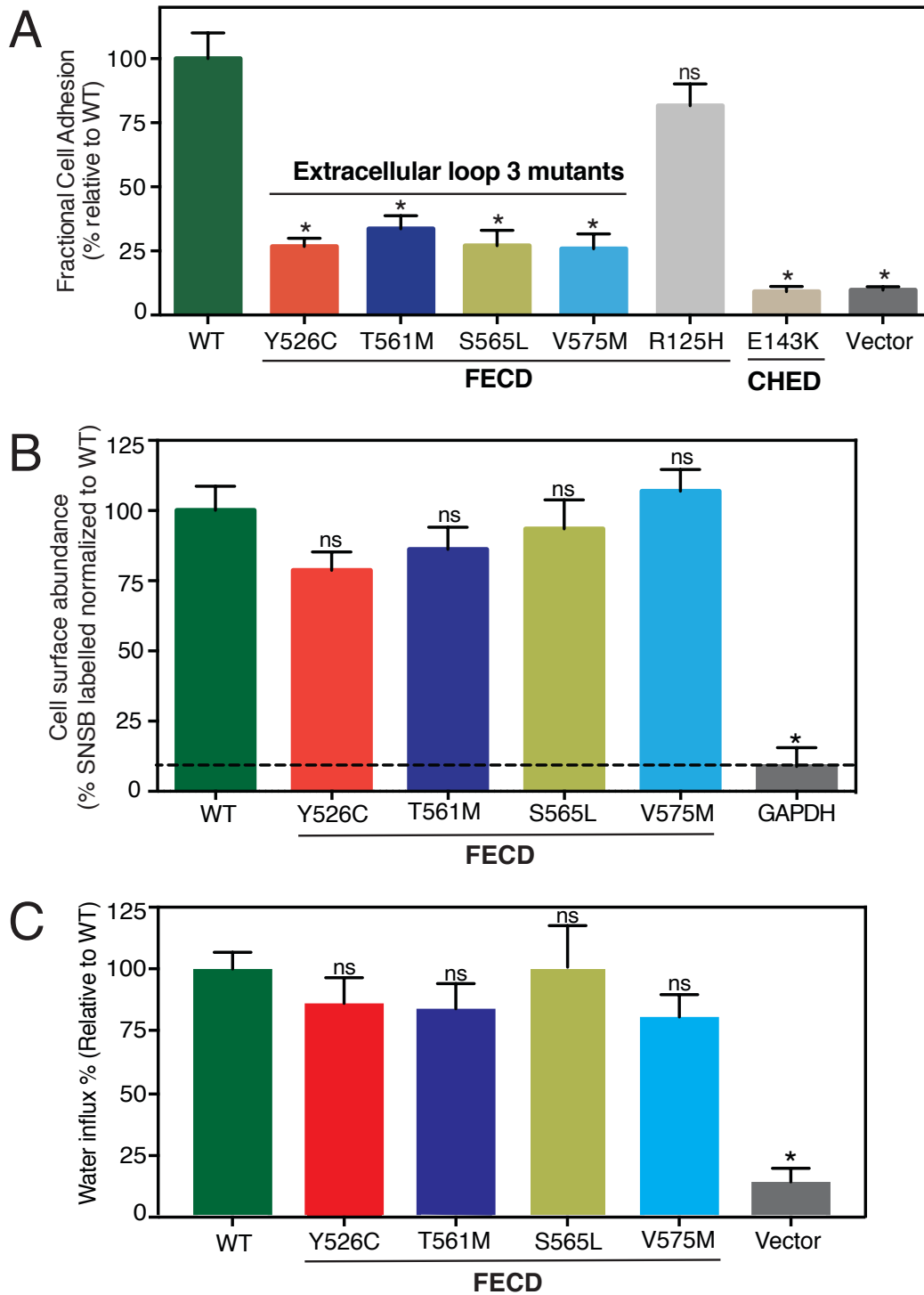


**Figure 4.5: FECD and CHED mutations in SLC4A11 compromise cell adhesion.**

Cells were transfected with cDNA encoding WT, Y526C, T561M, S565L, V575M, R125H, E143K-SLC4A11 or empty vector. (A) eGFP was co-transfected and cell adhesion assays were carried

out. Fractional cell adhesion was normalized to WT-SLC4A11 (n=12 from three independent replicates). **(B)** Transfected cells were incubated with membrane-impermeant SNSB and cell lysates were incubated with streptavidin agarose resin to bind the biotinylated protein. Cell surface abundance, calculated as the fraction of biotinylated protein, was normalized to the value for WT-SLC4A11. Dashed line marks the percentage of biotinylated GAPDH, which represents the background level of the assay (n=3). **(C)** HEK293 cells were co-transfected with cDNA encoding eGFP or indicated constructs. Cells were perfused with iso-osmotic medium followed by hypo-osmotic medium. Rate of change in GFP fluorescence in selected regions of cells was quantified as a surrogate for cell swelling. The initial rate of cell swelling was quantified upon switching to hypo-osmotic medium. Data were normalized to rate of WT-SLC4A11 (n= 5 to 8 independent replicates with 10-15 cells per coverslip). Data are presented as mean  $\pm$  SEM. \*p<0.0001 vs WT-SLC4A11 (One-way ANOVA and Bonferroni's post-tests).

To further refine the most energetically stable states we used the lowest-energy structures identified in ROSETTA-membrane modelling to generate an ensemble of structures for temperature Replica-Exchange simulations<sup>163</sup>. The k-means clustering performed on the parallel-tempering data from replicas run at ambient temperatures was done next<sup>164</sup>. The clustering algorithm was based on the RMS values of the C $\alpha$  positions and mapped 2-3 dominant structural states in each monomer sharing some general features. The predominant structure reveals an interweaving of the two EL3 monomers (Fig. 4.6A), each with a distinct structure (Fig. 4.6B). The model reveals the EL3 dimer to extend approximately 32 Å from the cell surface (Fig. 4.6A-C). The FECD-causing mutations cluster more in monomer 2 than in monomer 1. Space-filling models reveal that the residues mutated in FECD are buried in the EL3 structure (Fig. 4.6C), suggesting that they do not directly form a portion of the DM binding region, but likely give rise to disease through secondary alterations of the binding site.

We next examined the EL3 amino acid sequences of the three mammalian SLC4A11 orthologues tested for a role in cell adhesion (Fig. 4.2B). Sequences were highly conserved across the loop, suggesting an important role for this structure (Fig. 4.6D). The four EL3 amino acids mutated in FECD were not in fully conserved positions except V575M.

#### **4.2.5 STIC (SLC4A11-EL3 Transmembrane-GPA Integrated Chimera) restores cell adhesion**

To explore whether SLC4A11-EL3 alone can promote cell adhesion, we created a chimeric protein, STIC, a 143 amino acid protein consisting of the transmembrane region of GPA precursor with a mutated signal peptidase cleavage site to retain its signal peptide creating two transmembrane segments (Fig. 4.7A). The GPA extracellular region is replaced by SLC4A11-EL3 and a HA-tag is added at the C-terminus of the protein. GPA exists as a dimer in the plasma membrane<sup>165</sup> similar to SLC4A11<sup>162</sup>. On immunoblots, STIC ran as a dimer (~38 kDa) with

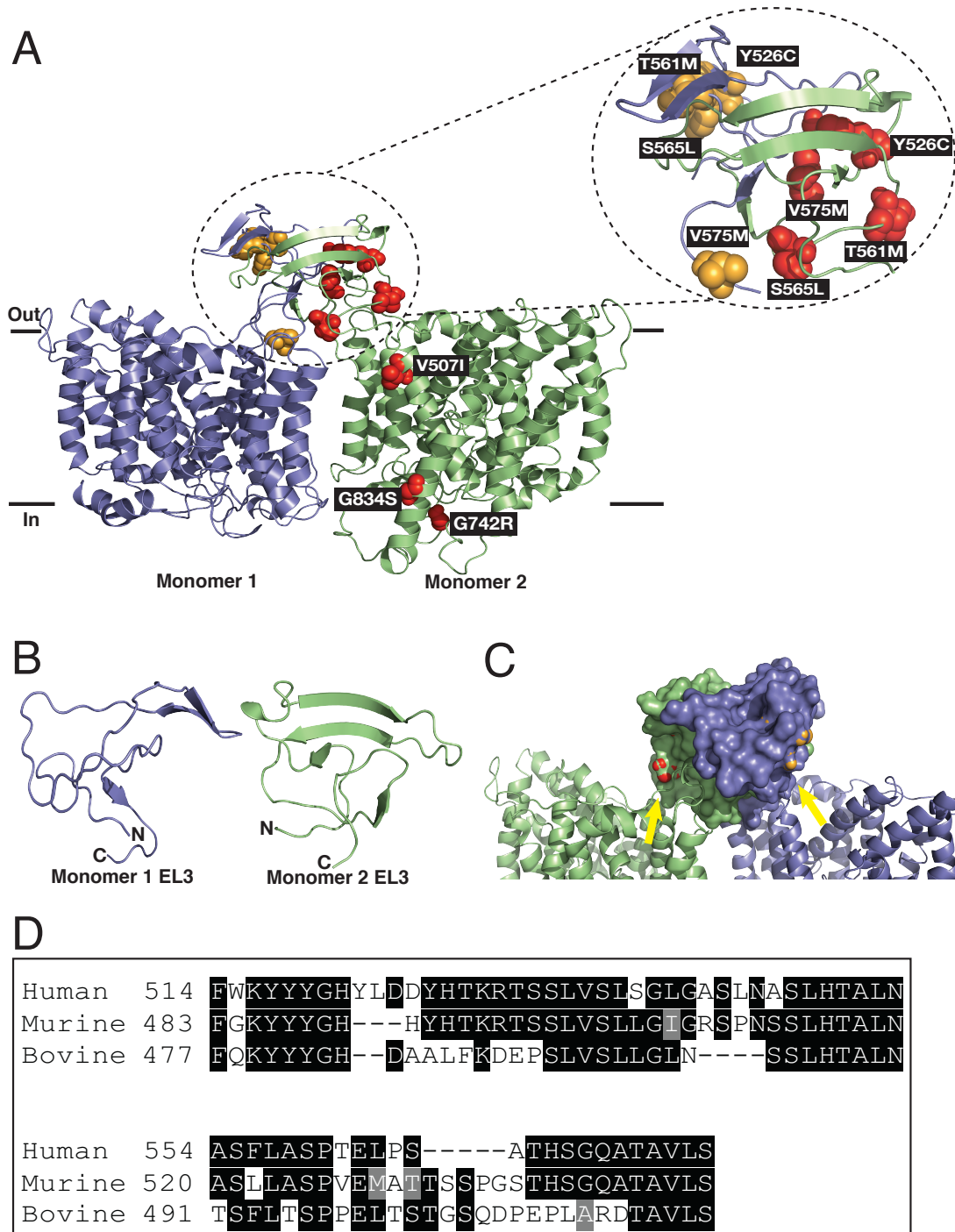


**Figure 4.6: Structural analysis of SLC4A11 Extracellular Loop 3.**

A three-dimensional energy minimized structural model of human SLC4A11 was prepared by homology to human Band 3 (SLC4A1)<sup>130</sup>. EL3 amino acid sequence is not conserved between

the two proteins and EL3 of Band 3 was not resolved in the published crystal structure. SLC4A11 EL3 structure was modelled, using molecular dynamics approaches. **(A)** Cartoon diagram of SLC4A11 dimer with the two individual monomers coloured purple and green, respectively. Circled is the EL3 structure, also shown in an expanded view. The four FECD mutations in EL3 are rendered in space filling format, coloured yellow in monomer 1 and red in monomer 2. Black lines indicate approximate position of lipid bilayer. **(B)** Cartoon diagrams of the structures of EL3 from the two SLC4A11 subunits, with amino- (N) and carboxy-terminal (C) ends of EL3 marked. **(C)** Model of the extracellular surface of human SLC4A11, with EL3 rendered in space-filling format. Monomer 1 is green and monomer 2 is purple. FECD mutant positions are coloured as in Panel A. Arrows indicate positions of partial surface exposure of these residues. **(D)** Human, bovine and murine SLC4A11 EL3 sequences were aligned. Black highlighting represents conserved residues, grey represents amino acids with similar characteristics, and white represents divergence. Asterisks indicate positions of FECD mutations at human residues 526, 561, 565 and 575.

expression levels comparable to SLC4A11 (Fig. 4.7B). In the cell adhesion assay, STIC promoted cell adhesion at levels similar to SLC4A11 suggesting that EL3 suffices to promote cell adhesion to DM (Fig. 4.7C).

#### **4.2.6 SLC4A11-EL3 interacts with DM components**

We next examined whether SLC4A11 interaction with DM was direct, and began to identify the SLC4A11 binding partner(s) in DM. We immobilized glutathione-S-transferase (GST) or GST fused to SLC4A11-EL3 (GST-SLC4A11-EL3) on glutathione resin and incubated with bovine DM extract. EL3 and interacting DM components were released upon treatment with PreScission protease. Proteins associated with GST and GST-SLC4A11-EL3 were resolved by reverse phase HPLC. Three peaks present in the GST-EL3-SLC4A11 elution profile, but not the GST-alone eluate, were subjected to mass spectrometry. Mass spectrometry analysis revealed COL8A1 and COL8A2 peptides as the predominant proteins interacting with SLC4A11-EL3 (Table 4.1, Fig. 4.8). This indicates that SLC4A11 promotes a direct interaction with DM through EL3 and suggests that the two collagens contribute to SLC4A11 binding.

#### **4.2.7 Role of DM in regulating SLC4A11 expression in primary HCEnC**

In primary cultured HCEnC, SLC4A11 expression declines during culture<sup>73,160,161</sup>. We isolated primary HCEnC from different donors and cultured them at P0 (passage 0) for 7 days. Cells were expanded to passage 1 (P1, seven days in culture after passage 0) and passage 2 (P2, seven days in culture after passage 1). We observed an almost complete loss of SLC4A11 expression (500-fold) after P2 (Fig. 4.9A).

We hypothesized that the presence of DM components promote SLC4A11 expression. HCEnC from three donors belonging to the same age range (Table 2.6) were cultured to P2. P2 cells were then cultured on DM-coated dishes in M5-endo

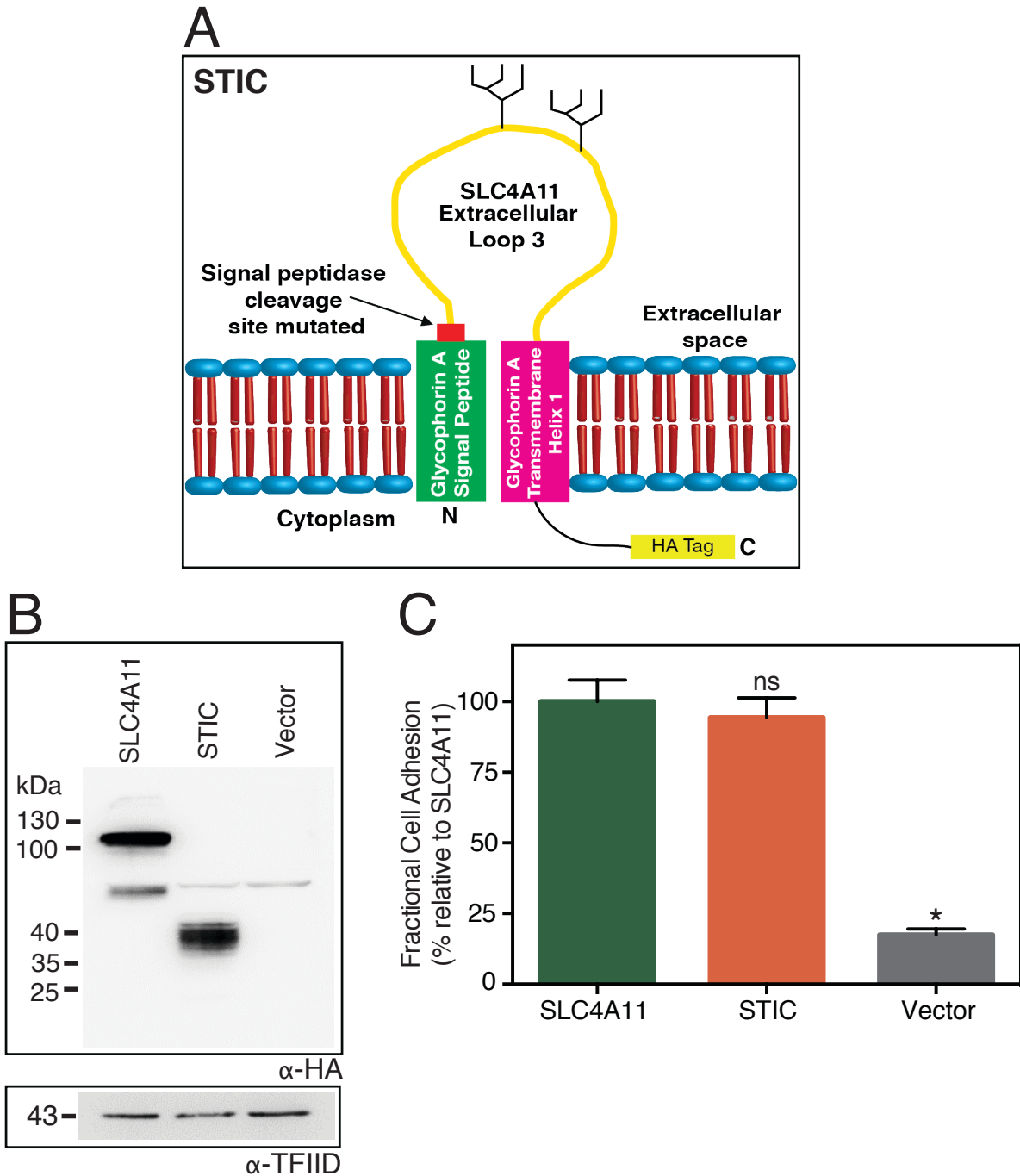


**Figure 4.7: STIC (SLC4A11-EL3 Transmembrane-GPA Integrated Chimera) restores cell adhesion.**

A chimeric protein (STIC) was constructed, using cDNA encoding GPA precursor and SLC4A11-EL3 (K516-Q571). **(A)** Topology model of STIC: extracellular GPA region replaced by SLC4A11-

EL3 (yellow) and the signal cleavage site mutated (red) to retain the GPA signal peptide (green) to create a second transmembrane segment followed by a C-terminal HA-epitope tag. **(B)** HEK293 cells were transfected with cDNA encoding HA-SLC4A11, STIC or vector. Cell lysates were probed on immunoblots with anti-HA and anti-TFIID antibodies. **(C)** HEK293 cells were co-transfected with cDNA encoding eGFP and indicated constructs, and cell adhesion assays were performed. Fractional cell adhesion was calculated and normalized to the value for SLC4A11. (n=16 from four independent replicates). Data are presented as mean  $\pm$  SEM. \*p<0.0001 versus SLC4A11 (One-way ANOVA and Bonferroni's post-tests).

**Table 4.1: Proteins associated with GST-SLC4A11-EL3 as identified by nano-liquid chromatography and mass spectrometry (nano-LC-ESI-MS<sup>2</sup>).**

Listed are the proteins exclusively identified in the three GST-SLC4A11-EL3 peak fractions. No corresponding peptide identifications were observed in the GST only (negative control) eluate. The total number of unique peptides and peptide spectrum matches (PSM) for each protein were pooled from all three peak fractions. Proteins are ordered according to the sum of PSMs of the identified peptides (in the last column). MW: Molecular weight.

#	Identified protein	Accession #	MW (kDa)	PSM
1	Collagen type VIII alpha-1 chain	CO8A1_HUMAN	73.3	55
2	Collagen type VIII alpha-2 chain	CO8A2_HUMAN	67.2	22
3	Basement membrane-specific heparan sulfate proteoglycan core protein	PGBM_HUMAN	468.5	17
4	Collagen type XII alpha-1 chain	COCA1_HUMAN	332.9	9
5	Emilin-1	EMIL1_HUMAN	106.6	2
6	Agrin	AGRIN_HUMAN	217.1	2
7	Inter-alpha-trypsin inhibitor heavy chain H5	ITIH5_BOVIN	104.3	2
8	Keratocan	KERA_MOUSE	40.4	1
9	Complement C1q tumor necrosis factor-related protein 5	C1QT5_RAT	25.3	1

10	Elastin	ELN_BOVIN	64.2	1
11	Transforming growth factor-beta-induced protein ig-h3	BGH3_PIG	74.4	1
12	Collagen type IV alpha-4 chain	CO4A4_BOVIN	46.4	1
13	Fibronectin	FINC_BOVIN]	272	1
14	Microfibril-associated glycoprotein 4	MFAP4_HUMAN	28.6	1
15	Olfactomedin-like protein 3	OLFL3_RAT	45.9	1
16	Nidogen-1	NID1_HUMAN	136.3	1

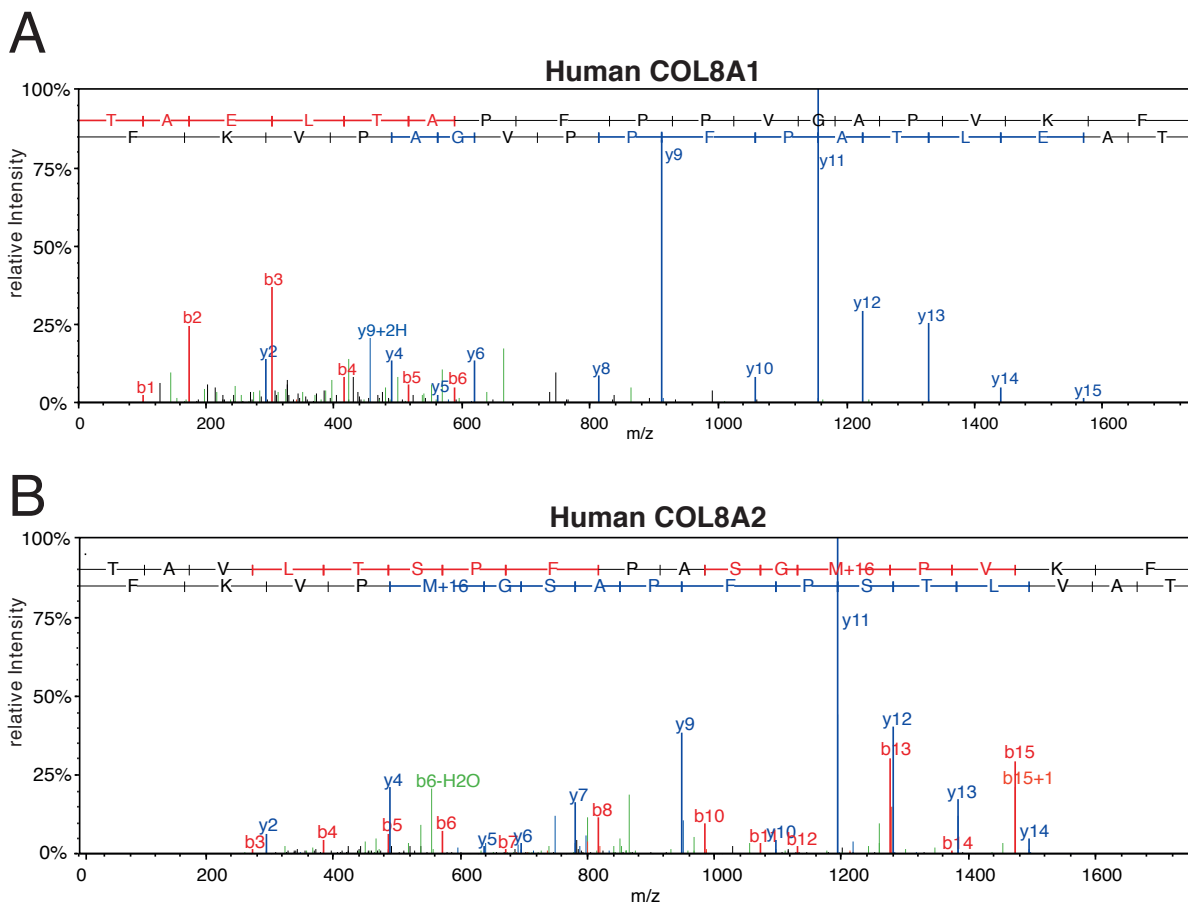


**Figure 4.8: Identification of DM proteins interacting with SLC4A11-EL3.**

MS/MS fragmentation spectra of peptides derived from the **(A)** Collagen type VIII alpha-1 chain (CO8A1\_human) and **(B)** Collagen type VIII alpha-2 chain (CO8A2\_human) which were identified in the eluted fractions of GST-SLC4A11-EL3. The relative intensity of peptide fragment spectra (y-axis) are shown for the m/z ratios (x-axis; m=mass of fragment, z=charge of peptide fragment) corresponding to the amino acid sequence (from N to C- and C to N-terminus, shown on the top). The identified fragments corresponding to the y-ion and b-ion series are colored in blue and red, respectively.

stabilization medium for 14 days. Transcript abundance was measured by quantitative RT-PCR (using primers listed in Table 2.9), revealing that SLC4A11 and COL8A2 transcript abundance increased approximately three and two-fold respectively at Day 14 compared to Day 0 (Fig. 4.9B). In contrast, abundance of COL8A1, N-Cadherin (NCAD) and LIM Homeobox Transcription factor 1 beta (LMX1B) transcripts did not change significantly. This suggests that SLC4A11 expression in HCEnC is sensitive to the presence of DM-environment. Interestingly, COL8A2 which was found as an interaction partner of SLC4A11 (Table 4.1), was also upregulated, suggesting a link between the two proteins.

HCEnC from three donors, belonging to the same age range were cultured to P2, then dissociated and grown on FNC or DM-coated dishes for 7 and 14 days. SLC4A11 protein expression on DM normalized to FNC control (Fig. 4.9C) increased by four-fold when compared to Day 0 (Fig. 4.9D). This further suggests the importance of DM environment on SLC4A11 expression in HCEnC and the role of SLC4A11 in HCEnC-DM physiology.

#### **4.2.8 Restoration of SLC4A11 expression increases HCEnC adhesion to DM**

Since HCEnC grown to P2 in the absence of DM lose SLC4A11 expression, we next examined whether adhesion to DM could be rescued by transfecting these P2 cells with SLC4A11. HCEnC isolated from three donors (Table 2.6) were transfected with SLC4A11 cDNA and cultured for 48 h. Microscopic inspection revealed transfected cells attained healthy hexagonal morphology and were further tested for SLC4A11 expression. HCEnC from three donors showed no SLC4A11 expression at P2 (NT) while the transfected cells showed abundant SLC4A11 (Fig. 4.10A). Densitometry quantified a 500-fold increase in SLC4A11 expression, which was similar to physiological SLC4A11 level in HCEnC at P1 (Fig. 4.9A).

The degree of adhesion of SLC4A11-transfected and NT primary HCEnC to DM was assessed for 24 h. Individual adhesion profiles for cells from each donor showed a two to three-

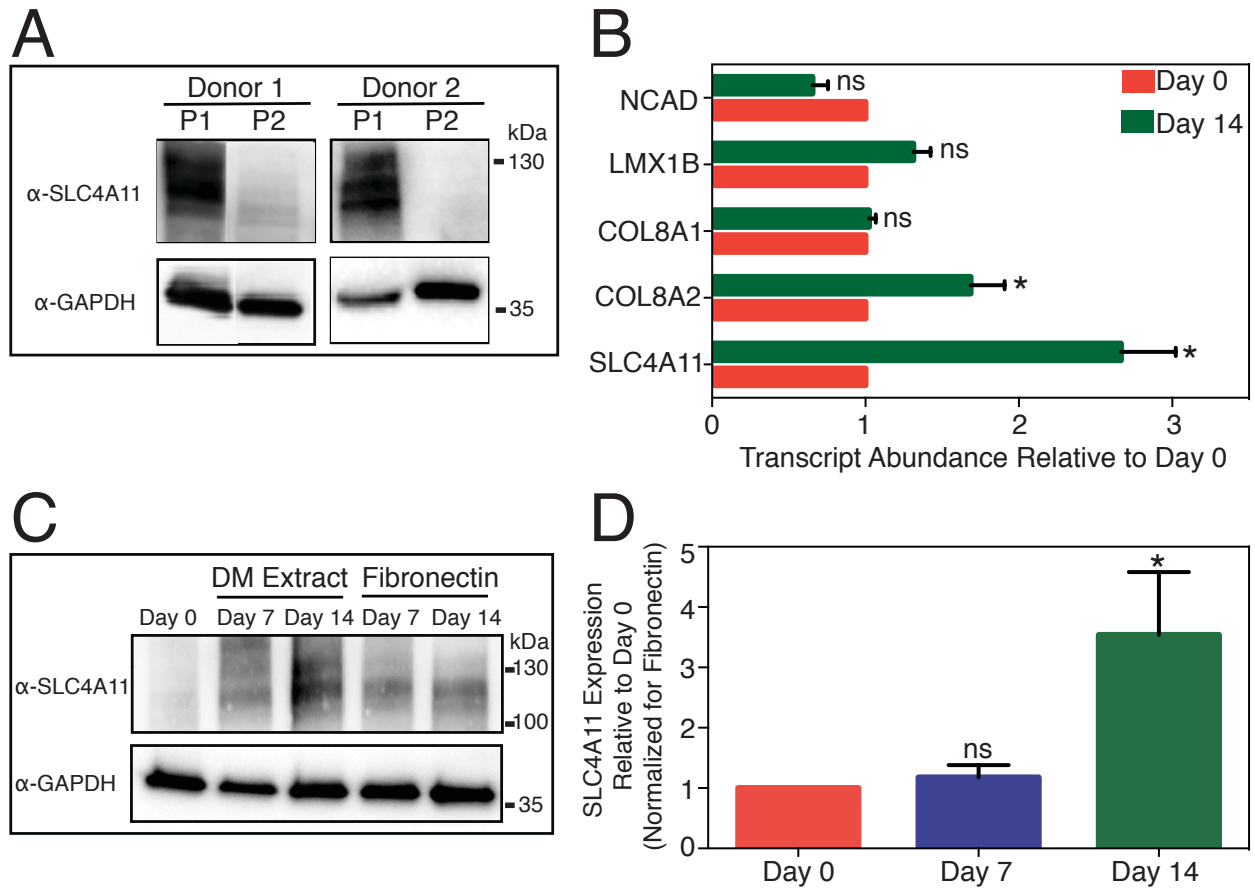


**Figure 4.9: Role of DM in regulating SLC4A11 expression in primary HCEnc.**

Primary HCEnc were cultured to P0, P1 and P2. **(A)** Cell lysates at P1 and P2 from two donors (Table 2.6) were probed on immunoblots with anti-SLC4A11 and anti-GAPDH antibodies. Note that intervening lanes have been removed between P1 and P2 lanes, indicated by the black lines. **(B)** P2 HCEnc were cultured on DM-coated dishes and harvested at Day 0 (before growth on DM) and Day 14 (following 14 days growth on DM). Total RNA was extracted from cells recovered at Day 0 and Day 14 from DM-coated dishes and real time PCR was performed.  $2^{-\Delta\Delta CT}$  was calculated and normalized for GAPDH and transcript abundance relative to Day 0 was plotted. (3 donors with n=3 for each donor). **(C)** P2 HCEnc were cultured on DM or FNC-coated dishes and harvested at Day 0, 7 and 14. Cell lysates were probed on immunoblots with anti-SLC4A11 and anti-GAPDH antibodies. (n=4 donors, data are representative from one donor). **(D)**

Densitometry quantified SLC4A11 expression in HCEnC grown on DM coated dishes normalized to level found for cells grown on FNC dishes. Data were plotted relative to SLC4A11 expression at Day 0 (n=4 donors). Data are presented as mean  $\pm$  SEM. \*p<0.05 versus Day 0 (One-tailed paired t-test).

-fold increase in impedance for SLC4A11-transfected cells over NT cells after 24 h (Fig. 4.10B-D). Data for average cell index for three donors was pooled at the 3 h timepoint (consistent with the adhesion data in HEK293 cells, Fig. 4.1A) and normalized to the value for SLC4A11-transfected cells (Fig. 4.10E). A two-fold increase in cell-index after 3h highlights the importance of SLC4A11 in HCEnC adhesion to DM.

#### **4.2.9 Anti-SLC4A11-EL3 antibody reduces primary HCEnC adhesion to DM**

HCEnC from five donors belonging to the same age range (Table 2.6) were cultured to P1. Cells were dissociated and incubated with anti-SLC4A11-EL3 antibody (Immune serum) or pre-immune serum from the same animal. Individual adhesion profiles for each donor showed a significant decline in HCEnC adhesion after incubation with immune serum (Fig. 4.11A-E). Pooled cell-index values from five donors at the 15 h time-point were normalized to data for cells incubated with pre-immune serum. Immune serum caused a decline in cell index by one-third of the pre-immune serum control (Fig. 4.11F), suggesting a significant role of SLC4A11-EL3 in mediating HCEnC attachment to DM. Incubation with anti-SLC4A11-EL3 antibody led to a 33% decline in primary HCEnC adhesion, while in SLC4A11-transfected HEK293 cells, there was an 80% decline (Fig. 4.3B). This suggests a higher level of cell adhesion functionality beyond SLC4A11 in HCEnC.

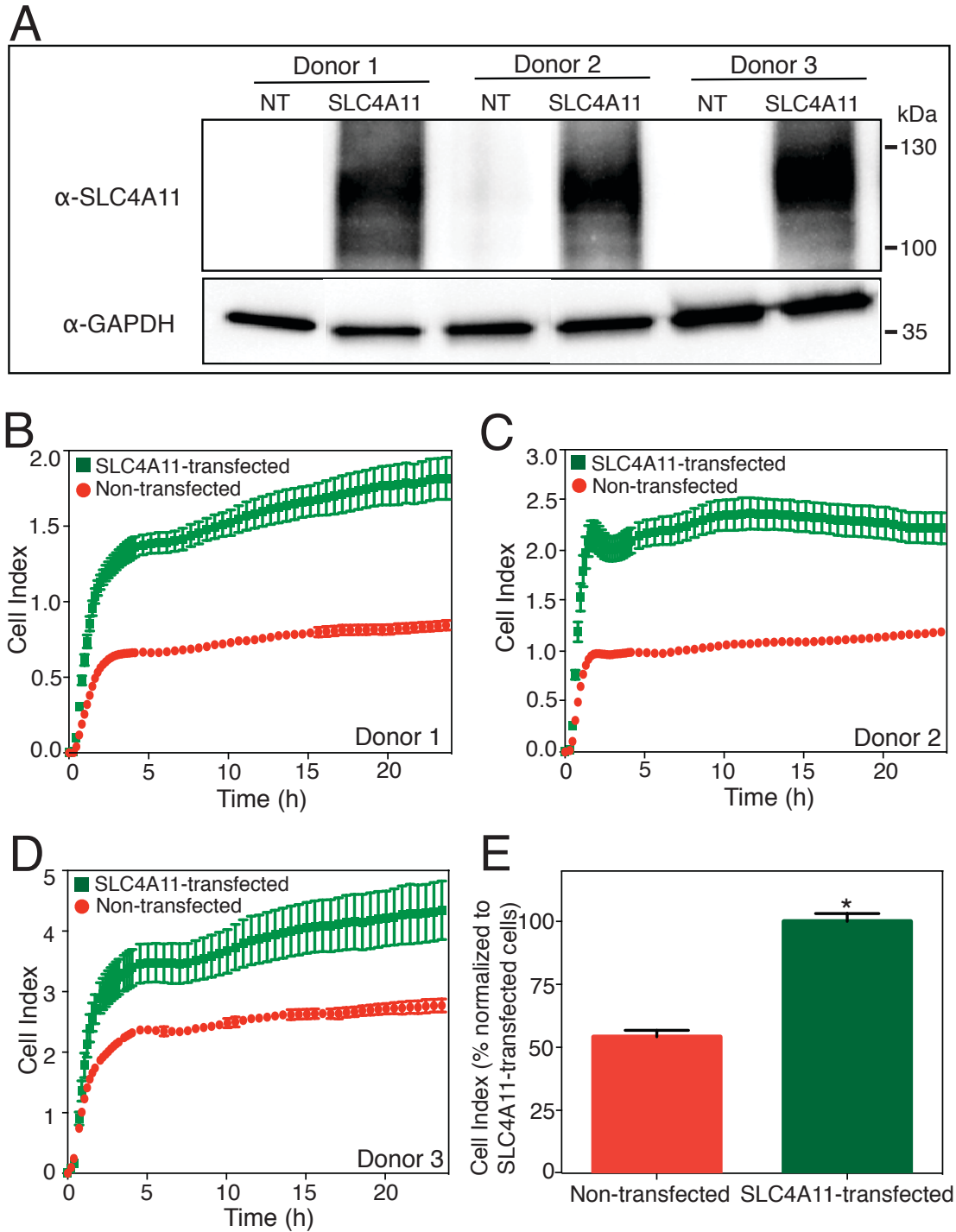


**Figure 4.10: Restoration of SLC4A11 expression increases HCEnc adhesion to DM.**

Primary HCEnc isolated from age-matched donor corneas were expanded to P2 and transiently transfected with cDNA encoding human SLC4A11. (A) Cell lysates from NT and SLC4A11-

transfected HCEnC were probed on immunoblots using anti-SLC4A11 and anti-GAPDH antibodies. (n=3 donors). Intervening lanes removed between NT and SLC4A11 lanes are indicated by black lines. **(B-D)** Cell adhesion to DM-coated dishes was analyzed with an xCELLigence real time impedance-based cell analyzer system for 24 h in three donors. (n=4). **(E)** Cell index (impedance) at 3 h time point was normalized to value for SLC4A11-expressing cells. Pooled data from three donors were plotted. (n=12 from three donors). Data are presented as mean  $\pm$  SEM. \* $p < 0.0001$  versus NT cells (Two-tailed t test).

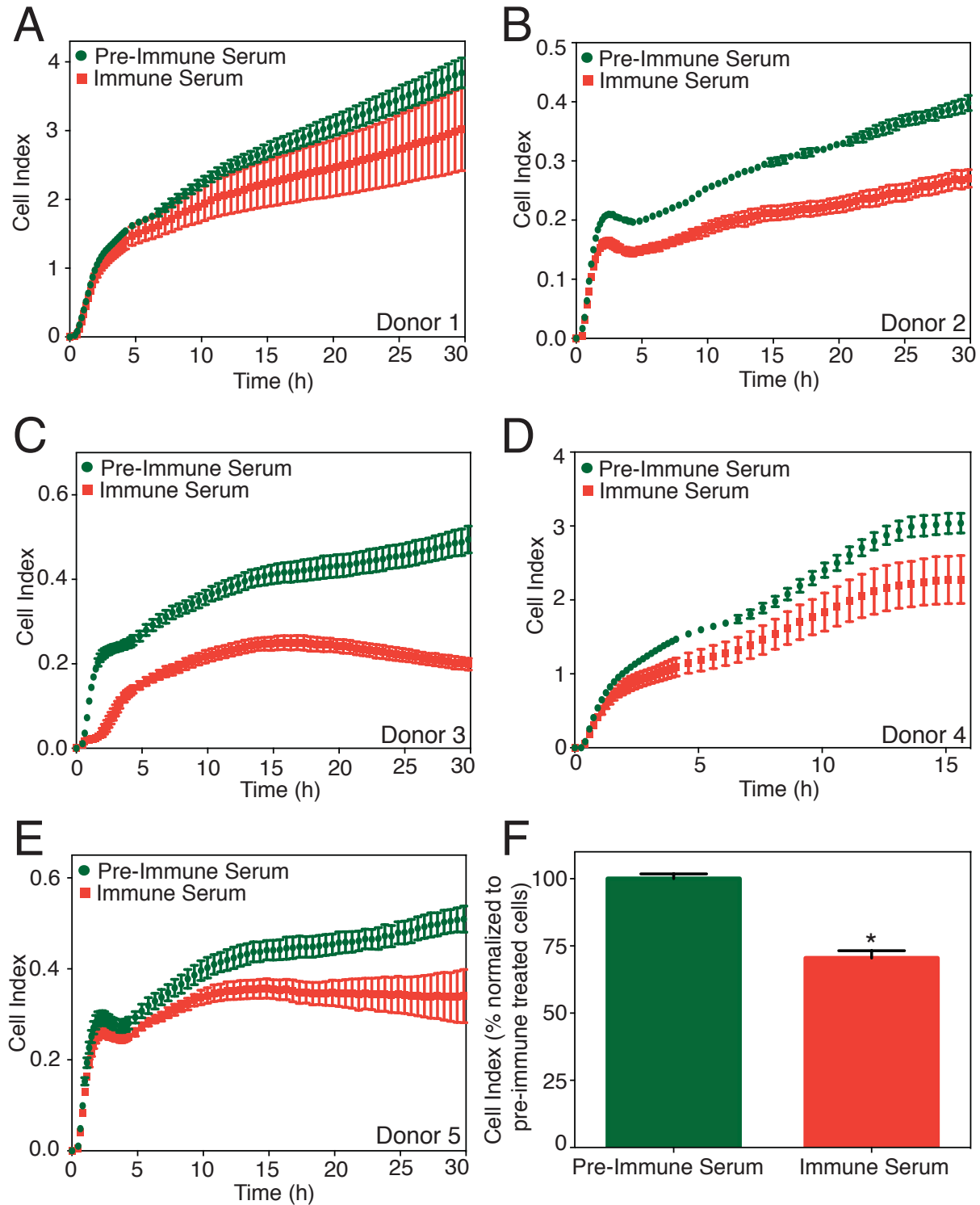


**Figure 4.11: Anti-SLC4A11-EL3 antibody reduces primary HCEnc adhesion to DM.**

Primary HCEnc from age-matched donors were expanded to P1. Cells from each donor were de-plated and incubated with anti-SLC4A11 EL3 immune serum or pre-immune serum for 30 min at

37 °C. **(A-E)** Cell adherence to DM-coated dishes was analyzed using an xCELLigence real time impedance-based cell analyzer for 30 h. (n=4). **(F)** Cell index (impedance) at median time point (15 h) was normalized to value for pre-immune serum incubated cells. Pooled data from five donors are plotted. (n=20 from five donors). Data are presented as mean  $\pm$  SEM. \* $p < 0.0001$  versus pre-immune serum (two-tailed t test).

### 4.3 Discussion

Experiments here provide support that solute transporter, SLC4A11, abundantly expressed in CEnC serves as a CAM to DM via its third extracellular loop (EL3) (Fig. 4.12A). FECD-causing mutations in SLC4A11-EL3 compromise endothelial cell adhesion to DM. Other SLC4A11 mutations that compromise its plasma membrane accumulation also impair endothelial cell adhesion. The cell adhesion role of SLC4A11 provides an explanation for the loss of CEnC seen in FECD and CHED patients. SLC4A11-EL3 containing chimeric protein, STIC, restores cell adhesion and provides a new therapeutic approach for disease treatment. Defective cell adhesion thus plays a previously unappreciated role in the pathogenesis of the genetic corneal dystrophies, CHED and FECD.

SLC4A11-mediated cell adhesion is proportional to its expression and is conserved across mammalian species. Loss of cell adhesion by anti-SLC4A11-EL3 antibody in transfected HEK293 cells and primary HCEnc suggests that SLC4A11-EL3 is the anchoring site of cells to DM. Furthermore, the four FECD-causing mutations in EL3, Y562C, T561M, S565L and V575M compromise cell adhesion, without any effect on protein-folding and osmotically driven-water flux. GST-SLC4A11-EL3 pull down assays and mass spectrometry analysis identified collagens, COL8A1 and COL8A2, as SLC4A11 interactors. COL8A2 mutations also cause FECD<sup>35</sup>. Primary HCEnc upregulate SLC4A11 and COL8A2 when grown on DM, suggesting an association between SLC4A11 expression in HCEnc and COL8A2 in DM. Together these data suggest cell adhesion as a defective pathway underlying CHED and FECD.

SLC4A11 is the first SLC protein reported to have cell adhesion function as far as we know. Although SLC3A2, a neutral amino acid transporter, has been tested for its cell adhesion role, it only regulates integrin-mediated adhesive signaling for cell growth and survival (protection from anoikis)<sup>166</sup>. Vascular Adhesion Protein-1 (VAP-1) is a cell surface glycoprotein, which

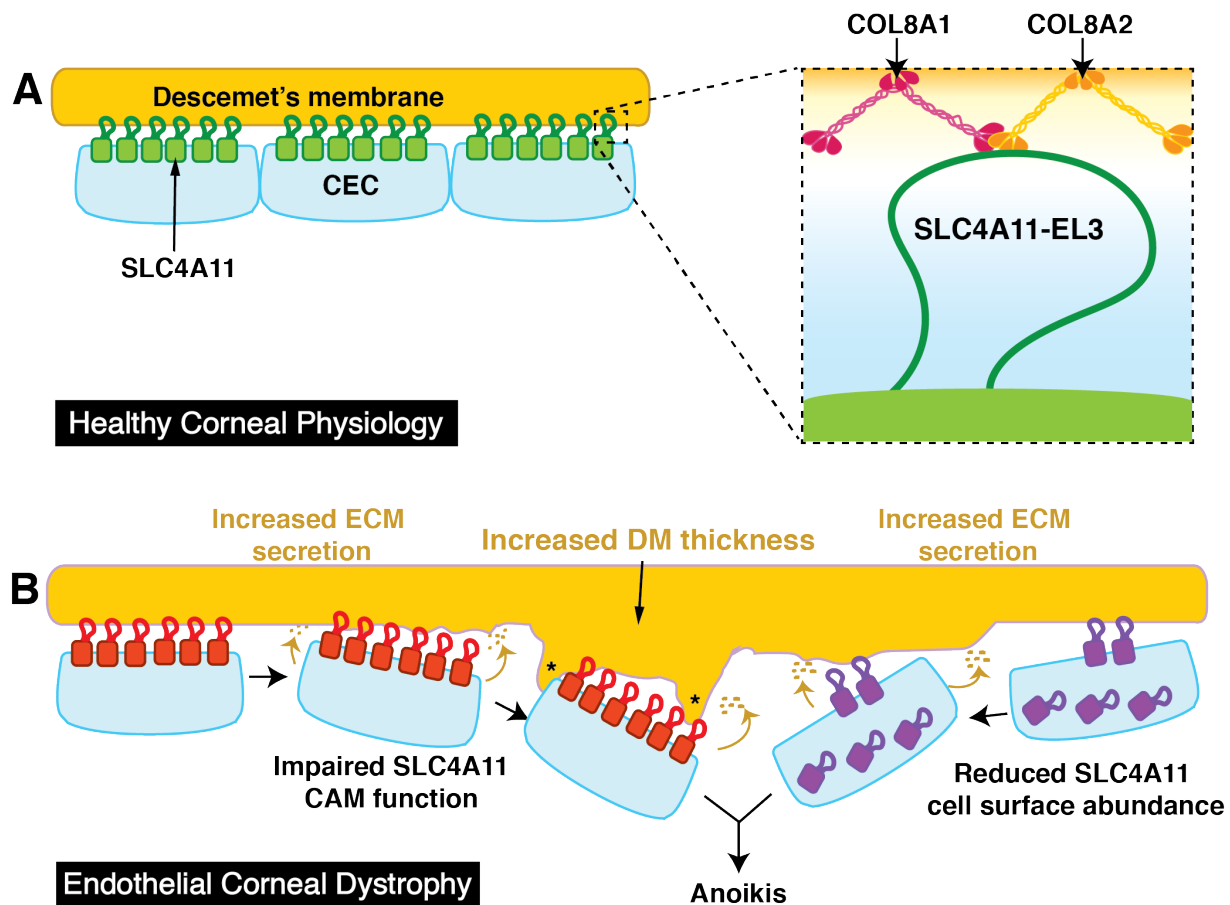


**Figure 4.12: SLC4A11 cell adhesion role in corneal physiology and endothelial corneal dystrophies.**

(A) In healthy cornea, WT-SLC4A11 (green) localized at the basolateral surface of HCEnc acts as a CAM to promote attachment to DM. (Inset) SLC4A11-EL3 interacts with DM proteins, COL8A2 and COL8A1, to promote adhesion. (B) In corneal dystrophies, SLC4A11 mutations compromising CAM function (red) or impairing trafficking/cell surface abundance (purple), reduce HCEnc-DM adhesion. Diseased HCEnc over-secrete ECM components in a futile attempt to compensate for weakened DM adhesion, ultimately leading to increased DM thickness and formation of guttae (\*). Loss of DM attachment triggers HCEnc anoikis.

functions as a mono-amine oxidase and as a CAM to promote leukocyte specific adhesion<sup>167</sup>, thus providing another example of a cell adhesion protein with dual functions.

SLC4A11 interaction with DM is direct, as suggested by the association of SLC4A11-EL3 with DM proteins, revealed by GST pull down combined with mass spectrometry. The ability of STIC to promote adhesion further argues for a direct role in cell adhesion. The region of SLC4A11 required for cell adhesion, EL3, lies at the center of the SLC4A11 dimer, where it would be relatively inaccessible to other integral membrane proteins. This suggests that EL3 directly binds DM, rather than through an intermediate. The mode of direct interaction of SLC4A11-EL3 with ECM would differ from that of some other cell adhesion proteins. In particular, integrins extend 110 Å from the cell surface<sup>168</sup>, whereas the molecular dynamics-derived SLC4A11-EL3 structure (Fig. 4.6A-C) suggests EL3 extends only about 32 Å, although the flexibility suggested by molecular dynamics could allow additional reach.

HCEnC downregulate SLC4A11 expression when isolated from their native environment<sup>72,73,161</sup>. Culturing these cells on DM re-induces SLC4A11 expression after two weeks as shown by the qPCR and protein analysis. This highlights the importance of DM environment in HCEnC biology, especially, SLC4A11 expression. This expression interplay between DM and SLC4A11 lends further support that CEnC adhesion to DM is the primary function of SLC4A11. Coordinated upregulation of COL8A2, the principal DM protein, and SLC4A11 upon growth on DM is consistent with this model. *Col8a2*, a FECD-causing gene, protein product interacts with SLC4A11 on the basis of GST pulldowns and MS analysis, further implicating this complex as critical in HCEnC-DM physiology.

Increased rates of HCEnC death in CHED and FECD may be explained by defective cell adhesion. Indeed, cells undergo a specific form of programmed cell death, anoikis, upon loss of basement membrane attachment<sup>158,159</sup>. Data here indicate SLC4A11 as a CAM promoting DM adhesion to prevent cell death by anoikis. Consistent with this, increased rates of cell death were

found in immortalized human CEnC after depletion of SLC4A11<sup>169</sup>. Additionally, *slc4a11* knock out mice manifest progressive CEnC loss with age<sup>107</sup>, consistent with a role of SLC4A11 in cell survival. Finally, COL8A2 has also been implicated in cell loss in FECD<sup>35,51</sup>. Thus, SLC4A11 interaction with COL8A2 implicates this complex as a critical in maintaining cell adhesion to prevent anoikis.

A role of SLC4A11 in preventing cell death by anoikis may also explain differences between CHED and FECD (Fig. 4.13). Unaffected individuals see a progressive loss of endothelial cells with age<sup>170</sup>. Decline in CEnC count below a critical threshold may lead to corneal edema<sup>171</sup>. Thus far, SLC4A11 is the only CHED gene identified (OMIM# 217700). CHED patients have negligible to 10-fold lower CEnC density than healthy infants<sup>57,172</sup>. Most CHED-causing mutations result in accumulation of little or no SLC4A11 at the cell surface<sup>89</sup>, which would clearly compromise cell adhesion (Fig. 4.12B, Fig. 4.13), explaining the appearance of CHED symptoms at birth. In contrast, most FECD-causing mutations do not impair SLC4A11 cell surface trafficking<sup>89</sup>, implying that the protein is defective in some critical function (Fig. 4.12B, Fig. 4.13). Data here for four SLC4A11 FECD mutants indicate that this function, in some cases, is cell adhesion (Fig. 4.5A). Symptoms may arise late in life in FECD because the mutated proteins retain their solute transport activity, as we revealed here for four FECD mutants (Fig. 4.5C). In the case of CHED, absence of cell surface SLC4A11 compromises transport and cell adhesion roles of the protein.

Diffuse and localized thickening of DM with formation of excrescences called guttae on the DM posterior surface also occur in ECDs. We propose that diseased CEnC, in a futile attempt to compensate for defective DM adhesion, may over-secrete ECM components. Aberrant deposition of these ECM components may lead to increased DM thickness and formation of guttae (Fig. 4.12B). Consistent with this, upregulated expression of ECM components including FNC occurs in CEnC from FECD patients<sup>173</sup>.

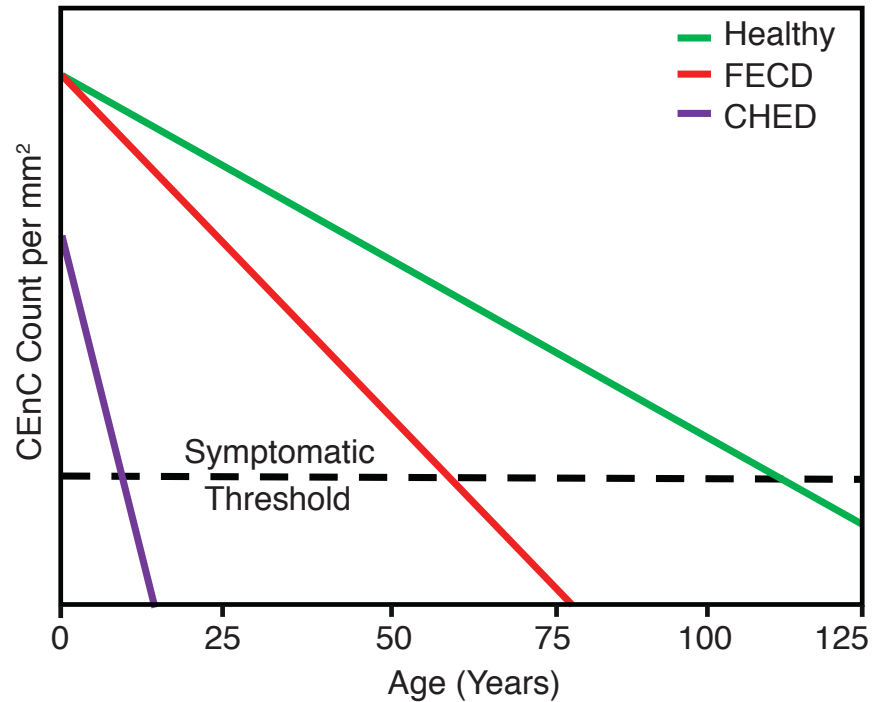


**Figure 4.13: SLC4A11 Cell Adhesion Role explains differences in FECD and CHED onset.**

CEnC count is critical in maintaining healthy corneal physiology. CEnC density is approximately 5000-7000 cells per mm<sup>2</sup> at birth and it decreases with age (green)<sup>171</sup>. Decline in CEnC density below a critical threshold may compromise the endothelial monolayer integrity which further compromises the endothelial pump, resulting in corneal edema. FECD-causing point mutations in SLC4A11 that affect the cell adhesion weaken the attachment of CEnC to DM, but the mutated protein still retains its transport functions (Fig. 4.5C). Disease symptoms are thus delayed and arise around 40-50 years, as seen in FECD (red). On the contrary, CHED-causing SLC4A11 mutations compromise the accumulation of protein at the cell surface<sup>89</sup>, which explains why CHED patients are born with 10-fold lower CEnC density when compared to healthy infants<sup>57,172</sup>. Absence of SLC4A11 at the cell surface clearly compromises cell adhesion, as seen in E143K-SLC4A11 (Fig. 4.5A) and the CEnC density declines rapidly giving rise to disease symptoms, as seen in CHED (purple).

FECD arises from alterations in several genes, with approximately 70% of FECD genetic load from TCF4 due to intronic trinucleotide repeat (TNR) expansion<sup>43</sup>. Expansion of the number of Cytosine-Thymine-Guanine (CTG) sequences beyond a threshold level sequesters MBNL1 (Muscleblind like 1 protein), whose normal role is as an activator or repressor of pre-mRNA splicing. This leads to accumulation of pre-mRNA-MBNL1 complexes in the cell that causes mRNA toxicity<sup>43</sup>. Increased rates of cell death have been proposed to be secondary to mRNA toxicity, but one report suggests no contribution to disease pathogenesis<sup>174</sup>. Loss of cell adhesion may also be a consequence of TCF4 alterations. TCF4 regulates expression of ZEB1<sup>55</sup>, another transcription factor whose mutations cause ECD<sup>44</sup>. ZEB1 acts as a transcriptional regulator of SLC4A11 by directly binding to its promoter<sup>175</sup>. Indeed, TCF4 controls the expression of other gene products involved in cell adhesion, including NRXN1<sup>176</sup>, CNTNAP2<sup>176</sup> and integrins<sup>177</sup>. This suggests that TCF4 may regulate SLC4A11 expression via ZEB1. TCF4 mutations that affect its expression and cause mRNA toxicity may induce loss of expression of its downstream genes, including SLC4A11. SAGE analysis in CEnC from pooled FECD corneas, also, revealed downregulation of SLC4A11 expression as a common FECD feature<sup>178</sup>. Altered expression of proteins required for CEnC-DM interaction could thus be an important component of FECD pathology.

The chimeric protein containing SLC4A11-EL3, STIC, increased cell adhesion to similar levels as full-length SLC4A11. Chimeric proteins like STIC may potentially improve the efficiency of regenerative cell therapy aimed at the treatment of FECD and CHED<sup>179,180</sup> when delivered into patient HEnC before injection into their anterior chamber.

The cell adhesion role of SLC4A11 may have significance to cancer progression. Indeed, high SLC4A11 expression is prognostic of poor outcomes in ovarian cancer<sup>87</sup>. The Cancer Genome Atlas (TCGA) database<sup>76</sup> and The Human Protein Atlas (THPA)<sup>71</sup> highlight multiple SLC4A11 mutations and differential SLC4A11 expression in cancers. Increased SLC4A11

expression may promote metastasis through increased cell adhesion at secondary sites following shedding from ECM, while SLC4A11 loss could disrupt signaling cascades needed for programmed cell death.

Complementary studies in transfected HEK293 cells and primary HCEnC are unified in supporting a central role of SLC4A11 in adhesion to DM. SLC4A11 is the first example of a solute transporter with a key role in cell adhesion. The discovery that SLC4A11 binds DM components implicates cell adhesion to ECM as a central pathway compromised in ECD. Some disease-causing SLC4A11 mutations compromise cell adhesion, without affecting cell surface trafficking or transport capacity. Cell adhesion defects thus suffice to cause corneal dystrophies. Restoration of cell adhesion using small chimeric protein, STIC that contains SLC4A11-EL3 may provide an intervention to increase CEnC-DM adhesion to slow ECD progression.

---

## **Chapter 5: Summary and Future Directions**

---

## 5.1 Summary

The objectives of this thesis were to 1) Identify the SLC4A11 translational product expressed in the human cornea. This is critical because SLC4A11 mutations cause two prominent genetic blinding diseases, FECD and CHED. Studies aimed at understanding the role(s) of SLC4A11 in the cornea should use the relevant SLC4A11 variant in order to generate reliable data. 2) Understand the role of SLC4A11 in HCEnC adhesion to DM. Progressive HCEnC loss is observed in FECD and CHED patients<sup>29</sup> but compromised solute transport function of SLC4A11 fails to explain this phenomenon. Defective cell adhesion role of SLC4A11 provides an explanation for HCEnC loss and proposes a defective cell biological pathway that underlies the pathology of these diseases. The data presented in this thesis have advanced our understanding of corneal physiology and its endothelial diseases through the discovery of a previously unidentified function of SLC4A11. Additionally, now we have potential strategies to treat FECD and CHED.

### 5.1.1 Human Corneal Expression of SLC4A11, a Gene Mutated in ECD

Three N-terminal SLC4A11 variants are expressed in humans: v1, v2 and v3, which are also called SLC4A11-A, -B and -C, respectively<sup>66</sup>. To identify the predominant variant(s) in human cornea, we used a combination of bioinformatic, RNA and variant specific-protein analysis. We began with the bioinformatics analysis to identify the variant with the strongest alignment with SLC4A11 from other mammalian species. We found that v2 has the strongest alignment with other mammalian species. Specifically, we observed a second methionine (M36) downstream of M1 which had a stronger degree of sequence conservation with other mammalian SLC4A11 proteins and a stronger Kozak consensus around M36, suggesting v2-M36 as the potential SLC4A11 start site in human cornea. We further performed RT-PCR and real time PCR analysis to quantify the abundance of SLC4A11 in the whole cornea and isolated endothelium, respectively. Both v2 and v3 transcripts were observed in whole cornea and isolated endothelium

but v2 was the predominant transcript. RT-PCR and real-time PCR data suggest that SLC4A11-v1 is not expressed in human cornea. To test the validity of these findings at the protein level, we raised custom antibodies corresponding to different variants and found that SLC4A11-v2 protein was four times as abundant as SLC4A11-v3 in the corneal endothelium.

Using custom antibodies, we further found that the translation start site in SLC4A11-v2 in human cornea is M36, instead of M1. Several *in vitro* studies have examined SLC4A11-v2 but all of them worked with SLC4A11-v2-M1, except a few recent studies from our group (Table 3.1). To test the validity of findings with SLC4A11 v2-M1, we compared SLC4A11 v2-M1 and v2-M36 in their cell surface abundance, localization and solute transport function. Interestingly, no significant differences were found suggesting the validity of the earlier studies with v2-M36.

We finally focused on the reason for presence of two N-terminal variants, v2-M36 and v3, in human corneas, differing only by 19 amino acids at their N-termini. No significant differences were observed in their solute transport activity (water flux), however, we found significant differences in the structure of their cytoplasmic domains as revealed by homology models created using i-TASSER and Phyre<sup>2</sup>. The unique N-terminus of v3 was surface exposed and has Threonine at position 5 (N-MAAA**T**RRVFHLQPC-C), which was predicted as a potential phosphorylation site for PKC and crucial in CEnC proliferation and cell cycle<sup>152</sup>. Overall, the results from Chapter 3 lead to the conclusion that v2-M36 is the predominant variant expressed in the human corneal endothelium. It is the relevant variant to be used in studies of SLC4A11 in human cornea and ECD. SLC4A11-v3 is, however, also present at significant levels and should be considered relevant based on the nature of the studies.

### **5.1.2 Defective Cell Adhesion Role of Solute Transporter, SLC4A11, in ECD**

Loss of HCEnc from their underlying basement membrane, DM, is a hallmark of blinding ECD<sup>29</sup>. Mutations in SLC4A11 cause ECD<sup>36,42</sup> but the link between SLC4A11 transport function and

HCEnC loss is unclear. We reasoned that SLC4A11 has roles beyond membrane transport. We hypothesized that SLC4A11, an abundant protein of the HCEnC basolateral surface<sup>73</sup>, promotes HCEnC adhesion to DM via its EL3. To test this hypothesis, we designed an *in vitro* cell adhesion assay using bovine DM extract on plates and SLC4A11 expressed in HEK293 cells. We found that SLC4A11 promotes cell adhesion to DM which is proportional to its expression and conserved across other mammalian species. Using custom antibody targeting SLC4A11-EL3, we observed that blocking EL3 with this antibody compromises cell adhesion, implicating EL3 in promoting DM attachment. Further, FECD-causing point mutations in EL3 compromise cell adhesion without any effect on cell surface processing and solute (water flux) transport, further implicating defective cell adhesion as critical in explaining HCEnC loss in patients. Pull down assays using GST-SLC4A11-EL3 fusion protein and DM extracts revealed COL8A2 (product of another FECD causing gene) and COL8A1 as interactors of SLC4A11 in the DM.

Complementary studies in primary CEnC isolated from donor human corneas revealed the importance of SLC4A11 in corneal physiology. Isolation of HCEnC from their native environment compromises SLC4A11 expression. Culturing HCEnC in the presence of DM causes upregulation of SLC4A11 and COL8A2, suggesting the importance of DM signaling in regulating SLC4A11 expression and its interaction partner. In parallel, restoring SLC4A11 expression to physiological levels by transfection increases HCEnC adhesion to DM. Blocking SLC4A11-EL3 with anti-SLC4A11-EL3 antibody compromises HCEnC adhesion by 30%, suggesting the contribution of SLC4A11 to HCEnC-DM adhesion via SLC4A11-EL3.

We created a three-dimensional energy-minimized model of SLC4A11-EL3 using ROSETTA-Membrane and Temperature Replica-Exchange Molecular Dynamics simulations. The model shows the FECD-causing point mutations are buried within the EL3 structure and they potentially cause disease by altering EL3-fold. Finally, we created a small chimeric protein, STIC, to understand if isolated EL3 promotes adhesion to DM. Interestingly, STIC promoted cell

adhesion to similar levels as full length SLC4A11. This suggests: 1) SLC4A11-EL3 is the key component of HCEnC that promotes a direct attachment to DM, and 2) Small chimeric proteins like STIC hold potential to correct defective cell adhesion in patients via gene delivery.

In conclusion, results from Chapter 4 found that SLC4A11 is the first solute transporter to show a cell adhesion function that provides an explanation to HCEnC loss in patients and suggests additional avenues for therapeutic intervention.

## **5.2 Future Directions**

The identified cell adhesion role of SLC4A11 and its association with COL8A2 in the human cornea creates a foundation to test new hypotheses to advance our understanding of solute transport proteins and cell adhesion mechanisms. It also suggests value in investigating the roles of SLC4A11 in tissues where endothelial cell loss is associated with disease pathophysiology. In this section, I discuss a few ideas stemming from the cell adhesion role of SLC4A11 that can help increase the understanding of the dynamics of this interaction and its application in other physiological systems.

### **5.2.1 Key amino acid residues involved in SLC4A11 and COL8A2 interaction**

Data in Chapter 4 suggest that interaction between SLC4A11-EL3 and COL8A2 promotes CEnC-DM attachment. The predicted length of SLC4A11-EL3 is 64 amino acids which includes four FECD-causing point mutations and two sites of N-linked glycosylation (Fig. 4.3A, Fig. 4.6D). Preliminary studies using peptide competition assays show the potential amino acids in SLC4A11-EL3 that play a role in this interaction lie between H527-L540 (Fig. 4.6D). The energy-minimized model of SLC4A11-EL3 maps this region at the surface of each EL3 where it can potentially interact with the DM (Fig. 5.1). Further analysis shows highly conserved residues, N-SLVSL-C, in this region (Fig. 4.6D). Interestingly, these residues are also present in the N-terminal extracellular

domain of secretin receptor (NCBI: NP\_002971) which plays a critical role in binding and recognition of the peptide hormone, secretin<sup>181</sup>. Zinc finger protein 717 (NCBI: XP\_011531546) and bacterial SapC proteins also have these residues, however, their role is unknown<sup>182,183</sup>. Additionally, the presence of hydrophobic amino acids, V and L, makes it a potential region to be involved in an interaction with DM.

COL8A2 also contains a C-terminal c1q-like domain<sup>184</sup>, which belongs to the c1q family of proteins that promote cell and ECM interactions<sup>185,186</sup>. COL8A2 C1q-like domain is a potential region for interaction with SLC4A11-EL3. Further studies focused on identifying the residues in SLC4A11-EL3 and COL8A2 are needed to understand the interaction between the two proteins. Site-directed mutagenesis can be used to mutate the SLVSL region in SLC4A11-EL3 and testing the mutant proteins in cell adhesion assay to identify the residues involved in interaction to DM. To identify the residues in COL8A2 that interact with SLC4A11-EL3, custom overlapping peptide arrays of c1q-like domains of COL8A2 can be made. These arrays can be incubated with HEK293 protein lysates expressing WT-SLC4A11 or empty vector and probing with anti-SLC4A11 antibody to identify the peptide spots that bind SLC4A11. Overlapping peptide arrays can be used to narrow down to the exact amino acid residues that are involved in the interaction. These results can be validated by reversing the experiment and making SLC4A11-EL3 peptide arrays that will be incubated with COL8A2 protein. GST-pull down assays and co-IP using WT and mutant proteins can further validate the findings from the previous experiments.

### **5.2.2 SLC4A11 and COL8A2 co-chaperone each other to maintain DM organization?**

DM is a highly organized array of ECM proteins arranged in hexagonal lattices. These ECM proteins are secreted by CEnC and deposited at the posterior surface of the DM<sup>34</sup>. In ECD, the DM assembly is disrupted by aberrant deposition of COL8A1 and COL8A2 proteins at the

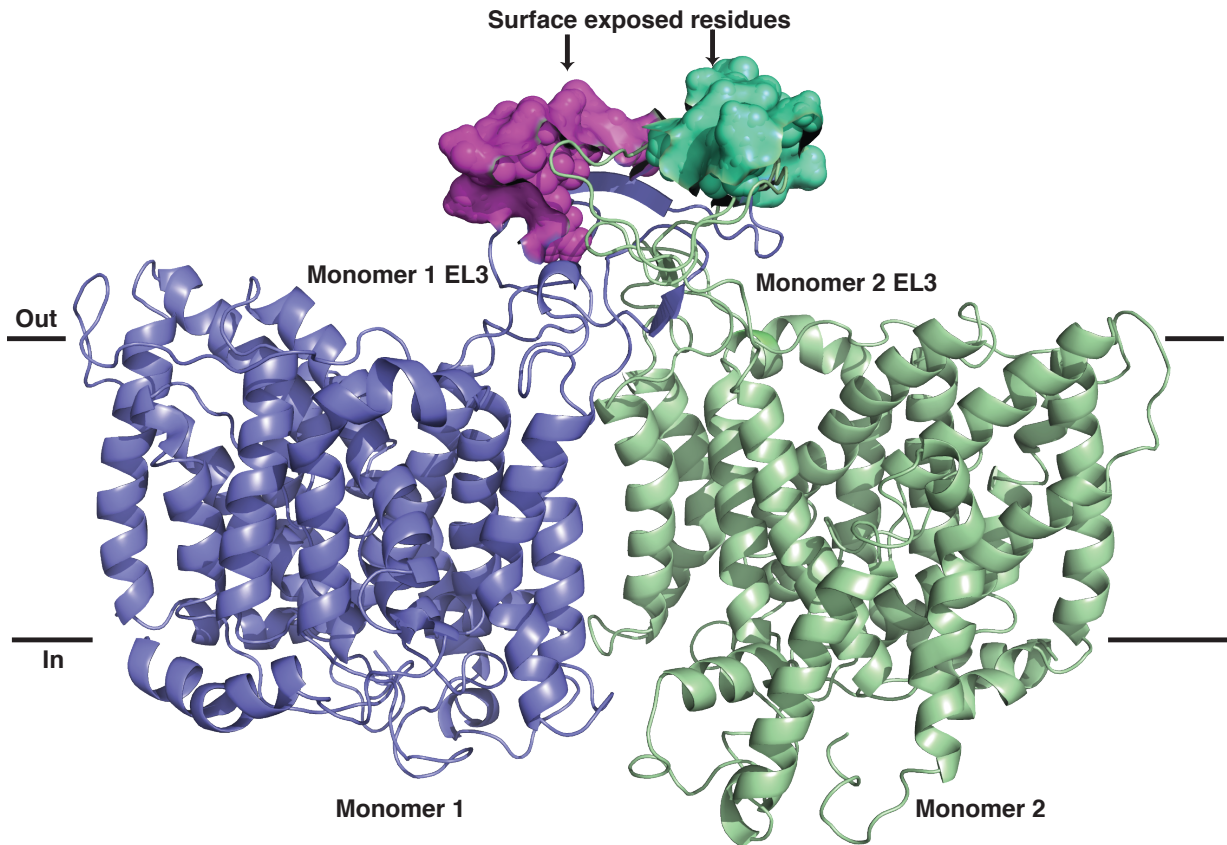


**Figure 5.1: Potential amino acids in SLC4A11-EL3 involved in DM interaction are surface exposed.**

Homology model of SLC4A11-EL3 showing two SLC4A11 monomers and their EL3 in the center. The amino acids H527-L540 rendered in space filling format, colored pink in monomer 1 and green in monomer 2, facing the DM. Amino acids H527-L540 in each loop contain the residues proposed to interact with DM.

posterior surface which results in DM thickening and guttae formation<sup>49</sup>. Data in Chapter 4 show that COL8A2 interacts with SLC4A11 (Table 4.1). Do these proteins traffic to the cell surface separately and interact after COL8A2 has been secreted onto the DM? If this is true, why does oversecreted COL8A2 and COL8A1 not assemble in the regular hexagonal pattern in ECD? The upregulation of SLC4A11 in HCEnC also leads to an upregulation of COL8A2, as seen in chapter 4 (Fig. 4.9). This suggests that SLC4A11 may bind COL8A2 at the ER during protein folding or trafficking and the two proteins may co-chaperone each other to the plasma membrane. This interaction may cause SLC4A11 to orient COL8A2 at the plasma membrane, so it is secreted and deposited on the posterior surface of the DM in an organized fashion. Loss or downregulation of SLC4A11 in ECD may affect the proper chaperoning and trafficking of COL8A2, resulting in unorganized secretion and deposition of COL8A2 on DM forming guttae. *In vitro* studies using overexpressed SLC4A11 and COL8A2 can be performed to understand the interaction between the two proteins. COL8A1 forms hexagonal array with COL8A2 and is also a potential SLC4A11 interactor (Table 4.1), making it an important component to be considered in this study. Protein expression analysis, pulse chase experiments, protein-pull down assays and immunofluorescence labelling can be used to test this hypothesis. This will help create a better understanding of the CEnC and DM physiology, and may provide a potential explanation for the presence of collagen-enriched guttae in patients.

### **5.2.3 Potential association of SLC4A11 with corneal integrins and focal adhesions**

SLC4A11 significantly contributes to CEnC adhesion as seen in Chapter 4 (Fig. 4.11F). Several integrins also contribute to CEnC-DM adhesion, for example, Integrin  $\alpha_v$  (ITGAV), Integrin  $\beta_3$  (ITGB3) and integrin  $\beta_5$  (ITGB5). These exist in heterodimers of  $\alpha_v\beta_3$ ,  $\alpha_v\beta_5$  in CEnC where they interact with FNC, collagens and laminins in the DM by binding to their RGD motifs<sup>116</sup>. Recent studies also implicate  $\alpha_4\beta_1$  and  $\alpha_6\beta_1$  in contributing to CEnC adhesion<sup>76</sup>. Focal adhesions are

multimeric complexes consisting of several proteins that interact to connect the inside of the cell to its ECM, promote cell adhesion and transduce signals across the plasma membrane<sup>187</sup>. Focal adhesions create strong regions of attachment between the cell and its ECM by clustering adhesion molecules to promote avidity. Integrins and its receptors are prominent transmembrane components of the focal adhesions that interact with the ECM proteins on their extracellular surface and with actin and other ancillary proteins on their cytosolic surface or membrane domains. The cell adhesion role of SLC4A11 in CEnC may be more efficient by avidity if it also functions via focal adhesions. SLC4A11 may interact with integrins to form focal adhesions in the plasma membrane. The presence of RGD motif in the N-terminal cytosolic domain of SLC4A11 further suggests a potential interaction between the cytosolic regions of SLC4A11 and integrins. Assays of protein-protein interaction can be used to test a potential association between SLC4A11 and corneal integrins that bind RGD motifs. Co-expression of these proteins can also test for a potential increase in strength of cell attachment to DM using the cell adhesion assays. This will further unravel the endothelial cell mechanisms of adhesion to their ECM.

#### **5.2.4 Role of SLC4A11 in anoikis**

Anoikis is programmed cell death due to loss of cell-ECM attachment. Cells require specific attachment to ECM, subtle changes in this attachment can break the communication between cells and ECM<sup>76</sup>. Anoikis is also a preventative mechanism to suppress metastasis of cells after loss of their ECM attachment<sup>188</sup>. Loss of DM attachment triggers anoikis in CEnC to prevent the migration of cells into the anterior chamber and the retina. Blocking integrin-mediated adhesion in focal adhesions of human endothelial cells triggers anoikis<sup>189</sup>. Does loss of SLC4A11-EL3 attachment to COL8A2 and COL8A1 triggers a pathway for cells to undergo cell death? SLC4A11 has a large (~44 KDa) cytoplasmic domain which is only implicated in solute transport functions. Data from Chapter 3 suggests additional roles of SLC4A11 cytoplasmic domain. Potential

phosphorylation sites present in SLC4A11 cytoplasmic domain that function with PKC to regulate CEnC proliferation and cell cycle, further supports this hypothesis<sup>152</sup>. SLC4A11 knockdown in an immortalized HCEnc line also leads to cell death by apoptosis<sup>169</sup>.

The role of SLC4A11 in promoting anoikis can be studied by blocking the SLC4A11-EL3 on the surface of HCEnc with anti-SLC4A11-EL3 antibody in adhesion assays and probing for anoikis-specific proteins. Using live cell staining reagents on the cells incubated with anti-SLC4A11-EL3 antibody versus pre-immune serum and subjecting them to flow cytometry cell sorting can also help understand the role of SLC4A11 in anoikis. Knocking out SLC4A11 in mice mimics the ECD pathophysiology as observed in humans. Comparing the protein profile of SLC4A11 KO mice versus WT mice can also be used for studying the changes in expression profiles of anoikis related proteins. Understanding the role of SLC4A11 in triggering cellular pathways responsible for mediating cell proliferation and death will be a major advancement to establish the versatility in functions of large solute carrier proteins and open doors for further investigations.

### **5.2.5 Potential exploitation of SLC4A11-mediated cell adhesion by cancer cells**

SLC4A11 is widely expressed in other tissues in the body including brain, kidneys, small intestine, liver, ovaries and breasts<sup>71</sup>. SLC4A11 expression is significantly upregulated in ovarian cancer cells<sup>87</sup>. Metastatic cells show higher SLC4A11 expression when compared to non-metastatic cells. High SLC4A11 expression is an independent predictor of poor patient survival. The Cancer Genome Atlas (TCGA) database<sup>76</sup> and The Human Protein Atlas (THPA)<sup>71</sup> also highlight multiple SLC4A11 mutations reported in cancer patients and differential SLC4A11 expression in several cancers, respectively. Despite several reports of SLC4A11 mutations and altered expression in cancerous tissues, the role of SLC4A11 in cancer is unclear. The cell adhesion role of SLC4A11 may explain the connection of SLC4A11 to cancer. Cancer cells may modulate SLC4A11

expression to shed from ECM and metastasize to secondary sites where they can further colonize. Downregulation of SLC4A11 may also suppress pathways of cell proliferation and death, as discussed in section 5.2.4. Further studies are needed to establish the role of SLC4A11 in tumor progression and metastasis. Similar correlations between integrin expression and cancer metastasis have been widely studied<sup>190</sup> and can be used as blueprints to investigate a potential role of SLC4A11 in cancer metastasis.

### **5.2.6 SLC4A11 and TCF4**

Approximately 70% of the genetic load of FECD comes from alterations in TCF4 but the effect of these alterations beyond mRNA toxicity are not understood. Another transcription factor, ZEB1 whose mutations also cause FECD, directly binds to SLC4A11 promotor<sup>175</sup>. Also, TCF4 and ZEB1 modulate each other expression and are a part of the Wnt and TCF4/ $\beta$ -catenin signaling pathways<sup>55</sup>. The association between TCF4 and ZEB1 hints that TCF4 may regulate SLC4A11 expression. Interestingly, TCF4 and ZEB1 also modulates the expression of another FECD causing gene, LAMC2<sup>55</sup>. If SLC4A11 is regulated by TCF4, SLC4A11 expression should be altered in FECD patients. Indeed, SAGE analysis in CEnC from FECD corneas revealed that downregulated SLC4A11 expression is a common feature of the disease<sup>178</sup>. Other CAMs like NRXN1<sup>176</sup>, CNTNAP2<sup>176</sup> and integrins<sup>177</sup> are also regulated by TCF4. Future efforts can be focused on studying the direct effect of TCF4 alterations on SLC4A11 expression. Knocking down TCF4 in primary HCEnc can easily address this question. Existing *pcf4*<sup>+/-</sup> mice can also be used to study the corneal expression of SLC4A11<sup>176</sup>. ECD-causing ZEB1 mutations also lead to downregulation of COL8A2 expression<sup>191</sup>, the interactor of SLC4A11, which further suggests that COL8A2 expression maybe regulated by similar upstream molecules as SLC4A11. If TCF4 acts as a transcription factor for SLC4A11 and COL8A2, the effect of TCF4 genetic load in FECD gets transferred to its downstream effectors SLC4A11 and COL8A2, implicating these proteins as

critical in FECD. This finding points towards CEnC-DM adhesion as the primary cell biological pathway defective in FECD, and the prime focus of FECD-related studies.

### **5.2.7 Cell adhesion in the inner ear**

CHED-causing SLC4A11 mutations also lead to sensorineural hearing loss which is termed as HS<sup>192</sup>. Now recognized as a variant presentation of CHED<sup>38</sup>. Patients harboring these mutations suffer both vision and hearing deficits, causes of which are unknown. CHED-mutations cause SLC4A11-misfolding and ER-retention<sup>89</sup> leading to loss of CEnC adhesion from DM (Fig. 4.5A). Does loss of SLC4A11 cell adhesion in specific cochlear tissues explain sensory deficits in patients? SLC4A11 is expressed in stria vascularis of the cochlear duct which produces endolymph for scala vestibuli, one of the two fluids of cochlea which helps in transmission of waves to receptors to promote sensory functions and coordinate balance<sup>76</sup>. These cells secrete their own ECM which is essential in cochlea function. Loss of cell attachment to their basement membrane in this region may disrupt the cochlear physiology leading to hearing deficits. SLC4A11 is also exclusively expressed in inner ear fibrocytes which lie under the sensory epithelia in the membranous labyrinth. Fibrocytes secrete their own ECM with cochlin as one of the abundant ECM proteins. SLC4A11 null mice show a complete collapse of the membranous labyrinth which affects the sensory functions of the mice<sup>193,194</sup>. However, cochlin expression did not change in their basement membrane. *slc4a11*<sup>-/-</sup> mice show hearing deficits with the altered ionic concentrations in the endolymph which is hypothesized to be the cause of hearing loss in mice and humans<sup>74</sup>. Future studies aimed at exploring SLC4A11 cell adhesion role in fibrocytes to promote attachment to their basement membrane and maintaining the integrity of the membranous labyrinth, and in cells of the stria vascularis are necessary to understand how SLC4A11 mutations cause sensorineural loss.

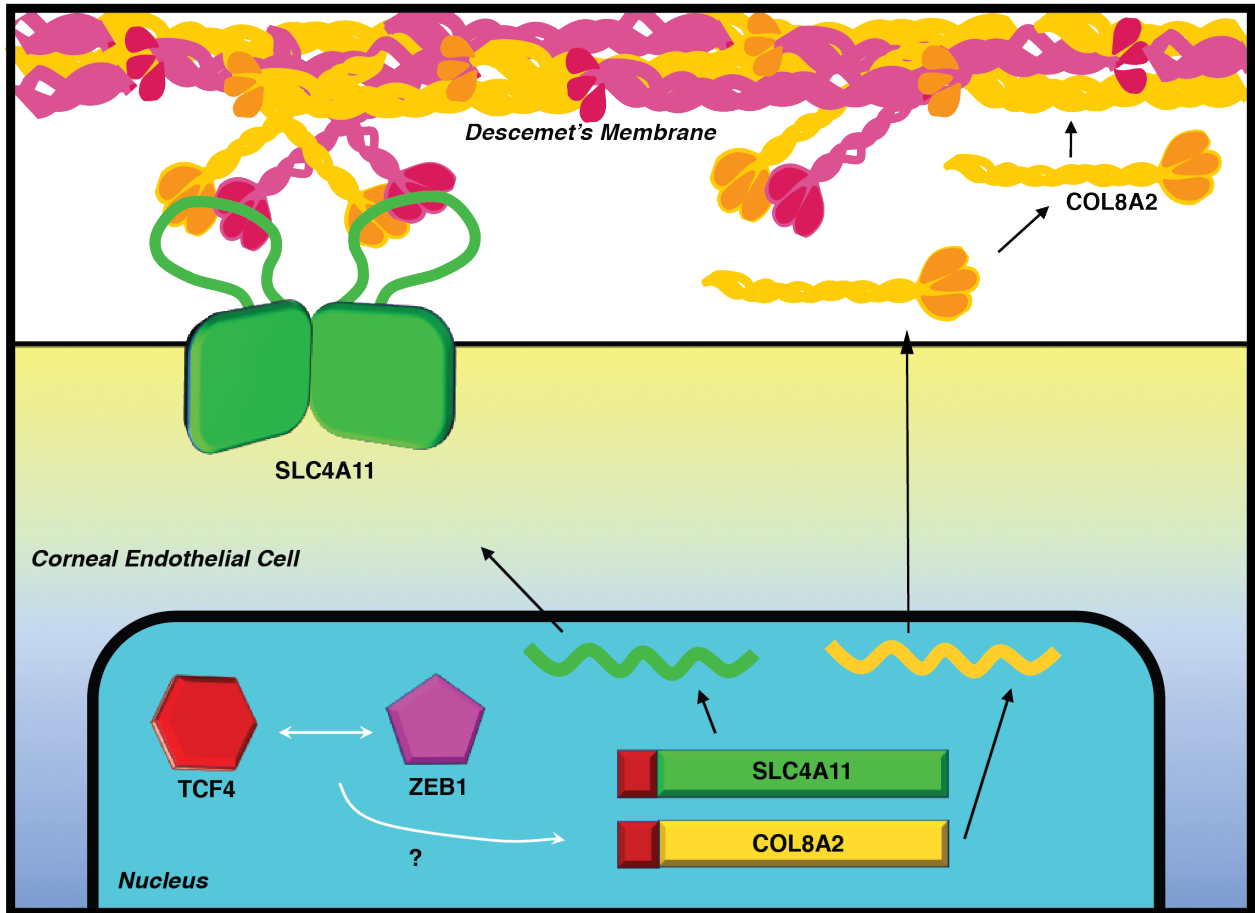


**Figure 5.2: Proposed cell biological pathway defective in FECD.**

Products of six out of nine genes mutated in FECD are players in this proposed pathway (SLC4A11, COL8A2, TCF4, ZEB1, LAMC1 and AGBL1) that contributes to CENC adhesion to DM by SLC4A11. Defects in any of these genes can result in loss of CENC-DM adhesion resulting in the loss of CENC, that contribute to FECD pathology. (LAMC1 and AGBL1 are not shown in the figure for simplicity).

### **5.2.8 Role of SLC4A11 during development**

Corneal endothelium is derived from the neural crest cells (NCC) that separate from the neural plate and migrate into the cleft formed between the surface ectoderm and the lens vesicle. This first wave of NCC migrate over a layer of FNC in the corneal stroma to form a layer of overlapping cells, which thin into a monolayer by the eighth week of gestation. This monolayer is the posterior cell layer of the cornea, also called corneal endothelium. Starting at the eighth week of human gestation, the CEnC in this monolayer start to secrete ECM components to lay down their basement membrane, the DM. The prenatal DM has a banded pattern and called anterior banded layer with an average thickness of 3  $\mu\text{m}$ . CEnC continue to deposit ECM components post-natally and throughout the life. The DM secreted post-natally has a non-banded granular appearance and called posterior non-banded layer whose average thickness in adults can reach 40  $\mu\text{m}$ . Migration pattern defects of NCC may lead to congenital anterior chamber defects, like CHED<sup>15,195</sup>. Transcriptional profiling shows the expression of SLC4A11 in NCC from developing mice embryos<sup>76</sup>. Cell adhesion role of SLC4A11 may be important for migrating NCC to accumulate at the site of corneal formation by differential regulation of SLC4A11 expression. Genetic defects that affect cell adhesion function or downregulate SLC4A11 expression may lead to a defect in NCC migration pattern. Indeed, *slc4a11* is the only gene reported whose mutations cause CHED (OMIM: 217700). The majority of CHED-causing mutations in SLC4A11 cause protein misfolding, leading to a partial or complete failure of SLC4A11 trafficking to the plasma membrane<sup>89</sup>. Additionally, CHED patients are born with a 10-fold lower CEnC density compared to healthy infants. This supports the argument that prenatal adhesion defects in migrating NCC may have a role in CHED pathology. Studies targeted towards investigating SLC4A11 cell adhesion function during embryonic development can test this hypothesis to provide a potential explanation for CHED pathology.

### **5.2.9 Strategies to use STIC as a therapeutic molecule in ECD**

With the global shortage of donor corneas, there is a growing need for new therapeutic strategies for ECD that can overcome the need for corneal transplants. As discussed in Chapter 4, cell adhesion is a cell biological pathway defective in ECD patients. Small proteins containing SLC4A11-EL3 like STIC, hold a potential to correct the cell adhesion defect in patients by gene delivery. The therapeutic potential of STIC or similar proteins containing SLC4A11-EL3 needs to be tested in an *in vivo* system closer to human physiology, like the primary HCEnC, to ensure its validity in disease treatment. Future studies to test the *in vivo* therapeutic potential of STIC should be designed while keeping in mind the long-term application in ECD patients. There are two potential strategies to deliver STIC to correct for adhesion defects: Direct or Indirect delivery. Direct method includes injecting viral particles like lentiviruses or adeno-associated viruses that contain the cDNA encoding STIC, into the anterior chamber of the eye. To suppress viral infection of neighboring tissues and increase the probability of viral particle delivery to CEnC, surface engineered viral vectors for CEnC-specific delivery should be used<sup>76</sup>. These vectors are designed by destruction of natural receptor used by the virus, followed by addition of a high-affinity ligand that attaches to a specific protein on the surface of the desired cell type. These high-affinity ligands could be a small peptide, single-chain antibody or a designed ankyrin repeat protein. NCAD<sup>76</sup> and peroxiredoxin 6 (PRDX6)<sup>76</sup> are specific markers of the apical surface of CEnC that are not expressed in the neighboring cells (corneal epithelium or stroma or trabecular meshwork), and can be used as targets to bind the viral vectors. *In vivo* expression of STIC in the diseased CEnC can strengthen their attachment to DM. Indeed, FECD and CHED patients are undergoing progressive CEnC loss which compromises their visual acuity. If the CEnC count is above the symptomatic threshold count (Fig. 4.13), the endothelium can retain the endothelial pump function to prevent corneal edema and compromised visual acuity. In adult corneas, this symptomatic

threshold is about one-tenth the number of cells in healthy corneas, i.e. 350-500 cells/mm<sup>2</sup> approximately<sup>76</sup>. Patients with CEnC counts higher than the threshold might be suitable candidates for direct gene delivery.

Indirect methods includes *ex vivo* gene delivery to tissue-engineered corneal constructs that are transplanted by EK, or transgene viral delivery to GMP-approved CEnC cultures before they are delivered to the anterior chamber by cell injection<sup>196</sup>. All strategies described above hold potential in ECD treatment, by delivery of SLC4A11-EL3 containing chimeric proteins which will successfully surpass the tests of therapeutic effectiveness and safety.

SLC4A11 was discovered in 2001<sup>197</sup> and its mutations were found in CHED patients in 2006<sup>36</sup>. Since then, many discoveries have helped us understand the role of this protein in corneal physiology and defects in ECD. However, loss of CEnC in ECD patients is a perplexing question. Several studies addressed the biology behind CEnC, suggesting loss as a consequence of oxidative stress<sup>198</sup>, ammonia accumulation<sup>203</sup> and mRNA toxicity<sup>108</sup>. However, none could provide an adequate mechanism to explain the increased CEnC loss. The cell adhesion function of SLC4A11 revealed in this thesis is unique in helping to explain normal corneal physiology and providing a potential explanation for progressive CEnC loss in patients. The cell adhesion role of SLC4A11 unifies the FECD genes as components of endothelial cell adhesion apparatus. Although, defective cell adhesion may only contribute to CEnC pathophysiology and additional effects of oxidative stress, mRNA toxicity and progressive ammonia accumulation may eventually trigger the pathways that cause the cells to ultimately detach and undergo anoikis. This study has advanced the field of SLC4A11, genetic corneal dystrophies and solute transport proteins. It has also put forward new ideas to help us better understand our biology and take the next steps for disease treatment. It was a long way to understand the roles of SLC4A11 in the human cornea, but we are not far away from understanding the diversity of its functions and their applications to create a better life quality for the ECD patients.

## BIBLIOGRAPHY

- 1 Silver, D. M. & Csutak, A. Human Eye Dimensions for Pressure-Volume Relations. *Invest Ophthalmol Vis Sci* **51**, 5019, (2010).
- 2 Willoughby, C. E., Ponzin, D., Ferrari, S., Lobo, A., Landau, K. & Omid, Y. Anatomy and physiology of the human eye: effects of mucopolysaccharidoses disease on structure and function—a review. *Clin Exp Ophthalmol*, 2-11, (2010).
- 3 Kels, B. D., Grzybowski, A. & Grant-Kels, J. M. Human ocular anatomy. *Clin Dermatol* **33**, 140-146, (2015).
- 4 DelMonte, D. W. & Kim, T. Anatomy and physiology of the cornea. *J Cataract Refract Surg* **37**, 588-598, (2011).
- 5 Torricelli, A. A., Singh, V., Santhiago, M. R. & Wilson, S. E. The corneal epithelial basement membrane: structure, function, and disease. *Invest Ophthalmol Vis Sci* **54**, 6390-6400, (2013).
- 6 Wilson, S. E. & Hong, J. W. Bowman's layer structure and function: critical or dispensable to corneal function? A hypothesis. *Cornea* **19**, 417-420, (2000).
- 7 Tisdale, A. S., Spurr-Michaud, S. J., Rodrigues, M., Hackett, J., Krachmer, J. & Gipson, I. K. Development of the anchoring structures of the epithelium in rabbit and human fetal corneas. *Invest Ophthalmol Vis Sci* **29**, 727-736, (1988).
- 8 Meek, K. M. & Knupp, C. Corneal structure and transparency. *Prog Retin Eye Res* **49**, 1-16, (2015).
- 9 Meek, K. M. & Boote, C. The organization of collagen in the corneal stroma. *Exp Eye Res* **78**, 503-512, (2004).
- 10 Torricelli, A. A. & Wilson, S. E. Cellular and extracellular matrix modulation of corneal stromal opacity. *Exp Eye Res* **129**, 151-160, (2014).
- 11 Johnson, D. H., Bourne, W. M. & Campbell, R. J. The ultrastructure of Descemet's membrane. I. Changes with age in normal corneas. *Arch Ophthalmol* **100**, 1942-1947, (1982).
- 12 Schlotzer-Schrehardt, U., Bachmann, B. O., Laaser, K., Cursiefen, C. & Kruse, F. E. Characterization of the cleavage plane in Descemet's membrane endothelial keratoplasty. *Ophthalmology* **118**, 1950-1957, (2011).

- 13 Kapoor, R., Bornstein, P. & Sage, E. H. Type VIII collagen from bovine Descemet's membrane: structural characterization of a triple-helical domain. *Biochemistry* **25**, 3930-3937, (1986).
- 14 Eghrari, A. O., Riazuddin, S. A. & Gottsch, J. D. Overview of the Cornea: Structure, Function, and Development. *Prog Mol Biol Transl Sci* **134**, 7-23, (2015).
- 15 Tuft, S. J. & Coster, D. J. The corneal endothelium. *Eye (Lond)* **4 ( Pt 3)**, 389-424, (1990).
- 16 Sanchis-Gimeno, J. A., Lleo-Perez, A., Alonso, L., Rahhal, M. S. & Martinez Soriano, F. Corneal endothelial cell density decreases with age in emmetropic eyes. *Histol Histopathol* **20**, 423-427, (2005).
- 17 Joyce, N. C. Proliferative capacity of corneal endothelial cells. *Exp Eye Res* **95**, 16-23, (2012).
- 18 Dua, H. S., Faraj, L. A., Said, D. G., Gray, T. & Lowe, J. Human corneal anatomy redefined: a novel pre-Descemet's layer (Dua's layer). *Ophthalmology* **120**, 1778-1785, (2013).
- 19 Bourne, W. M. Biology of the corneal endothelium in health and disease. *Eye (Lond)* **17**, 912-918, (2003).
- 20 Sweeney, D. F., Xie, R. Z., O'Leary, D. J., Vannas, A., Odell, R., Schindhelm, K., Cheng, H. Y., Steele, J. G. & Holden, B. A. Nutritional requirements of the corneal epithelium and anterior stroma: clinical findings. *Invest Ophthalmol Vis Sci* **39**, 284-291, (1998).
- 21 Petroll, W. M., Hsu, J. K., Bean, J., Cavanagh, H. D. & Jester, J. V. The spatial organization of apical junctional complex-associated proteins in feline and human corneal endothelium. *Curr Eye Res* **18**, 10-19, (1999).
- 22 Barry, P. A., Petroll, W. M., Andrews, P. M., Cavanagh, H. D. & Jester, J. V. The spatial organization of corneal endothelial cytoskeletal proteins and their relationship to the apical junctional complex. *Invest Ophthalmol Vis Sci* **36**, 1115-1124, (1995).
- 23 Olsen, E. G., Davanger, M. & Moen, T. The role of microfilaments in the healing of the corneal endothelium. *Acta Ophthalmol (Copenh)* **63**, 104-108, (1985).
- 24 Bonanno, J. A. Molecular mechanisms underlying the corneal endothelial pump. *Exp Eye Res* **95**, 2-7, (2012).
- 25 Bonanno, J. A. Identity and regulation of ion transport mechanisms in the corneal endothelium. *Prog Retin Eye Res* **22**, 69-94, (2003).
- 26 Fischbarg, J. Water channels and their roles in some ocular tissues. *Mol Aspects Med* **33**, 638-641, (2012).

- 27 Schey, K. L., Wang, Z., J, L. W. & Qi, Y. Aquaporins in the eye: expression, function, and roles in ocular disease. *Biochim Biophys Acta* **1840**, 1513-1523, (2014).
- 28 Vilas, G. L., Loganathan, S. K., Liu, J., Riau, A. K., Young, J. D., Mehta, J. S., Vithana, E. N. & Casey, J. R. Transmembrane water-flux through SLC4A11: a route defective in genetic corneal diseases. *Hum Mol Genet* **22**, 4579-4590, (2013).
- 29 Klintworth, G. K. Corneal dystrophies. *Orphanet J Rare Dis* **4**, 7, (2009).
- 30 Vincent, A. L. Corneal dystrophies and genetics in the International Committee for Classification of Corneal Dystrophies era: a review. *Clin Exp Ophthalmol* **42**, 4-12, (2014).
- 31 Feizi, S. Corneal endothelial cell dysfunction: etiologies and management. *Ther Adv Ophthalmol* **10**, 2515841418815802, (2018).
- 32 E.B.A.A. 2016 Eye Bank Statistical Report. (Eye bank Association of America, Washington, DC, USA, 2017).
- 33 Eghrari, A. O. & Gottsch, J. D. Fuchs' corneal dystrophy. *Expert Rev Ophthalmol* **5**, 147-159, (2010).
- 34 Elhalis, H., Azizi, B. & Jurkunas, U. V. Fuchs endothelial corneal dystrophy. *Ocul Surf* **8**, 173-184, (2010).
- 35 Biswas, S., Munier, F. L., Yardley, J., Hart-Holden, N., Perveen, R., Cousin, P., Sutphin, J. E., Noble, B., Batterbury, M., Kielty, C., Hackett, A., Bonshek, R., Ridgway, A., McLeod, D., Sheffield, V. C., Stone, E. M., Schorderet, D. F. & Black, G. C. Missense mutations in COL8A2, the gene encoding the alpha2 chain of type VIII collagen, cause two forms of corneal endothelial dystrophy. *Hum Mol Genet* **10**, 2415-2423., (2001).
- 36 Vithana, E. N., Morgan, P., Sundaresan, P., Ebenezer, N. D., Tan, D. T., Mohamed, M. D., Anand, S., Khine, K. O., Venkataraman, D., Yong, V. H., Salto-Tellez, M., Venkataraman, A., Guo, K., Hemadevi, B., Srinivasan, M., Prajna, V., Khine, M., Casey, J. R., Inglehearn, C. F. & Aung, T. Mutations in sodium-borate cotransporter SLC4A11 cause recessive congenital hereditary endothelial dystrophy (CHED2). *Nature Genetics* **38**, 755-757, (2006).
- 37 Desir, J. & Abramowicz, M. Congenital hereditary endothelial dystrophy with progressive sensorineural deafness (Harboyan syndrome). *Orphanet J Rare Dis* **3**, 28, (2008).
- 38 Siddiqui, S., Zenteno, J. C., Rice, A., Chacon-Camacho, O., Naylor, S. G., Rivera-de la Parra, D., Spokes, D. M., James, N., Toomes, C., Inglehearn, C. F. & Ali, M. Congenital hereditary endothelial dystrophy caused by SLC4A11 mutations progresses to Harboyan syndrome. *Cornea* **33**, 247-251, (2014).

- 39 Price, M. O., Gupta, P., Lass, J. & Price, F. W., Jr. EK (DLEK, DSEK, DMEK): New Frontier in Cornea Surgery. *Annu Rev Vis Sci* **3**, 69-90, (2017).
- 40 Vedana, G., Villarreal, G., Jr. & Jun, A. S. Fuchs endothelial corneal dystrophy: current perspectives. *Clin Ophthalmol* **10**, 321-330, (2016).
- 41 Weiss, J. S., Moller, H. U., Aldave, A. J., Seitz, B., Bredrup, C., Kivela, T., Munier, F. L., Rapuano, C. J., Nischal, K. K., Kim, E. K., Sutphin, J., Busin, M., Labbe, A., Kenyon, K. R., Kinoshita, S. & Lisch, W. IC3D classification of corneal dystrophies--edition 2. *Cornea* **34**, 117-159, (2015).
- 42 Vithana, E. N., Morgan, P. E., Ramprasad, V., Tan, D. T., Yong, V. H., Venkataraman, D., Venkataraman, A., Yam, G. H., Nagasamy, S., Law, R. W., Rajagopal, R., Pang, C. P., Kumaramanickevel, G., Casey, J. R. & Aung, T. SLC4A11 Mutations in Fuchs Endothelial Corneal Dystrophy (FECD). *Hum Mol Genet* **17**, 656-666, (2008).
- 43 Baratz, K. H., Tosakulwong, N., Ryu, E., Brown, W. L., Branham, K., Chen, W., Tran, K. D., Schmid-Kubista, K. E., Heckenlively, J. R., Swaroop, A., Abecasis, G., Bailey, K. R. & Edwards, A. O. E2-2 protein and Fuchs's corneal dystrophy. *N Engl J Med* **363**, 1016-1024, (2010).
- 44 Riazuddin, S. A., Zaghloul, N. A., Al-Saif, A., Davey, L., Diplas, B. H., Meadows, D. N., Eghrari, A. O., Minear, M. A., Li, Y. J., Klintworth, G. K., Afshari, N., Gregory, S. G., Gottsch, J. D. & Katsanis, N. Missense mutations in TCF8 cause late-onset Fuchs corneal dystrophy and interact with FCD4 on chromosome 9p. *Am J Hum Genet* **86**, 45-53, (2010).
- 45 Riazuddin, S. A., Vasanth, S., Katsanis, N. & Gottsch, J. D. Mutations in AGBL1 cause dominant late-onset Fuchs corneal dystrophy and alter protein-protein interaction with TCF4. *Am. J. Hum. Genet.* **93**, 758-764, (2013).
- 46 Riazuddin, S. A., Parker, D. S., McGlumphy, E. J., Oh, E. C., Iloff, B. W., Schmedt, T., Jurkunas, U., Schleif, R., Katsanis, N. & Gottsch, J. D. Mutations in LOXHD1, a recessive-deafness locus, cause dominant late-onset Fuchs corneal dystrophy. *Am J Hum Genet* **90**, 533-539, (2012).
- 47 Afshari, N. A., Igo, R. P., Jr., Morris, N. J., Stambolian, D., Sharma, S., Pulagam, V. L., Dunn, S., Stamler, J. F., Truitt, B. J., Rimmner, J., Kuot, A., Croasdale, C. R., Qin, X., Burdon, K. P., Riazuddin, S. A., Mills, R., Klebe, S., Minear, M. A., Zhao, J., Balajonda, E., Rosenwasser, G. O., Baratz, K. H., Mootha, V. V., Patel, S. V., Gregory, S. G., Bailey-Wilson, J. E., Price, M. O., Price, F. W., Jr., Craig, J. E., Fingert, J. H., Gottsch, J. D., Aldave, A. J., Klintworth, G. K., Lass, J. H., Li, Y. J. & Iyengar, S. K. Genome-wide

- association study identifies three novel loci in Fuchs endothelial corneal dystrophy. *Nat Commun* **8**, 14898, (2017).
- 48 Greenhill, N. S., Ruger, B. M., Hasan, Q. & Davis, P. F. The alpha1(VIII) and alpha2(VIII) collagen chains form two distinct homotrimeric proteins in vivo. *Matrix Biol* **19**, 19-28, (2000).
- 49 Gottsch, J. D., Zhang, C., Sundin, O. H., Bell, W. R., Stark, W. J. & Green, W. R. Fuchs corneal dystrophy: aberrant collagen distribution in an L450W mutant of the *COL8A2* gene. *Invest Ophthalmol Vis Sci* **46**, 4504-4511, (2005).
- 50 Meng, H., Matthaei, M., Ramanan, N., Grebe, R., Chakravarti, S., Speck, C. L., Kimos, M., Vij, N., Eberhart, C. G. & Jun, A. S. L450W and Q455K *col8a2* knock-in mouse models of Fuchs endothelial corneal dystrophy show distinct phenotypes and evidence for altered autophagy. *Invest Ophthalmol Vis Sci* **54**, 1887-1897, (2013).
- 51 Jun, A. S., Meng, H., Ramanan, N., Matthaei, M., Chakravarti, S., Bonshek, R., Black, G. C., Grebe, R. & Kimos, M. An alpha 2 collagen VIII transgenic knock-in mouse model of Fuchs endothelial corneal dystrophy shows early endothelial cell unfolded protein response and apoptosis. *Hum Mol Genet* **21**, 384-393, (2012).
- 52 Loganathan, S. K. & Casey, J. R. Corneal Dystrophy-Causing SLC4A11 Mutants: Suitability for Folding-Correction Therapy. *Hum Mutat* **35**, 1082-1091, (2014).
- 53 Mootha, V. V., Hussain, I., Cunnusamy, K., Graham, E., Gong, X., Neelam, S., Xing, C., Kittler, R. & Petroll, W. M. TCF4 Triplet Repeat Expansion and Nuclear RNA Foci in Fuchs' Endothelial Corneal Dystrophy. *Invest Ophthalmol Vis Sci* **56**, 2003-2011, (2015).
- 54 Vasanth, S., Eghrari, A. O., Gapsis, B. C., Wang, J., Haller, N. F., Stark, W. J., Katsanis, N., Riazuddin, S. A. & Gottsch, J. D. Expansion of CTG18.1 Trinucleotide Repeat in TCF4 Is a Potent Driver of Fuchs' Corneal Dystrophy. *Invest Ophthalmol Vis Sci* **56**, 4531-4536, (2015).
- 55 Sanchez-Tillo, E., de Barrios, O., Valls, E., Darling, D. S., Castells, A. & Postigo, A. ZEB1 and TCF4 reciprocally modulate their transcriptional activities to regulate Wnt target gene expression. *Oncogene* **34**, 5760-5770, (2015).
- 56 Riazuddin, S. A., Vasanth, S., Katsanis, N. & Gottsch, J. D. Mutations in *AGBL1* cause dominant late-onset Fuchs corneal dystrophy and alter protein-protein interaction with TCF4. *Am J Hum Genet* **93**, 758-764, (2013).

- 57 Sultana, A., Garg, P., Ramamurthy, B., Vemuganti, G. K. & Kannabiran, C. Mutational spectrum of the SLC4A11 gene in autosomal recessive congenital hereditary endothelial dystrophy. *Mol Vis* **13**, 1327-1332, (2007).
- 58 Wain, H. M., Lush, M. J., Ducluzeau, F., Khodiyar, V. K. & Povey, S. Genew: the Human Gene Nomenclature Database, 2004 updates. *Nucleic Acids Res* **32**, D255-257, (2004).
- 59 Lin, L., Yee, S. W., Kim, R. B. & Giacomini, K. M. SLC transporters as therapeutic targets: emerging opportunities. *Nat Rev Drug Discov* **14**, 543-560, (2015).
- 60 Cordat, E. & Casey, J. R. Bicarbonate transport in cell physiology and disease. *Biochem J* **417**, 423-439, (2009).
- 61 Jalimarada, S. S., Ogando, D. G., Vithana, E. N. & Bonanno, J. A. Ion transport function of SLC4A11 in corneal endothelium. *Invest Ophthalmol Vis Sci* **54**, 4330-4340, (2013).
- 62 Park, M., Li, Q., Shcheynikov, N., Zeng, W. & Muallem, S. NaBC1 is a ubiquitous electrogenic Na<sup>+</sup>-coupled borate transporter essential for cellular boron homeostasis and cell growth and proliferation. *Mol Cell* **16**, 331-341, (2004).
- 63 Loganathan, S. K., Schneider, H. P., Morgan, P. E., Deitmer, J. W. & Casey, J. R. Functional assessment of SLC4A11, an integral membrane protein mutated in corneal dystrophies. *Am J Physiol Cell Physiol* **311**, C735-C748, (2016).
- 64 Jalimarada, S. S., Ogando, D. G., Vithana, E. N. & Bonanno, J. A. Ion transport function of SLC4A11 in corneal endothelium. *Invest. Ophthalmol. Vis. Sci.* **54**, 4330-4340, (2013).
- 65 Myers, E. J., Marshall, A., Jennings, M. L. & Parker, M. D. Mouse *slc4a11* expressed in *Xenopus* oocytes is an ideally selective H<sup>+</sup>/OH<sup>-</sup> conductance pathway that is stimulated by rises in intracellular and extracellular pH. *Am J Physiol Cell Physiol* **311**, C945-C959, (2016).
- 66 Kao, L., Azimov, R., Abuladze, N., Newman, D. & Kurtz, I. Human SLC4A11-C functions as a DIDS-stimulatable H<sup>+</sup>(OH<sup>-</sup>) permeation pathway: partial correction of R109H mutant transport. *Am J Physiol Cell Physiol* **308**, C176-188, (2015).
- 67 Zhang, W., Ogando, D. G., Bonanno, J. A. & Obukhov, A. G. Human SLC4A11 Is a Novel NH<sub>3</sub>/H<sup>+</sup> Co-transporter. *J Biol Chem* **290**, 16894-16905, (2015).
- 68 Brown, B. F., Quon, A., Dyck, J. R. & Casey, J. R. Carbonic anhydrase II promotes cardiomyocyte hypertrophy. *Can J Physiol Pharmacol* **90**, 1599-1610, (2012).
- 69 Alka, K. & Casey, J. R. Bicarbonate transport in health and disease. *IUBMB Life* **66**, 596-615, (2014).

- 70 Parker, M. D., Ourmozdi, E. P. & Tanner, M. J. Human BTR1, a New Bicarbonate Transporter Superfamily Member and Human AE4 from Kidney. *Biochem. Biophys. Res. Commun.* **282**, 1103-1109, (2001).
- 71 THPA. *The Human Protein Atlas-SLC4A11*, (2019) (<https://www.proteinatlas.org/ENSG00000088836-SLC4A11/tissue>).
- 72 Frausto, R. F., Wang, C. & Aldave, A. J. Transcriptome analysis of the human corneal endothelium. *Invest Ophthalmol Vis Sci* **55**, 7821-7830, (2014).
- 73 Chng, Z., Peh, G. S., Herath, W. B., Cheng, T. Y., Ang, H. P., Toh, K. P., Robson, P., Mehta, J. S. & Colman, A. High throughput gene expression analysis identifies reliable expression markers of human corneal endothelial cells. *PLoS One* **8**, e67546, (2013).
- 74 Groeger, N., Froehlich, H., Maier, H., Olbrich, A., Kostin, S., Braun, T. & Boettger, T. Slc4a11 prevents osmotic imbalance leading to corneal endothelial dystrophy, deafness, and polyuria. *J Biol Chem* **285**, 14467-14474, (2010).
- 75 Parker, M. D. & Boron, W. F. The divergence, actions, roles, and relatives of sodium-coupled bicarbonate transporters. *Physiol Rev* **93**, 803-959, (2013).
- 76 TCGA. *The Cancer Genome Atlas-SLC4A11*, (2019) (<https://portal.gdc.cancer.gov/genes/ENSG00000088836>).
- 77 Vilas, G. L., Morgan, P. E., Loganathan, S., Quon, A. & Casey, J. R. Biochemical Framework for SLC4A11, the Plasma Membrane Protein Defective in Corneal Dystrophies. *Biochemistry* **50**, 2157-2169, (2011).
- 78 Vilas, G. L., Loganathan, S. K., Quon, A., Sundaresan, P., Vithana, E. N. & Casey, J. Oligomerization of SLC4A11 protein and the severity of FECED and CHED2 corneal dystrophies caused by SLC4A11 mutations. *Hum Mutat* **33**, 419-428, (2012).
- 79 Loganathan, S. K., Lukowski, C. M. & Casey, J. R. The cytoplasmic domain is essential for transport function of the integral membrane transport protein SLC4A11. *Am. J. Physiol.* **310**, C161-174, (2016).
- 80 Badior, K. E., Alka, K. & Casey, J. R. SLC4A11 Three-Dimensional Homology Model Rationalizes Corneal Dystrophy-Causing Mutations. *Hum Mutat* **38**, 279-288, (2017).
- 81 Takano, J., Noguchi, K., Yasumori, M., Kobayashi, M., Gajdos, Z., Miwa, K., Hayashi, H., Yoneyama, T. & Fujiwara, T. Arabidopsis boron transporter for xylem loading. *Nature* **420**, 337-340, (2002).

- 82 O'Neill, M. A., Ishii, T., Albersheim, P. & Darvill, A. G. Rhamnogalacturonan II: structure and function of a borate cross-linked cell wall pectic polysaccharide. *Annu Rev Plant Biol* **55**, 109-139, (2004).
- 83 Ogando, D. G., Jalimarada, S. S., Zhang, W., Vithana, E. N. & Bonanno, J. A. SLC4A11 is an EIPA-sensitive Na<sup>+</sup> permeable pHi regulator. *Am J Physiol Cell Physiol* **305**, C716-727, (2013).
- 84 Zhang, W., Li, H., Ogando, D. G., Li, S., Feng, M., Price, F. W., Jr., Tennessen, J. M. & Bonanno, J. A. Glutaminolysis is Essential for Energy Production and Ion Transport in Human Corneal Endothelium. *EBioMedicine* **16**, 292-301, (2017).
- 85 HGMD. *The Human Gene Mutation Database-SLC4A11*, (2019) (<http://www.hgmd.cf.ac.uk/ac/gene.php?gene=SLC4A11>).
- 86 COSMIC. *Catalogue of Somatic Mutations in Cancer-SLC4A11*, (2019) (<https://cancer.sanger.ac.uk/cosmic/gene/analysis?ln=SLC4A11>).
- 87 Qin, L., Li, T. & Liu, Y. High SLC4A11 expression is an independent predictor for poor overall survival in grade 3/4 serous ovarian cancer. *PLoS One* **12**, e0187385, (2017).
- 88 Kincaid, M. M. & Cooper, A. A. Misfolded proteins traffic from the endoplasmic reticulum (ER) due to ER export signals. *Mol Biol Cell* **18**, 455-463, (2007).
- 89 Alka, K. & Casey, J. R. Molecular phenotype of SLC4A11 missense mutants: Setting the stage for personalized medicine in corneal dystrophies. *Hum Mutat* **39**, 676-690, (2018).
- 90 Li, S., Hundal, K. S., Chen, X., Choi, M., Ogando, D. G., Obukhov, A. G. & Bonanno, J. A. R125H, W240S, C386R, and V507I SLC4A11 mutations associated with corneal endothelial dystrophy affect the transporter function but not trafficking in PS120 cells. *Exp Eye Res* **180**, 86-91, (2019).
- 91 Kao, L., Azimov, R., Shao, X. M., Frausto, R. F., Abuladze, N., Newman, D., Aldave, A. J. & Kurtz, I. Multifunctional ion transport properties of human SLC4A11: comparison of the SLC4A11-B and SLC4A11-C variants. *Am J Physiol Cell Physiol* **311**, C820-C830, (2016).
- 92 Chiu, A. M., Mandziuk, J. J., Loganathan, S. K., Alka, K. & Casey, J. R. High Throughput Assay Identifies Glafenine as a Corrector for the Folding Defect in Corneal Dystrophy-Causing Mutants of SLC4A11. *Invest Ophthalmol Vis Sci* **56**, 7739-7753, (2015).
- 93 Hemadevi, B., Veitia, R. A., Srinivasan, M., Arunkumar, J., Prajna, N. V., Lesaffre, C. & Sundaresan, P. Identification of mutations in the SLC4A11 gene in patients with recessive congenital hereditary endothelial dystrophy. *Arch Ophthalmol* **126**, 700-708, (2008).

- 94 Hemadevi, B., Srinivasan, M., Arunkumar, J., Prajna, N. V. & Sundaresan, P. Genetic analysis of patients with Fuchs endothelial corneal dystrophy in India. *BMC Ophthalmol* **10**, 3, (2010).
- 95 Ramprasad, V. L., Ebenezer, N. D., Aung, T., Rajagopal, R., Yong, V. H., Tuft, S. J., Viswanathan, D., El-Ashry, M. F., Liskova, P., Tan, D. T., Bhattacharya, S. S., Kumaramanickavel, G. & Vithana, E. N. Novel SLC4A11 mutations in patients with recessive congenital hereditary endothelial dystrophy (CHED2). *Hum Mutat* **28**, 522-523, (2007).
- 96 Riazuddin, S. A., Vithana, E. N., Seet, L. F., Liu, Y., Al-Saif, A., Koh, L. W., Heng, Y. M., Aung, T., Meadows, D. N., Eghrari, A. O., Gottsch, J. D. & Katsanis, N. Missense mutations in the sodium borate co-transporter SLC4A11 cause late onset Fuchs corneal dystrophy. *Hum Mutat* **31**, 1261-1268, (2010).
- 97 Desir, J., Moya, G., Reish, O., Van Regemorter, N., Deconinck, H., David, K. L., Meire, F. M. & Abramowicz, M. J. Borate transporter SLC4A11 mutations cause both Harboyan syndrome and non-syndromic corneal endothelial dystrophy. *J Med Genet* **44**, 322-326, (2007).
- 98 Aldave, A. J., Yellore, V. S., Bourla, N., Momi, R. S., Khan, M. A., Salem, A. K., Rayner, S. A., Glasgow, B. J. & Kurtz, I. Autosomal recessive CHED associated with novel compound heterozygous mutations in SLC4A11. *Cornea* **26**, 896-900, (2007).
- 99 Soumitra, N., Loganathan, S. K., Madhavan, D., Ramprasad, V. L., Arokiasamy, T., Sumathi, S., Karthiyayini, T., Rachapalli, S. R., Kumaramanickavel, G., Casey, J. R. & Rajagopal, R. Biosynthetic and functional defects in newly identified SLC4A11 mutants and absence of COL8A2 mutations in Fuchs endothelial corneal dystrophy. *J Hum Genet* **59**, 444-453, (2014).
- 100 Puangsricharn, V., Yeetong, P., Charumalai, C., Suphapeetiporn, K. & Shotelersuk, V. Two novel mutations including a large deletion of the SLC4A11 gene causing autosomal recessive hereditary endothelial dystrophy. *The British journal of ophthalmology* **98**, 1460-1462, (2014).
- 101 Kodaganur, S. G., Kapoor, S., Veerappa, A. M., Tontanahal, S. J., Sarda, A., Yathish, S., Prakash, D. R. & Kumar, A. Mutation analysis of the SLC4A11 gene in Indian families with congenital hereditary endothelial dystrophy 2 and a review of the literature. *Mol Vis* **19**, 1694-1706, (2013).

- 102 Shah, S. S., Al-Rajhi, A., Brandt, J. D., Mannis, M. J., Roos, B., Sheffield, V. C., Syed, N. A., Stone, E. M. & Fingert, J. H. Mutation in the *SLC4A11* gene associated with autosomal recessive congenital hereditary endothelial dystrophy in a large Saudi family. *Ophthalmic Genet* **29**, 41-45, (2008).
- 103 Aldahmesh, M. A., Khan, A. O., Meyer, B. F. & Alkuraya, F. S. Mutational spectrum of SLC4A11 in autosomal recessive CHED in Saudi Arabia. *Invest Ophthalmol Vis Sci* **50**, 4142-4145, (2009).
- 104 Kumawat, B. L., Gupta, R., Sharma, A., Sen, S., Gupta, S. & Tandon, R. Delayed onset of congenital hereditary endothelial dystrophy due to compound heterozygous SLC4A11 mutations. *Indian J Ophthalmol* **64**, 492-495, (2016).
- 105 Kaul, H., Suman, M., Khan, Z., Ullah, M. I., Ashfaq, U. A. & Idrees, S. Missense mutation in SLC4A11 in two Pakistani families affected with congenital hereditary endothelial dystrophy (CHED2). *Clin Exp Optom* **99**, 73-77, (2016).
- 106 Jiao, X., Sultana, A., Garg, P., Ramamurthy, B., Vemuganti, G. K., Gangopadhyay, N., Hejtmancik, J. F. & Kannabiran, C. Autosomal recessive corneal endothelial dystrophy (CHED2) is associated with mutations in SLC4A11. *J Med Genet* **44**, 64-68, (2007).
- 107 Han, S. B., Ang, H. P., Poh, R., Chaurasia, S. S., Peh, G., Liu, J., Tan, D. T., Vithana, E. N. & Mehta, J. S. Mice with a targeted disruption of *slc4a11* model the progressive corneal changes of congenital hereditary endothelial dystrophy. *Invest Ophthalmol Vis Sci* **54**, 6179-6189, (2013).
- 108 Wieben, E. D., Aleff, R. A., Tang, X., Butz, M. L., Kalari, K. R., Highsmith, E. W., Jen, J., Vasmatazis, G., Patel, S. V., Maguire, L. J., Baratz, K. H. & Fautsch, M. P. Trinucleotide Repeat Expansion in the Transcription Factor 4 (*TCF4*) Gene Leads to Widespread mRNA Splicing Changes in Fuchs' Endothelial Corneal Dystrophy. *Invest Ophthalmol Vis Sci* **58**, 343-352, (2017).
- 109 Wieben, E. D., Aleff, R. A., Tang, X., Kalari, K. R., Maguire, L. J., Patel, S. V., Baratz, K. H. & Fautsch, M. P. Gene expression in the corneal endothelium of Fuchs endothelial corneal dystrophy patients with and without expansion of a trinucleotide repeat in TCF4. *PLoS One* **13**, e0200005, (2018).
- 110 Gumbiner, B. M. Cell adhesion: the molecular basis of tissue architecture and morphogenesis. *Cell* **84**, 345-357, (1996).
- 111 Murray, P., Frampton, G. & Nelson, P. N. Cell adhesion molecules. Sticky moments in the clinic. *BMJ* **319**, 332-334, (1999).

- 112 Khalili, A. A. & Ahmad, M. R. A Review of Cell Adhesion Studies for Biomedical and Biological Applications. *Int J Mol Sci* **16**, 18149-18184, (2015).
- 113 Hohmann, T. & Dehghani, F. The Cytoskeleton-A Complex Interacting Meshwork. *Cells* **8**, (2019).
- 114 Gilmore, A. P. Anoikis. *Cell Death Differ* **12 Suppl 2**, 1473-1477, (2005).
- 115 Ishikawa, F., Ushida, K., Mori, K. & Shibamura, M. Loss of anchorage primarily induces non-apoptotic cell death in a human mammary epithelial cell line under atypical focal adhesion kinase signaling. *Cell Death Dis* **6**, e1619, (2015).
- 116 Stepp, M. A. Corneal integrins and their functions. *Exp Eye Res* **83**, 3-15, (2006).
- 117 Jacobus, A. P. & Gross, J. Optimal cloning of PCR fragments by homologous recombination in *Escherichia coli*. *PLoS One* **10**, e0119221, (2015).
- 118 Kozak, M. Point mutations define a sequence flanking the AUG initiator codon that modulates translation by eukaryotic ribosomes. *Cell* **44**, 283-292, (1986).
- 119 Gonzales, M. F., Brooks, T., Pukatzki, S. U. & Provenzano, D. Rapid protocol for preparation of electrocompetent *Escherichia coli* and *Vibrio cholerae*. *J Vis Exp*, (2013).
- 120 Ruetz, S., Lindsey, A. E., Ward, C. L. & Kopito, R. R. Functional activation of plasma membrane anion exchangers occurs in a pre-Golgi compartment. *J Cell Biol* **121**, 37-48, (1993).
- 121 Peh, G. S., Toh, K. P., Ang, H. P., Seah, X. Y., George, B. L. & Mehta, J. S. Optimization of human corneal endothelial cell culture: density dependency of successful cultures in vitro. *BMC Res Notes* **6**, 176, (2013).
- 122 Smith, P. K., Krohn, R. I., Hermanson, G. T., Mallia, A. K., Gartner, F. H., Provenzano, M. D., Fujimoto, E. K., Goeke, N. M., Olson, B. J. & Klenk, D. C. Measurement of protein using bicinchoninic acid. *Anal. Biochem.* **150**, 76-85, (1985).
- 123 Vilas, G. L., Loganathan, S., Quon, A., Sundaresan, P., Vithana, E. N. & Casey, J. R. Oligomerization of SLC4A11 protein and the severity of FECD and CHED2 corneal dystrophies caused by SLC4A11 mutations. *Human mutation* **33**, 419-428, (2012).
- 124 Kelley, L. A., Mezulis, S., Yates, C. M., Wass, M. N. & Sternberg, M. J. The Phyre<sup>2</sup> web portal for protein modeling, prediction and analysis. *Nat Protoc* **10**, 845-858, (2015).
- 125 Yang, J., Yan, R., Roy, A., Xu, D., Poisson, J. & Zhang, Y. The I-TASSER Suite: protein structure and function prediction. *Nat Methods* **12**, 7-8, (2015).

- 126 Carlson, E. C., Brendel, K., Hjelle, J. T. & Meezan, E. Ultrastructural and biochemical analyses of isolated basement membranes from kidney glomeruli and tubules and brain and retinal microvessels. *J. Ultrastr. Res.* **62**, 26-53, (1978).
- 127 Hou, G., Mulholland, D., Gronska, M. A. & Bendeck, M. P. Type VIII collagen stimulates smooth muscle cell migration and matrix metalloproteinase synthesis after arterial injury. *Am J Pathol* **156**, 467-476, (2000).
- 128 McClay, D. R., Wessel, G. M. & Marchase, R. B. Intercellular recognition: quantitation of initial binding events. *Proc Natl Acad Sci* **78**, 4975-4979, (1981).
- 129 Franco, C., Ho, B., Mulholland, D., Hou, G., Islam, M., Donaldson, K. & Bendeck, M. P. Doxycycline alters vascular smooth muscle cell adhesion, migration, and reorganization of fibrillar collagen matrices. *Am J Pathol* **168**, 1697-1709, (2006).
- 130 Arakawa, T., Kobayashi-Yurugi, T., Alguel, Y., Iwanari, H., Hatae, H., Iwata, M., Abe, Y., Hino, T., Ikeda-Suno, C., Kuma, H., Kang, D., Murata, T., Hamakubo, T., Cameron, A. D., Kobayashi, T., Hamasaki, N. & Iwata, S. Crystal structure of the anion exchanger domain of human erythrocyte band 3. *Science* **350**, 680-684, (2015).
- 131 Alford, R. F., Koehler Leman, J., Weitzner, B. D., Duran, A. M., Tilley, D. C., Elazar, A. & Gray, J. J. An Integrated Framework Advancing Membrane Protein Modeling and Design. *PLoS Comput Biol* **11**, e1004398, (2015).
- 132 Barth, P., Wallner, B. & Baker, D. Prediction of membrane protein structures with complex topologies using limited constraints. *Proc Natl Acad Sci* **106**, 1409-1414, (2009).
- 133 Subbotina, J., Yarov-Yarovoy, V., Lees-Miller, J., Durdagi, S., Guo, J., Duff, H. J. & Noskov, S. Y. Structural refinement of the hERG1 pore and voltage-sensing domains with ROSETTA-membrane and molecular dynamics simulations. *Proteins* **78**, 2922-2934, (2010).
- 134 Jiang, W., Hodoscek, M. & Roux, B. Computation of Absolute Hydration and Binding Free Energy with Free Energy Perturbation Distributed Replica-Exchange Molecular Dynamics (FEP/REMD). *J Chem Theory Comput* **5**, 2583-2588, (2009).
- 135 Lazaridis, T. Effective energy function for proteins in lipid membranes. *Proteins* **52**, 176-192, (2003).
- 136 Gallicchio, E., Andrec, M., Felts, A. K. & Levy, R. M. Temperature weighted histogram analysis method, replica exchange, and transition paths. *J Phys Chem B* **109**, 6722-6731, (2005).

- 137 *Gene Expression Analysis Using TaqMan Assays (Thermo Fisher Scientific)*, (2019) (<https://www.thermofisher.com/ca/en/home/life-science/pcr/real-time-pcr/real-time-pcr-assays/taqman-gene-expression.html>).
- 138 Patel, S. P. & Parker, M. D. SLC4A11 and the Pathophysiology of Congenital Hereditary Endothelial Dystrophy. *Biomed Res Int* **2015**, 475392, (2015).
- 139 Desir, J., Moya, G., Reish, O., Van Regemorter, N., Deconinck, H., David, K. L., Meire, F. M. & Abramowicz, M. Borate transporter SLC4A11 mutations cause both Harboyan syndrome and non-syndromic corneal endothelial dystrophy. *J. Med. Genet.* **44**, 322-326, (2007).
- 140 Loganathan, S. K., Schneider, H. P., Morgan, P. E., Deitmer, J. W. & Casey, J. R. Functional Assessment of SLC4A11, an Integral Membrane Protein Mutated in Corneal Dystrophies. *Am. J. Physiol.* **311**, C735-748, (2016).
- 141 Jennings, M. L., Howren, T. R., Cui, J., Winters, M. J. & Hannigan, R. Transport And Regulatory Characteristics Of The Yeast Bicarbonate Transporter Homolog Bor1p. *Am. J. Physiol.* **293**, C468-476, (2007).
- 142 Park, M., Li, Q., Shcheynikov, N., Zeng, W. & Muallem, S. NaBC1 is a ubiquitous electrogenic Na<sup>+</sup> -coupled borate transporter essential for cellular boron homeostasis and cell growth and proliferation. *Mol. Cell* **16**, 331-341, (2004).
- 143 Alka, K. & Casey, J. R. Molecular Phenotype of SLC4A11 Missense Mutants: Setting the Stage for Personalized Medicine in Corneal Dystrophies. *Human Mutat.* **39**, 676-690, (2018).
- 144 Li, S., Hundal, K. S., Chen, X., Choi, M., Ogando, D. G., Obukhov, A. G. & Bonanno, J. A. R125H, W240S, C386R, and V507I SLC4A11 mutations associated with corneal endothelial dystrophy affect the transporter function but not trafficking in PS120 cells. *Exp Eye Res* **180**, 86-91, (2018).
- 145 Vilas, G. L., Morgan, P. E., Loganathan, S., Quon, A. & Casey, J. R. A Biochemical Framework for SLC4A11, the Plasma Membrane Protein Defective in Corneal Dystrophies. *Biochem* **50**, 2157-2169, (2011).
- 146 Aldahmesh, M., Khan, A., Meyer, B. & Alkuraya, F. Mutational Spectrum of SLC4A11 in Autosomal Recessive CHED in Saudi Arabia. *Investigative ophthalmology & visual science* **50**, 4142-4145, (2009).

- 147 Kumar, A., Bhattacharjee, S., Prakash, D. R. & Sadanand, C. S. Genetic analysis of two Indian families affected with congenital hereditary endothelial dystrophy: two novel mutations in SLC4A11. *Mol Vis* **13**, 39-46, (2007).
- 148 Roy, S., Praneetha, D. C. & Vendra, V. P. Mutations in the Corneal Endothelial Dystrophy-Associated Gene SLC4A11 Render the Cells More Vulnerable to Oxidative Insults. *Cornea* **34**, 668-674, (2015).
- 149 Guha, S., Chaurasia, S., Ramachandran, C. & Roy, S. SLC4A11 depletion impairs NRF2 mediated antioxidant signaling and increases reactive oxygen species in human corneal endothelial cells during oxidative stress. *Scientific reports* **7**, 4074, (2017).
- 150 Alka, K. & Casey, J. R. Ophthalmic Nonsteroidal Anti-Inflammatory Drugs as a Therapy for Corneal Dystrophies Caused by SLC4A11 Mutation. *Investigative ophthalmology & visual science* **59**, 4258-4267, (2018).
- 151 Blom, N., Gammeltoft, S. & Brunak, S. Sequence and structure-based prediction of eukaryotic protein phosphorylation sites. *J Mol Biol* **294**, 1351-1362, (1999).
- 152 Graham, M. A., Rawe, I., Dartt, D. A. & Joyce, N. C. Protein kinase C regulation of corneal endothelial cell proliferation and cell cycle. *Invest Ophthalmol Vis Sci* **41**, 4124-4132, (2000).
- 153 Geiger, B., Bershadsky, A., Pankov, R. & Yamada, K. M. Transmembrane crosstalk between the extracellular matrix--cytoskeleton crosstalk. *Nat. Rev. Mol. Cell Biol.* **2**, 793-805, (2001).
- 154 Musch, D. C., Niziol, L. M., Stein, J. D., Kamyar, R. M. & Sugar, A. Prevalence of corneal dystrophies in the United States: estimates from claims data. *Invest. Ophthalmol. Vis. Sci.* **52**, 6959-6963, (2011).
- 155 Li, S., Hundal, K. S., Chen, X., Choi, M., Ogando, D. G., Obukhov, A. G. & Bonanno, J. A. R125H, W240S, C386R, and V507I SLC4A11 mutations associated with corneal endothelial dystrophy affect the transporter function but not trafficking in PS120 cells. *Exp. Eye Res.* **180**, 86-91, (2018).
- 156 Fairbanks, G., T.L. Steck & Wallach., D. F. H. Electrophoretic analysis of the major polypeptides of the human erythrocyte membrane. *Biochemistry* **10**, 2606-2617, (1971).
- 157 Bennett, V. & Stenbuck, P. J. The membrane attachment protein for spectrin is associated with band 3 in human erythrocyte membranes. *Nature* **280**, 468-473, (1979).
- 158 Frisch, S. M. & Francis, H. Disruption of epithelial cell-matrix interactions induces apoptosis. *J. Cell Biol.* **124**, 619-626, (1994).

- 159 Olie, R. A., Boersma, A. W., Dekker, M. C., Nooter, K., Looijenga, L. H. & Oosterhuis, J. W. Apoptosis of human seminoma cells upon disruption of their microenvironment. *Br. J. Cancer* **73**, 1031-1036, (1996).
- 160 Frausto, R. F., Le, D. J. & Aldave, A. J. Transcriptomic Analysis of Cultured Corneal Endothelial Cells as a Validation for Their Use in Cell Replacement Therapy. *Cell Transplant* **25**, 1159-1176, (2016).
- 161 Shei, W., Liu, J., Htoon, H. M., Aung, T. & Vithana, E. N. Differential expression of the Slc4 bicarbonate transporter family in murine corneal endothelium and cell culture. *Mol Vis* **19**, 1096-1106, (2013).
- 162 Vilas, G. L., Loganathan, S., Quon, A., Sundaresan, P., Vithana, E. N. & Casey, J. R. Oligomerization of SLC4A11 protein and the severity of FECD and CHED2 corneal dystrophies caused by SLC4A11 mutations. *Human Mutation* **33**, 419-428, (2012).
- 163 Noskov, S. Y., Rostovtseva, T. K., Chamberlin, A. C., Tejjido, O., Jiang, W. & Bezrukov, S. M. Current state of theoretical and experimental studies of the voltage-dependent anion channel (VDAC). *Biochim Biophys Acta* **1858**, 1778-1790, (2016).
- 164 Shao, J., Tanner, S. W., Thompson, N. & Cheatham, T. E. Clustering Molecular Dynamics Trajectories: 1. Characterizing the Performance of Different Clustering Algorithms. *J Chem Theory Comput* **3**, 2312-2334, (2007).
- 165 Trenker, R., Call, M. E. & Call, M. J. Crystal Structure of the Glycophorin A Transmembrane Dimer in Lipidic Cubic Phase. *J Am Chem Soc* **137**, 15676-15679, (2015).
- 166 Feral, C. C., Nishiya, N., Fenczik, C. A., Stuhlmann, H., Slepak, M. & Ginsberg, M. H. CD98hc (SLC3A2) mediates integrin signaling. *Proc. Natl. Acad. Sci. U S A* **102**, 355-360, (2005).
- 167 Salmi, M. & Jalkanen, S. VAP-1: an adhesin and an enzyme. *Trends Immunol.* **22**, 211-216, (2001).
- 168 Ye, F., Liu, J., Winkler, H. & Taylor, K. A. Integrin alpha IIb beta 3 in a membrane environment remains the same height after Mn<sup>2+</sup> activation when observed by cryoelectron tomography. *J. Mol. Biol.* **378**, 976-986, (2008).
- 169 Liu, J., Seet, L. F., Koh, L. W., Venkatraman, A., Venkataraman, D., Mohan, R. R., Praetorius, J., Bonanno, J. A., Aung, T. & Vithana, E. N. Depletion of SLC4A11 causes cell death by apoptosis in an immortalized human corneal endothelial cell line. *Invest. Ophthalmol. Vis. Sci.* **53**, 3270-3279, (2012).

- 170 Wilson, R. S. & Roper-Hall, M. J. Effect of age on the endothelial cell count in the normal eye. *Br. J. Ophthalmol.* **66**, 513-515, (1982).
- 171 Costagliola, C., Romano, V., Forbice, E., Angi, M., Pascotto, A., Boccia, T. & Semeraro, F. Corneal oedema and its medical treatment. *Clin. Exp. Optom.* **96**, 529-535, (2013).
- 172 Kenyon, K. R. & Antine, B. The pathogenesis of congenital hereditary endothelial dystrophy of the cornea. *Am. J. Ophthalmol.* **72**, 787-795, (1971).
- 173 Goyer, B., Theriault, M., Gendron, S. P., Brunette, I., Rochette, P. J. & Proulx, S. Extracellular Matrix and Integrin Expression Profiles in Fuchs Endothelial Corneal Dystrophy Cells and Tissue Model. *Tissue Eng. Part A*, (2017).
- 174 Oldak, M., Ruszkowska, E., Udziela, M., Ozieblo, D., Binczyk, E., Scieczynska, A., Ploski, R. & Szaflik, J. P. Fuchs Endothelial Corneal Dystrophy: Strong Association with rs613872 Not Paralleled by Changes in Corneal Endothelial TCF4 mRNA Level. *Biomed. Res. Int.* **2015**, 640234, (2015).
- 175 Zhang, W., Aldave, A.J. Corneal endothelial dystrophies belong to the same series of disorders connected by transcriptional factors ZEB1 and TCF4/E2-2. *Invest. Ophthalmol. Vis. Sci.* **59**, 1351, (2018).
- 176 Forrest, M., Chapman, R. M., Doyle, A. M., Tinsley, C. L., Waite, A. & Blake, D. J. Functional analysis of TCF4 missense mutations that cause Pitt-Hopkins syndrome. *Hum. Mutat.* **33**, 1676-1686, (2012).
- 177 Plantefaber, L. C. & Hynes, R. O. Changes in integrin receptors on oncogenically transformed cells. *Cell* **56**, 281-290, (1989).
- 178 Gottsch, J. D., Bowers, A. L., Margulies, E. H., Seitzman, G. D., Kim, S. W., Saha, S., Jun, A. S., Stark, W. J. & Liu, S. H. Serial analysis of gene expression in the corneal endothelium of Fuchs' dystrophy. *Invest. Ophthalmol. Vis. Sci.* **44**, 594-599, (2003).
- 179 Bartakova, A., Kunzevitzky, N. J. & Goldberg, J. L. Regenerative Cell Therapy for Corneal Endothelium. *Curr Ophthalmol Rep* **2**, 81-90, (2014).
- 180 Soh, Y. Q. & Mehta, J. S. Regenerative Therapy for Fuchs Endothelial Corneal Dystrophy. *Cornea* **37**, 523-527, (2018).
- 181 NCBI. *Conserved Protein Domain Family (7tmB1\_secretin)*, (2019)  
(<https://www.ncbi.nlm.nih.gov/Structure/cdd/cd15275>).
- 182 SNPEffect. *ZN717\_HUMAN*, (2019)  
([http://snpeffect.switchlab.org/uniprot/ZN717\\_HUMAN](http://snpeffect.switchlab.org/uniprot/ZN717_HUMAN)).

- 183 NCBI. *Conserved Protein Domain Family (SapC)*, (2019) (<https://www.ncbi.nlm.nih.gov/Structure/cdd/PF07277>).
- 184 Desronvil, T., Logan-Wyatt, D., Abdrabou, W., Triana, M., Jones, R., Taheri, S., Del Bono, E., Pasquale, L. R., Olivier, M., Haines, J. L., Fan, B. J. & Wiggs, J. L. Distribution of COL8A2 and COL8A1 gene variants in Caucasian primary open angle glaucoma patients with thin central corneal thickness. *Mol Vis* **16**, 2185-2191, (2010).
- 185 Nayak, A., Pednekar, L., Reid, K. B. & Kishore, U. Complement and non-complement activating functions of C1q: a prototypical innate immune molecule. *Innate Immun* **18**, 350-363, (2012).
- 186 Tas, S. W., Klickstein, L. B., Barbashov, S. F. & Nicholson-Weller, A. C1q and C4b bind simultaneously to CR1 and additively support erythrocyte adhesion. *J Immunol* **163**, 5056-5063, (1999).
- 187 Wehrle-Haller, B. Structure and function of focal adhesions. *Curr Opin Cell Biol* **24**, 116-124, (2012).
- 188 Kim, Y. N., Koo, K. H., Sung, J. Y., Yun, U. J. & Kim, H. Anoikis resistance: an essential prerequisite for tumor metastasis. *Int J Cell Biol* **2012**, 306879, (2012).
- 189 Maubant, S., Saint-Dizier, D., Boutillon, M., Perron-Sierra, F., Casara, P. J., Hickman, J. A., Tucker, G. C. & Van Obberghen-Schilling, E. Blockade of alpha v beta3 and alpha v beta5 integrins by RGD mimetics induces anoikis and not integrin-mediated death in human endothelial cells. *Blood* **108**, 3035-3044, (2006).
- 190 Seguin, L., Desgrosellier, J. S., Weis, S. M. & Cheresh, D. A. Integrins and cancer: regulators of cancer stemness, metastasis, and drug resistance. *Trends Cell Biol* **25**, 234-240, (2015).
- 191 Lechner, J., Dash, D. P., Muszynska, D., Hosseini, M., Segev, F., George, S., Frazer, D. G., Moore, J. E., Kaye, S. B., Young, T., Simpson, D. A., Churchill, A. J., Heon, E. & Willoughby, C. E. Mutational spectrum of the *ZEB1* gene in corneal dystrophies supports a genotype-phenotype correlation. *Invest Ophthalmol Vis Sci* **54**, 3215-3223, (2013).
- 192 Abramowicz, M. J., Albuquerque-Silva, J. & Zanen, A. Corneal dystrophy and perceptive deafness (Harboyan syndrome): CDPD1 maps to 20p13. *J Med Genet* **39**, 110-112, (2002).
- 193 Lopez, I. A., Rosenblatt, M. I., Kim, C., Galbraith, G. C., Jones, S. M., Kao, L., Newman, D., Liu, W., Yeh, S., Pushkin, A., Abuladze, N. & Kurtz, I. Slc4a11 gene disruption in mice: cellular targets of sensorineuronal abnormalities. *J Biol Chem* **284**, 26882-26896, (2009).

- 194 Delprat, B., Ruel, J., Guitton, M. J., Hamard, G., Lenoir, M., Pujol, R., Puel, J. L., Brabet, P. & Hamel, C. P. Deafness and cochlear fibrocyte alterations in mice deficient for the inner ear protein otospiralin. *Mol Cell Biol* **25**, 847-853, (2005).
- 195 Williams, A. L. & Bohnsack, B. L. Neural crest derivatives in ocular development: discerning the eye of the storm. *Birth Defects Res C Embryo Today* **105**, 87-95, (2015).
- 196 Peh, G. S. L., Ong, H. S., Adnan, K., Ang, H. P., Lwin, C. N., Seah, X. Y., Lin, S. J. & Mehta, J. S. Functional Evaluation of Two Corneal Endothelial Cell-Based Therapies: Tissue-Engineered Construct and Cell Injection. *Scientific reports* **9**, 6087, (2019).
- 197 Parker, M. D., Ourmozdi, E. P. & Tanner, M. J. Human BTR1, a new bicarbonate transporter superfamily member and human AE4 from kidney. *Biochem Biophys Res Commun* **282**, 1103-1109, (2001).
- 198 Jurkunas, U. V., Bitar, M. S., Funaki, T. & Azizi, B. Evidence of oxidative stress in the pathogenesis of fuchs endothelial corneal dystrophy. *Am J Pathol* **177**, 2278-2289, (2010).